Downloaded from orbit.dtu.dk on: May 05, 2023

DTU Library

Operation and Design of Diabatic Distillation Processes

Bisgaard, Thomas

Publication date:
2016

Document Version
Peer reviewed version

Link back to DTU Orbit

Citation (APA):
Bisgaard, T. (2016). *Operation and Design of Diabatic Distillation Processes*. Technical University of Denmark.

General rights
Copyright and moral rights for the publications made accessible in the public portal are retained by the authors and/or other copyright owners and it is a condition of accessing publications that users recognise and abide by the legal requirements associated with these rights.

- Users may download and print one copy of any publication from the public portal for the purpose of private study or research.
- You may not further distribute the material or use it for any profit-making activity or commercial gain
- You may freely distribute the URL identifying the publication in the public portal

If you believe that this document breaches copyright please contact us providing details, and we will remove access to the work immediately and investigate your claim.

Technical University of Denmark

PhD Thesis

Operation and Design of Diabatic Distillation Processes

Thomas Bisgaard

2016-02-28

DTU Chemical Engineering
Department of Chemical and Biochemical Engineering

Technical University of Denmark
Anker Engelundsvej 1
Building 101A
DK-2800, Kgs. Lyngby
Denmark
CVR-nr. 30 06 09 46
Phone: (+45) 45 25 25 25
Email: dtu@dtu.dk
www.dtu.dk

©2016-02-28 Thomas Bisgaard
Printed by GraphicCo

Preface

This thesis is submitted as a partial fulfilment of the requirements for obtaining a Doctor of Philosophy (PhD) degree at the Technical University of Denmark. The thesis presents the main research results obtained during a three year period between September 2012 to February 2016.

The PhD project was conducted at the Department of Chemical and Biochemical Engineering (CAPEC-PROCESS) under the supervision of Associate Professor Jakob Kjøbsted Huusom and Associate Professor Jens Abildskov as main supervisors and Associate Professor Nicolas von Solms and Professor Kim Pilegaard as co-supervisors. A part of the work was conducted in collaboration with Professor Sigurd Skogestad at the Department of Chemical Engineering, Norwegian University of Science and Technology (NTNU), Norway.

As the author of this thesis, I sincerely hope that this work will be considered as a significant contribution to the development of the field of diabatic distillation. Furthermore, I hope that the obtained results will seed and inspire future researchers to contribute to the field and that the developed materials and method will be found useful in the process.

I would like to thank the Technical University of Denmark for funding the project. A significant influence on the work is the supervision. I would hereby thank all my supervisors, in particular Jakob and Jens, for their valuable social and professional support, guidance, motivation, and criticism of the work. Positive contributions to the motivation by other sources during the PhD has been highly appreciated. In particular, I would mention Professor Emeritus Sten Bay Jørgensen for providing feedback and showing interest in the work. Finally, I would like to thank all the colleagues in CAPEC-PROCESS for providing a friendly, supporting and attractive working environment. Especially, my "office mates" have made every day - spent in the office - brighter.

During the three year duration of the PhD, I was granted the opportunity to

spend three of the months in Trondheim (Norway) as an external research stay under the supervision of Professor Sigurd Skogestad. This research stay resulted in a new approach to the project, which led to significant contributions. I am very grateful for the support from Professor Sigurd Skogestad and the colleagues at NTNU. I am grateful to have been sharing three months with the friendly and helpful colleagues at NTNU and I hope the contact will persist.

Thomas Bisgaard
Kgs. Lyngby, 2016

Summary

Diabatic operation of a distillation column implies that heat is exchanged in one or more stages in the column. The most common way of realising diabatic operation is by internal heat integration resulting in a heat-integrated distillation column (HIDiC). When operating the rectifying section at a higher pressure, a driving force for transferring heat from the rectifying section to the stripping section is achieved. As a result, the condenser and reboiler duties can be significantly reduced.

For two-product distillation, the HIDiC is a favourable alternative to the conventional distillation column. Energy savings up to 83% are reported for the HIDiC compared to the CDiC, while the reported economical savings are as high as 40%. However, a simpler heat-integrated distillation column configuration exists, which employs compression in order to obtain a direct heat integration between the top vapour and the reboiler. This configuration is called the mechanical vapour recompression column (MVRC). Energy and economic savings of similar magnitude as the HIDiC are reported for the MVRC. Hence, it is important to develop methods and tools for assisting the selection of the best distillation column configuration.

The contributions of this work can be divided in three parts. The first part involves the identification of the preferred distillation column configuration (CDiC, MVRC, or HIDiC) for a given mixture to be separated. Correlations between physical parameters, distillation column design variables, and preliminary feasibility indicators are investigated through simulations studies. The simulation studies include case studies, where different mixtures are separated in different distillation column configurations. The considered mixtures are industrially relevant and their thermodynamic behaviours vary considerable from one another. The HIDiC was found to be the preferred configuration in terms of operating expenditures for mixtures of normal boiling point differences below 10 K.

The second part involves the investigation of the technological feasibility of the

HIDiC. The impact on the column capacity (required tray area, entrainment flooding, weeping) of different column arrangements of the internal heat transfer is investigated. Furthermore, the ability to achieve stable operation of a concentric HIDiC is investigated by systematically designing a regulatory control layer and a supervisory control layer. Stable operation, in terms of column capacity and setpoint tracking, is demonstrated by simulation.

The final part covers the developed simulation tools and methods. A new distillation column model is presented in a generic form such that all the considered distillation column configurations can be described within the same model framework. The following distillation column configurations are considered:

- The conventional distillation column (CDiC)
- The mechanical vapour recompression column (MVRC)
- The heat-integrated distillation column (HIDiC)
- The secondary reflux and vaporisation column (SRVC)

The generic nature of the modelling framework is favourable for benchmarking distillation column configurations. To further facilitate benchmarking of distillation column configurations, a conceptual design algorithm was formulated, which systematically addresses the selection of the design variables. The conceptual design of the heat-integrated distillation column configurations is challenging as a result of the increased number of decision variables compared to the CDiC. Finally, the model is implemented in Matlab and a database of the considered configurations, case studies, pure component properties, and binary interaction parameters is established.

Resumé

Diabatisk drift af en destillationskolonne indebærer, at varme udveksles på en eller flere bunde i kolonnen. En udbredt metode til at realisere diabatisk operation er ved brug af indre varmeveksling, hvilket resulterer i den varmeintegrerede destillationskolonne (engelsk forkortelse: HIDiC). Ved at operere forstærkersektionem ved et højere tryk, kan en temperaturdrivkraft opnås, således at en varmeovergang fra forstærkersektionen til afdriversektionen kan realiseres. Dette resulterer i, at den krævede mængde energi, som fjernes fra kondensatoren og tilføres i kedlen, reduceres betydeligt.

For destillationskolonner med to produkter, anses HIDiC som et favorabelt alternativ til den konventionelle destillationskolonne (engelsk forkortelse: CDiC). Energibesparelser på op til 83 % er rapporteret for HIDiC'en sammenlignet med en CDiC , mens de rapporterede økonomiske besparelser er op til 40 %. Imidlertid, eksisterer en enklere varmeintegreret destillationskolonnekonfiguration, som udnytter kompression til at opnå en direkte varmeintegration mellem den øverste damp og kedlen. Denne konfiguration kaldes den mekaniske dampgenkompressionskolonne (engelsk forkortelse: MVRC). Energimæssige og økonomiske besparelser af lignende størrelsesorden som for HIDiC'en er rapporteret for MVRC'eren. Derfor er det vigtigt at udvikle værktøjer og metoder til at udvælge den mest favorable destillationskolonnekonfiguration.

Bidragene fra dette arbejde kan opdeles i tre dele. Den første del involverer identificering af den foretrukne destillationskolonnekonfiguration (CDiC, MVRC, or HIDiC) for en given blanding, der skal separeres. Sammenhænge mellem fysiske parametre, designvariable, og simple evalueringsindikatorer undersøges via simuleringersstudier. Simuleringersstudierne omfatter casestudier, hvor forskellige blandinger bliver udført i forskellige destillationskolonnekonfigurationer. De betragtede blandinger er industrielt relevante og deres termodynamiske egenskaber

afviger betragteligt fra hinanden. HIDiC'en har vist sig at være den foretrukne konfiguration, hvad angår driftsomkostninger, for blandinger med normalkogepunktsforskelle under 10 kelvin.

Den anden del omfatter en undersøgelse af den teknologiske gennemførlighed af en HIDiC. Inflydelsen af valget af måden, hvorpå HIDiC kolonnen arrangeres, på kolonnenkapaciteten undersøges. Dette dækker over undersøgelser af kravet til bundareal, samt risiko for væskelækage og -oversvømmelse på bundene. Endvidere er evnen til at opnå stabil drift undersøgt ved systematisk at designe et stabiliserende kontrollag efterfulgt af et tilsynsførende kontrollag. Stabil drift, hvad angår kolonne kapacitet og setpunktsporing, demonstreres ved simulering.

Den sidste del dækker over de udviklede simuleringsværktøjer og -metoder. En ny destillationskolonnemodel præsenteres i en generisk form, således at alle de betragtede destillationskolonnekonfigurationer kan beskrives inden for de samme modelrammer. De betragtede destillationskolonnekonfigurationer er:

- Den konventionelle destillationskolonne (CDiC)
- Den mekaniske dampgenkompressionskolonne (MVRC)
- Den varmeintegrerede destillationskolonne (HIDiC)
- Sekundær refluks og fordampningskolonne (SRVC)

På grund af den generiske karakter af modelleringsrammen, kan sammenligningsstudier af destillationskolonnekonfigurationer fortages på systematisk og konsistent vis. For yderligere at forenkle sammenlingingsstudier af destillationkolonnekonfigurationer er en konceptuel designalgoritme formuleret, som leder til en systematisk bestemmelse af designvariablene. Det konceptuelle design af varmeintegrerede destillationkolonnekonfigurationer er udfordrende som følge af det øgede antal af designvariable sammenligning med CDiC'en. Endeligt, er en Matlab-implementering af modellen, samt en database over de betragtede konfigurationer og separationer, etableret.

Contents

Chapter 1

Thesis Overview

This chapter contains a general overview of the PhD project with emphasis on its contributions. A brief introduction outlining the motivation, challenges and perspectives of diabatic distillation is presented. The project goals and the overall structure of the thesis document is provided here as well. Finally, dissemination activities related to the project and the main achievements are briefly outlined.

1.1 Motivation

Multi-stage distillation has been known since the 16th century. Today, distillation is the most widely used technique for separating chemical mixtures. In fact, it is estimated that more than 40,000 columns are currently operating worldwide [85] accounting for 40% of the energy consumed in the chemical industry. The energy consumed by distillation in 1978 was estimated to be 1458 PJ distributed among the different sectors shown in Figure 1.1. In particular, improvements in the petrochemical sector will lead to significant energy reductions. Many of the well-established industries have a reputation of being conservative and therefore, it is believed that the data fairly represents modern distillation energy consumption.

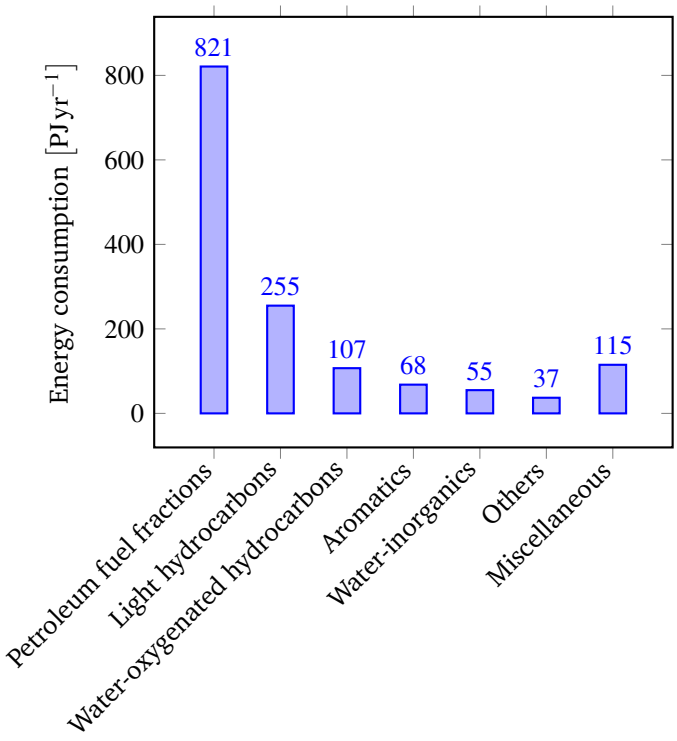

Figure 1.1. Estimated total U.S. distillation energy consumption 1978 [105]. The total energy consumption is 1458 PJ yr^{-1}.

Distillation offers a large number of advantages; it is usually the most economical method of separating liquid mixtures [162], it has a wide application range, and it is a technologically mature process. The key disadvantages are the high energy input requirement and its low thermodynamic efficiency. Industrial distillation columns operate at thermodynamic efficiencies in the range of 5-20% [26]. The

low thermodynamic efficiency is related to the heat addition at a relative high temperature in the bottom of the distillation column and energy removal at a relative low temperature in the top of a column. As a consequence, conventional heat integration within a distillation column is limited to feed preheating using the sensible heat of the bottoms product stream.

Improvements in distillation have been investigated since its industrial implementation. Particularly, the oil and energy crises during the 70's contributed to a significant interest in improved energy efficiency. In 1978 it was estimated that a decrease of energy consumption of 10% in distillation would conserve the equivalent of 100,000 barrels of oil per day [105]. To put things in perspective, the US imported twice the amount of crude oil per month (approx. 200,000 barrels of crude oil per month) during the same year [3]. The focus on effective energy management is not only driven by economics. It is widely acknowledged that the increasing CO_2 emissions associated with energy consumption, are correlated with the global climate change. Predictions foresee an increase in the average global temperature of up to 6°C by 2050 if current emission trends persist [65]. With all industrial processes accounting for 5% of the global CO_2 emissions in 2009 [65], a strong motivation exists to improve current technologies in every sector within the chemical industry. This includes distillation as it takes up 40% of the energy consumption in the chemical industry.

Several attempts to save energy have been proposed. These can be divided into the categories listed in Table 1.1. The improvements either involve changes with impact on the separation process or changes without impact on the separation process. These can further be divided in separation and energy efficiency-related improvements. Examples of each category are listed. This thesis focuses on the energy related categories. Examples of energy efficiency-related improvements with impact on the separation are intensified distillation configurations including the heat-integrated distillation columns [94]. Examples of the efficiency-related improvements without impact on the separation are the heat pump assisted distillation columns [34]. These configurations reflect types of heat integration for stand-alone distillation columns and cover external and internal heat integration, corresponding to vapour recompression and diabatic operation [43], respectively. Configurations, containing either or both types of heat integration, typically require compression. Electricity is invested in compression in order to reuse the latent heat removed in the top of a column, which is otherwise discarded in conventional distillation columns. Significant energy savings are reported for the heat-integrated distillation configurations. Potentially, this can lead to reductions in operation costs, overcoming the increased investment costs associated with additional heat exchange

Table 1.1. Options and classification of energy conservation methods in distillation inspired by Mix et al. [105].

Without impact on the process		With impact on the process	
Separation efficiency	Energy efficiency	Separation efficiency	Energy efficiency
• Control retrofit (adjust/update tuning, structure etc.) • Tray internals retrofit	• Insulation • Reboiler maintenance • Feed/product heat exchange • heat pump (vapour compression and vapour recompression)	• Side draw • Alternate techniques (e.g. extractive distillation)	• Thermal coupling (e.g. dividing wall column) • Intermediate heat exchangers • Internal heat integration (diabatisation)

equipment and compression. For example, energy savings up to 90% have been demonstrated by simulation of the heat-integrated distillation column separating propylene/propane [158]. An interesting catagory of separations that show a significant potential for energy improvements are the close-boiling mixtures, typically found in the petrochemical industry. This catagory includes the propylene/propane separation. The separations of close-boiling mixtures are typically very energy demanding and requires tall distillation towers with large internal flow rates. According to Figure 1.1, 90% of the 255 PJ energy spent on separating light hydrocarbons almost corresponds to a quarter of the brutto energy consumption of Denmark [2]. Hence, improvements in distillation in the light hydrocarbon industry appears to have a potential for large energy savings.

1.2 Thesis Objective and Goals

Employing heat pump in distillation is a relatively old concept but its advantages appears not to be fully exploited. Several options exist for intensified binary distillation [85] but the potentials among the different heat pump assisted distillation configurations are not fully understood. Extensive efforts have been made to develop the diabatic distillation technology since the late 70's. Despite demonstrations of large energy savings and manageable operability of e.g. the internally heat-integrated distillation column compared to the conventional distillation column, it has not yet been widely adopted by the industry. It is expected that this is due to lack of mature methods for designing these more complex configurations

and the investment cost associated with additional equipment (the compressor). These two factors constitute a significant psychological barrier for choosing such configurations over the familiar conventional ones [87].

The aim of this PhD project is to shed light on the potential benefits of diabatic operation and address some of the barriers for industrial application/acceptance of diabatic distillation columns. There is a need for research and comparative studies that can help to provide analysis of the pros and cons of novel and intensified distillation processes compared to conventional columns, while considering a broader range of separations. These studies must address both static as well as dynamic analysis. The following topics have been identified to comprise an important contribution:

1. **Modelling:** Improvements in the modelling is an important task, since the use of simplistic models can represent limitations. For example, in several published models, pressure dynamics or sensible heat effects are often ignored. Furthermore, it is important that models for conducting benchmark studies of distillation column configurations are consistent (same level of detail, economic parameters etc.).

2. **Analysis and benchmarking:** Consistent and systematic analysis of the potential benefits of intensified distillation solutions are required. It is observed that different means of analysis are reported in literature, which can lead to bias towards certain configurations. Current studies report very different figures for potential energy savings, which clearly constitutes a problem in relations to achieving industrial acceptance. Few authors have addressed this issue by proposing systematic evaluations. In addition, published case studies of industrial relevance are limited to a quite narrow range of separations. For example, benchmarking results of the separation of benzene/-toluene are often reported. Furthermore, it is desired (if possible) to link the desired distillation configurations to the physical properties of the components in the mixture to be separated. This is an advantage in computer-aided design frameworks as e.g. that of Jaksland et al. [72].

3. **Conceptual design:** The availability of simple, conceptual design methods of heat-integrated distillation columns is limited compared to conventional distillation columns. Furthermore, the realisation of the internals in the internally heat integrated columns still appears to be a challenge.

4. **Operation:** It is important to model and simulate a heat-integrated distillation column as realistic as possible in order to conclude, whether it has

acceptable operability for industrial application. Hence, all actuators must be considered. Furthermore, it is important to devise a control structure, which resembles that of the industrial practice.

1.3 Thesis Outline and Contributions

The thesis is divided into the following chapters listed with a short summary:

- **Chapter 2 Heat-Integrated Distillation Overview:** Literature overview of heat-integrated distillation column configurations. A more detailed literature review is provided of the internally heat-integrated distillation column (HIDiC), with the purpose of collecting, classifying, presenting, and discussing the literature in order to identify perspectives and challenges of industrial implementation. In contrast to the existing literature, the focus in the HIDiC review is on the technical feasibility. Hence, the possibilities of physical realisation in terms of achieving the required heat transfer areas, of choosing appropriate column arrangements, and of obtaining stable operation are discussed. In particular, attention is paid to the implications of internal heat transfer in distillation w.r.t. separation performance and heat transfer performance is discussed in relation to conventional equipment.

- **Chapter 3 Distillation Column Model:** This chapter represents the core of the work, in the sense it provides the modelling basis - the model framework - which is used throughout the thesis. The implementation and the solution procedure are presented end exemplified.

- **Chapter 4 Conceptual Design:** A simulation-based, conceptual design procedure for heat-integrated distillation columns with compressors is presented. The design method can be used to produce a conceptual design of any distillation configuration by iteratively, minimising the total annualised cost (TAC). Depending on the required design, the method can provide a design for a given configuration or a design of the configuration with the lowest TAC (with no configurations specifications in advance). The method is explained step by step and illustrated through examples. The presented method is a generalisation of the procedure for arriving at an optimal design, based on experience from numerous rigorous simulations studies covering most possibilities of the pairing of heat integrated stages.

- **Chapter 5 Techno-Economic Feasibility Analysis:** An extensive feasibility study is presented, covering the separation of ten fundamentally different

mixtures (nine binary and one multicomponent), carried out in four different distillation column configurations. Links between mixture component physical properties, simple feasibility measures and the actual economic feasibilities are established. Two case studies involving the separations of benzene/-toluene and propylene/propane are highlighted. The presentations of the case studies consist of illustrations of the basic features of the HIDiC, the conceptual designs, the technical feasibilities, and elaborate benchmarking studies. In this regard, uncertainty analysis and sensitivity analysis are used on two classes of mixtures (low/high normal boiling point differences) in order to quantify the uncertainty of operating expenditure estimates and to identify the more significant uncertain variables.

- **Chapter 6 Stabilising Control:** A regulatory control structure design is proposed. Stable operation, in terms of setpoint tracking and avoiding entrainment flooding and weeping, was achieved in the simulation of a concentric HIDiC separating benzene/toluene. The necessity of including pressure dynamics in modelling of the heat-integrated distillation columns is illustrated by benchmarking dynamic open-loop responses against a constant molar overflow-model.

- **Chapter 7 Optimising Control:** A supervisory control structure design is devised based on the systematic, economic plant-wide control method by Larsson and Skogested [89]. Optimal operation of HIDiC is defined. The optimal operating point is determined for a concentric HIDiC, separating a mixture of benzene/toluene. The combined supervisory and regulatory control structures are evaluated by simulation and good performance is achieved w.r.t. setpoint tracking of all controlled variables. Furthermore, good economic performance is demonstrated for realistic disturbance scenarios.

- **Appendices:** In Appendix A, the model implementation documentation is supplied, while mathematical derivations are collected in Appendix B. Additional material for the economic model is provided in Appendix C. The common model solution algorithm, known as the Wang-Henke boiling-point method, is extended to cover heat-integrated distillation column configurations. This extension is documented in Appendix D. Finally, Appendix E contains the application examples of two existing graphical design methods.

Apart from the text, the thesis contains figures, tables and illustrations. The illustrations are distinguished from the main text using shaded boxes. These illustrations are used to elaborate on certain aspects in more detail and cover e.g.

investigations of assumptions or analytical expressions, with the aim to provide an order of magnitude perception. A consistent notation throughout the thesis is used and listed in the very end (page 251).

1.4 Publications

All the scientific publications produced during the PhD work are listed in this section according to journal articles, peer-reviewed conference publications, and additional publications. Chapter references in boldface brackets are used to indicate which material, the corresponding publications are based upon. Hence, this section can be used as a reference work if more condensed descriptions are preferred. The contributions are published unless otherwise stated.

1.4.1 Journal Papers

Ordered list of journal papers, starting from the most recent contribution:

- T. Bisgaard, J.K. Huusom, and J. Abildskov. Conceptual design of heat-integrated distillation columns with compressors. 2016 **(Chapter 4)** (in preparation)
- T. Bisgaard, J.K. Huusom, and J. Abildskov. Modeling and analysis of conventional and heat-integrated distillation columns. *AIChE Journal*, 61(12):4251–4263, 2015 **(Chapter 3)**
- M. Mauricio-Iglesias, T. Bisgaard, H. Kristensen, K.V. Gernaey, J. Abildskov, and J.K. Huusom. Pressure control in distillation columns: A model-based analysis. *Ind Eng Chem Res*, 53(38):14776–14787, 2014 **(Chapter 3)**

1.4.2 Reviewed Conference Papers

Ordered list of reviewed conference papers, starting from the most recent contribution:

- T. Bisgaard, S. Skogestad, J.K. Huusom, and J. Abildskov. Optimal operation and stabilising control of the concentric heat-integrated distillation column. *11th IFAC International Symposium on Dynamics and Control of Process Systems – Trondheim, Norway*, 2016 **(Chapter 6 and 7)**
- T. Bisgaard, J.K. Huusom, and J. Abildskov. Impact on model uncertainty of diabatization in distillation columns. *Proceedings of Distillation and Absorption*, pages 909–914, 2014 **(Chapter 5)**

- K. Meyer, L. Ianniciello, J.E. Nielsen, T. Bisgaard, J.K. Huusom, and J. Abildskov. Hidic – design, sensitivity and graphical representation. *Proceedings of Distillation and Absorption*, pages 727–732, 2014 **(Chapter 4)**
- T. Bisgaard, J.K. Huusom, and J. Abildskov. A modeling framework for conventional and heat integrated distillation columns. *10th IFAC International Symposium on Dynamics and Control of Process Systems – Mumbai, India*, pages 373–378, 2013 **(Chapter 3)**
- T. Bisgaard, J.K. Huusom, and J. Abildskov. Dynamic effects of diabatization in distillation columns. *Computer-aided Chemical Engineering*, 32:1015–1020, 2013 **(Chapter 6)**
- T. Bisgaard, J.K. Huusom, and J. Abildskov. Dynamic effects of diabatization in distillation columns. *Proceedings of the 10th European Workshop on Advanced Control and Diagnostics (ACD 2012)*, 2012 **(Chapter 6)**

1.4.3 Other Documentation

An extensive Matlab library has been developed, consisting of databases of physical parameters, simulation case studies, and models. More details are provided in Appendix A.

Chapter 2

Heat-Integrated Distillation Overview

This chapter contains an overview of different heat-integrated distillation configurations proposed in literature. During the overview, the concept of diabatic distillation is introduced. The following section presents a literature review of the heat-integrated distillation column. The focus is on its techno-economic feasibility. Experimental experiences, reported in literature, are summarised and discussed in relation to the possibilities and the challenges of equipment for the realisation of the HIDiC.

2.1 Introduction

Section 2.2 (below) will provide a step-by-step introduction to the concepts of the HIDiC. At the end of Section 2.2 some more recent configurations are presented and discussed.

Elaborate overviews of heat-integrated distillation technologies exist in literature [111, 37, 73, 86, 100, 85, 87, 126]. The present HIDiC review (Section 2.3) deviates from the existing reviews in the sense that it aims to combine all aspects of technological feasibility and economic feasibility.

Here, technological feasibility covers the possibilities of

- obtaining a feasible conceptual design,
- realising the obtained conceptual design in physical equipment, and
- maintaining stable, continuous operation when subject to disturbances.

Economic feasibility is when an economic benefit of a heat-integrated distillation configuration, compared to conventional distillation, can be reaped. Thus, the economic basis for benchmark studies is examined. The economic basis involves design variables (heat exchange areas), model parameters (overall heat transfer coefficient), and economic parameters (steam price, cooling water price, and electricity price). Based on the findings in the HIDiC literature review, Section 2.4 presents the identified areas of research, which are covered in this thesis.

2.2 Distillation Methods

Distillation is a physical, multiphase separation technique that exploits the differences in relative volatilities of components and the counter-current movement of the contacting vapour and liquid phases. The most common industrial distillation column configuration is the conventional distillation column (CDiC), which are described below.

2.2.1 Conventional Distillation Column

A conventional distillation column (CDiC) consists of a vertical column tower, a reboiler and a condenser as illustrated in Figure 2.1. The most common configuration has two product streams and one feed stream. Gravity transports liquid downwards inside the column because of the vertical orientation of the column, while vapour moves upwards due to pressure differences between the bottom and the top, initiated by the reboiler. At each vertical position, a part of the entering vapour is

condensed and mixed with the entering liquid and the present liquid (holdup), while a liquid amount of similar magnitude is vaporised due to the added latent heat from the condensation. To generate these flows, the CDiC is equipped with a heat exchanger in the top (the condenser) and in the bottom (the reboiler). The role of the condenser is to fully or partly condense the vapour leaving the column in the top. A fraction of the condensed vapour is recycled to the top of the column (the reflux). The reboiler generates vapour flow (i.e. pressure) in the bottom by evaporation (boilup). The products of the distillation column (see Figure 2.1) are typically a distillate in the top (A) that is rich in the most volatile component(s) and a bottom product (B) that is rich in the least volatile component(s). The column is divided in two column sections: The rectifying section, which is above the feed location, and the stripping section, which is below the feed location. The column itself (excluding the condenser and the reboiler) is thermally insulated from the surroundings and is therefore considered adiabatic.

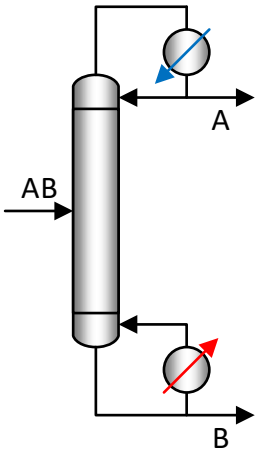

Figure 2.1. Conventional distillation column (CDiC).

The internals of a distillation column consists either of trays, structured packing material or random packing material.The purpose of the internals is to facilitate efficient mass transfer between the contacting liquid and vapour phases. For tray columns, a stage is identical to a tray when assuming equilibrium.For packed columns, the theoretical stage is often translated into an equivalent column height (HETP, height equivalent to theoretical plate). In modelling, liquid-vapour equilibrium is typically assumed on each stage and is thus also called a theoretical stage

or an equilibrium stage.

Stand-alone heat integration in a CDiC is limited to feed preheating using the bottoms stream, where only sensible heat can be recovered. In the following sections, different distillation column configurations are presented that are able to overcome this limitation by employing compression. The radical idea of introducing new equipment in distillation (e.g. a compressor), can potentially revolutionise the old and well-known unit operation of distillation.

2.2.2 Heat Pump-Assisted Distillation

The heat pump-assisted distillation column, which was introduced in the 1950's [34], received renewed interest during the oil and energy crises in the 1970's as significant energy savings can be obtained. The heat pump enables the absorption of heat from a cold source and the rejection of heat at a higher temperature sink, which can directly translate into the condenser as the cold energy source (due to condensation) and the reboiler as the hot temperature sink (due to vaporisation). The simplest distillation configuration employing this principle is called the vapour compression column (VCC) shown in Figure 2.2(a). In this configuration, an appropriate working fluid acts as an energy carrier between the condenser and reboiler. As shown, compression and throttling is required.

Alternatively, the top vapour can be used as the working fluid thereby resulting in the configuration illustrated in Figure 2.2(b). This configuration is commonly known as the mechanical vapour recompression column (MVRC). A review on heat pump assisted distillation technologies is provided by Jana [74]. The MVRC circumvents the additional compression cycle by letting the compressor work directly on the top vapour. As vapour recompression can be obtained by different means [86], the term "mechanical" is used to differentiate from e.g. the thermal vapour recompression column (TVRC). In the TVRC, the required work for compression is provided by a steam ejector thus limiting its application to systems with water produced as the distillate. The TVRC is not considered in this work. Both the VCC and the MVRC can be classified as externally heat integrated distillation columns since the heat exchange takes place outside the conventional distillation equipment. A significant advantage of both the VCC and the MVRC is that the heat pump has no impact on the separation. Therefore, such configurations appears to be very desired in new applications as well as retrofitting, as they constitute a minimal technical risk [127]. Furthermore, heat pump-assisted distillation has good operability as proven by both simulation [107, 134, 135, 78] and experimentally [6, 90]. Furthermore, significant economic and energy savings are reported [44, 127, 128, 30, 8, 32]. In fact, it has already been successfully applied in the industry in the productions of 1-

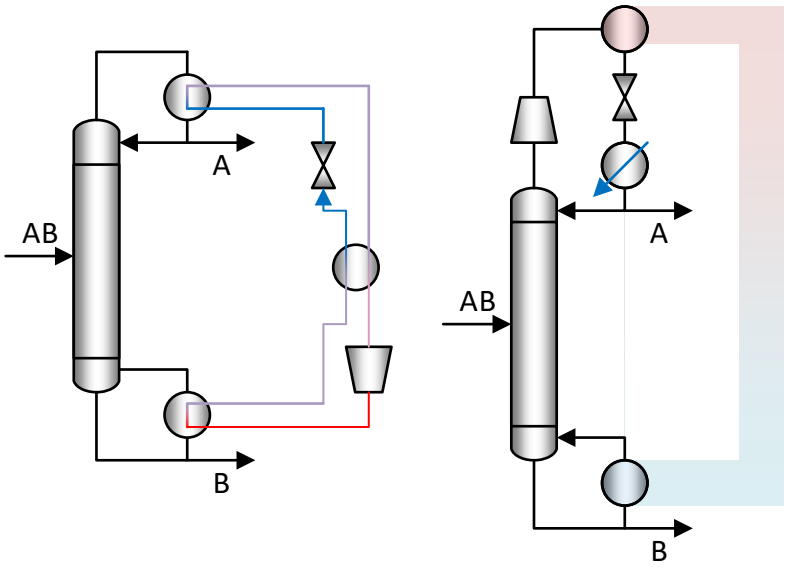

(a) Vapour Compression Column (VCC).

(b) Mechanical Vapour Recompression Column (MVRC).

Figure 2.2. Externally heat-integrated distillation columns.

butene, chlorobenzene, ethanol, isopropanol and more [49]. Table 2.1 summarises some feasibility studies from the open literature. The table clearly illustrates the large savings compared to conventional distillation for a range of separations. It also illustrates the dependency of the conclusions on the economic models. For instance, separating the benzene/toluene in an MVRC is economically feasible according to one study [51] but economically infeasible according to another study [139]. However, the overall trend suggests that heat pump-assisted distillation is an attractive alternative to conventional distillation as an economic benefit is achieved for most reported separations.

2.2.3 Diabatic Distillation

In most cases, the column shell in conventional distillation is thermally insulated causing adiabatic operation. If, instead, heat transfer is taking place at two or more locations in the column (e.g. in the column trays), the column is said to be diabatic. A general representation of a diabatic distillation column is given in Figure 2.3(a).

The distillation column with sequential heat exchangers (DSHE) is an example of a diabatic distillation column (Figure 2.3(b)). In this configuration, heat is

Table 2.1. Reported energy and economic savings of the mechanical vapour recompression column. The energy and economic savings are reported with reference to a CDiC performing the same separation; positive savings are in favour of the MVRC. Electrical energy is weighted by a factor of three for estimating the total energy consumption in the HIDiC.

System	Savings		Reference
	Energy	Economy	
Binary			
Acetic acid/acetic anhydride	48%	-	[22]
Propylene-propane	-	21%	[125]
	-	44.1%	[139]
Benzene/fluoro-benzene	-	54%	[51]
Benzene/n-heptane	66%	42%	[51]
Benzene/toluene	-	17%	[51]
	-	-24.9%	[139]
Benzene/chloro-benzene	-	0%	[51]
Ethanol/water	67%	36%	[51]
Ethylbenzene/styrene	74%	69%	[30]
Methanol/water	50%	3.1%	[141]
Multicomponent			
Styrene/benzene/toluene/ethylbenzene	79%	39%	[51]
Ethylbenzene/xylenes blend	62%	56%	[30]
Xylene blend	24%	47%	[8]

removed in the rectifying section by letting a cold stream pass the inside of the column, thereby acting as an energy sink. As this stream is introduced in the top and removed at a lower location the temperature can reach a higher value than what can be obtained from a condenser. The stages in the rectifying sections can thus be considered as sequential heat exchangers. In the same manner, a heating stream is introduced in the bottom of the column and is extracted at a higher location.

This configuration has been studied as a means of improving the thermodynamic efficiency of a distillation column by various authors [43, 77, 144]. Furthermore, the concept of diabatic distillation has been proven experimentally by de Koeijer and Rivero [25]. For a diabatic distillation column, a reduction in exergy loss of 39% can be obtained, meaning that the degradation of the energy quality is reduced compared to conventional distillation. Reports on economic savings have not been encountered in the literature. This is likely due to the fact that no direct benefits (i.e. energy requirement reductions) are achieved. Instead, the streams for removing/adding energy in the condenser/reboiler become more potent for heat integration, which can not easily be quantified in terms of economic improvements.

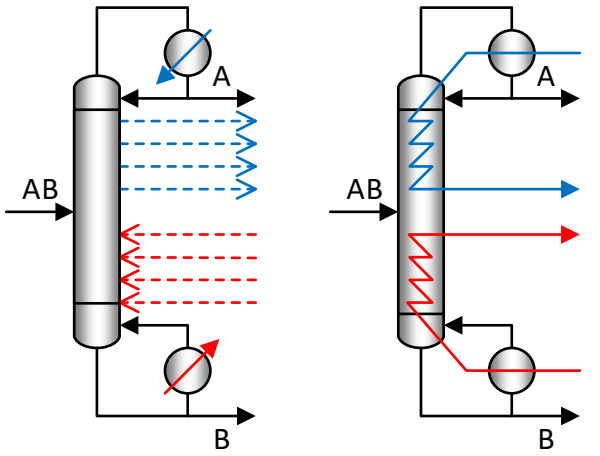

(a) General diabatic distillation column.

(b) Distillation column with sequential heat exchangers (DSHE).

Figure 2.3. Diabatic distillation columns.

2.2.4 Internal Heat-Integrated Distillation

The principles of heat pump-assisted distillation can be used for enabling diabatic operation in such a way that the rectifying section acts as a heat source and the stripping section acts as a heat sink. Hence, the rectifying section must be operated at a higher pressure in order to achieve the necessary temperature driving forces among the heat-integrated stages. The two column sections are physically separated (i.e. the rectifying section is not necessarily on top of the stripping section) and a compressor is connected to the vapour leaving the stripping section, i.e. from the feed stage. In accordance with the differences in pressures between the column sections, a throttling valve is connected to the liquid stream leaving the rectifying section. The obtained configuration is commonly referred to as the heat-integrated distillation column (HIDiC) but was originally introduced along with the concept of secondary reflux and vaporisation by Mah et al. [94]. The HIDiC is also referred to as the internal thermally coupled distillation column by some authors [92] but the term "thermal coupling" is commonly associated with the principle of the Petluyk arrangement discussed in Section 2.2.6. In Figure 2.4(a), a conceptual representation of the HIDiC is presented. The variant of the HIDiC, where feed preheating is used such that reboiler and condenser duties are avoided, is often called the ideal

HIDiC (i-HIDiC) [73]. More recently, the term HIDiC is used to describe both internally heat integrated (diabatic) columns and columns, which have external heat exchangers for realising heat integration between the column sections.

Additional energy can be recovered by using vapour recompression of the top vapour in the HIDiC. This column was introduced along with the HIDiC by Mah and Fitzmorris [31]. As the HIDiC abbreviation is fairly well established, the name secondary reflux and vaporisation column (SRVC) will be used for a HIDiC having condenser/reboiler heat integration using an additional compressor on the top vapour. The SRVC is illustrated in Figure 2.4(b). Later, Mane et al. [98] considered a configuration, which is conceptually identical to the SRVC. However, Mane et al. used the name Intensified HIDiC.

The HIDiC is an intensified distillation column [5], which represent a radical, stand-alone way of carrying out heat integration. Because of the promising features of the HIDiC, extensive efforts have been made to develop this technology during the past 15 years, both theoretically and experimentally. A more elaborate description of the HIDiC is provided in Section 2.3.

2.2.5 Advanced Internal Heat-Integrated Distillation

Jana [73] provides an overview of applications of advanced distillation techniques transferred to the HIDiC. Pressure-swing distillation is an apparent application of internal heat integration because two different column pressures already exist. However, two distillation columns are required rather than two column sections. Following the concepts of the HIDiC by choosing a high pressure rectifying section as heat source and a low pressure stripping section as heat sink, the two configurations in Figure 2.5 are obtained for the two cases: (a) for a minimum-boiling azeotropic mixture and (b) for a maximum-boiling azeotropic mixture [62]. Huang et al. [62] provides a framework for designing the heat-integrated pressure swing distillation columns and found for the separation of acetonitrile/water that up to 15% operating cost reductions and 14% capital cost reductions could be achieved compared to a conventional sequence. However, it was concluded that this rectifying/stripping section type heat integration fails to compete with the condenser/reboiler (multi-effect) type heat integration for the considered separation [62]. The internally heat-integrated pressure-swing distillation columns arrangement is a special case of the arrangement, referred to as the heat-integrated double distillation columns (HIDDiC). The HIDDiC provides an alternative to a multi-effect distillation sequence for separations with more than two product splits (conceptually includes water/ethanol/azeotropic ethanol). The HIDDiC has been studied with the heat integration of entire column sections [82] and with few heat-integrated stages

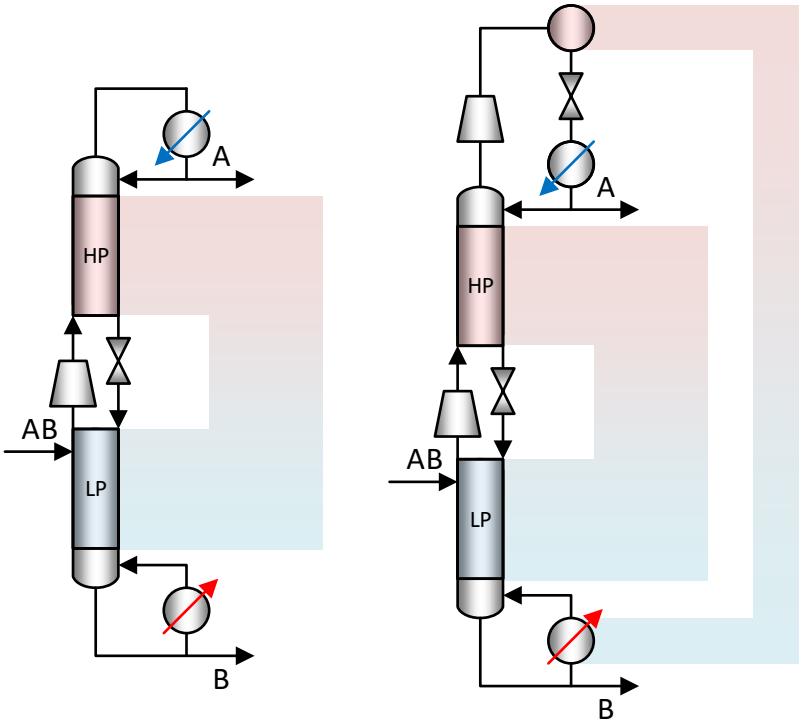

(a) The Heat-Integrated Distillation Column (HIDiC).

(b) Secondary reflux and vaporisation Column (SRVC).

Figure 2.4. Internally heat-integrated distillation columns. LP is the low-pressure section and HP is the high-pressure section.

[167, 172, 59]. However, the benefit over a conventional multi-effect distillation column arrangement has not been fully demonstrated. Furthermore, it is important to note that the HIDDiC can potentially be operated without a compressor [82], which is also the case for a multi-effect distillation sequence. Multi-effect distillation denotes a distillation sequence, in which the columns operate at different pressure such that e.g. condenser/reboiler type heat integration can be realised.

A more unconventional approach was adopted by Mulia-Soto et al. [108] and Ponce et al. [131], where the entire distillation columns in a pressure-swing sequence were heat integrated. For the ethanol/water separation this leads to the arrangement illustrated in Figure 2.5(c), which is referred to as an internally heat-integrated pressure swing distillation process (IHIPSD). It was shown that by in-

vesting 0.28 MW, the total reboiler duty could be reduced from 6.33 MW from a conventional sequence to 4.30 MW for the IHIPSD. Condenser/reboiler type heat integration was not considered in the mentioned studies [108, 131]. The study by Mulia-Soto was later questioned [143], as reproducing the ethanol/water separation in conventional equipment was deemed extremely difficult. The separation of ethanol/water, in particular, suffers from relatively low sensitivity of the azeotropic composition to pressure. In the case of low pressure sensitivity, pressure swing distillation becomes practically impossible as the internal flow rates varies significantly with small changes in product purities.

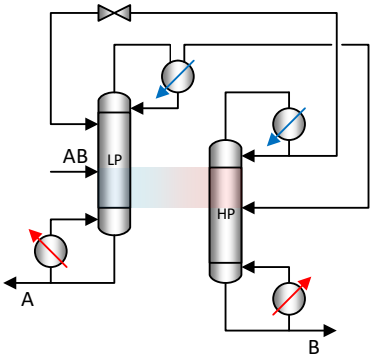

(a) Internally Heat-Integrated Pressure-swing Distillation Column separating minimum-boiling azeotrope [62].

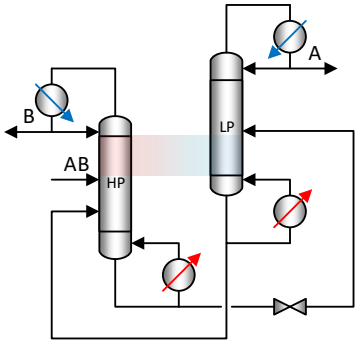

(b) Internally Heat-Integrated Pressure-swing Distillation Column separating maximum-boiling azeotrope [62].

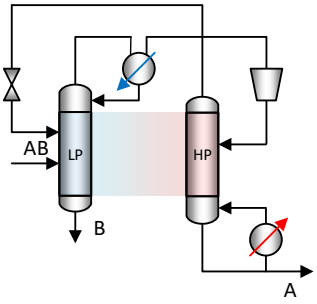

(c) Internally Heat-Integrated Pressure-swing Distillation Column (IHIPSDC) for separating ethanol/water [108].

Figure 2.5. Advanced internally heat-integrated distillation columns. LP is the low-pressure section/column and HP is the high-pressure section/column.

2.2.6 Thermally Coupled Distillation Columns

Based on the patent by Brugma [18], Petlyuk et al. [129] introduced thermal coupling in a distillation with a prefractionation column as illustrated in Figure 2.6(a). By supplying the reflux and boil-up flows in the prefractionation column by directly taking fractions of the internal vapour and liquid flows from the main column, significant energy savings can be obtained for multicomponent separations. As a result, an intensified arrangement was achieved called the Petlyuk arrangement. A ternary distillation process is illustrated in Figure 2.6. A thermodynamically equivalent configuration was filed as a patent [169] in 1949, in which both prefractionation and distillation takes place in the same column shell (Figure 2.6(b)). This configuration is known as the dividing wall column (DWC). In 1985 (35 years after its introduction [169]), the DWC was introduced in an industrial application by BASF [126]. Since then, it has been industrially recognised as a common separation technique of multicomponent mixtures.

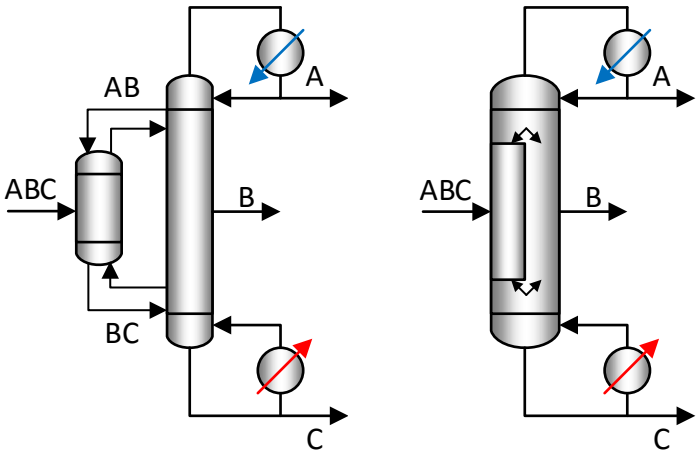

(a) Petlyuk configuration. (b) Dividing Wall Column (DWC).

Figure 2.6. Thermally coupled distillation columns.

2.2.7 Summary of Heat-integrated Distillation Methods

The previous sections only illustrate a handful of the many possibilities for intensifying distillation. It is important, as a chemical plant design engineer, to be able to identify the best distillation column configuration among the alternatives. Hence,

it is important to investigate the feasibility of all alternatives when designing distillation units for chemical and biochemical plants. Kiss et al. [86] systematically addressed this investigation for a wider range of configurations and proposed a flow chart for selecting an appropriate distillation configuration for a given class of separation. In the case of binary distillation, four distinct configurations were covered in this chapter; the CDiC, the MVRC, the HIDiC, and the SRVC. According to Kiss et al. [86], the HIDiC or the MVRC are among the preferred choices if (i) it is a binary distillation, (ii) water is not a top product (distillate), and (iii) separation is above atmospheric pressure. In terms of separation involving more than two product splits, i.e. multicomponent separations, the DWC or multi-effect distillation sequences are typically the preferred option [86].

This issue of linking the feed mixture to the preferred distillation column configuration has been the topic of various studies [51, 142, 155, 47]. These studies conclude that the economic advantage of either configuration is a complex function of mixture identity, whereas correlations between optimality and relative volatility have been shown for ideal mixtures. In particular, the study by Shenvi et al. [142] concluded that the efficacy of the HIDiC can not be solely decided, based on the feed and product specification, and pointed out that the shape of the column temperature profile is the dominant factor. However, no direct and simple guidelines of selecting a configuration among the binary distillation techniques (e.g. the MVRC and the HIDiC) have been encountered in literature. Hence, there is still a need for systematically mapping the choice of superior configuration w.r.t. selected performance criteria.

2.3 The Heat-Integrated Distillation Column

The heat-integrated distillation column (HIDiC) has a great potential as a standalone distillation solution, due to following benefits:

- It provides reuse of otherwise wasted latent heat in the CDiC (like the MVRC) but requires a lower compression ratio than that of the MVRC [94].

- The equipment size can potentially be reduced as one of the column sections contains a denser, high-pressure vapour. Furthermore, a concentric arrangement [45] can realise the HIDiC within one column shell.

- A compressor is a more reliable energy source/sink than steam/cooling water due to elimination of temperature and pressure disturbances [49].

- The usage of electricity instead of steam can potentially result in lower harmful emissions provided that electricity can be generated from renewable sources. In addition, this might also affect the energy prices through regulations.

Kim [82] pointed out the limitations of the HIDiC based on a claimed long history on development of an industrially applicable HIDiC:

- The required compressor (turbo-blower) is big and expensive
- The HIDiC is legally classified as a pressure vessel subject to safety regulation
- The HIDiC cannot be applied for feeds containing dirty, sticky, corrosive, and heat-sensitive compounds
- Startup and shutdown as well as normal operation are not easy

Due to the listed, potential benefits and limitations, the HIDiC has received increased attention the past decades with the leading research groups located in The Netherlands (TU Delft) and Japan (AIST). In Japan, a collaboration between academia and industry takes place and there is currently an ongoing project about industrial implementation of the HIDiC [1]. This particular HIDiC configuration is termed the Super HIDiC [87].

A broad overview of the HIDiC literature is summarised and classified in Table 2.2. The purpose of this table is to provide a reference work of the literature that is cited in the following subsections. Hence, if the reader has identified a research topic related to the HIDiC, Table 2.2 will provide the references to consult.

When consulting the references in Table 2.2, it shows that the HIDiC literature dates back to more than 35 years ago with the introduction of the secondary reflux and vaporisation concept. Considering the history of the DWC (Section 2.2.6), a time span of roughly 35 years was required to industrialise the DWC concept. According to this observation, the HIDiC should be in a stage for industrial implementation – but is this the case? In the following sections, the published state-of-the-art research will be presented and discussed within the topics of experimental verification, conceptual design and equipment design, benchmarking, and operation. Conclusions of the findings are reported in the end of this chapter in order to answer the above stated question.

2.3.1 Experimental Studies

The first section is dedicated to the experimental studies related to the HIDiC since such studies report valuable experience and insights in design and operation. Table

[1] Personal communication with Toshihiro Wakabayashi during Distillation & Absorption 2014, Friedrichshafen, Germany

Table 2.2. Reference work of the HIDiC classified according to research topics.

Publication type	Research topic(s)	References
Reviews	Configurations	[73]
	Simulation	[100, 111]
	Design	[37]
	Applications	[95]
	Benchmarking	[86]
	HIDiC realisation	[87]
	Distillation equipment	[126]
Experiment	CFD	[132]
	Proof-of-concept	[109, 28, 27, 66, 81, 58, 170, 19, 118, 121, 122]
	Start-up	[123]
Dynamic modelling	Simple model	[60, 92]
	Stage-based model	[55, 14]
	Rate-based model	[99, 66]
Benchmarking	Energy and economics	[94, 136, 158, 125, 31, 20, 139, 141, 50]
	Exergy	[114, 115]
	Intensified HIDiC	[98, 84, 83, 97]
	Pressure swing HIDiC	[62, 108, 131]
	Vacuum separation	[22]
Design	Graphical methods	[156, 56, 159, 118]
	Simulation-based methods	[23, 38, 41, 39, 40, 38]
	Mathematical Programming	[51, 140, 47, 91]
	Sensitivity analysis	[112, 142, 154, 67, 155, 68, 171]
	Sequence	[61]
Dynamics and control	Control strategy	[116, 110, 113, 174, 93, 36]
	Steady state multiplicity	[96, 164, 165, 80, 79]
	Temperature control	[63]
	Controllability	[106]
	Intenfied HIDiC	[113]
	High purity control	[173]
	Start-up	[166]

2.3 contains a summary of the experimental studies obtained in the literature. Further details on the reported experience from the experimental studies are discussed in the following sections, and in particular, w.r.t. equipment in Section 2.3.4 and operation in Section 2.3.6.

The primary focus of the experimental studies is on determining the overall

heat transfer coefficient for such devices in addition to delivering proof-of-concept. In Table 2.3, several means of quantifying the performance of the reported HIDiC studies w.r.t. mass transfer and heat transfer are reported. The table lists the height equivalent theoretical plates (HETP), the specific heat transfer area (Φ, area available for heat transfer per column volume), and the overall heat transfer coefficient (U_{ihx}). These values have either been directly reported in the studies or calculated using relevant information if possible. The HETP is a measure of the separation performance, which is useful to compare similar equipment (with or without internal heat transfer). The specific heat transfer area is a measure of feasibility in the sense that maximal achievable values are dictated by conventional heat exchange equipment. Finally, the overall heat transfer coefficient quantifies the relation between the required heat exchange area and the required internal heat transfer rate. Thus, the overall heat transfer coefficient is an essential parameter, which must be reported along with the heat exchange area. In addition, the experimental studies are classified in tray columns and packed columns with more geometric data provided in the table. The majority of the experimental efforts are directed towards packed columns in the shell-and-tube arrangement or the concentric arrangement with only one tube. But also a concentric tray HIDiC has been considered.

Table 2.3. Reported experimental results of the HIDiC. The details on the column internal cover number of tubes, tube diameter, and internals type. ID is inner diameter, HETP is height-equivalent theoretical plates, Φ is the specific heat transfer area, and U_{ihx} is the overall heat transfer coefficient responsible for the internal heat exchange.

Experimental set-up description			Performance			Ref.
Height	Outer diameter	Details on internals and system	HETP	Φ	U_{ihx}	
mm	mm		m	$m^2\,m^{-3}$	$kW\,m^{-2}\,K^{-1}$	
Tray columns						
2640	800	Concentric column: 1× tube 500 mm (rectifier), dual flow "lift" trays, and a total of 4 trays with 400 mm spacing. system: Benzene/toluene.	- (50-75% tray efficiency*)	19.9 (calc. from $4\,m^2\,stage^{-1}$ and tray spacing)	0.50-0.95*	[122]
2600	-	Parallel columns: Dual flow "lift" trays (no downcomers) with heat tubes, and a total of 5 trays with 400 mm spacing. system: Benzene/toluene.	- (45-85% tray efficiency*)	-	0.40-1.0	[121]
1500	800	1× tube 300 mm (rectifier), sieve trays with heat panels, and a total of 3 trays with 500 mm spacing. System: Cyclohexane/n-heptane.	- (Approx. 81% tray efficiency)	-	0.40-1.90*	[28]

Continued on next page

Table 2.3 – continued from previous page

Experimental set-up description			Performance			Ref.
Height	Outer diameter	Details on internals and system	HETP	Φ	U_{ihx}	
mm	mm		m	$m^2\,m^{-3}$	$kW\,m^{-2}\,K^{-1}$	
Packed columns						
1900	-	Shell-and-tube: 21× 300 mm tubes. System: Benzene/toluene.	0.420 (tube) and 0.330 (shell)	-	0.60-1.0*	[118]
16,000	254	Concentric: 1× tube with varying diameter: 140, 165, and 190 mm (rectifier) containing MC PACK structured packing (widest in bottom). System: Benzene/-toluene.	-	-	-	[109, 66]
20,000	318.5	Shell-and-tube: 3× 101.6 mm tubes (rectifier). System: Benzene/-toluene.	0.29*	-	0.450-0.600*	[123]
20,000	318.5	Concentric: 1× tube 139.8 mm (rectifier). System: Benzene/-toluene.	0.26*	-	0.500-0.810*	[123]

Continued on next page

Table 2.3 – continued from previous page

Experimental set-up description			Performance			Ref.
Height	Outer diameter	Details on internals and system	HETP	Φ	U_{ihx}	
mm	mm		m	$m^2\,m^{-3}$	$kW\,m^{-2}\,K^{-1}$	
20,000	318.5	Concentric: 1× tube 198 mm (rectifier). System: Benzene/toluene.	0.27*	-	0.530-0.810*	[123]
27,000	1,400	Shell-and-tube: 7× double-tube (rectifier) packed column in 2x35 theoretical stages. System: C4-C6 hydrocarbon mixture.	0.77 (calc. from column height)	1.9 (calc. from column height and $2.25\,m^2\,stage^{-1}$)	0.67	[58]
1,000	200 (width)	Structured plate-fin: 40 parallel channels (phase contact $528\,m^2\,m^{-3}$). System: Cyclohexane/n-heptane.	1.20-1.44	52.7	0.214-0.321	[19]
1,000	200 (width)	Structured plate-packing: Corrugations inclined in opposites direction (phase contact $600\,m^2\,m^{-3}$). System: Cyclohexane/n-heptane.	0.22-0.40	52.7	0.373-0.550	[19]

Continued on next page

Table 2.3 – continued from previous page

Experimental set-up description			Performance			Ref.
Height	Outer diameter	Details on internals and system	HETP	Φ	U_{ihx}	
mm	mm		m	$m^2\,m^{-3}$	$kW\,m^{-2}\,K^{-1}$	
1,000	150	Concentric: 1× inner tube with varying diameter 88-108 mm (ID, widest in bottom) with Dixon packing and 150 mm	0.12-0.15 (inner) and 0.35-0.59 (outer)*	-	0.780-1.00 (Eq (2.5))	[170]
Combined tray and packed columns						
6,800	250 mm (ID)	Concentric: Stripper=Outer shell with packing (250 mm (ID), 5.2 m height). Rectifier= 25 trays in inner tube (150 mm ID, 6.8 m height). System: Ethanol/water.	-	9.6 (calc. from 0.09426 $m^2\,stage^{-1}$)	0.3249	[81]

*Obtained from figure in reference

2.3.2 Dynamic Modelling

In dynamic distillation column simulations, the "constant molar overflow" assumption is widely applied. As a consequence, the energy holdup derivatives are converted into algebraic equations [146]. This assumption has been adopted in a HIDiC model by Huang et al. [60] and Liu et al. [92], which has been applied for both static and dynamic applications. The models of Huang et al. and Liu et al. require constant pressures in the two column sections and ideal mixtures, but these models have proven useful in dynamic simulations and optimisation due to the low computational efforts required. However, the models of Huang et al. [60] and Liu et al. [92] do not take liquid and vapour hydraulics into account. In conventional distillation columns, vapour dynamics are usually fast and have a minor impact on the overall distillation column performance. However, the liquid hydraulics are important, as propagations of changes in the top of a real distillation column do not affect the bottom immediately [147]. Because internal heat transfer causes local pressure changes, it can be argued that both liquid and vapour hydraulics should be accounted for in the dynamic modelling of the HIDiC. The expression for linearised tray liquid hydraulics [151] was adopted by Zheng et al. [172] for a HIDiC, while the Franscis weir formula is more common (used by e.g. Ho et al. [55]). Ho et al. [55] included pressure hydraulics in their HIDiC simulation study by modelling the propagation of pressures through each stage in the rectifying section as having first-order dynamics. However, the impact of the propagation of pressure changes in the stripping section was neglected in the study of Ho et al. [55]. The concept of first-order dynamics in the pressure dynamics is similar to that of the linearised tray liquid dynamics, but the pressure dynamics are occuring in a smaller time scale. For conventional distillation columns, the first-order dynamic approximation is typically adequate for describing the vapour dynamic responses [151]. Alternatively, the propagation of pressure in a HIDiC can be accounted for by correlating vapour flow rates through pressure gradients between column stages as Wang et al. [166]. For conventional distillation columns, a detailed dynamic model is presented by e.g. Gani, Cameron and Ruiz [42, 21, 133], and Gross et al. [46].

2.3.3 Conceptual Design

The transition from conventional to the heat-integrated distillation configurations result in a significantly higher number of design degrees of freedom. This leads to complicated design problems. The methods for their solution often require models for simulation. However, for binary mixtures, graphical design methods have been described. In order for heat-integrated distillation configurations to become in-

creasingly recognised as a feasible alternative to conventional configurations, finding a compromise between investment cost, operating cost and operability is essential.

Simulations of conventional distillation columns require specification of five variables:

- Operating pressure
- Total number of stages
- Feed location
- Reflux ratio
- Vapour boil-up ratio

A common way of selecting these variables is using the McCabe-Thiele or Ponchon-Savarit methods [54] for (pseudo)binary mixtures. The Fenske-Underwood-Gilliland method applies to both binary and multicomponent mixtures but is limited to ideal behaviours. These methods require specifications of the feed, the operating pressure, and typically two product purities.

Assuming internal heat integration takes place between pairs of stages, the HIDiC has additional degrees of freedom: The pressure ratio between the sections, the heat exchange area per pair, and the variables characterising the arrangement of heat integration between the stages. In equilibrium stage-based distillation column models, the assignment of heat-integrated stages contribute as additional discrete variables to the existing discrete design variables, namely the number of stages and the feed stage location. A complex combinatorial problem is resulted, which has many alternative designs. It has been demonstrated that the pairing of heat-integrated stages is crucial in obtaining an economically feasible HIDiC design [158, 154]. This comprises a significant challenge to the HIDiC design because it is not always recommended to pair all possible stages [23, 142, 51].

Approaches that do not rely on mathematical optimisation, commonly assume uniform heat exchange areas or uniform heat duties throughout the heat-integrated stages. However, optimal arrangements often involve non-uniform heat exchange areas as well as non-uniform internal heat duties [155]. The optimum pressure ratio differs little from the one required to obtain a minimum temperature driving force between the paired stages [155].

Graphical design approaches for the HIDiC has been the focus of several works. Takamatsu et al. [156] developed a stepping procedure resembling McCabe-Thiele

constructions. Nakanishi et al. [118] proposed a relation between the minimum reflux ratio and the total heat exchange area for evaluation of the separation feasibility. Ho et al. [56] extended the Ponchon-Savarit graphical method to demonstrate binary HIDiC design by the use of enthalpy-composition-diagrams (*hxy*-diagram). By specifying the column section pressures and the amount of internal heat transfer, constructions can be established in a fashion resembling that of a conventional column design, leading to the required number of stages and feed stage location. From these, the compressor duty and reboiler duty can be estimated, and the required heat exchange area can be calculated. Due to the simplicity of this method, a constant heat duty on every pair (decision variable) is assumed and no suggestions for the pairing of the stages for internal heat integration are provided. Later, the Ponchon-Savarit method was slightly adjusted and a graphical tool was introduced [159], called reversible distillation curves (RDCs). The RDCs were incorporated in the *hxy*-diagram to guide the identification of thermodynamically preferred heat-integrated stages. The extended Ponchon-Savarit method requires specifications of the total number of stages, reboiler duty, the compressor duty, and the number of heat-integrated stages, inspired by a corresponding design of a conventional column.

The discrete nature of the design problem has been tackled by reducing the mixed integer non-linear mathematical programming (MINLP) problem into a continuous formulation by Harwardt and Marquardt [51]. The solution strategy for this NLP is based on a superstructure optimisation approach to determine the optimal number of stages and the position and the heat transfer areas of internal heat exchangers for both column sections. Solutions with the total annualised cost (TAC) and the total energy consumption as objective functions were presented. The advantage of using a mathematical formulation of the problem is the flexibility of being able to impose e.g. physical constraints on the optimisation variables. The MINLP was solved by Shahandeh et al. [140] by using a genetic algorithm and innovative decision variables called "the layout numbers". Furthermore, a method with an integrated Boltzmann Estimation of Distribution Algorithm was adopted by Gutierrez-Guerra et al. [47] in order to solve the design problem as an optimisation problem. Provided the simulation tools are accessible, these mathematical programming-based methods can give relatively fast optimal CDiC, HIDiC, SRVC or MVRC design solutions. However, due to the high degree of non-linearity imposed by e.g. thermodynamic relations, the extensive number of discrete variables, and the overall magnitude of the design problem of HIDiC configurations, advanced and robust solution procedures are required. Optimal solutions in simulation studies agree that the internal heat exchange areas should be focused in the top of the

rectifying section (near conventional cold utility) and in the bottom of the stripping section (near conventional hot utility) [51, 140, 47].

After specifying the heat-integrated stages, it has been proposed by Chen et al. [23] and Gadalla [41] to reduce the number of heat-integrated stages taking the ideal HIDiC as a reference. The design of the ideal HIDiC is in both cases based on iterative algorithms requiring experience-based decisions on e.g. compression ratio and pairing. Chen et al. [23] proposed an iterative algorithm requiring the designer to specify the desired number of heat-integrated pairs (three by default) and then modifying their locations by sensitivity analysis of a specified objective function. Gadalla [41], on the other hand, propose to eliminate the pairs having the lowest temperature driving forces, i.e. the pinched stages considering the impact on a specified objective function. In addition, the method of Gadalla includes a hydraulic feasibility analysis step, which provides a means of quantifying the feasibility of different internal heat exchanger/column shell arrangements based on geometrical considerations.

For the simpler configuration with only external heat integration between the condenser and the reboiler as e.g. in the MVRC, a design procedure is proposed by e.g. Omideyi et al. [127]. The SRVC is a combination of internal heat integration from the HIDiC and external heat integration from the MVRC. Hence, the SRVC has two compressors and two throttling valves as indicated in Figure 2.4(b). Simulations indicated that larger energy and cost savings can be obtained for some separations in the SRVC compared to the HIDiC [31] and this type of heat integration was superior to a HIDiC with heat integration between reboiler and the condenser realised only by increased compression ratio [98].

As shown, the topic of design of heat-integrated distillation columns, particular HIDiC, has been addressed by various methods. The methods can be resolved into three classes, as reported in Table 2.4 together with literature examples and pros and cons. Due to the significantly increased degrees of freedom, most methods have design decisions that require insights in the performance of the considered configuration. In the graphical design methods, most design decisions are extensive variables (duties or flows), which might lead to infeasible designs. For example, the compressor duty in the extended Ponchon-Savarit method must be specified prior to knowing the actual feasible temperature gradients for internal heat transfer. In the simulation-based approaches, column profiles are available at each iteration step, and thus decisions can be taken as the design gradually arises. Also the mathematical programming methods can cope with this. However, the solution algorithms are tailored to the considered systems and the associated assumptions/simplifications.

Table 2.4. Design methods overview with their pros and cons.

Class	Method and, reference	Pros	Cons
Graphical	• McCabe-Thiele [156] • Ponchon-Savarit [56] • Extended Ponchon-Savarit [159]	• Intuitive • Balance equations are solved graphically	• Limited to (pseudo)binary mixtures (2D representations) • Risk of infeasible design • Decision variables directly related to energy or mass balances (flows or duties)
Mathematical Programming	• Superstructure optimisation [51] • Genetic Algorithm [140] • BUMDA Algorithm [47]	• Generic and flexible cost function and constraints • Multicomponent mixtures	• Requires full model implementation • Convergence of non-linear problem • Appearance of flat and/or local minima
Simulation-based	• Simplified HIDiC [23] • Thermo-hydraulic Approach [41]	• Incremental design • Multicomponent mixtures	• Requires full model implementation • Convergence (without optimiser)

2.3.4 Equipment Design

The distillation equipment, which is affected by the introduction of internal heat integration in the HIDiC is discussed in this section. This covers the column internals and the possibilities for realising internal heat transfer inside the internals. Moreover, new equipment is introduced compared to conventional distillation. A compressor is required to realise internal heat transfer and a throttling valve is required to reduce the pressure of the liquid entering the low-pressure section from the high-pressure section. Details about the choice of e.g. compressor is rarely mentioned in the HIDiC literature. However, it has a consequence for the economic models. Therefore this subsection provide suggestions for suitable equipment for the HIDiC application.

2.3.4.1 Compressor

Two different groups of commercially available compressors are existing: Rotodynamic compressors and positive displacement compressors. The rotodynamic compressors have rotating parts, which translates motion into momentum in the gas particles and ultimately into pressure. As a result, the gas flow is continuous. The positive displacement compressors work, as the name implies, by directly increasing pressure by displacing gas volumes. Such compressors operate at fixed gas flow rate but high pressure differentials can be achieved. The two groups of compressors can further be divided into the following types [162]:

- Rotodynamic types:
  - Centrifugal compressor, producing radial discharge flow at a high flow rate and a compression ratio of up to 4.5.
  - Axial flow compressor, which can handle large flow rates and small compression ratios in the range of 1.2-1.5 (or up to 5-6.5 per machine consisting of several stages). Axial flow compressors have higher efficiencies than centrifugal compressors but their stable operation ranges are relatively narrow.
- Positive displacement types:
  - Reciprocating piston compressors operate at low gas flow rates and relative large compression ratios (up to 10).
  - Rotary compressors (screws, blades, lobes etc.), can boost the discharge pressures by up to 690 kPa thereby providing very large compression ratios for smaller throughput. Such compressors are typically used for vacuum services operating at high efficiencies around 80-95%.

The centrifugal/motor type compressor appears to be most suited type in distillation processes due to the high vapour capacity and the robustness under varying flow rates. A compression ratio limit of up to five should be sufficient for the HIDiC. Compression ratios above five are expected to become economically infeasible due to both high operation cost and high investment cost. Sulzer [49] reports that the compressor types turboblowers, radial turbo compressors, screw-type or axial compressors are used for heat pump-assisted distillation (e.g. MVRC and VCC applications). These are mainly rotodynamic type compressors.

The relevant models for the HIDiC application is the temperature change for a giving compression ratio and the required compressor duty. These can be modelled

by considering an ideal gas and by introducing an isentropic efficiency [162]. From thermodynamic analysis, the discharge temperature and the compression duty are:

$$T_{out} = T_{in}\left(1+\frac{1}{\eta_{is}}\left[\left(\frac{P_{out}}{P_{in}}\right)^{(k-1)/k}-1\right]\right) \tag{2.1}$$

$$E = \frac{1}{\eta_{is}}\left(\frac{k}{k-1}\right)RT_{in}\left[\left(\frac{P_{out}}{P_{in}}\right)^{(k-1)/k}-1\right] \tag{2.2}$$

$$k = \frac{C_P^V}{C_V^V} = \frac{C_P^V}{R-C_P^V} \tag{2.3}$$

where

$T_{out} =$ outlet (discharge) temperature [K]
$T_{in} =$ inlet temperature [K]
$E =$ work of compression [kW]
$\eta_{is} =$ isentropic effeciency (isentropic work divided by actual work) [-]
$P_{out} =$ outlet (discharge) pressure [kPa]
$P_{in} =$ inlet pressure [kPa]
$C_P^V =$ constant pressure heat capacity [$\mathrm{kJ\,mol^{-1}\,K^{-1}}$]
$C_V^V =$ constant volume heat capacity [$\mathrm{kJ\,mol^{-1}\,K^{-1}}$]
$R =$ universal gas constant [$\mathrm{kJ\,mol^{-1}\,K^{-1}}$]

Equations (2.1)-(2.2) are based on isentropic efficiencies and these equations typically appear in the HIDiC literature [112, 51]. However, the efficiency of a compressor is an empirically derived quantity and thus depends on the compressor layout/type. It is therefore believed that the precision loss related to the selection of a constant efficiency makes it unnecessary to account for vapour phase non-ideality. In modelling, Eq. (2.2) is therefore found sufficient.

When it comes to operation of a compressor, Muhrer et al. [107] considered different operation modes of the compressor in an MVRC. They showed that a compressor variables speed mode and a mode, where the integrated heat exchange area was adjusted, were the best operation mode alternatives of the MVRC to compensate for disturbances. Hence, in dynamic modelling of a compressor, it is important to incorporate the compressor duty as a possible actuator variable, as it closely resembles the variable speed mode. A detailed dynamic model of a compressor is formulated by Jiang et al. [76]. They show that the compressor time constants are in the order of fractions of a second. Therefore, it is expected that the dynamics of a compressor, as an actuator, are unimportant in the dynamic simulations of e.g. the HIDiC.

2.3.4.2 Internal Heat Exchangers

Introducing heat transfer inside equipment, which conventionally is designed to provide mass transfer (separation) using phase contact, involves a risk of arriving at a trade-off between mass transfer and heat transfer efficiencies. In conventional heat exchangers, compact plate-and-fin heat exchangers can achieve specific heat exchange areas up to $1200\,m^2\,m^{-3}$ while shell-and-tube heat exchangers can achieve up to $300\,m^2\,m^{-3}$ [162]. When heat transfer is combined with mass transfer, approximate specific heat exchange areas from $1.9\,m^2\,m^{-3}$[58] and up to $52.7\,m^2\,m^{-3}$[19] have been reported (Table 2.3). Higher numbers are in practice difficult to achieve in distillation, since the liquid flow pattern is difficult to alter because gravity is the only driving force for the liquid flow. In conventional heat exchangers, baffles are being used in the shell side in order to effectively increase the possible contact area with the tube side. Note that the specific area is reported in heat exchange area per column volume. Alternatively this number could be reported per column area. However, in order to compare structured columns with tray columns, the third dimension (height) is important due to physical limitations in the different internals layout.

Table 2.5 reports the encountered arrangement suggestions for realising internal heat integration in distillation. The arrangements can be classified in dividing wall arrangement, which is suited for both tray columns and packed columns, and the partitioning wall arrangement, which can only be employed with packed columns. However, as the Table 2.5 clearly shows, most attention has been paid to the concentric column and the shell-and-tube arrangements, both inspired by the conventional shell-and-tube heat exchangers. As heat exchange takes place in the height of the column, gradual condensation and vaporisation occurs inside the column. Hence, the ideal diameter varies along the column height. For the concentric arrangement, this corresponds e.g. to an inner rectifying section with a diameter, which is small in the top and increases towards the bottom. In practice, the construction of such tubes is particularly challenging [109], but this challenge has been overcome more recently [170]. A simpler arrangement, yet effective, is the structured plate column arrangement proposed by Bruinsma et al. [19]. This arrangement has the highest reported specific heat transfer area among the experimental columns.

If the tube walls do not provide sufficient heat transfer area, heat panels can be installed inside the trays [27, 28]. Gadalla et al. [37] used geometrical considerations to propose relations of maximum achievable internal heat transfer area when including heat panels for a concentric arrangement based on the column dimensions. These relations are described in detail in Section 3.4.3, as they are used to evaluate the feasibility of conceptual HIDiC designs.

The challenge in achieving a sufficient heat exchanger area can be overcome in the separate columns type (Table 2.5). One way of realising this arrangement is to withdraw liquid from the holdup of one tray in the high-pressure column and let it exchange heat with the holdup of a tray in the low-pressure column. This can be done using a conventional heat exchanger located outside both columns or inside in either of the columns. The latter option has been patented by Wakabayashi and Nakao [161], in which stabbed-in type heat exchangers were inserted in the trays of the high-pressure section. However, the application of stabbed-in type heat exchangers is limited to cases, where only a few trays are heat integrated. De Koijer et al. [25] presented an alternative to the stabbed-in type heat exchanger, which is suitable for sieve trays. This alternative consisted of coils, hanging slightly above the tray, containing a cooling media. This configurations corresponds to the DSHE but the principle can also be transferred to the HIDiC configuration.

A trend in the layout of the experimental HIDiC studies is the small employed diameter-to-height ratios (heights and diameters are reported individually in Table 2.3). Consider for example the tallest reported packed HIDiC with a height of 27.000 mm and a diameter of 1.400 mm resulting in a diameter-to-height ratio of 0.05. None of the reported experimental experiences concern industrial-scale equipment, in which only the dividing wall constitutes the heat exchange area (Table 2.3). This comprises an issue when evaluating the technical feasibility of the HIDiC, as the achievable heat transfer area, in many cases, decreases with increasing column diameter. The specific heat exchange area for example a shell-and-tube arrangement is given by:

$$\Phi = \frac{N_{tubes}\pi d_i H}{\pi d_o^2 H/4} = \frac{4N_{tubes}d_i}{d_o^2} \tag{2.4}$$

where

$\Phi =$ specific heat transfer area (heat exchange area per column volume) [$m^2\,m^{-3}$]
$N_{tubes} =$ number of tubers inside the column shell [-]
$d_i =$ inner (tube) diameter [m]
$d_o =$ outer (shell) diameter [m]
$H =$ height of control volume [m]

In a conventional distillation column, the required tray cross sectional area typically scales linearly with the internal vapour flow rate, which scales linearly with the feed flow rate (throughput). In order to maintain the same internal heat transfer rate during scale-up, provided that the temperature driving force remain constant, the specific heat exchange area must remain constant. This means that the heat exchange area must be proportional to the feed flow rate. In the simple case of a

concentric arrangement ($N_{tubes} = 1$), the specific heat exchange area in Eq. (2.4) does not satisfy this requirement as argued in Illustration 2.1. By designing a distillation column with small diameter, the specific heat exchange area can be large. But in the bulk chemical industry, the conventional column areas can exceed 14 m in diameter and 100 m in elevation [153]. As heat panels inside a distillation column has proven efficient [28] for tray columns, such installations has not been encountered for packed columns.

A correlation between the overall heat transfer coefficient (U_{ihx}) and the compression ratio (CR) has proposed by Xu et al. [170]:

$$U_{ihx} = 4.139 - 4.154CR + 1.290CR^2 \text{ kW K}^{-1} \tag{2.5}$$

$CR =$ compression ratio [-]

Despite the fact that it is based on an ethanol/water mixture in a concentric packed column, the tendency of decreasing overall heat transfer coefficient with increasing compression ratio (or increasing temperature driving force) has been confirmed for tray columns elsewhere [27]. The appearing of dry spots on the heat exchange surface was believed to cause this decreasing trend, which might represent a significant challenge in industrial set-ups.

2.3.4.3 Column Internals

In conventional distillation columns, the phase contact between the liquid and the vapour is crucial for the separation performance. Different means of creating phase contact are:

- Tray/plate columns (sieve, valve or bubble-cap): The column is vertically divided in sub volumes called the trays, which makes accessibility and, thus, maintainance easy. The most common types are: Sieve trays, valve and bubble-cap trays. Some typical dimensions are [162]: Weir heights are 50.8 mm, weir lengths about 75% of tray diameter. Pressure drop per tray is of the order of 0.70 kPa. Sieve tray perforations are 6.35-12.7 mm diameter with hole area being 10% of the active cross section. Single-pass sieve and valve trays with crossflow are the most widely used trays [57].

- Packing (random or structured): These type of columns often has a high specific area for separation (contact area per column volume). They have low pressure drops and low holdups, and they are typically used for low column diameters, low pressures, or when proof materials are required. However, liquid maldistribution can be a limitation and the prices are typically higher than tray columns [162].

Table 2.5. Suggestions for realisation of internal heat exchangers. The table column "origin" refers to the literature, in which the arrangement was proposed.

Class	Cross section	Type	References	
			Origin	Experimental
Dividing wall		Separate columns	[52, 117, 161]	[25, 121]
	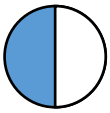	Partitioning wall column	[138, 75]	
		Concentric column	[45, 24]	[28, 66, 81, 170, 81, 122] [132]*
Partitioning wall		Multiconcentric column	[124]	
	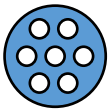	Shell-and-tube column	[7]	[109, 123, 66, 58]
		Structured plate column	[4]	[19]
Single tower		Alternating trays	[71]	

* Simulated experiments using computational fluid dynamics

The question remains, how does the introduction of internal heat exchangers affect the separation and what is possible in conventional equipment? The answers depend on many factors such as how much heat transfer area is required and what is the column cross sectional area etc. It has been found that heat panels lead to a slightly increased tray separation efficiency (10%), which could be due to the hindrance of backmixing of the froth [28]. Furthermore, the pressure drops in the concentric sieve trays are independent of the presence of heat panels [27].

For packed columns, a decrease in the separation efficiency in the outer column (concentric arrangement) is observed [170]. This decrease is separation efficiency is believed to be caused by liquid accumulation (maldistribution) near the inner col-

umn wall due to its increasing diameter towards the bottom. In the structured plate arrangement, also no significant impact on the separation efficiency was observed for neither stripping nor rectifying operations [19].

2.3.5 Benchmark Studies

Various studies concern benchmarking of the HIDiC but the overall conclusion are often contradictory due to numerical dissimilarities (in e.g. overall heat transfer coefficients and utility prices) and different basis of comparisons.This was for example discussed in relation to the achievable heat exchange area in section 2.3.4.2.

The steady state performances of simulation and experimental studies of the HIDiC compared to the CDiC are summarised in Table 2.6 based on a variety of literature sources. Since the internal heat transfer is a key element in such studies, the parameters related to this, namely the internal heat exchange area(s) and the overall heat transfer coefficient(s), are reported along with the simulation results (if stated).

Illustration 2.1. Dependence of specific area on column diameter in the concentric arrangements.
Consider a larger and a smaller concentric HIDiC with trays of the dimensions given in the below:

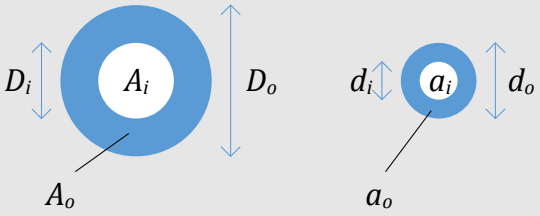

Assume that the required active area of a tray is proportional to the vapour flow, that the molar vapour flows are identical in each of the sections (inner and outer tube) and that the temperatures are similar (applies to close-boiling component separations). If the HIDiC is operated at a compression ratio of two, which is a common value, then the density of the vapour in the inner tube is twice of that in the outer tube when considering ideal vapour phases. The ratio between the temperatures in the inner section and the outer section is approximately unity since small temperature driving forces are preferred for internal heat integration. Therefore the volumetric vapour flow in the outer tube is twice that of in the inner tube, and similarly the tray area of the outer tube is twice of that of the inner tube. This translates into

$$\begin{aligned} A_o = 2A_i,\ a_o = 2a_i \Rightarrow \\ D_o = \sqrt{2}D_i,\ d_o = \sqrt{2}d_i, \end{aligned}$$

which, when combining with Eq. (2.4), gives

$$\begin{aligned} \Phi|_{D_o=5\,\mathrm{m}} &= 2/D_o = 0.4\,\mathrm{m}^2\,\mathrm{m}^{-3} \\ \Phi|_{d_o=0.5\,\mathrm{m}} &= 2/d_o = 4\,\mathrm{m}^2\,\mathrm{m}^{-3} \end{aligned}$$

Hence, the smaller column has a larger available, specific heat exchange area. Provided the given assumptions apply, the ratio of the specific heat transfer areas scales linearly with the ratios of the outer column diameters.

Table 2.6. Benchmarking of the HIDiC. Symbols: A_{ihx} is the heat exchange area per stage, U_{ihx} is the overall heat transfer coefficient. In some cases, only the product $U_{ihx}A$ is supplied. The energy and economic savings are reported with reference to a CDiC performing the same separation; positive savings are in favour of the HIDiC. Electrical energy is weighted by a factor of three for estimating the total energy consumption in the HIDiC.

System	Parameters		Savings		Ref.
	Design parameters	U_{ihx} [$\mathrm{kW\,m^2\,K^{-1}}$]	Energy	Economy	
Binary mixtures					
Benzene/toluene	$UA = 10.0 - 23.0\,\mathrm{kW\,K^{-1}}$		40%	-	[114]
	-	-	40%	-	[109]
	$A = 20\,\mathrm{m^2}$	>0.800	35%	-	[118]
*	-	-	40%	-	[66]
	$\sum A = 229.7\,\mathrm{m^2}$	-	-	-45%	[139]
	Optimal design	-	-	-11%	[51]
Acetic acid/acetic anhydride	$A = 270 - 1000\,\mathrm{m^2}$ / $A = 50 - 420\,\mathrm{m^2}$	0.6	4%	-	[22]
Propylene/propane	$A = 399\,\mathrm{m^2}$ / $A = 779\,\mathrm{m^2}$	1.0	-	35%	[125]
	$A = 400\,\mathrm{m^2}$	1.0	25% vs MVRC	20% vs MVRC	[158]
	$\sum A = 46.277\,\mathrm{m^2}$	-	-	35.6%	[139]
	$A = 18.58\,\mathrm{m^2}$	0.5678	13%	-	[94]
Benzene/ fluorobenzene	Optimal design	-	-	44%	[51]

Continued on next page

Table 2.6 – continued from previous page

System	Parameters		Savings		Ref.
	Design parameters	U_{ihx} [$kW\,m^2\,K^{-1}$]	Energy	Economy	
Benzene/ chlorobenzene	Optimal design	-	-	-17%	[51]
Benzene/n-heptane	Optimal design	-	-	46%	[51]
Cyclohexane/n-heptane*	$A = 21\,m^2$ (given $53\,m^2\,m^{-3}$ and HETP)	0.3-0.5	65%	40%	[19]
Ethylene/ethane	$A = 18.58\,m^2$	0.5678	-22%	-	[94]
Trans-2-butene/ cis-2-butene	$A = 18.58\,m^2$	0.5678	6%		[94]
Methanol/water	$A = 54991.4\,m^2$ (1 internal HEX)	0.8	56%	27.2%	[141]
Ethanol/water	Optimal design	-	38%	6%	[51]
*	0.09426	0.3249	-	-	[81]
Multicomponent mixtures					
Benzene/toluene/p-xylene	$U_{ihx}A = 0.5\,kW\,K^{-1}$	-	34%	-	[67]
n-pentane/cyclopentane/ 2-methylpentane	$UA = 0.9\,kW\,K^{-1}$	-	51%	-	[68]
Propane/n-butane/n-pentane	$U_{ihx}A = 6.33\,kW\,K^{-1}$	-	39%	2%	[84]
12 hydrocarbons*	-	-	52%		[67]
Styrene/benzene/toluene/ ethylbenzene	Optimal design	-	74%	37%	[51]

The utility prices comprise the basis of economic benchmarking. Utility prices vary with time and location because they depend on various factors such as availability, feedstock source, tax regulations, inflation and more. In fact, large installations often negotiate electricity price levels. Especially steam, produced in excess locally, will reduce the price significantly. The benchmark studies report different utility prices, which is illustrated in Table 2.7. In estimations of the operating costs of distillation column configurations with compressors, the ratio of electricity cost to steam cost is of utmost importance as the electricity usually is several times more expensive than steam. This ratio can bias a conclusion towards a particular configuration. For example, a high ratio favours a CDiC, while a low ratio potentially favours heat pump-assisted configurations (MVRC, HIDiC etc.). This ratio is provided in Table 2.7 along with utility prices and the references. It can be seen that the ratio varies from 1.8 and up to 23.3. Furthermore, this ratio is also commonly used to scale the relative contributions of the duties (reboiler duty and compressor duty) when reporting energy savings (Table 2.6). Hence, a consistent treatment of this ratio is essential in the benchmarking of distillation column configurations. Even in benchmarking studies, electrical energy weight factors from one to three are observed, which complicates direct comparisons of the reported energy savings. In Table 2.6, all duties were identified and converted into unified energy saving measures using a factor of three.

Ulrich and Vasudevan [157] provide correlations for estimating electricity, steam and cooling water prices based on the following expressions:

$$S_{\text{electricity}} = 1.3 \cdot 10^{-1}(\text{CR PCI}) + 0.010(S_{s,f}) \tag{2.6}$$

$$S_{\text{steam}} = 2.7 \cdot 10^{-5} m_{steam}^{-0.9}(\text{CR PCI}) + (0.0034 P_{steam}^{0.05})(S_{s,f}), \tag{2.7}$$

$$1 < P_{\text{steam}} < 46\,\text{barg},\ 0.06 < m_{\text{steam}} < 40\,\text{kg s}^{-1}$$

$$S_{\text{cw}} = (0.0001 + 3.0 \cdot 10^{-5} v_{\text{cw}}^{-1})(\text{CR PCI}) + 0.003(S_{s,f}), \tag{2.8}$$

$$0.01 < v_{\text{cw}} < 10\,\text{m}^3\,\text{s}^{-1}$$

Where

$S_{\text{electricity}} =$ electricity price [\$kWh^{-1}]
CR PCI= historical inflation parameter for projects in the U.S. [-]
$S_{s,f} =$ fuel price [\$GJ^{-1}]
$S_{\text{steam}} =$ steam price [\$kg^{-1}]
$m_{\text{steam}} =$ nominal steam production rate [kg s^{-1}]
$P_{\text{steam}} =$ steam pressure [barg]
$S_{\text{cw}} =$ cooling water price [\$m^{-3}]
$v_{\text{cw}} =$ nominal cooling water production rate [m^3 s^{-1}]

Table 2.7. Comparison of reported utility prices.

Utility prices				Ref.
Electricity, $\$\,kWh^{-1}$	Steam, $\$\,t^{-1}$	Cooling water, $\$\,t^{-1}$	Electricity/Steam price, -	
-	6.82	-	-	[137]
0.05	17.2	-	1.8	[8]
0.081	-	-	-	[23]
0.1	10.88	0.025	5.7	[32]
-	-	-	2.5	[44]
0.0739	22.19	0	2.1	[51]
0.084	17	0.06	3.0	[62]
-	25	0.06	-	[59]
0.084	17	0.06	3.0	[83]
0.0843	16.85	0.059	3.1	[111]
0.1	13	0.03	4.7	[158]
0.12	30		2.5	[160]
0.1	13	0.06	4.7	[171]
0.1	2.65	0.014	23.3	[9]
0.1	-	-	-	[3]
0.06	9.5	-	3.9	[30]
0.14*	23*	0.08*	3.8	[157]

* Estimated based on correlations provided by reference
Note: Conversion factors have been used to obtain comparable units. These are currency $1.1094\,\$\,euro^{-1}$, heat of vaporisation of steam $2220\,kJ\,kg^{-1}$, heat capacity cooling water $4.1813\,kJ\,kg^{-1}\,K^{-1}$, allowable temperature change of cooling water 5 K, and density of cooling water $1000\,kg\,m^{-3}$.

Later, during benchmarking in this work, the expressions in Eq. (2.6)-(2.8) have been employed for utility prices using the parameters $S_{s,f} = 4\,\$\,GJ^{-1}$, CR PCI = 584.6 [1] for 2012, $m_{\text{steam}} = 10\,kg\,s^{-1}$, $v_{\text{cw}} = 5\,m^3\,s^{-1}$, and pressure dependence in Eq. (2.7) preserved.

2.3.6 Operation

The operational aspect of the HIDiC is discussed in this section with emphasis on start-up, dynamics, and controllability. The general operation implications from process intensification (PI) are [119]:

- Increased operational complexity because of stronger interaction between the inputs.
- Fewer degrees of freedom.
- Increased sensitivity to disturbances.

- Narrower operating windows.

The dynamic implications of internal heat integration is described below.

2.3.6.1 Start-up

One crucial element of operating the HIDiC is its start-up procedure. Especially two observations must addressed; (i) a trim condenser and a trim reboiler are strictly necessary for start-up, and (ii) inverse heat transfer does not only lead to consumption of extra energy, but also risks of potential operation problems. A start-up procedure (Table 2.8) is devised and validated experimentally by [109]. Later a similar procedure was simulated by Wang et al. [166]. Feasibility of continuous

Table 2.8. Operation sequence for HIDiC start-up starting from cold and empty state [109].

Phase	Procedure as formulated by Naito et al. [109]
1	Liquid feed is introduced and propagates through the stripping section until reaching the bottom.
2	As the liquid holdup reaches a pre-specified value, heating is initiated. Vapour starts to move up the stripping section.
3	The compressor is started as the stripping section is filled.
4	As vapour moves through the rectifying section, pressure starts to build up. As the pressure reaches a pre-specified value, the condenser is started. Vapour is condensed in the top and the condensate accumulates in the reflux drum.
5	When the holdup in the reflux drum reaches a pre-specified value, total reflux operation is initiated.
6	When the flow rate of the overhead reaches a pre-specified value, distillate product is draw out and composition controllers are activated and the reboil rate is gradually decreased.
7	Continuous operation starts.

operation of the HIDiC has been documented for bench-scale experiment [109, 66] and in pilot plant [58]. Both former references report more than 100 hours of smooth, continuous operation for separation of hydrocarbons. The duration of the start-up phase of a bench-scale HIDiC separating $0.89\,\mathrm{mol\,s^{-1}}$ benzene/toluene was reported as 10 hours [109].

2.3.6.2 Dynamics

The ideal HIDiC was studied with respect to step changes in input variables (feed preheater and compression ratio) by Huang et al. [60]. The ideal HIDiC displays significant difference in positive and negative responses indicating a strong process

non-linearity. Furthermore, strong input-output interactions were found. The analysis was extended to cover dynamic responses of all feed flow rates, feed composition, feed thermal condition, section pressures, and heat exchange area per stage resulting in the same conclusion, i.e. strong non-linearity is present [92]. However, it was noticed that the ideal HIDiC is a self-balancing process. The process is self-balancing in the sense that effects of disturbances in the feed are reduced compared to conventional distillation columns. This can be illustrated by the example of increased feed flow rate. If the feed is composed of both liquid and vapour, the concentration of the heavy component increases in the rectifying section and decreases in the stripping section. This leads to increased internal heat transfer, which has the opposite effect of the composition responses.

Simulations showed that high purity HIDiC has slower responses and stronger non-linearity [173] leading to e.g. asymmetric and inverse composition responses. The inverse responses were concluded to be severe for responses in the top composition subject to changes in the feed thermal condition and thus, using the feed duty is manipulated variable is not recommended for feedback control [173]. A similar significant increase in the process non-linearity is also observed for conventional distillation [35]. Usually fast control action can reduce model mismatch by keeping the process operated close to the nominal operating point, where the effect of non-linearity is least.

Steady state multiplicity is well documented for the CDiC (e.g. Jacobsen and Skogestad [69]). Doherty and Perkins [29] report that no steady state multiplicity occurs for binary distillation in the case of constant molar overflow (CMO) assumption or in a ternary flash unit but only occur in ternary distillation. Multiple steady states are also reported for e.g. the VCC [90]. Furthermore, simulation results suggest that steady state multiplicity also occurs for the HIDiC [79]. The presence of steady state multiplicity depends on the HIDiC control structure and the operation policy and, in particular, strongly depends on the compressor operating policy. Hence, it is recommended to operate the compressor at a fixed duty or rotation speed rather than a fixed compression ratio [79, 96]. Alternatively, *DV* or *LB* control structures for composition control can be adopted for avoiding steady state multiplicity [165]. Later, Kano et al. [80] developed a graphical instability criteria for the HIDiC.

2.3.6.3 Controllability

Nakaiwa et al. [110] considered the general HIDiC with four variables controlled, namely the distillation composition, the bottoms composition, the reflux drum holdup and the reboiler holdup using single input-single-output (SISO) controllers

paired with four of the candidates $\mathbf{u} = [D, B, L_{cnd}, V_{rbl}, L_{cnd}/D, V_{rbl}/B, \Delta P, f_F]$. The reboil flow rate ($V_{rbl}$) is used instead of the reboiler duty (Q_{rbl}), the pressure elevation (ΔP) is used instead of the compressor duty (E), and the feed thermal condition (f_F) is used instead of feed preheater (Q_F). All stabilising control loops were assumed perfectly controlled and no further attention was paid to these. The present control problem has 70 possible solutions and it was solved by evaluating steady state control performance indices including the condition number (CN) and the relative gain array (RGA). The study showed that the feed preheater and the compressor are feasible candidates as manipulated variables for dual composition control. In addition, a conventional control scheme such as dual ratio control is feasible in the HIDiC. Closed-loop simulation showed that control schemes utilising f_F or ΔP have oscillatory servo and regulatory responses. This is not surprising as f_F has a direct impact on the overall mass balance on the column affecting both composition while ΔP also affects both compositions by only affecting the internal flows. Especially, the control schemes including f_F as a manipulated variable show strong interactive behaviour, as changes in external flows have significantly larger impact on compositions than internal flows [151]. It was shown that the operability of the HIDiC was more complicated than that of a CDiC due to diabatisation, while closed-loop simulations confirmed this analysis [36].

Various authors have investigated PI-controllers for composition control in the HIDiC and demonstrated stable operation by simulation of simple models [92, 173, 116, 174]. Huang et al. [63] used temperature to infer compositions and concluded that simple temperature control (STC) can not work as effectively as in conventional distillation columns. A similar temperature control scheme was adopted by Ho et al. [55] using a more rigorous model accounting for pressure dynamics with acceptable control performance.

2.4 Research Areas

Based on the presented literature review, the following topical conclusions related to the state-of-the-art research can be made:

- **Equipment design:** Centrifugal compressors are suitable for heat pump applications due to moderate compression ratios and high allowable throughput. Based on the required heat exchange areas, it appears that relatively large internal heat transfer areas are required. Therefore, focus should be directed towards experimental set-ups with more industrially relevant dimensions. In particular, the specific heat transfer area is relatively small for the majority of the experimental set-ups, which indicates that one tube in a concentric dis-

tillation column does not provide sufficient heat transfer area. Adding heat panels inside the column can significantly improve the specific heat transfer area without affecting the separation, but it has only been investigated in tray columns. In packed columns, the structured plate HIDiC can provide exceptional high specific heat exchange areas. This topic of equipment design not covered further in this work.

- **Modelling and parameters:** It appears that there is a mismatch in the reported dynamic simulation results. The literature related to dynamic modelling spans from simple models ignoring pressure dynamics and employ the "constant molal overflow" assumption, whereas other models address these simplifications to some extent. This leads to different conclusions when it comes to the controllability and the development of control structures for the HIDiC. One physical parameter of particular significance is the overall heat transfer coefficient. This has been found to depend on operation conditions and column arrangement. Based on reported literature values in Section 2.3.1, a value of $0.60\,\mathrm{kW\,m^{-2}\,K^{-1}}$ appears to be a representative value.

- **Conceptual design:** Many alternative design approaches exist. The different approaches are classified in graphical methods, simulation-based methods and mathematical programming-based methods. Different classes are suited for different applications depending on the modelling and simulation efforts. However, a common denominator of the described methods is that they all require expert decisions due to the large number of design degrees of freedom.

- **Controller design:** Followed by the conceptual design, a design of instrumentation and controllers is often followed. A formulation of the control structure and philosophy must be conducted and evaluated for models accounting for pressure dynamics, in particular. No literature has been encountered, which addresses the root of this problem, i.e. how to obtain a stabilising control structure in a systematic manner. After stable operation is ensured, additional control objectives can be investigated (purity control etc.). In addition, the stabilising control structure is of utmost importance in industrial context due to operational and safety concerns.

- **The HIDiC among alternatives:** It is clear that the HIDiC, in many applications, is an energy-wise and economically preferred alternative to conventional distillation. However, many authors includes only the conventional distillation column when benchmarking the HIDiC instead of including the simpler MVRC, which is already used in the industry. It has also been found,

that comparing results across references is essentially impossible, since the benchmark study conclusions are very case specific due to the significant variations in the economic parameters.

The present conclusions can be considered as a more detailed motivation for the research targeted in this thesis. The order of the presented conclusions, closely resembles the structure of the thesis in terms of the covered topics. However, the first topic of experimental validation is not covered in this thesis, as relevant set-ups have not been available.

Chapter 3

Distillation Column Model

A generic model of the conventional, the heat-integrated, the mechanical vapour recompression distillation columns, and related configurations, is presented. The solution procedure of the model is outlined and illustrated using examples.

The model is different from the existing literature for four reasons. The first reason relates to the way the compressor model is incorporated in relation to the dynamic energy balances. Second, the way pressure dynamics are accounted for, which is because of the former reason and the incorporation of a well-known expression for vapour flow through perforations. Third, the high degree of detail in the description of the trays, which enables investigation of entrainment flooding and weeping. And finally, the fact that the model is formulated in a generic framework, which is tailor-made for benchmarking of heat-integrated distillation column configurations. Thus, while many of the phenomena accounted for within the modelling framework have appeared before in other contexts, they have not been combined together in a consistent framework that puts things on suitable form for maximum utility. The BP method of Wang and Henke [163] for conventional distillation columns is extended here such that it can cover the considered heat-integrated distillation columns. An effective tear variable initialisation procedure was developed and provided along with the method documentation. Experience using an extended version of the BP method has been reported by Mah et al. [94].

However, it does not seem to have been documented in the open literature.

The main contribution of this chapter is published in an article [T. Bisgaard, J.K. Huusom, and J. Abildskov. Modeling and analysis of conventional and heat-integrated distillation columns. *AIChE Journal*, 61(12):4251–4263, 2015]. An early state of the model was published for the DYCOPS 2013 proceedings [T. Bisgaard, J.K. Huusom, and J. Abildskov. A modeling framework for conventional and heat integrated distillation columns. *10th IFAC International Symposium on Dynamics and Control of Process Systems – Mumbai, India*, pages 373–378, 2013].

3.1 Introduction

Three heat pump-assisted distillation column configurations has been targeted along with the conventional distillation column for modelling with the aim of providing a consistent basis for comparison. All four configurations are illustrated in Figure 3.1. One purpose of the model is to compare the performances of e.g. the HIDiC,

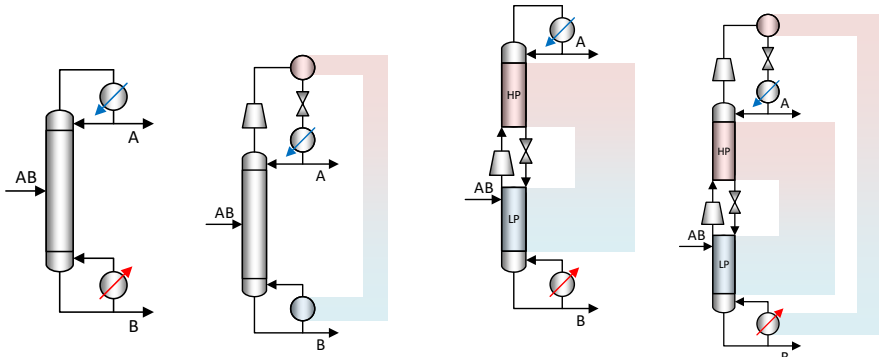

(a) Conventional distillation column (CDiC).

(b) Mechanical vapour recompression column (MVRC).

(c) The heat-integrated distillation column (HIDiC).

(d) Secondary reflux and vaporisation column (SRVC).

Figure 3.1. Conceptual illustrations of four configurations indicating conceptual similarities.

the MVRC, and the SRVC for the purpose of benchmarking. This is addressed in Chapter 5 based on static simulations and in Chapters 6 and 7 based on dynamic simulations.

The model is organised in such way that it can be used for both static and dynamic simulations while covering several heat-integrated distillation column configurations. Furthermore, the incorporation of pressure dynamics using dynamic energy balances comprises an additional improvement compared to previous dynamic HIDiC models (Section 2.3.2). The key features of the model are:

- Dynamic mass and energy balances.
- Temperature dependence of physical properties.
- Liquid phase non-ideality by activity coefficient models in static and dynamic formulations (possibility of liquid and vapour phase non-ideality for static formulation by incorporating equation of state models).

- Accounts for tray geometry.
- Dynamic tray pressures.
- Liquid and vapour hydraulics.
- Generic in the sense that it can cover various different heat-integrated distillation configurations (including the MVRC, the HIDiC, and the SRVC).

The presentation of the model is divided in conservation equations and constitutive equations. A section describing the proposed performance indicators is followed by the model equations. The implementation strategy of the model equations is presented in the final part of the chapter, where also the solution procedure and the simulation workflow are outlined. A model application example, followed by a discussion, concludes the chapter.

3.2 Conservation Equations

A supplementary list of symbols and abbreviations is located in the notation section in the very end of the thesis (page 251). The conservation equations are derived using the control volumes indicated in Figure 3.2 and cover both mass and energy balances. Individual mass and energy balances are presented for the two stage classifications: A mixing stage and a non-mixing stage.

The mixing stage is defined as a stage in which both a liquid phase and a vapour phase constitute the control volume. A mixing stage allows withdrawal of both phases and mixing of two entering counter-current flows (liquid and vapour flows). A tray, a condenser, and a reboiler are mixing stages, which are conventionally used in distillation column modelling. Equilibrium between the phases is assumed in a mixing stage. The condenser and the reboiler are special cases of mixing stages, as in most cases, no liquid enters the condenser and no vapour enters the reboiler.

In a non-mixing stage, the liquid and vapour phases are not mixed. In this context, a pseudo steady state is assumed for the liquid meaning that it is passed unchanged through the non-mixing stage. Hence, the control volume only covers the vapour holdup, which is present inside the compressor. A non-mixing stage is not at equilibrium.

Molar holdups are used as the state variables in the mass balances. The energy holdup derivatives in the energy balances are converted into temperature derivatives using chain rule algebra (Appendix B.2). In order to maintain a simple representation of the energy balances, these are presented as energy holdup derivatives.

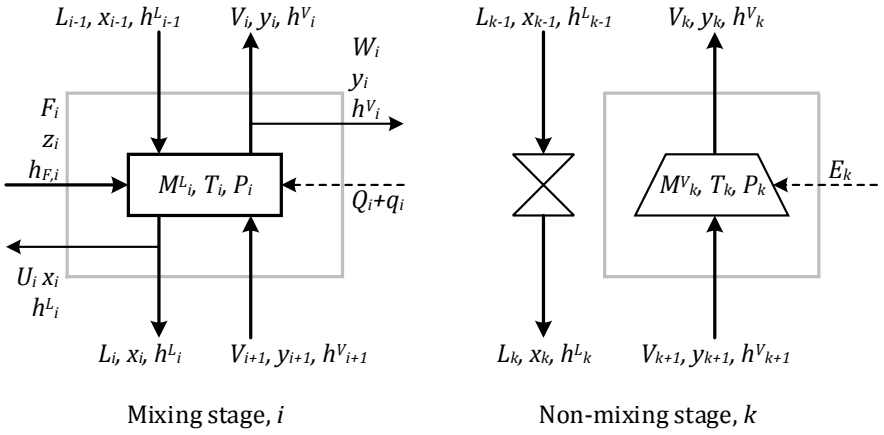

Figure 3.2. General representation of mixing and non-mixing distillation column stages with nomenclature. Mass transport is represented by solid lines and energy transport is represented by dashed lines. The gray contours represent control volumes.

3.2.1 Mixing Stage

Let $j = 1,2,\ldots,N_C$ denote a component in an N_C-component mixture. As no component specific relations are presented, the index j implicitly covers all components in an equation unless otherwise stated. Furthermore, let $i = 1,2,\ldots,N_S$ denote a column stage counted from the top including mixing stages (trays, condenser, reboiler) and non-mixing stages (compressor/valve) as indicated in Figure 3.2. Consider the subset $\mathbf{n}_{cpr} = [k(1),k(2),\ldots,k(N_{cpr})]$, where N_{cpr} is the number of compressors. Conservation of the mass of a mixing stage is expressed in moles for each component j:

$$\begin{aligned}\frac{d}{dt}(M_{i,j}) =& L_{i-1}x_{i-1,j} + V_{i+1}y_{i+1,j} + F_i z_{i,j} \\ &- (L_i + U_i)x_{i,j} - (V_i + W_i)y_{i,j}, \qquad i = \{1,2,...,N_S\} \notin \mathbf{n}_{cpr}\end{aligned} \tag{3.1}$$

where

$M_{i,j} =$ liquid the molar holdup [mol]
$L_i =$ liquid flow rate [$\mathrm{mol\,s^{-1}}$]
$U_i =$ liquid draw flow rate [$\mathrm{mol\,s^{-1}}$]
$x_{i,j} =$ liquid composition [-]
$V_i =$ vapour flow rate [$\mathrm{mol\,s^{-1}}$]
$W_i =$ vapour draw flow rate [$\mathrm{mol\,s^{-1}}$]

$y_{i,j} =$ vapour composition [-]
$F_i =$ feed flow rate [mol s^{-1}]
$z_{i,j} =$ feed composition [-]

Conservation of energy is expressed:

$$\frac{d}{dt}\left(M_{T,i}h_i^L\right) = L_{i-1}h_{i-1}^L + V_{i+1}h_{i+1}^V + F_i h_{F,i} + Q_i + q_i - \left(L_i + U_i\right)h_i^L - \left(V_i + W_i\right)h_i^V, \qquad i = \{1,2,...,N_S\} \notin \mathbf{n}_{cpr} \tag{3.2}$$

where

$M_{T,i} =$ total molar holdup [mol]
$h_i^L =$ liquid phase enthalpy [kJ mol^{-1}]
$h_i^V =$ vapour phase enthalpy [kJ mol^{-1}]
$Q_i =$ external heat transfer rate [kW]
$q_i =$ internal heat transfer rate [kW]

The left-hand side of Eq. (3.2) is a simplification of the total energy holdup by neglecting the vapour holdup and assuming incompressible liquid [146]:

$$\frac{d}{dt}\left(M_{T,i}^L u_i^L + M_{T,i}^V u_i^V\right) \approx \frac{d}{dt}\left(M_{T,i}^L h_i^L\right), \qquad M_{T,i}^V \approx 0, \quad u_i^L \approx h_i^L \tag{3.3}$$

where

$u_i =$ internal energy [kJ mol^{-1}]

This assumption is reasonable to the same extent as the ideal gas assumption. A numerical example is provided in Illustration 3.1 as motivation for this statement.

3.2.2 Non-mixing Stage

The assignment of $\mathbf{n}_{cpr}$ with $k \in \mathbf{n}_{cpr}$ depends upon the distillation configuration to be considered. An example of the assignment of $\mathbf{n}_{cpr}$ is given in Illustration 3.2. This variable allows the consideration of heat pump-assisted distillation columns with one or more compressors. A description of the assignment of $\mathbf{n}_{cpr}$ is provided in Section 3.5.

For a non-mixing stage, k, the total holdup dynamics are neglected. This applies to the valve and the compressor, where the total molar holdup is assumed constant, leading to the mass balances:

$$\frac{d}{dt}\left(y_{k,j}\right) = \frac{V_k}{M_{T,k}}(y_{k+1,j} - y_{k,j}), \qquad k \in \mathbf{n}_{cpr} \tag{3.4}$$
$$V_k = V_{k+1}$$

Illustration 3.1. Analysis of assumption related to negligible vapour holdup
Consider a distillation column tray with a weir height of 50 mm and tray spacing of 609.6 mm. Assuming that the total liquid height including the liquid over the weir is 1.2 times the weir height, the volume fraction of the liquid of a tray is $1.2 \cdot 50\,\text{mm}/609.6\,\text{mm} = 0.10$ corresponding to 10% of the tray volume. If the tray contains just one component (water and benzene considered), the molar fraction becomes:

$$x = \frac{0.10\rho^L/MW}{0.10\rho^L/MW + (1-0.10)\frac{P}{RT^{sat}(P)}}$$

Where ρ^L is the liquid density, MW is the molar mass, P is the pressure, R is the universal gas constant, and $T^{sat}(T)$ is the saturation temperature given by the Antoine equation.
The liquid molar fraction of water can thus be estimated for different values of the pressure (P):

	Liquid molar fraction, x	
P	Water	Benzene
kPa	-	
10	0.999	0.997
100	0.995	0.973
500	0.978	0.896
1000	0.959	0.823
1500	0.942	0.764

Since the application range of the ideal gas equation typically is 50-1000 kPa, it has been illustrated that the vapour molar holdup roughly contributes to less then 10% of the total holdup for $P \leq 500\,\text{kPa}$ and hence it is reasonable to neglect it. The employed parameters are provided below.
Water: $\rho^L = 1000\,\text{kg}\,\text{m}^{-3}$, MW =0.018 kg mol^{-1} and $T^{sat}(P) = 1810.94/(8.14019 - \log_{10}P) - 244.485$ expressed in Torr and °C.
Benzene: $\rho^L = 877\,\text{kg}\,\text{m}^{-3}$, $MW = 0.078\,\text{kg}\,\text{mol}^{-1}$, and $T^{sat}(P) = 1660.652/(4.72583 - \log_{10}P) + 1.461$ expressed in Torr and °C.

Note that Eq. (3.4) only applies to the compressor whereas the valve is at steady state:

$$\begin{aligned} x_{k,j} &= x_{k-1,j}, \qquad k \in \mathbf{n}_{cpr} \\ L_k &= L_{k-1} \end{aligned} \tag{3.5}$$

As a result of assuming constant holdup, the fast dynamics associated with transient

Illustration 3.2. Indexing for non-mixing stages.
Consider an SRVC with seven stages (i.e. $N_S = 7$) illustrated below.

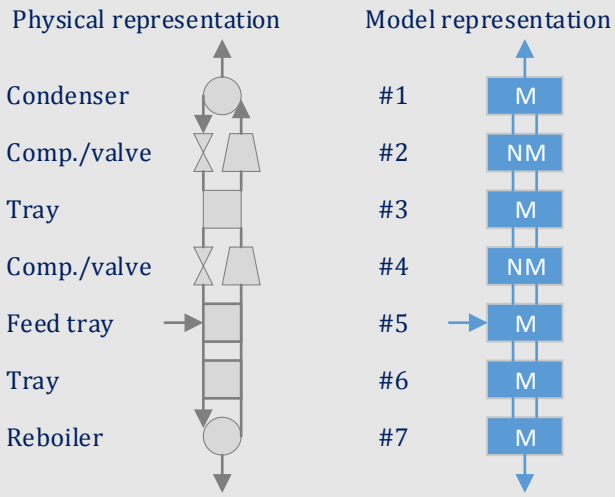

The condenser is stage #1, which is a mixing stage (M). Stage #2 is a non-mixing stage (NM) as it represent a compressor/valve. Stage #3 is a tray in the rectifying section. Stage #4 is also a non-mixing stage, while stage #5 is the feed tray and stage #6 is a tray, both in the stripping section. Stage #7 is the reboiler. This can be represented as $\mathbf{n}_{cpr} = [2,4]^T$ with $N_{cpr} = 2$.

vapour densities of the inlet and outlet flow rates are ignored. Dynamic simulations of a centrifugal compressor [76] support this assumption.

Conservation of energy gives:

$$\frac{d}{dt}(u_k^V) = \frac{V_k}{M_{T,k}}\left[h_{k+1}^V - h_k^V + \frac{E_k}{V_k}\right], \qquad k \in \mathbf{n}_{cpr} \tag{3.6}$$
$$h_k^L = h_{k-1}^L$$

where

$E_k =$ power input to the compressor [kW]

Throttling is assumed isenthalpic and the compression is assumed dry, i.e. no condensation occurs. For the vapour phase holdup, the internal energy must be applied, which is related to the enthalpy through the definition, $u = h - Pv$, where v is the molar volume.Note that the internal energy is given in Eq. (3.6) since the

vapour phase is considered. Hence, this must be accounted for when expressing the equation in terms of temperature derivatives (see derivation in Appendix B).

3.3 Constitutive Equations

This section presents a default set of constitutive equations that can be replaced according to application as various pure component (heat capacity, vapour pressure etc.) and mixture (activity coefficient models, fugacity coefficient models) relations are available.

3.3.1 Vapour-Liquid Equilibrium

The vapour-liquid equilibrium (VLE) is modelled using two approaches, the $(\gamma-\phi)$-approach and the $(\phi-\phi)$-approach. In the $(\gamma-\phi)$-approach, non-ideal liquid and ideal vapour phases are considered, leading to the modified Raoult's law. For the $(\phi-\phi)$-approach, non-ideal liquid and vapour phases are considered. In both approaches, a negligible contribution from the Poynting correction is assumed resulting in the following VLE condition:

$$y_{i,j} = \begin{cases} \dfrac{\gamma_{i,j} P^{sat}_{i,j}}{P_i} x_{i,j} & (\gamma-\phi)-\text{approach} \\ \dfrac{\phi^V_{i,j}}{\phi^L_{i,j}} x_{i,j} & (\phi-\phi)-\text{approach} \end{cases} \tag{3.7}$$

where

$\gamma_{i,j} =$ liquid phase activity coefficient of component j at stage i [-]
$P^{sat}_{i,j}$ liquid phase component saturation pressure [kPa]
$P_i =$ stage pressure [kPa]
$\phi^V_{i,j} =$ vapour phase fugacity coefficient [-]
$\phi^L_{i,j} =$ liquid phase fugacity coefficient [-]

The employed thermodynamic model(s) should be chosen carefully depending on the system, and its prediction of the liquid phase stability should be tested if relevant [152].

The vapour pressure of component j in the liquid on stage i is in this work calculated by the DIPPR 101 correlation:

$$P^{sat}_{i,j} = \exp\left[A_j + B_j T_i^{-1} + C_j \ln(T_i) + D_j T_i^{E_j}\right] \tag{3.8}$$

where

$A_j, B_j, C_j, D_j, E_j =$ pure component parameters
$T_i =$ stage i temperature [K]

Finally, in the case of an ideal vapour phase, the pressure can be calculated by a bubble pressure calculation, derived from Eq. (3.7):

$$P_i = \sum_{j=1}^{N_C} x_{i,j}\gamma_{i,j}P_{i,j}^{sat} \tag{3.9}$$

For non-ideal vapour phases, the pressure can not be expressed explicitly.

3.3.2 State Functions

The calculations of the state functions are based on a pure gas reference state at 298.15 K and 101.325 kPa. An illustration of the path is provided in Table 3.1. The ideal gas heat capacity form has been adopted from the DIPPR 107 correlation:

$$c_{P,i,j}^{V} = A_j + B_j\left(\frac{C_j}{T_i\sinh\left(C_j/T_i\right)}\right)^2 + D_j\left(\frac{E_j}{T_i\cosh\left(E_j/T_i\right)}\right)^2 \tag{3.10}$$

$$c_{P,i,j}^{L} = c_{P,i,j}^{V} - \frac{d}{dT}\left(\Delta h_{vap,i,j}\right) \tag{3.11}$$

where

$c_{P,i,j}^{L} =$ constant pressure heat capacity of liquid [kJ mol^{-1} K^{-1}]
$c_{P,i,j}^{V} =$ constant pressure heat capacity of vapour [kJ mol^{-1} K^{-1}]
$\Delta h_{vap,i,j} =$ heat of vaporisation [kJ mol^{-1}]

The ideal gas vapour enthalpy is expressed relative to its value at a reference, T_{ref}:

$$h_{i,j}^{V} = h_{ref,j}^{\circ} + \int_{T=T_{ref}}^{T_i} c_{P,i,j}^{V}\,dT \tag{3.12}$$

$$h_i^{V} = \sum_{j=1}^{N_C} y_{i,j}h_{i,j}^{V} \tag{3.13}$$

where

$A_j, B_j, C_j, D_j, E_j =$ pure component parameters

The heat of vaporisation of component j is given by the DIPPR 106 correlation:

$$\Delta h_{vap,i,j} = A_j(1 - T_{r,i,j})^{B_j + C_j T_{r,i,j} + D_j T_{r,i,j}^2} \tag{3.14}$$

$$T_{r,i,j} = T_i / T_{c,j} \tag{3.15}$$

where

$A_j, B_j, C_j, D_j =$ pure component parameters
$T_{c,j} =$ critical temperature of a component [K]
$T_{r,i,j} =$ reduced temperature [-]

The liquid enthalpy is obtained from the following expression:

$$h_{i,j}^{L} = h_{i,j}^{V} - \Delta h_{vap,i,j} \tag{3.16}$$

$$h_{i}^{L} = \sum_{j=1}^{N_C} x_{i,j} h_{i,j}^{L} \tag{3.17}$$

The excess enthalpy contribution of non-ideal liquid mixtures has been ignored since models may not be sufficiently accurate and thus little advantage exists in including the term. The significance of including the excess enthalpy contribution has been investigated by Fredenslund et al. [33] and a deviation in the total flow rates of 3-5% was observed.

The entropy of the vapour phase (s^V) is given by that of an ideal gas:

$$s_{i,j}^{V} = s_{ref,j}^{\circ} + \int_{T=T_{ref}}^{T_i} \left(c_{P,i,j}^{V}/T \right) dT - R \ln \left(P_i/P_{ref} \right) \tag{3.18}$$

$$s_{i}^{V} = \sum_{j=1}^{N_C} y_{i,j} s_{i,j}^{V} - R \sum_{j=1}^{N_C} y_{i,j} \ln y_{i,j} \tag{3.19}$$

where

$R =$ universal gas constant [$\mathrm{kJ\,mol^{-1}\,K^{-1}}$]

Since the tray temperature is equal to the bubble temperature, the liquid entropy is:

$$s_{i,j}^{L} = s_{i,j}^{V} - \Delta h_{vap,i,j}/T_i \tag{3.20}$$

$$s_{i}^{L} = \sum_{j=1}^{N_C} x_{i,j} s_{i,j}^{L} - R \sum_{j=1}^{N_C} x_{i,j} \ln x_{i,j} \tag{3.21}$$

The contribution of non-ideality on the entropy has been neglected for the same reason as the enthalpy.

3.3.3 Miscellaneous Equations

The following definitions are used for respectively the liquid mole fraction and the total stage holdup:

$$x_{i,j} = M_{i,j}/M_{T,i} \tag{3.22}$$

$$M_{T,i} = \sum_{j=1}^{N_C} M_{i,j} \tag{3.23}$$

Table 3.1. Paths for state functions starting from reference condition (T_{ref}, P_{ref}) of pure substances $\mathbf{x}^0$. The mixtures are considered ideal.

Path	State	Conditions	Enthalpy	Entropy
Start	Gas, elements	$T_{ref}, P_{ref}, \mathbf{x}^0$	h^0_{ref}	s^0_{ref}
Isobaric change	Gas, pure	$T, P_{ref}, \mathbf{x}^0$	$\int_{t=T_{ref}}^{T} c^V_{P,j} dt$	$\int_{t=T_{ref}}^{T} \frac{c^V_{P,j}}{t} dt$
Isothermal change P	Gas, pure	$T, P, \mathbf{x}^0$	0	$-R \ln \frac{P}{P_{ref}}$
Optional: Condense at T, P	Liquid, pure	$T, P, \mathbf{x}^0$	Δh_{vap}	$-\frac{\Delta h_{vap}}{T}$
Isothermal and isobaric mixing	Liquid or vapour mixture	$T, P, \mathbf{x}$	0	$-R \sum_j x_j \ln x_j$

Average molecular weights (MW_i) of the liquid and vapour phases can be calculated from those of the pure components, as follows:

$$MW_i^L = \sum_{j=1}^{N_C} x_{i,j} MW_j \tag{3.24}$$

$$MW_i^V = \sum_{j=1}^{N_C} y_{i,j} MW_j \tag{3.25}$$

The pure component liquid density is calculated from the DIPPR 105 correlation:

$$\rho^L_{i,j} = \frac{MW_j A_j}{B_j^{1+(1-T_i/C_j)^{D_j}}} \tag{3.26}$$

The liquid mixture density (ρ_i^L) is approximated by the ideal expression by assuming no excess volume:

$$\rho_i^L = MW_i \left(\sum_{j=1}^{N_C} x_{i,j} MW_{i,j} / \rho^L_{i,j} \right)^{-1} \tag{3.27}$$

Vapour density can be calculated based on the ideal gas expression:

$$\rho_i^V = \frac{MW_i^V P_i}{Z_i^V R T_i} \tag{3.28}$$

where

$Z_i^V =$ compressibility factor [-]

According to its definition, $Z_i^V = 1$ for ideal gases.

3.3.4 Internal Heat Transfer

A pair of heat-integrated stages describes the link, which enables heat transfer between two stages in a column.Consider a column with a total of N_{ihx} internally

heat-integrated pairs, corresponding to $2N_{ihx}$ heat-integrated stages in the column. A pair of heat-integrated stages, n, can be represented mathematically as a heat source stage ($r(n)$) being paired with a heat sink stage ($s(n)$). This representation of the pairing enables a description of complex heat integration arrangements, including e.g. a heat source stage being paired with multiple heat sink stages [160] or a few stages being paired, which are not in the same vertical height [23, 51]. The application of the pair description is shown in Illustration 3.3.

Let $n = 1,2,\ldots,N_{ihx}$, denote the n'th pair of heat-integrated stages $r(n)$ and $s(n)$. The heat transfer rate due to heat integration is given by Eq. (3.29):

$$\begin{aligned} q_{s(n)} &= U_{ihx}A_{ihx,n}(T_{r(n)} - T_{s(n)}), \quad n = 1,2,\ldots N_{ihx} \\ q_{r(n)} &= -q_{s(n)} \\ q_i &= 0, \quad i \neq n \end{aligned} \tag{3.29}$$

where

$U_{ihx} =$ overall heat transfer coefficient [$\mathrm{kW\,m^{-2}\,K^{-1}}$]

$A_{ihx,n} =$ internal heat transfer area [$\mathrm{m^2}$]

The relations between $r(n)$ and $s(n)$ and n can be specified as a matrix on the form $\mathbf{n}_{ihx} \in \mathbf{Z}^{N_{ihx}\times 2}$ where $r(n)$ is the first column element in row $\mathbf{n}_{ihx}$, $s(n)$ is the second column element in row $\mathbf{n}_{ihx}$, and $\mathbf{Z}$ denote the natural numbers (positive integers). An illustration of the indices is provided in Illustration 3.3.

3.3.5 Non-mixing Stage Relations

The non-mixing stage accounts for the compressor/valve stage. The mass and energy dynamics for the compressor are described in Eq. (3.4)-(3.6), whereas the throttling is assumed adiabatic and at steady state. The throttled liquid is considered as superheated until it reaches the stage below. Hence, the following applies to the liquid phase of the non-mixing stage:

$$c_k^L = c_{k-1}^L \tag{3.30}$$

$$MW_k^L = MW_{k-1}^L \tag{3.31}$$

$$\rho_k^L = \rho_{k-1}^L \tag{3.32}$$

The pressure of the compressor outlet is related to that of the inlet, by the following simplified expression resulting from an isentropic balance for ideal gases (Eq. (2.1)):

$$P_k = P_{k+1}\left[\eta_{is}\left(\frac{T_k}{T_{k+1}} - 1\right) + 1\right]^{\kappa_k/(\kappa_k - 1)} \tag{3.33}$$

where

Illustration 3.3. Indexing for internal heat transfer.
Consider the HIDiC with four heat-integrated stages realised by installing stabbed-in type heat exchangers into the stripping section by Wakabayashi and Hasebe [160]. The column separates a multicomponent mixture of mainly C8 and C9 aromatics. This design has 30 stages in the rectifying section and 25 stages in the stripping section. In this work, the condenser in the top, the compressor above the feed stage, and the reboiler in the bottom are counted as stages and therefore 58 stages constitutes the HIDiC. According to the notation in this work, the heat integration takes place between stages #2-#37, #2-#47, #7-#54, and #23-#57 corresponding to R1-S5, R1-S15, R6-S22, and R22-S25 where the R refers to a tray in the rectifying section and S refer to the tray in the stripping section. According to the suggested notation the paring can be described by

$$\mathbf{n}_{ihx} = \begin{bmatrix} r(1) & s(1) \\ r(2) & s(2) \\ r(3) & s(3) \\ r(4) & s(4) \end{bmatrix} = \begin{bmatrix} 2 & 37 \\ 2 & 47 \\ 7 & 54 \\ 23 & 57 \end{bmatrix}.$$

By adopting this representation, the model offers a great flexibility of covering many types of heat integration such as internal as well as external, and even condenser/reboiler type integration as these are counted as stages as well.

$\eta_{is} =$ isentropic efficiency of compression [-]

$\kappa_k =$ isentropic expansion factor, which is given by the ratio of constant pressure and constant volume heat capacities [-]

For ideal gasses, the isentropic expansion factor is:

$$\kappa_k = \frac{c^V_{P,k}}{c^V_{V,k}} = \frac{c^V_{P,k}}{c^V_{P,k} - R} \tag{3.34}$$

Despite the fact that the constant pressure heat capacity is assumed constant in the derivation of Eq. (3.33)-(3.34), the temperature dependency is still considered according to Eq. (3.10).

3.3.6 Tray Hydraulics

The liquid and vapour flow rates must be expressed as functions of the state variables. In a tray column, liquid is entering a tray from the downcomer and leaving by flowing over the weir. The liquid flow rate can be described by the Francis weir

formula, which states [168]:

$$L_i = \begin{cases} \dfrac{C_i^L \rho_i^L H_{oW,i}^{3/2}}{MW_i^L}, & H_{oW,i} > 0 \\ 0, & H_{oW,i} \leq 0 \end{cases} \tag{3.35}$$

$$H_{oW,i} = H_{cl,i} - H_W \tag{3.36}$$

$$h_{cl,i} = \frac{M_{T,i} MW_i^L}{\rho_i^L A_{a,i}} \tag{3.37}$$

where

$C_i^L =$ a constant depending on the liquid loading of the individual trays [$m^{1.5}\,s^{-1}$]

$A_{a,i} =$ active area of tray covered by the liquid phase [m^2]

$H_W =$ weir height [m]

$H_{cl} =$ clear liquid height (froth ignored) [m]

$H_{oW} =$ liquid height above the weir [m]

Both $A_{a,i}$, H_W, and C_i^L are dimensional parameters of the column internals. The value of C_i^L is obtained from steady state simulations. A general representation of a tray in a column with notation is given in Figure 3.3. The different areas of a tray are listed in Table 3.2. In addition, the table reports typical tray dimensions, including the relevant tray parameters appearing in Eq. (3.35).

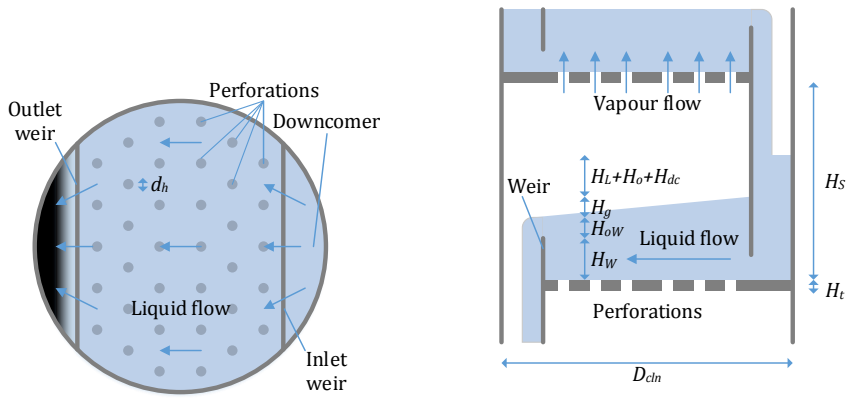

(a) Cross section of a sieve tray.

(b) Notation illustrated on tray.

Figure 3.3. Conventional tray layout.

From the vapour phase, a flow, caused by a pressure gradient, leaves the tray into the above tray. The vapour flow through perforated trays can be described as

Table 3.2. Definition of regions in a column tray.

Illustration	Name	Area symbol	Comments and sieve tray typical dimensions
	Total area	A_T	Column cross sectional area. Given by conventional sizing methods.
	Downcomer are	A_d	$A_d = \theta_{dT} A_T$. Roughly $\theta_{dT} = A_d/A_T$ is in the range 0.1-0.2 [37].
	Tray area	A_t	$A_t = (1-\theta_{dT})A_T$
	Active area	A_a	$A_a = (1-2\theta_{dT})A_T$
	Perforations area	A_p	Holes 6.35-12.7 mm diameter, $\theta_{pa} = A_p/A_a = 0.1$ [57]

done by Kolodzie and van Winkle [88]. In this work, the volumetric flow rate is simplified to be proportional to the square root of the pressure gradient in terms of liquid height:

$$V_i = \text{sgn}(\Delta P_i) \frac{10^{-3/2} C_i^V (\rho_i^V)^{0.5}}{MW_i^V} |\Delta P_i|^{0.5} \tag{3.38}$$

$$\Delta P_i = P_i - P_{i-1}$$

where

$C_i^V =$ a constant depending on the vapour loading (Note that the conversion factor $10^{-3/2}$ appears when kPa is used for pressure) [m^2]

$g =$ gravitational acceleration [m s^{-2}]

The operator sgn returns the sign of the pressure driving force, thereby providing the direction of the vapour flow. In addition, the change in density was neglected such that a mean density is obtained in Eq. 3.38. This mean density is assumed to be the density of the vapour in stage i.

3.4 Performance Indicators

In this section a set of performance indicators with expressions for evaluating distillation columns are provided. Suitable expressions for conventional equipment have been carefully identified and employed for estimation of investment cost of the new equipment present in e.g. the HIDiC (internal heat transfer equipment). Note that the models of the performance indicators are independent of the physical model given in the previous sections. The simulation results obtained by the physical model are input to the performance indicator models. Therefore, there will be distinguished between model parameters and economic parameters.

3.4.1 Second-law Efficiency

The second-law efficiency, η_{2nd}, provides insights into the column energy efficiency and is given by [31]:

$$\begin{aligned}
\eta_{2nd} &= \frac{W_{min}}{W_{lost} + W_{min}} \\
W_{min} &= \sum_{i=1}^{N_S} \left(U_i b_i^L|_{T=T_\sigma} + W_i b_i^V|_{T=T_\sigma} - F_i b_{F,i}|_{T=T_\sigma} \right) \\
W_{lost} &= \sum_{i=1}^{N_S} \left(U_i b_i^L + W_i b_i^V - F_i b_{F,i} + Q_i(1 - T_\sigma / T_{s,i}) + E_i \right) \\
b_i^L &= h_i^L - T_\sigma s_i^L \\
b_i^V &= h_i^V - T_\sigma s_i^V \\
b_{F,i} &= h_{F,i} - T_\sigma s_{F,i}
\end{aligned} \tag{3.39}$$

where

$W_{min} =$ minimum, isothermal work [kW]
$W_{lost} =$ lost work [kW]
$b_i =$ availability function [kJ mol^{-1}]
$T_\sigma =$ temperature of the surroundings [K]
$T_{s,i} =$ temperature of the energy sink or source [K]

The internal heat transfer (q_i) does not appear in Eq. (3.39) and hence it is distinguished from the external heat transfer rate (Q_i).

3.4.2 Operating and Capital Expenditures

One method to estimate the capital expenditures (CAPEX) is Guthrie's Modular Method as described by e.g. Biegler et al. [9]. This method reflects the median of equipment cost data, which have deviations of up to 20% for some units.

The CAPEX calculation consists of a summation of the updated bare module costs (UBMC) corresponding to vessels, trays, heat exchangers, and compressors (see following sections):

$$\text{CAPEX} = \sum_{\text{i modules}} \text{UBMC}_i \tag{3.40}$$

The updated bare module cost (UBMC) is given by the expression:

$$\text{UBMC} = (\text{UF})(\text{BC})(\text{MPF} + \text{MF} - 1) \tag{3.41}$$

where

UF = update factor (UF=(CE PCI)/115) [-]
BC = base cost [$]
MPF = material and pressure factor [-]
MF = module factor [-]

The estimation of the updated bare module cost is based on empirical correlations of direct cost of equipment taking historical data into account. The annual index of the chemical engineering plant cost index is taken from Chemical Engineering Plant Cost Index (CE PCI) [1] and the value from 2012 is 584.6. The MPF is the material and pressure factor, which accounts for operating conditions and construction material of the individual equipment. The module factor (MF) accounts for direct and indirect costs (equipment cost, installation, shipping, taxes, and supervision) in a simple manner. It depends on the bare module cost:

$$\text{MF} = \begin{cases} \text{MF2}, & \text{BC} < 200,000 \\ \text{MF4}, & 200,000 \leq \text{BC} < 400,000 \\ \text{MF6}, & 400,000 \leq \text{BC} < 600,000 \\ \text{MF8}, & 600,000 \leq \text{BC} < 800,000 \\ \text{MF10}, & 800,000 \leq \text{BC} < 1,000,000 \end{cases} \tag{3.42}$$

The values for MF2, MF4, MF6, MF8, and MF10 for the different types of equipment are reported by Biegler et al. [9].

The operating expenditures (OPEX) is estimated based on the contributions of the individual equipment:

$$\text{OPEX} = \sum_{\text{i modules}} \text{OC}_i \tag{3.43}$$

where

OC= operating cost [$\$\,\text{s}^{-1}$]

The estimation of the contributions on CAPEX and OPEX in terms of UBMC and OC, respectively, are described in the following sections.

3.4.2.1 Column

The distillation column itself consists of a vessel module and a tray stack module. Only tray columns are considered. Given a steady state column simulation, the algorithm for sizing and costing is as follows:

1. Provide vapour flow profile V_i and liquid flow profile L_i for all trays i
2. Retrieve physical properties MW_i^L, MW_i^V, ρ_i^L, ρ_i^V, and σ_i^L for all trays i
3. Select tray spacing (H_S), downcomer area per total tray area (θ_{dT}), and flooding factor (FF). Typical values for sieve trays: $\theta_{dt} = 0.10$ (Table 3.2), $FF = 0.80$, and $H_S = 609.6\,\text{mm}$ (24") [9].
4. Determine column diameter
   a) Calculate $F_{lv,i} = \dfrac{L_i MW_i^L}{V_i MW_i^V}\left(\dfrac{\rho_i^V}{\rho_i^L}\right)^{0.5}$
   b) Read Souders and Brown factor (C_{sb}) from Figure C.1 in Appendix C
   c) Calculate the linear vapour velocity $u_{nf,i} = C_{sb}\left(\dfrac{\rho_i^L - \rho_i^V}{\rho_i^V}\right)^{0.5}\left(\dfrac{\sigma_i^L}{\sigma_{\text{ref}}}\right)^{0.2}$ with $\sigma_{\text{ref}} = 0.020\,\text{N s}$.
   d) Calculate the total tray area $A_{T,i} = \dfrac{V_i MW_i^V}{\varepsilon u_{nf} FF \rho_i^V}$, where $\varepsilon = 0.75$ is the area available for vapour flow. Any correction factor [57] to the vapour velocity is neglected
   e) Calculate the column diameter $d_i = (4A_{T,i}/\pi)^{0.5}$
   f) Select largest diameter for cost estimation $d_{max} = \max_i d_i$ for i trays
5. Calculate UBMC for tray stack
   a) Calculate the number of trays $N_T = N_S - N_{cpr} - N_{cnd} - N_{rbl}$, where $N_{cnd} = 1$ is the number of condensers, $N_{rbl} = 1$ is the number of reboilers, and N_{rbl} is the number of compressors.
   b) The tray stack height is calculated based on the tray spacing according to $H_{\text{tray stack}} = \dfrac{N_T H_S}{\eta_{tray}}$ where N_T is the number of trays and η_{tray} is the tray efficiency.
   c) Calculate $\text{BC}_{\text{tray stack}} = 125 H_{\text{tray stack}}^{0.97} d_{max}^{1.45}$
   d) Calculate UBMC using Eq. (3.41) and appropriate MF and MPF
6. Calculate UBMC for column

a) Calculate the column height $H_{\text{column}} = 1.20 H_{\text{tray stack}}$. The column must encase both the tray stack and also an extra feed space, disengagement space in top and bottom and skirt height, which totals approximately 20% of the total tray stack height.

b) Calculate $\text{BC}_{\text{column}} = 963 H_{\text{column}}^{0.81} d_{max}^{1.05}$

c) Calculate UBMC using Eq. (3.41) and appropriate MF and MPF

7. No operating costs are associated with the column or the tray stack

3.4.2.2 Internal Heat Transfer

The cost estimation of the internal heat exchangers is based on conventional heat exchangers. A U-tube heat exchanger is used to represent one pair of heat integrated stages. Since the provided cost estimate includes both shell and tubes it is assumed to be an overestimate of the real cost. Instead the estimate reflects the increased complexity of incorporating and adapting heat exchangers to fit inside the column trays. The algorithm for estimating the cost is as follow:

1. Provide internal heat transfer areas ($A_{ihx,n}$)
2. Calculate $\text{BC} = \sum_{n=1}^{N_{ihx}} 477 A_{ihx,n}^{0.65}$
3. Calculate UBMC using Eq. (3.41) and appropriate MF and MPF
4. No operating costs are associated with internal heat exchangers

3.4.2.3 Condenser and Side Heat Exchangers

The approach for estimating the required heat exchange area for a condenser or any side heat exchangers is described below. Only cooling water is considered as the heat sink.

1. Provide the duty (Q) and the heat source temperature (T)
2. Specify the cooling water inlet temperature ($T_{cw,in}$), the allowed temperature change of the cooling water (ΔT_{cw}), and overall heat transfer coefficient $U_{hex} = 0.60\,\text{kW}\,\text{m}^{-2}\,\text{K}^{-1}$ (or assign appropriate)
3. Retrieve physical properties of cooling medium. Cooling water parameters: $MW_{cw} = 0.018\,\text{kg}\,\text{mol}^{-1}$ and $C_{P,cw} = 0.0753\,\text{kJ}\,\text{mol}^{-1}\,\text{K}^{-1}$
4. Calculate the temperature driving force

   a) Calculate the cooling water outlet temperature $T_{cw,out} = T_{cw,in} + \Delta T_{cw}$

b) Assume that the heat source temperature is constant. Check that $T_{cw,out} \leq T$ (or reasonable lower than T) is satisfied, otherwise cooling water can not be used at the specified $T_{cw,in}$

c) Calculate the logarithmic mean temperature difference $\Delta T_{lm} = \frac{(T - T_{cw,out}) - (T - T_{cw,in})}{\log(T - T_{cw,out}) - \log(T - T_{cw,in})}$

5. Calculate UBMC

a) The area is thus $A = \frac{Q}{U_{hex} \Delta T_{lm}}$

b) Calculate BC $= 477A^{0.65}$

c) Calculate UBMC using Eq. (3.41) and appropriate MF and MPF

6. Calculate operating cost

a) Calculate mass flow rate $f_{cw} = MW_{cw} \frac{Q}{\Delta T_{cw} C_{P,cw}}$

b) Calculate operating cost OC $= S_{cw} f_{cw}$. The cost of cooling water can be obtained using Eq. (2.8)

3.4.2.4 Reboiler and Side Heat Exchangers

The approach for estimating the required heat exchange area for every condenser or side heat exchanger using is as follows. Only steam is considered as a heat source.

1. Provide the duty (Q) and the heat sink temperature (T)

2. Specify the minimum temperature driving force $\Delta T = 10\,\mathrm{K}$ and overall heat transfer coefficient $U = 1.420\,\mathrm{kW\,m^{-2}\,K^{-1}}$ for a reboiler or $U_{hex} = 0.60\,\mathrm{kW\,m^{-2}\,K^{-1}}$ for heat exchangers (or assign appropriately)

3. Retrieve physical parameters of steam: Molecular weight $MW_{steam} = 0.018\,\mathrm{kg\,mol^{-1}}$

4. Calculate steam condition

a) Calculate the required steam temperature $T_{steam} = T + \Delta T$

b) Calculate steam saturation pressure from Eq. (3.8)

c) Calculate steam heat of vaporisation from Eq. (3.14)

5. Calculate UBMC

a) The area is thus $A = \frac{Q}{U_{hex} \Delta T}$

b) Calculate BC $= 477A^{0.65}$

c) Calculate UBMC using Eq. (3.41) and appropriate MF and MPF

6. Calculate operating cost

   a) Calculate mass flow rate $f_{steam} = MW_{steam} \dfrac{Q}{\Delta h_{vap,steam}}$ [kg s^{-1}]

   b) Calculate operating cost OC $= S_{steam} f_{steam}$. The cost of steam can be obtained using Eq. (2.7).

3.4.2.5 Compressor

Since the duty of the compressor is given from simulation, no further calculations are required for sizing. The compressor is assumed to be of centrifugal/motor type. The investment and operating costs for each compressor are:

1. Provide the duty (E)
2. Specify motor efficiency η_{cpr}
3. Calculate actual compressor power $E_{actual} = E/\eta_{cpr}$
4. Calculate UBMC

   a) Calculate BC $= 831 E_{actual}^{0.77}$

   b) Calculate UBMC using Eq. (3.41) and appropriate MF and MPF

5. Calculate operating cost OC $= S_{electricity} E_{actual}$. The cost of electricity can be obtained using Eq. (2.6).

3.4.3 Hydraulic Feasibility Indicator

The hydraulic feasibility indicator (HFI) is a simple indicator for a concentric column arrangement that describes whether a specified heat exchange area is feasible or not. The derivation is based on relatively simple geometric considerations, which are provided by Gadalla et al. [37]. A numerical example is provided in Illustration 3.4 in order to give an order of magnitude of the potential available heat exchange area in a tray. The definition of HFI is:

$$\text{HFI} = \min_n \frac{A_{ihx,n}}{A_{HP,n}} \tag{3.44}$$

where

$A_{ihx,n} =$ required/specified heat exchange area of pair n [m^2]
$A_{HP,n} =$ available heat exchange area of pair n [m^2]

Based on the provided models, the algorithm for estimation the HFI for a concentric column arrangement is:

1. Provide column profile of the required cross sectional area ($A_{T,i}$) and heat exchange areas ($A_{ihx,n}$). The following steps requires the tray areas of the heat-integrated stages. These are identified using the indices described in Section 3.3.4, i.e. $A_{T,r(n)}$ for heat source stages and $A_{T,s(n)}$ for heat sink stages that matches $A_{ihx,n}$.

2. Specify the downcomer area per total cross sectional area ($\theta_{dT} = 0.10$), and heat panel height (H_{HP}) and thickness (T_{HP}), and the fraction of the liquid flow path to be covered by heat panels ψ. Some realistic values are [37]: $H_{HP} = 0.30\,\text{m}$, $T_{HP} = 0.030\,\text{m}$, and $\psi = 0.8$.

3. Calculate a new concentric total cross sectional area $A_{CT,max} = \max_n(A_{T,r(n)} + A_{T,s(n)})$

4. Normalise the total cross sectional areas of the column sections such that the sums of the two sections are constant and equal to $A_{CT,max}$.

   a) Update $A_{T,r(n)} := A_{CT,max}\frac{A_{T,r(n)}}{A_{T,r(n)}+A_{T,s(n)}}$ for all $n = 1,2,\ldots N_{ihx}$

   b) Update $A_{T,s(n)} := A_{CT,max}\frac{A_{T,s(n)}}{A_{T,r(n)}+A_{T,s(n)}}$ for all $n = 1,2,\ldots N_{ihx}$

   Note that this approach does not result in a linear change in the stripping section diameter.

5. Calculate the inner column diameter $d_{inner,n} = \sqrt{\frac{4A_{T,r(n)}}{\pi}}$ (assumed to be rectifying section in a concentric column)

6. Calculate the outer column diameter $d_{outer,n} = \sqrt{\frac{4(A_{T,r(n)}+A_{T,s(n)})}{\pi}}$ (assumed to be stripping section in a concentric column)

7. Calculate heat panel heat transfer area of each pair

   a) Calculate the heat exchange area per heat panel $A_{1HP} = H_{HP}\psi(d_{outer,n} - d_{inner,n})$

   b) Calculate the number of heat panels available $N_{HP,n} = \frac{\pi}{2T_{HP}}\left(d_{outer} + d_{inner} - \frac{\theta_{dt}d_{outer}^2}{d_{outer}-d_{inner}}\right)$

   c) Calculate total heat transfer area available $A_{HP,n} = A_{1HP,n}N_{HP,n}$

8. Calculate HFI using Eq. (3.44)

It should be noted that the calculation of HFI is restricted to the concentric column arrangement and heat panels in the outer (stripping) section.

3.5 Model Implementation

The model work flow is summarised in Figure 3.4. Steps 1-9 concern steady state simulations and Steps 10-12 concern dynamic simulations. The figure illustrates the progress of the steps for implementation depending on the simulation task purpose, i.e. whether it is static or dynamic. Steps 1–2 are conventional steps for separation by distillation where Step 3 requires user input for specifying the particular configuration of interest. This is addressed in more details in Section 3.5.1. In Step 4, a column design must be selected. A suitable design method is proposed in Chapter 4. Step 5 serves as an evaluation of the choice of thermodynamic models based on the selected operating pressures. Steps 6–7 result in a steady state solution. The purpose of Step 6 is to significantly improve the convergence rate by providing an initial guess for the solver in Step 7. An extension of the Wang-Henke Boiling-point (BP) method is used in Step 6. The fsolve function in Matlab was adopted to simultaneously solve all model equations, design specifications and separation specifications. Section 3.4 provides a basis for evaluating a distillation column design for Step 8, where graphical representations such as an xy-diagram and/or xy-enthalpy diagram can be useful for evaluating the simulation results. If dynamic simulations are required, one has to proceed to Steps 10–12, beginning in Step 10 with fixing hydraulic parameters appearing in Eqs. (3.35) and (3.38). The required dynamic parameters cover for example the active tray area(s) and the weir height. These parameters are converted to the proportionality constants in the mentioned equations in Step 10 such that dynamic simulations can be carried out in Step 11. Detailed considerations on the model parameters, the model implementation and the model solution procedure are outlined in the following subsections.

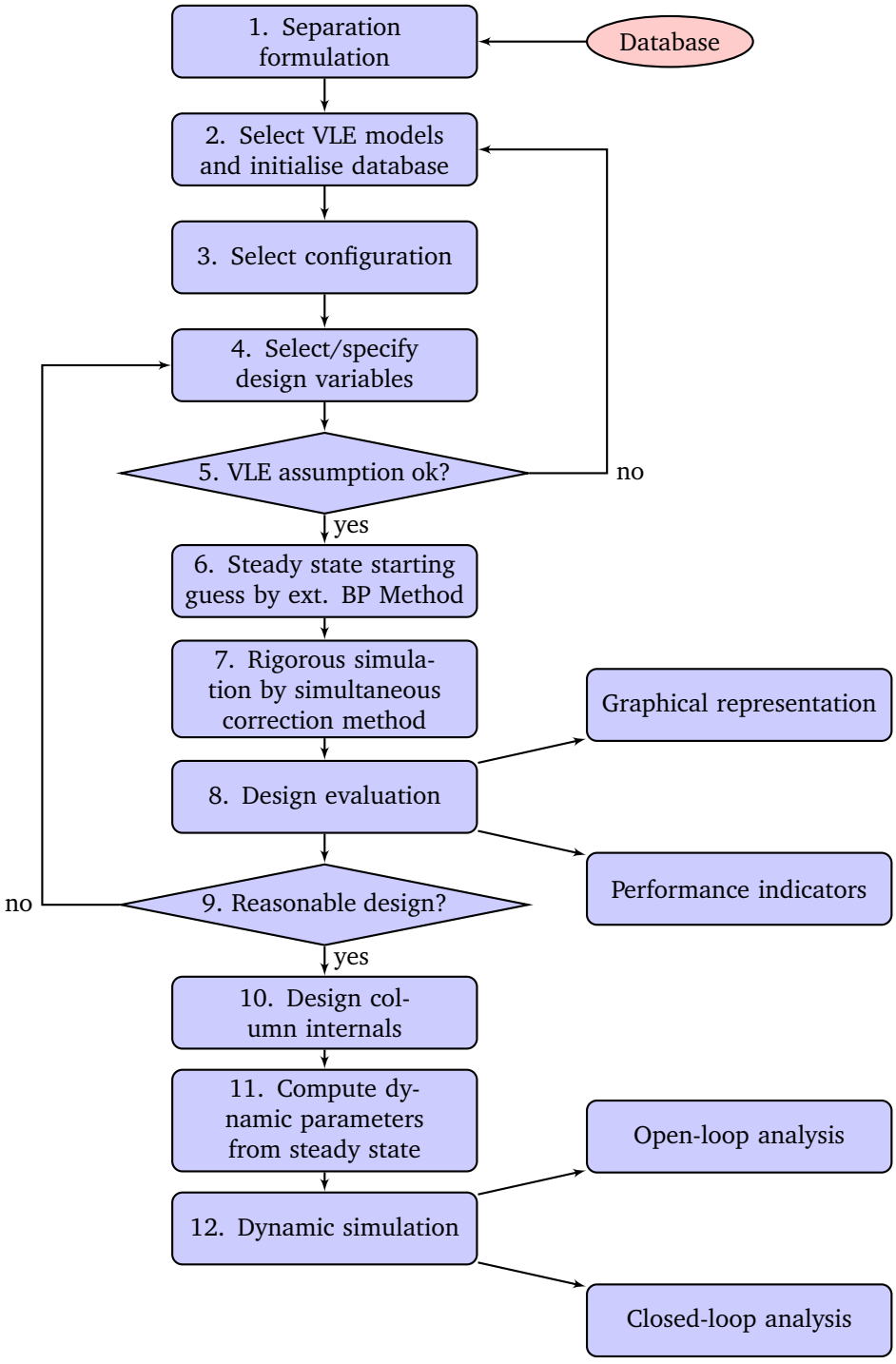

Figure 3.4. Overview of the workflow required in different simulation studies.

3.5.1 Configuration Parameters

The proposed model framework offers a great flexibility with respect to the selection of distillation configurations, and ultimately a generalised foundation for comparisons. The four configurations introduced in Figure 3.1 can be represented using the guidelines of parameter selection in Table 3.3. Take for example the MVRC for which the position of the compressor/valve stage must be at stage 2, whereas for the HIDiC, the compressor must located above the feed stage. Other positions of the compressor can also be modelled for the exploration of new configurations. Furthermore, the framework enables studies, which incorporate for example additional compressors to cope with separations having complex column temperature profiles or for higher energy utilisation. For example, the SRVC is conceptually a combination of the MVRC and the HIDiC. A more detailed example on choosing the configurations parameters is given in Illustration 3.5.

Table 3.3. Characterisation of the three heat-integrated configurations.

Position	Set size	Index name	Index range		
			MVRC	HIDiC	SRVC
Compressor/valve	N_{cpr}	k	2	$k = N_F - 1$	Combined
Heat integrated stages in rectifying section	N_{ihx}	r	1	$1 \leq r \leq N_F - 1,\ r \neq k$	HIDiC and MVRC
Heat integrated stages in stripping section	N_{ihx}	s	N_S	$N_F \leq s \leq N_S,\ s \neq k$	

3.5.2 Proposed Specifications

The type and the number of the required specifications (i.e. degrees of freedom) depends on the purpose of the study to be carried out. In the general case (considering the control volumes in Figure 3.2), a distillation column is fully specified when the variables listed in Table 3.4 are supplied. However, various combinations of specifications can by supplied in order to eliminate the degrees of freedom. The link between these, i.e. between the proposed specifications and the degrees of freedom, is provided in the table. Furthermore, remarks on the link between the degrees of freedom associated with conventional distillation columns and the considered heat-integrated distillation configurations are provided.

The dynamic model contains additional parameters compared to simpler approaches [60]. This is a result of maintaining the energy balances in a dynamic

Table 3.4. Degrees of freedom analysis for the general distillation column representation constituted by the stages in Figure 3.2. The mentioned steps refer to the model workflow in Figure 3.4.

Degree of freedom	Remark
Number of stages (N_S)	This variable is essential as it influences the total number of degrees of freedom. It is specified in Step 4.
Feed flow rate (F_i)	The feed flow rate is specified in Step 1. The integer variable N_F is introduced to impose constraints $F_i = 0, i \neq N_F$. N_F is specified in Step 4. Conceptually, it is possible to increase the number of feed stages but it is not considered in this work.
Feed composition ($z_{i,j}$)	The same as the feed flow rate applies to the feed composition. However, the number of degrees of freedom is $N_S(N_C - 1)$ before introducing N_F.
Feed Pressure (P_F)	The same as the feed flow rate applies to the feed pressure.
Feed enthalpy (h_F)	The same as the feed flow rate applies to the feed enthalpy.
Liquid side draw flow rate (U_i)	In this work, no liquid side draws on the trays are considered. However, the distillate and the bottom product streams are considered as liquid side draws. This implies that $U_i = 0, i \neq \{1, N_S\}$. It is common to impose purity constraints, thereby eliminating the degrees of freedom U_1 and U_{N_S}. As a result, all U_i is typically fixed in Step 1.
Vapour side draw flow rate (W_i)	No vapour side draws are considered in this work. However, this variable is relevant if, for example, a partial condenser is employed.
Pressure (P_i)	In order to consume the thermodynamic degrees of freedom, the pressure must be specified. The specification of pressure is a design decision covered in Step 4. An important remark, is that the specification of the column pressure profile also consumes the degrees of freedom associated of the non-mixing stages (i.e. the compressor duty E_k). This is because the constraint of isentropic compression is imposed in Eq. (3.33).
Internal heat transfer rate (q_i)	The matrix $\mathbf{n}_{ihx}$ is obtained through Steps 3-4. Then q_i can either be specified directly or obtained by Eq. (3.29).

form, i.e. expressed in terms of time derivatives rather than using a pseudo-steady state approximation. The reason for this is to maintain a system of ordinary differential equations (ODE) rather than a system of differential-algebraic equations (DAE), which is computationally more complex to solve.

An advantage of the model is that it accounts for the liquid holdup present both below and over the weir in a tray. Furthermore, the model accounts for dynamic tray pressure drops. As a result of these two considerations, the model enables studies of entrainment flooding and weeping. This is of particular interest in relation to heat-integrated trays because the liquid and vapour loadings vary significantly throughout a heat-integrated distillation column. However, for more general dynamic studies, the additional model parameters can also represent a disadvantage in the sense that the model contains more parameters with physical meaning (e.g. weir height and active tray area). Such parameters are bound within reasonable/realistic limits, which has to be taken into account.

A list of recommendations for fixing these parameters is compiled in Table 3.5. For liquid and vapour hydraulics, it is suggested to specify the driving forces. Note that the specification of the dynamic parameters relies on the steady state solution. Furthermore, note that dynamic simulations can only be performed if tray pressure drops are non-zero.

Table 3.5. Recommendation for selection of the dynamic column design parameters based on a steady state simulation. N_{cnd} is the number of condensers (0 or 1), and N_{rbl} is the number of reboilers (0 or 1).

Variable	Appearing in Eq.	Number of Appearance	Recommended constraint
C_i^L	(3.35)	$N_S - N_{cnd} - N_{rbl} - N_{cpr}$	Fix height over weir ($H_{oW,i}$) as e.g. 20% of weir height, i.e. $H_{oW,i} = 0.2H_W$
C_i^V	(3.38)	$N_S - N_{cnd} - N_{cpr}$	Fix tray pressure drop ΔP_i as e.g. 0.70 kPa
$A_{a,i}$	(3.35)	$N_S - N_{cnd} - N_{rbl} - N_{cpr}$	Use conventional column sizing method (Section 3.4.2.1) for $A_{T,i}$, and calculate $A_{a,i} = (1 - 2\theta_{dT})A_{T,i}$ using e.g. $\theta_{dT} = 0.10$
$M_{T,cnd}$ and $M_{T,rbl}$	(3.1)-(3.2)	$N_{cnd} + N_{rbl}$	Fix time constant defined as total holdup divided by steady state throughput, e.g. 5 min
$M_{T,k}$ (compressor/-valve)	(3.4)-(3.6)	N_{cpr}	Fix time constant defined as total holdup divided by steady state throughput, e.g. 10 s

3.5.3 Implementation

The calculation sequence of the model equations is based on the framework provided by Gani et al. [42]. The set of model equations is decomposed into smaller subsets that can be solved sequentially and independently of one another as illustrated in Figure 3.5. As a result, the dynamic model can be solved as a system of

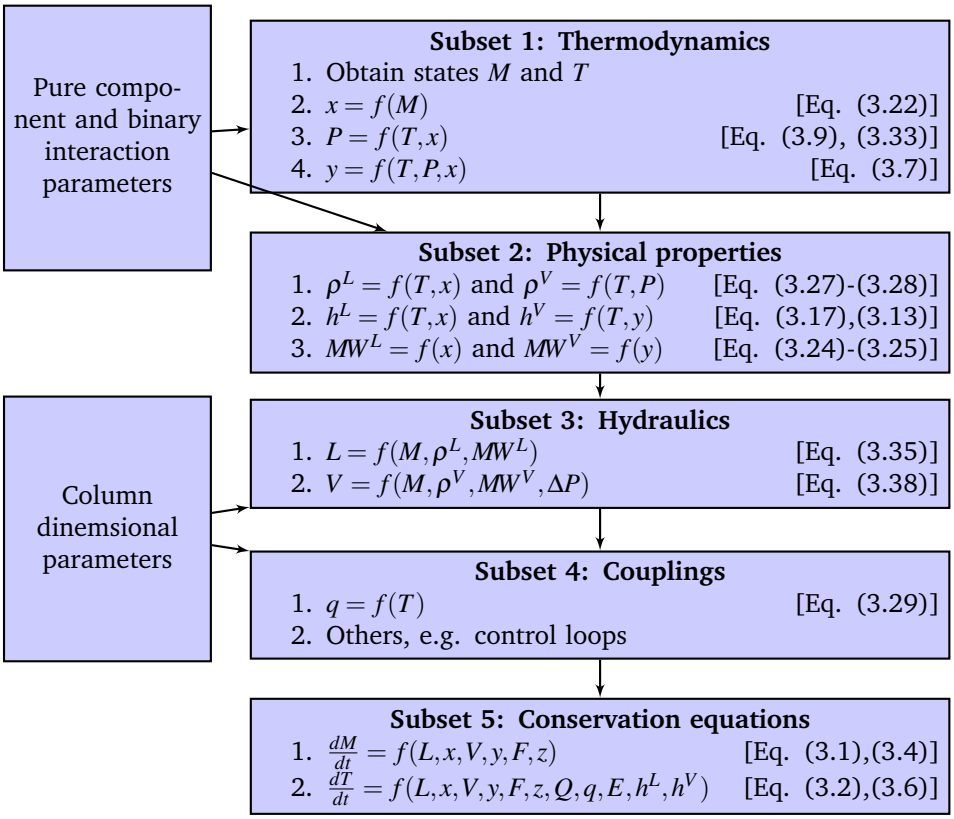

Figure 3.5. Implementation sequence to obtain a system of ordinary differential equations in the case of ideal vapour phases.

coupled, ordinary differential equations if vapours are considered ideal and when deviation from non-ideality of the liquid phase is described as a function of liquid phase state variables temperature and composition. When non-ideality of the vapour phase is the case, a differential-algebraic equation solver (DAE) must be used, which increases the complexity of the solution procedure. One might argue that the HIDiC has a main application in the low-to-medium pressure range since the pressure elevation is often minimised to reduce both the OPEX and the CAPEX associated with the compressor. The full model is implemented in Matlab and will

be employed throughout this work. For dynamic simulations, the model has been implemented in Matlab Simulink.

3.5.4 Static Model Solution Procedure

In this work, static simulations are carried out involving mixtures of varying degrees of complexity. These simulations cover studies concerning mixtures with (i) ideal vapour and liquid phases, (ii) non-ideal liquid phases and ideal vapour phase, and (iii) non-ideal liquid and vapour phase. The Matlab command fsolve is adopted as a means to obtain a steady state solution. However, arriving at a converged solution of the model is not straightforward. Despite efforts were put in to provide appropriate input and output scaling, the starting guess was found to have a significant impact on the possibility of obtaining a converged solution.

In order to address the problem of providing a good starting guess for the fsolve command, the Wang-Henke boiling-point method (BP method) was adopted. The BP method was originally proposed by Wang and Henke [163] for conventional distillation columns only. In this work, the BP method was extended such that it can cover the considered heat-integrated distillation columns. The resulting method is termed the extended BP method and its documentation is provided in Appendix D. An effective tear variable initialisation procedure was developed and provided along with the method documentation. Experience using an extended version of the BP method has been reported by Mah et al. [94]. However, it has not been documented in the open literature.

For a two product and one feed distillation configuration, the extended BP method requires the specification of the pressure profile, the distillate flow rate, and the reflux ratio in addition to the general feed specifications. In return, it provides a solution to the model, which is reasonable robust for all the considered distillation column configurations. By using the extended BP method solution as starting guess, it was observed that the convergence of the fsolve command was obtained for most feasible values of the reflux flow rate. This observation can be explained by the fact that the reflux flow rate is directly treated as an adjustable variable in the optimisation problem.

3.6 Example: Separation of Benzene/toluene

This example serves to illustrate the model framework described in Section 3.5 using the steps in Figure 3.4. A feed consisting of a partly vaporised equi-molar mixture of benzene/toluene is fed at $83.3\,\mathrm{mol\,s^{-1}}$. The overall feed composition is 50% benzene and 50% toluene and it consists of 50% liquid and 50% vapour. It is desired

to produce 99.5% pure benzene in the top and 99.5% pure toluene in the bottom. These specifications complete Step 1 (Figure 3.4) and thus the database must be accessed for pure component and mixture properties. The benzene/toluene mixture can be described satisfactorily using the assumption of ideal liquid and vapour phases in Step 2, and the HIDiC is chosen as the considered configuration in Step 3. In Step 4, the design is provided by Nakaiwa et al. [111]: An operating pressure in the feed stage of 101.3 kPa, a compression ratio of 2.553, an overall heat transfer coefficient of $0.60\,\mathrm{kW\,m^{-2}\,K^{-1}}$, a heat exchange area $5.0\,\mathrm{m^2\,stage^{-1}}$, 40 trays in the rectifying section, and 40 trays in the stripping section. All 40 trays are heat integrated from top to bottom in each section. In terms of stages, the HIDiC consists of 83 stages including all trays and the condenser, reboiler and the compressor/valve. In this example, an additional tray pressure drop of 0.70 kPa is assumed. The thermodynamic models are reasonable in Step 5 for the selected operating conditions. The resulting model has 249 states and 421 equations to be solved simultaneously. The following additional input were provided for the extended BP method: The distillate flow rate, which can be calculated from overall mass balance $D = 41.7\,\mathrm{mol\,s^{-1}}$ and a reflux ratio initial estimate $RR = 0.5$. Convergence of a steady state solution is obtained after 47 iterations and it proceeds according to Figure 3.6. As the temperature profile is among the tear variables its convergence is also shown in Figure 3.6.

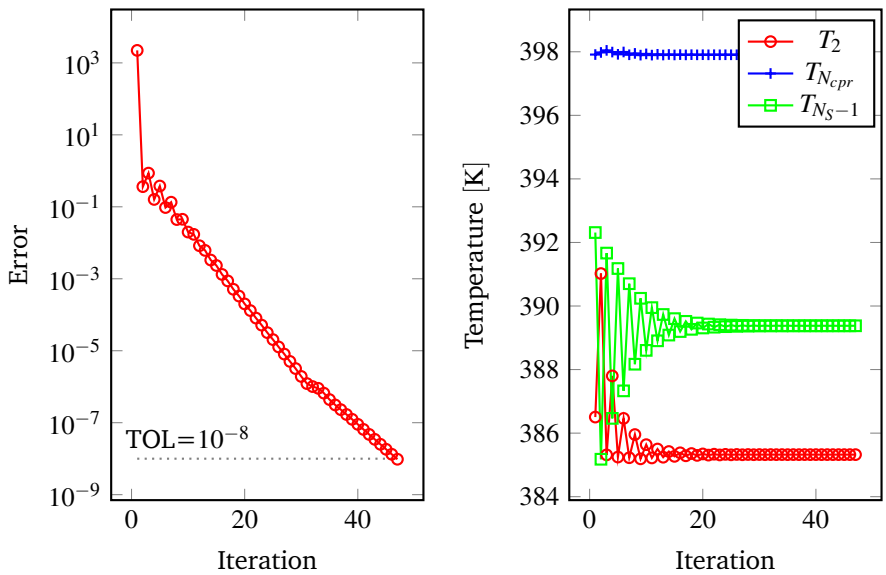

Figure 3.6. Convergence plot of error and selected tear variables.

The design is evaluated w.r.t. performance indicators described in Section 3.4 and compared to the results reported by Nakaiwa et al. [111]. All economic parameters are listed in Table 3.7 and as many as possible of the parameters are taken from Nakaiwa et al. The results are summarised in Table 3.6. One factor of the significant differences between the simulation results and the reference results is the fact that pressure drops are included. Other factors are dissimilarities in economic models and economic model parameters as many of them are not reported by Nakaiwa et al.

Table 3.6. Selected performance indicators based on the presented model compared to literature example. The economic parameters are adopted from reference if possible.

Indicator	Unit	This work	Nakaiwa et al. [111]
Column area	m^2	2.668	-
Second-law efficiency	-	0.14	-
CAPEX	$\$\,yr^{-1}$	3.72	2.58
OPEX	$\$\,yr^{-1}$	0.836	0.303
Water consumption	$kg\,yr^{-1}$	$3.69 \cdot 10^6$	-
HFI	-	3.1	-

Provided that the design seems reasonable (Step 9), the column internals must be designed in Step 10. The total tray cross sectional area is already estimated based on conventional methods during the design evaluation in Step 8 when estimating the CAPEX. This resulted in $2.67\,m^2$. However, ideally it is found that the total tray area changes gradually throughout the column. Therefore, a suitable column arrangement must be selected to justify the selected total tray area column profile. For example, when simulating a concentric arrangement, the varying tray area is reasonable. In addition, a weir height of 50 mm is assumed. Both the total tray area and the weir heights influence the dynamic simulation results. The suggestions in Table 3.5 are used to convert the steady state solution into a dynamic formulation, which finally can be used for dynamic simulations in Step 10.

3.7 Discussion

3.7.1 Model Evaluation

No dynamic, experimental data of the HIDiC have been encountered in the literature. Therefore, it has not been possible to evaluate the model. The presented model was, however, employed in the simulation of a CDiC with particular emphasis on pressure dynamics by Mauricio-Iglesias et al. [101]. In the study of

Table 3.7. Economic parameters for performance indicators. The parameters are grouped in column parameters, which has impact on the model itself, and economic parameters, which has only impact on the performance indicators (see Section 3.4).

Class	Parameter	Unit	Value
Column parameters			
Internal heat exchanger	Heat transfer coefficient	$kW\,m^{-2}\,K^{-1}$	0.60
	Heat exchange area	m^2	5
Tray	Active area per tray area	-	0.70
	Weir height	m	0.05
	Weir overfill fraction	-	0.20
	Pressure drop	kPa	0.70
Condenser	Time constant	min	5
Reboiler	Time constant	min	5
Compressor	Isentropic efficiency	-	0.80
	Time constant	s	10
Economic parameters			
General	Electricity price	$\$\,kWh^{-1}$	0.0843
	Steam	$\$\,t^{-1}$	16.8634
	Cooling water (at 300 K)	$\$\,t^{-1}$	0.0590
	Year	-	2012
	Project life time	yr	5
	Service factor	-	1
	Materials	-	Carbon steel
Tray	Efficiency	-	1
	Flooding factor	-	0.80
	Void fraction	-	0.75
	Type	-	Sieve
	Spacing	mm	609.60 (24")
Condenser	Water temperature increase	K	5.0
	Heat transfer coefficient	$kW\,m^{-2}\,K^{-1}$	0.60
	Type	-	Floating head
Reboiler	Heat transfer coefficient	$kW\,m^{-2}\,K^{-1}$	1.420
	Type	-	Kettle reboiler
Compressor	Motor efficiency	-	0.90
	Type	-	Centrifugal/ motor

Mauricio-Iglesias et al., the implications of different control structures for controlling the column pressure were assessed by simulations. The simulation results were benchmarked against experimental results of an industrial distillation column separating a mixture of 2-propanol/water azeotrope. Mauricio-Iglesias et al. [101] concluded, that the model could satisfactorily account for the pressure dynamics

in relation to the considered separation. Based on this experience, it is assumed that the presented model provides a reasonable representation of a heat-integrated distillation column. However, it is expected that the pressure dynamics play a more important role in the HIDiC due to the strong interactions with the internal heat transfer.

3.7.2 Internals Limitation

One significant limitation of the presented model is that it is based on equilibrium-stages, resembling those in tray columns. In certain separations, packed column internals are preferred, e.g. in the structured plate HIDiC [19]. Modelling of these configurations requires alternative, rate-based approaches. However, for benchmarking studies without further detailed information on the layout of the column internals, it is reasonable to consider tray columns. In addition, equilibrium-based models are typically preferred because of fewer required model parameters.

3.7.3 Economic Models

As mentioned in the benchmarking case study, the evaluation of the techno-economic feasibility of the HIDiC is not a straightforward task. In fact, great uncertainty is associated with this task. Since the HIDiC was introduced in 1977 [94] a major concern has been to demonstrate the benefit w.r.t. energy consumption compared to conventional distillation by either comparing utility consumptions or second-law efficiencies. A more direct measure of the economic feasibility is total annualised cost (TAC). TAC calculation, however, relies heavily on the selected economic model. Typically the installation of internal heat exchangers and a compressor appear to be the major expenses in the HIDiC. Hence, the costing procedures of these units, e.g. selection of types of internal heat exchangers will have a significant impact on the TAC. Some authors [111, 158] add an additional penalty in the magnitude of 20-50% on the HIDiC capital expenditures to account for increased complexity of the column layout. It is thus vital, that more research is carried out in order to improve the accuracy of the costing procedure of the HIDiC. Furthermore, the estimation of operation expenditures depends upon the utility prices and availability. For example, steam prices might be significantly lower if steam is present in excess in the process or at neighbouring facilities. Hence, it is essential to employ identical costing scenarios in benchmark studies, which is made possible within the provided framework. It should be noted, that the installation of internal heat transfer does not only affect the economic feasibility but also the technical feasibility since these might reduce the separation performance. Many of the economic and technical

feasibility aspects are covered in Chapter 5.

Two distinct uncertainties are expected in the economic models presented in Section 3.4: Estimation of the bare module cost of (i) an internal heat exchanger and (ii) the column. A conventional shell-and-tube heat exchanger economic model is used for (i), which means that the module cost accounts for both the shell and the tubes. To realise internal heat transfer in a real HIDiC, it is unlikely that the heat exchanger shell is required. Furthermore, simpler layouts of the internal heat exchangers (e.g. heat panels) are proposed in the literature. Both arguments suggest that the presented economic model gives rise to conservative estimates (overestimates) of the internal heat exchanger bare module costs. For the column bare module cost (including the tray stack), one single tower having the widest diameter and the maximum pressure among all the trays is assumed. This approach does not restrict the bare module cost estimation to certain column arrangements, since a wide selection of arrangements is proposed in literature (see Table 2.5). This assumption might lead to a bare module cost estimate, which is smaller than the case where the column is physically divided in the two column sections. But as the required column diameter is gradually changing in e.g. the concentric HIDiC, using the maximum column diameter is assumed to compensate for the above cost underestimate.

3.8 Conclusion

A generic distillation column model is presented and demonstrated. It can describe both adiabatic and diabatic distillation columns covering among others the conventional, the heat-integrated, and the mechanical vapour recompression distillation column. In addition, the framework offers the flexibility of expanding the current existing configuration library due to the generic structure. The model is embedded in a framework enabling studies to gain insights into e.g. static properties and the dynamic behaviours in a consistent manner. A Matlab simulation platform was developed containing a full implementation of the model and a database of the different configurations and pure component and mixture properties. A solution algorithm was developed in order to obtain robust convergence of the model.

Illustration 3.4. Derivation and estimation of the available tray heat transfer area given the tray dimensions [37].
The heat panels are assumed to be placed on the outside of the wall of the inner tube in the concentric arrangement according to the figure below:

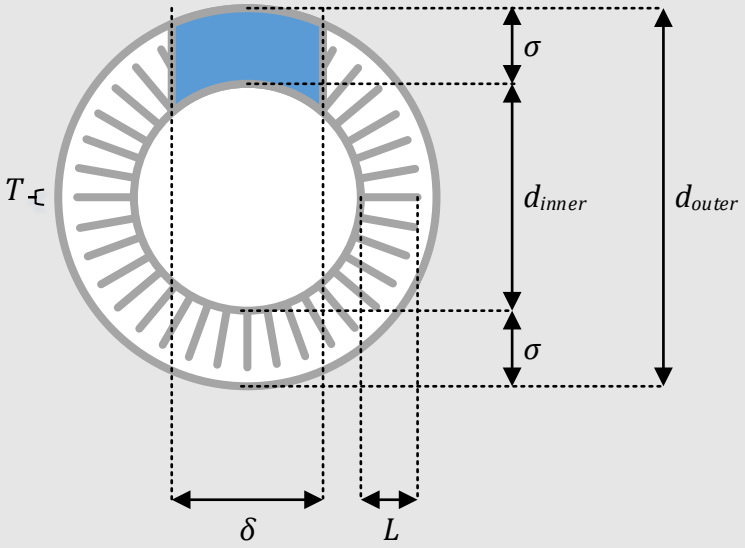

The area of one heat panel is

$$A_{1HP} = 2LH_{HP},$$

where H_{HP} is the height. The areas associated with the thickness of the panels are ignored. In this work, an additional parameter ψ is introduced that is defined as the fraction of liquid flow to be covered by heat panels, i.e. $\psi = L/\sigma$. The number of heat panels

$$N_{HP} = \frac{L_{inner}}{T} + \frac{L_{outer} - L_{inner}}{2T},$$

where $L_{inner} = \pi d_{inner} - \delta$ is the circumference of the inner tube minus δ and $L_{outer} = \pi d_{outer} - \delta$ is the circumference of the outer tube minus δ. The downcomer width is given by $\delta = A_d/\sigma = \theta_{dT} A_{outer}/\sigma$. The curvatures are ignored such that the downcomer can be approximated by a rectangle. It is assumed that no gaps between the heat panels are required on the outer wall of the inner tube.

In Illustration 2.1 it was argued that the rectifying section area is half that of the stripping section given the provided assumptions. If the inner tube is the rectifying section with the area of $1.0\,\mathrm{m}^2$ and the outer tube is the stripping section with area $2.0\,\mathrm{m}^2$. The dimensions thus become:

$$
\begin{aligned}
d_{inner} &= \sqrt{4/\pi \cdot 1.0\,\mathrm{m}^2} = 1.13\,\mathrm{m} \\
d_{outer} &= \sqrt{4/\pi \cdot (1.0\,\mathrm{m}^2 + 2.0\,\mathrm{m}^2)} = 3.39\,\mathrm{m} \\
\sigma &= (3.39\,\mathrm{m} - 1.13\,\mathrm{m})/2 = 1.13\,\mathrm{m} \\
\delta &= \frac{0.10\pi(3.39\,\mathrm{m})^2}{2(3.39\,\mathrm{m} - 1.13\,\mathrm{m})} = 0.799\,\mathrm{m} \\
L_{inner} &= \pi \cdot 1.13\,\mathrm{m} - 0.799\,\mathrm{m} = 2.75\,\mathrm{m} \\
L_{outer} &= \pi \cdot 3.39\,\mathrm{m} - 0.799\,\mathrm{m} = 9.85\,\mathrm{m} \\
L &= 0.80 \cdot 1.13\,\mathrm{m} = 0.904\,\mathrm{m} \\
A_{1HP} &= 2 \cdot 0.904\,\mathrm{m} \cdot 0.30\,\mathrm{m} = 0.542\,\mathrm{m}^2 \\
N_{HP} &= \frac{2.75\,\mathrm{m}}{0.030\,\mathrm{m}} + \frac{9.85\,\mathrm{m} - 2.75\,\mathrm{m}}{2 \cdot 0.030\,\mathrm{m}} = 210 \\
A_{HP} &= 210 \cdot 0.542\,\mathrm{m}^2 = 114\,\mathrm{m}^2
\end{aligned}
$$

The dimensional parameters are taken from Section 3.4. Thus the specific heat area can be calculated based on a tray spacing of 24":

$$
\Phi = \frac{114\,\mathrm{m}^2}{2.0\,\mathrm{m}^2 \cdot 0.6096\,\mathrm{metre}} = 93.5
$$

This specific heat transfer area is much larger than the values obtained in experimental setups (see Table 2.3).

Illustration 3.5. Obtaining an MVRC, a HIDiC, and an SRVC by adjusting configurations parameters.
Provided a distillation column with nine stages where stage #6 is the feed stage. The first #1 and the last #9 are respectively condenser and reboiler. According to Table 3.3, selecting the compressor/valve stage $k = 2$ and heat integrated stage in the rectifying section as $r = 1$ and in the stripping section $s = N_S = 9$ the resulting configurations is the MVRC. In order to obtain a HIDiC, the compressor/valve stage is set to $k = N_F - 1 = 5$ and as many trays as possible are heat integrated, i.e. $r = [2,3,4]$ and $s = [6,7,8]$. Finally, the SRVC is obtained by using a combination of the MVRC and the HIDiC although one additional stage is used as compressor/valve and thus only two stages can be heat-integrated in each section. The illustration below summarises this example.

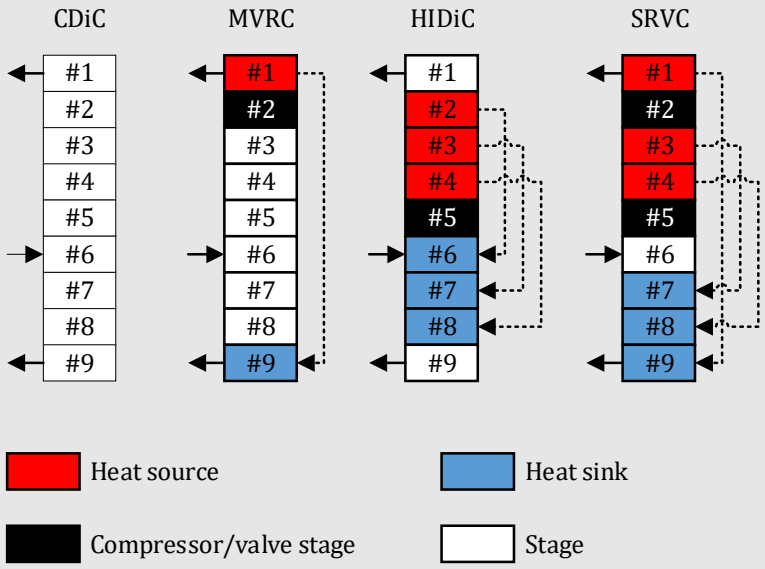

Illustration 3.6. Calculation of the hydraulic constants given the steady state flow profiles.

Consider a distillation column tray with a weir height of 50 mm. Assume at a given tray, the physical properties can be approximated by that of water:

	Liquid	Vapour
Density, $\mathrm{kg\,m^{-3}}$	958	0.598
Flow, $\mathrm{mol\,s^{-1}}$	50	75
Molecular weight, $\mathrm{kg\,mol^{-1}}$	0.018	

Assuming a liquid height over the weir corresponding to 20% of the weir height and a pressure drop of 0.70 kPa (Table 3.5), the liquid and vapour flow hydraulic constants can be calculated and fixed by using Eqs. (3.35) and (3.38):

$$C^L = \frac{LMW}{\rho^L H_{oW}^{3/2}} = \frac{50\,\mathrm{mol\,s^{-1}} \cdot 0.018\,\mathrm{kg\,mol^{-1}}}{958\,\mathrm{kg\,m^{-3}} \cdot (0.2 \cdot 0.050\,\mathrm{m})^{3/2}} = 0.9395\,\mathrm{m^{1.5}\,s^{-1}}$$

$$C^V = \frac{VMW}{(\rho^V)^{0.5}(\Delta P)^{0.5}} = \frac{75\,\mathrm{mol\,s^{-1}} \cdot 0.018\,\mathrm{kg\,mol^{-1}}}{(0.598\,\mathrm{kg\,m^{-3}})^{0.5}(700\,\mathrm{Pa})^{0.5}} = 0.0660\,\mathrm{m^2}$$

In dynamic simulations, the total liquid holdups and pressures vary in time when subject to disturbances and hence the liquid and flow rates are calculated by fixing the constants using the steady state as illustrated in this example.

Chapter 4

Conceptual Design

An iterative design method for the conceptual design of the mechanical vapour recompression column (MVRC), the heat-integrated distillation column (HIDiC), and the secondary reflux and vaporisation column (SRVC), is presented. The method is tailor-made for the developed model framework and allows relatively fast conceptual design of considered configurations for a given separation (binary or a multicomponent mixture). An economic objective function is used to direct the progress of the design towards optimality and a generic distillation column configuration is used to represent the considered configurations. The method is more intuitive and takes a more stepwise approach to the design problem, compared to other superstructure-based MINLP approaches relying on mathematical programming. However, on present form, a fully optimal design is not guaranteed.

The application of the design method on the MVRC, the HIDiC, and the SRVC is outlined. Finally, the method is discussed and exemplified for a binary mixture of benzene/toluene and a multicomponent mixture of aromatic compounds.

The design method was presented at the AIChE Annual Meeting 2015 in Salt Lake City, Utah, in a presentation entitled "Design Methods for the Heat-Integrated Distillation Column (HIDiC)". Furthermore, an early stage of the design method was presented at the Distillation and Absorption conference

[K. Meyer, L. Ianniciello, J.E. Nielsen, T. Bisgaard, J.K. Huusom, and J. Abildskov. Hidic – design, sensitivity and graphical representation. *Proceedings of Distillation and Absorption*, pages 727–732, 2014].

4.1 Introduction

As a basis for the benchmarking of distillation column configuration alternatives, a satisfactory design method is required. Furthermore, such a method is essential for obtaining economically feasible designs for investigating dynamics and control. Based on the model presented in Chapter 3, a simulation-based design method for exploring various distillation column configuration alternatives by allowing gradual conversion between the configurations would be useful. However, existing design methods can not directly be extended to all the configurations, studied in this thesis. Thus, the need for developing the present design algorithm was identified. The presented design algorithm is a generalisation of the experience gained in simulations of a variety of mixtures taking into account a relative large design space. Hence, common trends in the resulting optimum designs w.r.t. TAC have been identified and systematised. Furthermore, the experiences are verified by qualitative considerations (see Section 4.6).

4.1.1 Configuration Generalisation

The mechanical vapour recompression column (MVRC), the heat-integrated distillation column (HIDiC), and the secondary recompression column (SRVC) are targeted as potential candidates for improvements as alternatives to the conventional distillation column (CDiC). In the scope of this work, economic improvements are essential, while reductions in e.g. energy consumption are optional. However, energy reductions are closely related to economic improvements. A generalised distillation column structure has been defined, which is capable of describing the targeted potential candidates (HIDiC, MVRC, and SRVC) and the CDiC. This generalised distillation column structure is illustrated in Figure 4.1. The considered configurations in this work are limited to one feed and two product stream separations, which is reflected in the figure.

4.1.2 Design Reservations

All obtainable designs by the design algorithm are restricted to the four configurations: CDiC, MVRC, HIDiC and SRVC. Additional design reservations are made in order to reduce the complexity of the design problem. These are listed and motivated below:

- **Sequenced heat-integrated trays:** It was previously concluded that the concentric HIDiC, in particular, is a potential arrangement of the HIDiC for tray columns. This arrangement limits the pairing to stages of the same vertical

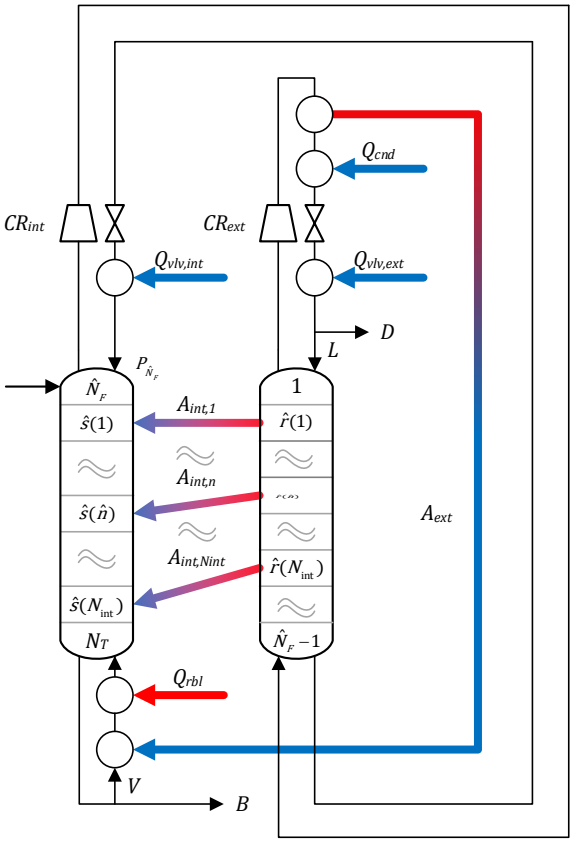

Figure 4.1. A generalised distillation column structure indicating the design degrees of freedom with symbols.

height. Furthermore, no significant additional complexity/investment cost associated with the installation of heat panels gradually along the height in the concentric HIDiC is expected. Various authors [23, 142, 51] claim that the optimal design only contain few pairings with large heat exchange areas. However, such conclusions are often favoured because of the high CAPEX of the required heat exchangers when conventional economic models are used. The economic model of a conventional heat exchanger is typically valid for a shell-and-tube heat exchange. Clearly, such a model can not accurately describe the cost of simple heat panels inside a distillation column tray.

- **Uniform heat exchange area approach:** This approach implies a constant

heat exchange area between every pair of heat-integrated trays. An alternative approach represented in the design literature is the uniform heat transfer rate approach [41, 154]. However, an optimal approach w.r.t. economy lies between the two approaches [155]. This conclusion relies again on the economic models for the heat exchangers and the column, although no experimental data have confirmed such models. It was previously concluded that heat panels must be installed in order to achieve sufficient heat transfer area. Hence, it is argued that the uniform heat exchange area approach reflects a solution, which is most likely to be realised when using heat panels. In particular in relation to the reservation of using sequenced heat-integrated trays, it is presumed that the costs of construction of trays with e.g. heat panels can be reduced; uniform trays that can be massproduced in modules thus favours the uniform heat exchange area approach.

- **Compression ratio(s):** The compression ratio is not considered as a means to improve the economic performance of a design. The compression ratio is solely used for achieving the specified minimum temperature driving force(s) among the paired stages. This is reasonable, as the compressor duty has a relatively small impact on the total annualised cost [155].

- **Economic design approach:** Despite the fact that the available economic models are not properly validated, the total annualised cost (TAC) is employed as the design objective function. It is important to account for the existing trade-off between operating costs and investment costs, which the TAC provides.

- **Only tray/tray and condenser/reboiler type heat integration:** The allowable pairings are restricted to only tray/tray and condenser/reboiler type heat integration. The argument for this reservation is that tray/condenser or tray/reboiler type heat integration can be approximated by involving the tray just below the condenser or above the reboiler rather that the condenser or reboiler. Condenser/tray type heat integration is encountered in the graphical design method by Wakabayashi and Hasebe [159].

- **Reboiler duty rather than feed preheat duty:** The ideal HIDiC has neither a condenser nor a reboiler duties. However, in order to realise such a configuration, the feed has to be partly vaporised. To obtain this, the feed can either be preheated or exist on this form prior to the distillation column. Since only the separations of liquid saturated mixtures are considered in work, a feed preheater or a reboiler is required. During this work, it has been found that the

heat input is utilised more efficiently when it is added in the reboiler rather than to the feed. Therefore, feed preheating is not considered in the method.

4.2 Nomenclature

The design degrees of freedom associated with the generalised column representation are provided in Figure 3.1. Adopted definitions in this chapter are explained in the following subsections.

4.2.1 Design Degrees of Freedom

Consider the general two-product distillation column illustrated in Figure 4.1 with N_T trays (i.e. excluding condenser and reboiler) and one feed introduced at stage $\hat{N}_F$ counted from the top. A bottom product is removed from the reboiler, located below stage N_T at a rate B, while a fraction is vaporised at a rate V and returned to the bottom stage, denoted by the boil-up ratio (V/B). The external heat duty, required for vaporising the returned stream, is termed the reboiler duty and denoted Q_{rbl}. The column section spanning the feed tray to the bottom tray is the stripping section (abbreviated "str"). The pressure of the feed tray is denoted $P_{\hat{N}_F}$. The top vapour of the stripping section is compressed at a compression ratio CR_{int} before it enters the bottom of the rectifying section (abbreviated "rct"). The pressure in the bottom tray of the rectifying section is thus $CR_{int}P_{\hat{N}_F}$. The liquid from the rectifying section is throttled by a valve before entering the feed stage. The top vapour of the rectifying section is compressed at a compression ratio CR_{ext} before it is condensed using an external energy sink with the condenser duty (Q_{cnd}). The distillate is removed at a rate D from the condenser while the rest of the overhead vapour stream L is returned to the column top stage consistent with the value of the reflux ratio ($RR = L/D$). The possibility of considering valve cooling for the two throttling valves is addressed by the duties $Q_{vlv,int}$ and $Q_{vlv,ext}$.

4.2.2 Pairs – Heat-integrated Stages

In order to simplify the nomenclature, there will be distinguished between internal heat integration and external heat integration. Internal heat integration takes place between the column trays and external heat integration takes place between the condenser and the reboiler. Both types of heat integration are described by Eq. (3.29) but subscripts ("int" and "ext") are used to distinguish between the types when needed. The influence on the selection of the variables indicated in Figure 4.1 are summarised in Table 4.1. As indicated in the table, a compression ratio of

unity is a mathematical indication of the absence of a compression stage. The same applies to a heat exchanger; a heat exchange area of zero corresponds to absence of a heat exchanger. Using this representation, the four configurations of Figure 4.1 can be represented.

Table 4.1. Characterisation of different heat-integrated distillation column configurations.

Configuration	Internal heat integration		External heat integration	
	CR_{int}	$A_{int,\hat{n}}$	CR_{ext}	A_{ext}
CDiC	1	0 (all)	1	0
MVRC	1	0 (all)	>1	>0
HIDiC	>1	>0	0	0
SRVC	>1	>0	>1	>0

4.2.3 Indexing

It is more convenient to refer to tray numbers instead of stage numbers because stages describe trays, compressors, condensers and reboilers. The tray basis is therefore more intuitive in this context. When a compressor is added/removed during the design procedure, the stage numbers of certain trays are altered, whereas the tray numbers remain unchanged. A new set of indices are introduced by adding a circumflex on the indices introduced in Chapter 3. Hence, the tray number ($\hat{i}$) spans $\hat{i} = 1,2,\ldots,N_T$. The feed tray is $\hat{i} = \hat{N}_F$. Furthermore, the number of heat-integrated pairs (N_{ihx}) can be partitioned in N_{int} internal pairings and one external pairing. A pair of heat-integrated trays, $\hat{n}$, can be represented mathematically as a heat source tray, $\hat{r}(\hat{n})$, being paired with a heat sink tray, $\hat{s}(\hat{n})$. Thus, let $\hat{n} = 1,2,\ldots,N_{int}$, denote the $\hat{n}$'th pair of heat-integrated stages $\hat{r}(\hat{n})$ and $\hat{s}(\hat{n})$. The index $\hat{n}$ does not cover the condenser/reboiler type heat integration. The usage of the tray based indices is illustrated on an SRVC configuration in Illustration 3.3.

4.3 Design Method Overview

The conceptual design algorithm is illustrated in Figure 4.2. An overview is presented below and the steps are further elaborated in the following section. Step 1 requires the following input: (i) what is to be separated, (ii) the purity demands of the product stream(s), (iii) a formulation of the objective function that should direct the design to an optimal solution, and (iv) a minimum temperature driving force for heat integration. In Step 2, a conceptual design of the CDiC must be established by minimising/maximising the specified objective function in Step 1, item

Illustration 4.1. Introducing the tray basis notation for the CDiC and the SRVC from Illustration 3.3.
The tray basis indexing for the simple case of a CDiC and the SRVC is illustrated below:

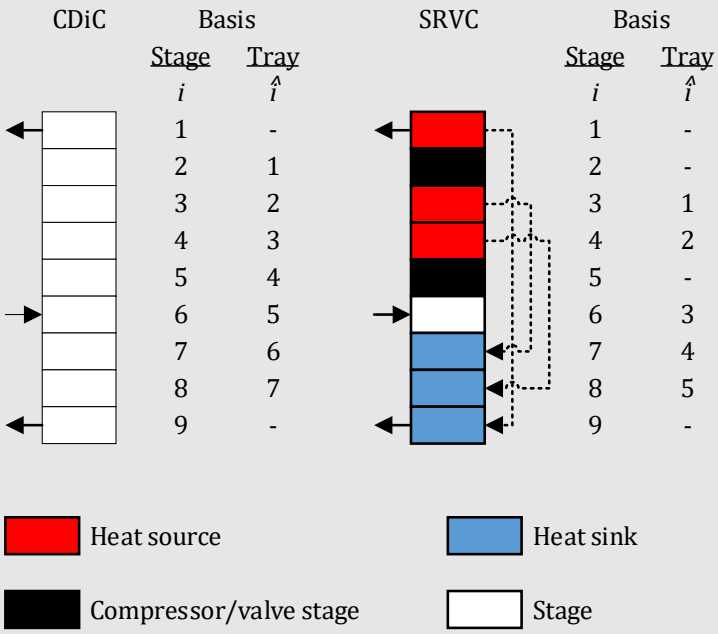

As illustrated, the adopted tray basis is visual. When conducting the simulation required for this method, simple relation are used to convert the tray basis to stage basis. For example, the total number of stages is $N_S = N_T + N_{cnd} + 1 + 1$, i.e. the sum of the total number of trays, the number of condensers, and the number of reboilers. In addition, the feed location N_F in stage basis is simply $N_F = \hat{N}_F + N_{cpr} + 1$, i.e. the sum of compressors plus one condenser provided that the compressors are only located above the feed stage.

(iii). In Step 3, the CDiC is converted into one of the considered configurations (Figure 3.1) by including either or both internal and external heat integration. In the following step, the remaining design degrees of freedom being the heat exchange area for each pairing (Step 4a), the total number of trays (Step 4b), and the pairing arrangement (Step 4c) are adjusted by iteration. In Step 5, column simulations are repeated as the compression ratio (*CR*) is adjusted (in Step 6) until a specified

minimum temperature gradient among the heat-integrated stage(s) is obtained by iteration. A column simulation means obtaining a converged simulation satisfying mass and energy balances and specified product purity constraints formulated in Step 1. In Step 7, the design objective function (specified in Step 1) is calculated and evaluated in Step 8, if further iterations must be carried out.

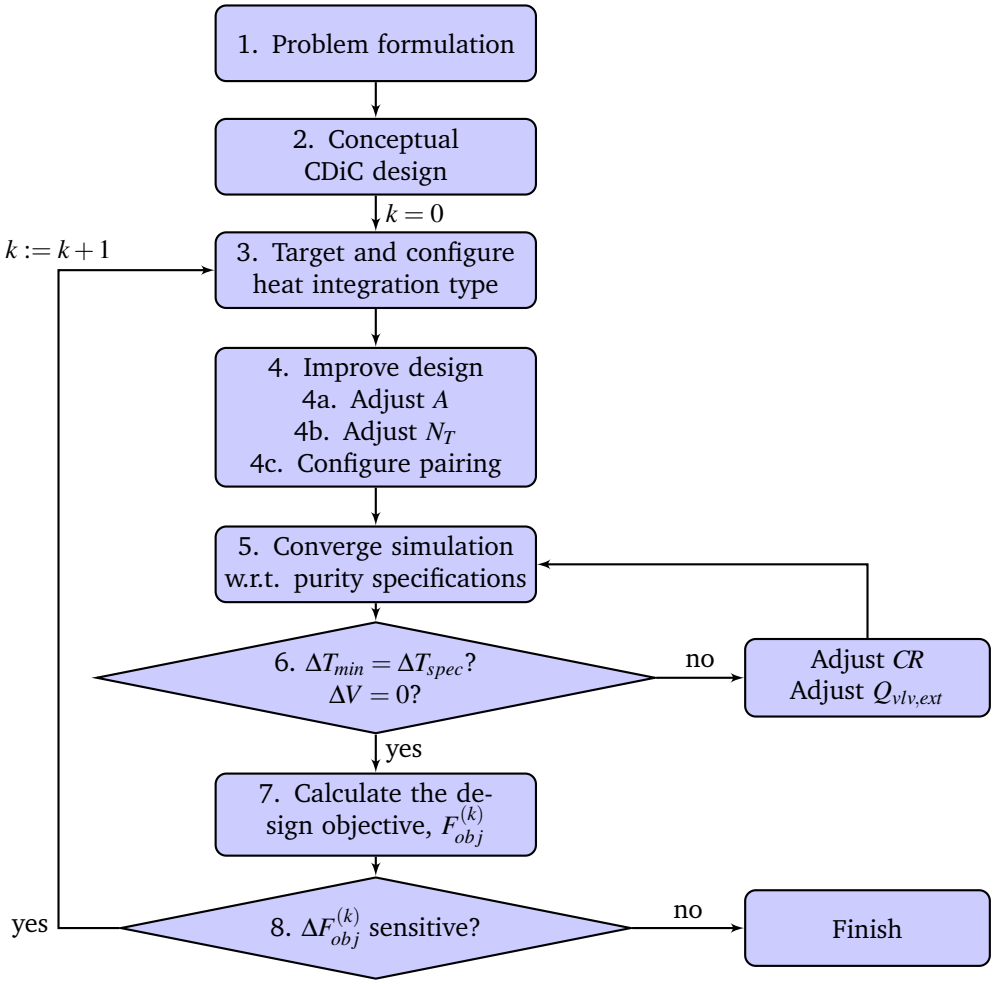

Figure 4.2. Conceptual design of a heat-integrated distillation column.

4.4 Detailed Description of the Design Method

This section provides a detailed description of the design method by describing all the required actions and the tools needed to use the method.

4.4.1 Step 1: Problem formulation

The feed stream(s) to be separated must be identified w.r.t. composition, pressure, and temperature such that no thermodynamic degrees of freedom remain. This can have influence on the available design methods of the CDiC. This design method only requires a CDiC design as explained in Step 2 and therefore relies on better established conventional methods. Along with a complete specification of the feed, the purity requirements of the distillate and the bottoms streams must be specified.

Step 1 requires a formulation of the design objective function. This objective function facilitates iterations as it both serves as a means to steer the design to a near-optimal solution, and as a stop criteria when a configuration becomes unfavoured according to the objective function. The total annualised cost is suggested as the design objective function because it represents a trade-off between the OPEX and the CAPEX.

Finally, a minimum temperature approach of $\Delta T_{spec} = 5\,\mathrm{K}$ is proposed.

4.4.2 Step 2: Conceptual CDiC design

The second step requires a design of a conventional distillation column, i.e. specification of the number of trays in the stripping section (N_{str}), the number of trays in the rectifying section (N_{rct}), a column pressure (here $P_{\hat{N}_F}$), the reflux ratio (L/D), and the boil-up ratio (V/B).

Typically the selection of distillation column pressure depends on a wide variety of factors, including possibility of plant-wide heat integration, availability of utilities (steam temperature, cooling water temperature) and so on. In this design method, the feed pressure has been chosen as the design variable as the feed stage resembles the top stage of the section with the lowest pressure in the HIDiC and the SRVC. After a stage pressure drop has been assumed (e.g. $0.7\,\mathrm{kPa}$), the column operating pressure, $P_{\hat{N}_F}$, must be selected in a defined pressure range being $P_{min} \leq P_{\hat{N}_F} \leq P_{max}$. The specification of P_{min} and P_{max} are important as they will affect the design of the heat-integrated distillation configurations with compressors. This pressure range is determined by the thermal stability of the components in the mixture to be separated, by the mechanical strength of the equipment, or by the temperature of the accessible cooling water. By default $P_{min} = 101.325\,\mathrm{kPa}$ and $P_{max} = \infty$ (unbounded).

Based on the obtained operating pressure and the product specification from Step 1, the Ponchon-Savarit method is adopted for binary mixtures and the Fenske-Underwood-Gilliland method is adopted for multicomponent mixtures [54]. As the design objective function is the TAC, this should be taken into account already in the CDiC design. Both methods require the reflux to minimum reflux ratio as input.

Thus the design is carried out as a one-dimensional optimisation procedure, where this ratio is manually adjusted until a minimum TAC is obtained. A minimum TAC is often resulted as CAPEX increases with an increasing number of stages, while the OPEX decreases as external utility requirements are reduced. In the end of Step 2, the iteration variable k is initialised as $k = 0$.

4.4.3 Step 3: Target and configure heat integration type

Two types of heat integration are possible; internal heat integration and external heat integration. Only one type can be targeted when Step 3 is considered. The following actions are required, depending on the targeted heat integration type:

- Internal heat integration: This results in the splitting of the two column sections. A compressor is added to the vapour exiting the stripping section, and a throttling valve is added to the liquid exiting the rectifying section. By doing this, additional design degrees of freedom are obtained: (i) the compression ratio ($CR_{int} = P_{\hat{N}_F-1}/P_{\hat{N}_F}$), (ii) how the stages are paired, (iii) the heat exchange areas for heat-integrated stage pairs, and (iv) the possibility for valve cooling. When targeting the internal heat integration, the variables CR, A, and Q_{vlv} of Figure 4.2 refer to the compressor (CR_{int}), the area ($A_{int,\hat{n}}$), and the valve cooling ($Q_{vlv,int}$), responsible for the internal heat integration respectively. These variable are initialised ($k = 0$) as $CR_{int} = 1$, and the pairing as in Table 4.2 with $A_{int,\hat{n}} = 0\,\mathrm{m}^2$, $\hat{n} = 1,2,\ldots,N_{int}$ and $Q_{int,vlv} = 0\,\mathrm{kW}$. In this way, a CDiC is maintained from a simulation perspective. The argument behind the initial pairing in Table 4.2 is based on the fact that the integration should be located as close as possible to the conventional utilities (condenser and reboiler). A numerical example of the initial pairing is provided in Illustration 4.2.

- External heat integration: The compressor and throttling valve are installed in the overhead vapour, exiting the top of the rectifying section, and the liquid reflux, respectively. By definition, the condenser is paired with the reboiler (according to Figure 4.1). Initialisation ($k = 0$) is carried out using $CR_{ext} = 1$, $A_{ext} = 0\,\mathrm{m}^2$, and $Q_{vlv,ext} = 0\,\mathrm{kW}$. When targeting the external heat integration, the variables CR, A, and Q_{vlv} refer respectively to the compression ratio (CR_{ext}), heat exchange area (A_{ext}), and the valve cooling ($Q_{vlv,ext}$) responsible for the external heat integration.

Table 4.2. Initialisation of the paired trays. Trays are counted from top.

Case	N_{int}	Energy source	Energy sink
$N_{rct} = N_{str}$	N_{rct}		
$N_{rct} \geq N_{str}$	N_{str}	$\hat{r} = [1,2,\ldots,N_{int}]^T$	$\hat{s} = [N_T + 1 - N_{int}, N_T + 2 - N_{int}, \ldots, N_T]^T$
$N_{rct} \leq N_{str}$	N_{rct}		

Illustration 4.2. Initial pairing in an HIDiC.
Consider a HIDiC with $N_T = 10$ with $\hat{N}_F = 4$. Hence, the HIDiC has three trays in the rectifying section $N_{rct} = 3$ and six trays in the stripping section $N_{str} = 6$. According to Table 4.2, the number of heat-integrated stages becomes $N_{int} = N_{rct} = 3$ as $N_{rct} \leq N_{str}$. As a result, the pairing becomes

$$\hat{r} = [1,2,\ldots,N_{int}]^T = [1,2,3]$$

and

$$\hat{s} = [N_T + 1 - N_{int}, N_T + 2 - N_{int}, \ldots, N_T]^T = [8,9,10]^T.$$

4.4.4 Step 4: Improve design

Here, the design is improved with respect to the defined objective function in Step 1. Three options for improving the design are proposed. The options are (a) adjust A, (b) adjust N_T, and (c) configure pairing. The options are ranked in decreasing priority. Only one option should be chosen per iteration loop. Furthermore, it is suggested to change a variable gradually in order to investigate the sensitivity in the objective function. The iterations are carried out manually. In the first encounter of Step 4 ($k = 0$), no improvements should be made, as the objective function must be evaluated in Step 7 for the current design.

4.4.5 Step 4a: Adjust A

The uniform heat transfer area approach is adopted, meaning $A_{int,n} = A_{int},\ n = 1,2,\ldots,N_{int}$. The magnitude of A_{int} is bound between zero and a maximum value, which leads a value of zero in one of the internal flow rates or the external duties. The magnitude of the changes in A in this step depends on the separation and the distillation column configuration. Assume that the maximum achievable heat exchange area A_{max} is given (estimation provided below), then the procedure for adjusting A is:

(i) Initialise $\beta = 0.30$

(ii) For $k = 1$, set $A^{(k)} = A^{(k-1)} + \beta A_{max}$

(iii) For $k > 1$, evaluate $\delta = \frac{\Delta F_{obj}^{(k-1)}}{A^{(k-1)} - A^{(k-2)}}$ for $\Delta F_{obj}^{(k-1)} = F_{obj}^{(k-1)} - F_{obj}^{(k-2)}$

a. If $\delta < 0$, set $A^{(k)} = A^{(k-1)} + \beta A_{max}$ (TAC reduced from previous iteration)

b. If $\delta > 0$, restore $A^{(k)} = A^{(k-1)}$ (TAC increased from previous iteration)

(iv) If an infeasible design is encountered ($A^{(k)}$ becomes too large)

a. Restore $A^{(k)} = A^{(k-1)}$

b. Set $\beta := 0.8\beta$

c. Repeat from (ii).

Here, $\Delta F_{obj}^{(k-1)}$ is the change in the objective function, caused by the previous iteration. This value can be obtained after the initialisation and one iteration (i.e. $k > 1$). The initial value and the factor in Step (iv)b can be chosen differently according to experience. Note that the maximum achievable heat exchange area (A_{max}) is used to express the step size and it does not directly impose a constraint on A. This is because the estimate of A_{max} does not necessarily reflect the real value. This approximation depends upon the type of targeted heat integration. In internal heat integration, the latent heat of the reflux flow or the boil-up flow dictate the maximum required area. For external heat integration, the external duties directly provides the estimate. These results can be summarised as:

$$A_{int,max} = \frac{\min(\Delta h_{vap,cnd} L, \Delta h_{vap,rbl} V)}{N_{int} U_{ihx} \Delta T_{spec}} \tag{4.1}$$

$$A_{ext,max} = \frac{\min(|Q_{cnd}|, |Q_{rbl}|)}{U_{ihx} \Delta T_{spec}} \tag{4.2}$$

where

$\Delta T_{spec} =$ the minimum specified temperature gradient as defined in Step 1 [K].

The maximum $A_{int,max}$ estimate in Eq. (4.1) is inspired by the minimum reflux ratio provided by Nakanishi et al. [118], while Eq. (4.2) reflects the fact that $A_{ext,max}$ is limited by external duties.

If needed, the uniform heat transfer rate approach can be used as iteration variable instead of A_{int}. However, this has not been adopted in this work.

4.4.6 Step 4b: Adjust N_T

Similar to varying the total number of stages for obtaining a trade-off between OPEX and CAPEX by minimising the TAC for a CDiC (Step 2), it is proposed to increase the number of heat-integrated stages by one in each column section in the same vertical height. These must be paired in order to reduce the required heat exchange area in the remaining stages. As for a CDiC, the column dimension should not exceed a certain height (typically a maximum of 100 m). Experience show that the optimal number of trays is usually 10-20% higher than that of a CDiC.

4.4.7 Step 4c: Configure pairing

The algorithm of Chen et al. [23] for reducing the number of internal heat exchangers can be directly incorporated in this design algorithm. Configuring the pairing should only be done if the cost of internal heat integration is significant (e.g. comprises more than 50% of the CAPEX).

4.4.8 Step 5: Converge simulation w.r.t. purity specifications

For fixed $A_{int,\hat{n}}$, A_{ext}, CR_{int} and CR_{ext}, Step 5 requires a column simulation similar to a CDiC simulation by simultaneously adjusting the reflux ratio, L/D, and the boil-up ratio, V/B, by iteration until the two purity specifications are satisfied.

4.4.9 Step 6: Satisfy minimum temperature driving force and vapour flow rate specifications

Increased pressure is used to elevate the temperature in the heat sources, i.e. the condenser and/or the rectifying section. The increase in temperature depends upon the employed compression ratio, CR, which is essential for obtaining the desired, positive temperature driving forces ($\Delta T_{\hat{n}} \geq 0$) in Eq. (3.29). Given the N_{int} internally heat-integrated pairs or the externally heat-integrated condenser/reboiler pair, a minimum temperature driving force must be defined as:

$$\Delta T_{min} = \begin{cases} \min\limits_{1 \leq \hat{n} \leq N_{int}} \left(T_{\hat{r}(\hat{n})} - T_{\hat{s}(\hat{n})} \right) & \text{(internal heat integration)} \\ T_{cnd} - T_{rbl} & \text{(external heat integration)} \end{cases} \tag{4.3}$$

The CR must be adjusted until following condition is satisfied:

$$\Delta T_{min} = \Delta T_{spec} \tag{4.4}$$

where

$\Delta T_{spec} =$ the minimum temperature driving force approach [K]

The initial guess of CR is based on an order of magnitude estimate, which applies to a binary mixture separated into pure components by distillation assuming similar heats of vaporisation. This order of magnitude estimate is:

$$CR = \alpha_{12} \tag{4.5}$$

where

$\alpha_{12} =$ the relative volatility [-]

For multicomponent mixtures, the relative volatility of the key components in top to the key component in the bottom can be employed when applying Eq. (4.5). The derivation is given in Appendix B.4.

The following rules apply for the adjustment of $CR = P_{out}/P_{in}$ in order to adjust ΔT_{min} in Eq. (4.4) based on the initial design pressures of the CDiC, and the pressure range specified in Step 2. The rules - in prioritised order - are:

(i) Reduce P_{in} while $P_{in} \geq P_{min}$

(ii) Increase P_{out} while $P_{out} \leq P_{max}$

Note the possibility of reducing the stripping pressure. This is beneficial in the HIDiC, as the CDiC operating pressure has been selected for enabling the use of cooling water.

The product of the internal and external compression ratios for any given configuration approximately satisfies Eq. (4.6). This relation can be useful in estimating the remaining compression ratio for the SRVC if one is provided.

$$CR_{int} CR_{ext} = \alpha_{12} \tag{4.6}$$

where

$CR_{int} =$ the compression ratio responsible for internal heat integration $[-]$

$CR_{ext} =$ the compression ratio responsible for the external heat integration $[-]$

As a part of Step 6, the required valve cooling for the external heat integration must obtained by adjusting $Q_{vlv,ext}$ until the flow rates of the vapour leaving and the vapour entering the tray below the compressor are equal:

$$V_1 - V_2 = 0 \tag{4.7}$$

When isenthalpic throttling of a liquid takes place, it flashes upon reaching a tray at a lower pressure condition (see Figure 4.3). This can have a significant impact on the economics as this formed vapour passes directly through the following tray and into the compressor. Therefore, cooling in external heat integration (e.g. the

MVRC) must be performed upon throttling the liquid by using $Q_{vlv,ext}$. $Q_{vlv,ext}$ has a similar magnitude of the compressor duty. The iterations of CR and $Q_{vlv,ext}$ can be combined in one step because they do not affect each other.

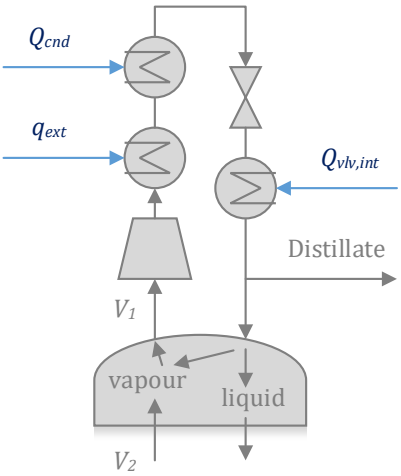

Figure 4.3. The fate of a throttled liquid in the MVRC. The amount of vapour from the throttled stream that joins the internal vapour flow in the tray depends on the amount of valve cooling.

4.4.10 Step 7: Calculate design objective (F_{obj})

This step contains an evaluation of the resulting design. The TAC is estimated based on the approach outlined in Section 3.4. One iteration loop is defined as the loop composed of Step 3 through Step 8 (Figure 4.2). The objective function sensitivity ($\Delta F_{obj}^{(k)}$) of iteration k, is defined as:

$$(\Delta F_{obj})^{(k)} = (F_{obj})^{(k)} - (F_{obj})^{(k-1)} \tag{4.8}$$

4.4.11 Step 8: ΔF_{obj} sensitive?

The stop criteria for any of the considered improvements in Step 4, is evaluated and additional iterations are required if the sensitivity of the objective function to the current design adjustment is sufficient. For F_{obj} =TAC, design improvements are obtained when $(\Delta F_{obj})^{(k)} < 0$, i.e. TAC is reduced. The stop criteria for the targeted improvement strategy becomes:

$$\left| \frac{(\Delta F_{obj})^{(k)}}{(F_{obj})^{(k-1)}} \right| \leq 0.01 \tag{4.9}$$

Table 4.3. Specifications for the separation of benzene/toluene.

Variable	Unit	Value
Components	-	Benzene/toluene
VLE Models (liquid/vapour)	-	Ideal/ideal
Feed flow rate	$\mathrm{mol\,s^{-1}}$	83.3
Composition	-	0.50
Feed pressure	kPa	101.3
Feed temperature	K	365.3
Distillate benzene composition	-	0.995
Bottoms benzene composition	-	0.005

Hence, if the relative change in the objective function caused by all investigated improvements is less than 1%, the final design is obtained.

4.5 Method Illustration

The method is exemplified on two case studies below. The case studies are a separation of benzene/toluene and a separation of a multicomponent mixture of aromatic compounds.

4.5.1 Separation of Benzene/toluene

A binary mixture of benzene/toluene is a candidate mixture for separation using a heat-integrated distillation column configuration. This time, the feed specifications from the example in Section 3.6 are employed and a design should be obtained with the proposed method. The design specifications are listed in Table 4.3. Initially the cases are illustrated, where a considered configuration is specified in advance. Hence, the resulting HIDiC, MVRC, and SRVC designs are presented. In the last example, a general approach is illustrated, where no specification on the desired configurations is made in advance. The objective function is F_{obj} =TAC and a minimum temperature approach of $\Delta T_{spec} = 5.0\,\mathrm{K}$ is used. The economic parameters are listed in Table 4.4 and no constraints are imposed on the objective function.

4.5.1.1 CDiC design

To select the column operating pressure, $P_{\hat{N}_F}$, the bubble-point pressure of the distillate is calculated giving 35 kPa. This suggests a total condenser is sufficient and an atmospheric column is preferred, i.e. $P_{\hat{N}_F} = 101.3\,\mathrm{kPa}$. In addition, the bubble point temperature of the bottom of the column (395.6 K) is below the pure component

Table 4.4. Model parameters.

Class	Parameter	Unit	Value
Internal heat exchanger	Heat transfer coefficient	$\mathrm{kW\,m^{-2}\,K^{-1}}$	0.60
General	Electricity price	$\mathrm{\$\,kWh^{-1}}$	0.14
	Steam ($P_{steam} > 200\,\mathrm{kPa}$)	$\mathrm{\$\,t^{-1}}$	$1.99 + 16.2(P_{steam} - 101.3\,\mathrm{kPa})^{0.05}$
	Cooling water (at 300 K)	$\mathrm{\$\,t^{-1}}$	0.080
	Year	-	2012
	Project life time	yr	5
	Service factor	-	0.904
	Materials	-	Carbon steel
Tray	Pressure drop	kPa	0.70
	Efficiency	-	0.80
	Flooding factor	-	0.80
	Void fraction	-	0.75
	Type	-	Sieve
	Spacing	mm	609.60 (24")
Condenser	Water temperature increase	K	5.0
	Heat transfer coefficient	$\mathrm{kW\,m^{-2}\,K^{-1}}$	0.60
	Type	-	Floating head
Reboiler	Heat transfer coefficient	$\mathrm{kW\,m^{-2}\,K^{-1}}$	1.420
	Difference between steam and reboiler temperature	K	10
	Type	-	Kettle reboiler
Compressor	Isentropic efficiency	-	0.80
	Motor efficiency	-	0.90
	Type	-	Centrifugal/motor

critical temperatures. The column pressure limits are assumed as $P_{min} = 101.3\,\mathrm{kPa}$ and $P_{max} = 1000\,\mathrm{kPa}$. Furthermore, a tray pressure drop of $0.70\,\mathrm{kPa}$ is assumed.

The required total number of stages and the feed location are estimated using the Ponchon-Savarit method for a given reflux ratio. The reflux ratio is adjusted until a minimum TAC was obtained, resulting in TAC$=1.50\,\mathrm{M\$\,yr^{-1}}$ with 19 equilibrium stages in the rectifying section (excluding condenser), and 18 equilibrium stages in the stripping section (including reboiler). The one-dimensional optimisation problem is illustrated in Figure 4.4. A tray column is adopted resulting in 19 trays in rectifying section and 17 trays in stripping section as the reboiler is an equilibrium stage. Simulation gives a reflux ratio of 1.45, a condenser duty of $Q_{cnd} = -3170\,\mathrm{kW}$ and $Q_{rbl} = 3240\,\mathrm{kW}$.

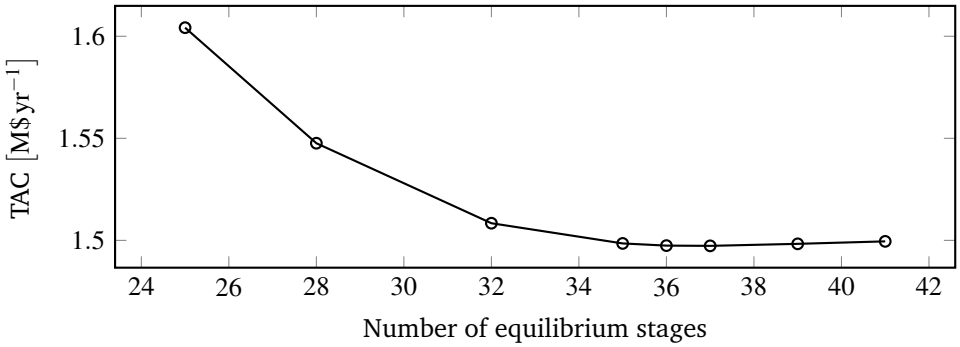

Figure 4.4. Design of CDiC based on TAC.

4.5.1.2 HIDiC Design

The base case CDiC design consists of a total condenser, 19 trays in rectifying section, 17 trays in stripping section, and a partial reboiler resulting in 36 trays in total. According to Step 3, a type of heat integration must be targeted and configured. In this example, internal heat integration is targeted, eventually resulting in a HIDiC design. A compressor and a valve are introduced above the feed tray. The internal heat integration is configured according to Table 4.2 such that as many trays in each section are heat-integrated. As a result, $N_{int} = 17$. All the trays in the stripping section are paired one by one with the first 17 trays in the rectifying section.

Initially, no improvements should be made in Step 4. Based on the initialisations of $A_{int} = 0\,\mathrm{m}^2$ and $CR = 1$, a simulation is carried out in Step 5. Here, a reflux ratio and a boil-up ratio are obtained such that the required purity specifications are satisfied. This simulated configuration is numerically identical to the CDiC simulated in Step 2. Evaluating the minimum temperature force $\Delta T_{min} = -22.5\,\mathrm{K}$ reveals that a significant temperature lift is required by the compressor. The compression ratio is altered in Step 6 until the condition in Eq. (4.4) is satisfied. An initial value of $CR_{int} = 2.4$ is used, corresponding to the relative volatility (Eq. (4.5)). In Step 2, the minimum allowed pressure was $P_{min} = 101.3\,\mathrm{kPa}$ and maximum allowable pressure was $P_{max} = 1000\,\mathrm{kPa}$. Since the stripping section pressure is already at its minimum pressure, the rectifying section pressure is increased in order to obtain the desired compression ratio. Iterations of the compression ratio are carried out (Steps 5-6) until the temperature condition in Eq. (4.4) is satisfied. Typically, the final compression ratio does not deviate strongly from this initial value. Therefore, the changes in CR are in the order of 0.1 down to 0.001. The dependency of ΔT_{min} on the changes in CR depends on the system considered and on the magnitude of

A. When $A > 0$, the pair location of ΔT_{min} (pinch) can move during iterations. This is the case for the separation of benzene/toluene. This observation is believed to be the reason for the failed attempt in automating this algorithm. For $A = 0\,\mathrm{m}^2$, a compression ratio of 2.13 results. The key design variables and the resulting TAC from the mentioned designs are listed in Table 4.5.

The maximum expected heat exchange area can be calculated using $U_{ihx} = 0.60\,\mathrm{kW\,m^{-2}\,K^{-1}}$ using Eq. (4.1):

$$A_{max} = \frac{31\,\mathrm{kJ\,mol^{-1}} \cdot 60.4\,\mathrm{mol\,s^{-1}}}{17 \cdot 0.60\,\mathrm{kW\,m^{-2}\,K^{-1}} \cdot 5\,\mathrm{K}} = 36.7\,\mathrm{m}^2$$

The procedure for improving the design by changing the heat exchange area through Step 4a is as follows: Based on $A_{int,max}$ the first improvement is $A^{(1)} = 0 + 0.30 \cdot 36.7\,\mathrm{m}^2 = 11.0\,\mathrm{m}^2$. Simulation in Step 5 and adjustments in CR are followed in Step 6 until $\Delta T_{min} = 5.0\,\mathrm{K}$. A reduction in TAC of 6% is achieved so more iteration should be followed. In the following iteration $A^{(2)} = 11.0\,\mathrm{m}^2 + 0.30 \cdot 36.7\,\mathrm{m}^2 = 22.0\,\mathrm{m}^2$ and a new compression ratio is obtained. These iterations are listed in Table 4.5. An infeasible design is encountered for $A^{(3)} = 33.0\,\mathrm{m}^2$, the change in A is reduced and the iterations are repeated. A maximum limit of A was achieved giving $A = 30.1\,\mathrm{m}^2$ and $CR_{int} = 2.49$. In this design, no reflux is required and thus L/D becomes zero. Furthermore, TAC=$1.76\,\mathrm{M\$\,yr^{-1}}$.

Proceeding, the number of trays (N_T) is incrementally increased by two in each section. These trays are added in the same vertical height and are heat-integrated with each other. The total number of stages is increased until a minimum TAC is obtained similar to the CDiC design. Each time the number of stages is increased, the pair and the determination of heat exchange area and compression ratio must be repeated. Only the cases, where A is maximised are shown in Table 4.5 (referred to as no reflux). These were found to give the lowest TAC.

The design with a minimum TAC ($1.72\,\mathrm{M\$\,yr^{-1}}$) has 48 trays in total and 23 pairings. At this point, a design of the HIDiC has been obtained with the simulation results of the procedure illustrated in Table 4.5. The duties in the final HIDiC design are $Q_{cnd} = -1213\,\mathrm{kW}$, $Q_{rbl} = 1124\,\mathrm{kW}$ and $E = 402\,\mathrm{kW}$, corresponding to a reduction in the reboiler duty of 65%. Note however, that the TAC is increased compared to the CDiC.

As can be seen, the TAC is minimum when the heat exchange area is maximised leading to no external reflux condition ($L/D = 0$). An important observation is that when the total number of stages is increased, the HIDiC design becomes infeasible for unchanged A and CR. This is due to the fact that the total heat exchange area ($N_{int}A$) increases since N_{int} increases.

Table 4.5. Design Progress of the HIDiC.

A m^2	CR -	N_{rct} -	N_{str} -	ΔT_{min} K	OPEX M\$ yr^{-1}	CAPEX M\$	TAC M\$ yr^{-1}	Note
0	1	19	17	-22.5	1.33	0.840	1.50	Step 2
0	2.13	19	17	5.0	1.69	2.12	2.12	Step 3-6
11	2.13	19	17	4.27	1.42	2.79	1.98	Step 4a
11	2.188	19	17	5.0	1.41	2.83	1.98	Step 4a-6
22	2.188	19	17	3.55	1.24	3.24	1.89	Step 4a-6
22	2.369	19	17	5.0	1.17	3.38	1.84	Step 4a-6
33	2.369	19	17	3.79	1.03	3.75	1.78	Step 4a-6
30.1	2.46	19	17	4.7	1.02	3.73	1.77	Step 4a
30.1	2.49	19	17	5.0	1.01	3.76	1.76	Step 5-8 (no reflux)
24.8	2.48	21	19	5.0	1.00	3.71	1.74	Step 4b-8 (no reflux)
21.5	2.47	23	21	5.0	0.98	3.70	1.72	Step 4b-8 (no reflux)
19.3	2.46	25	23	5.0	0.97	3.73	1.72	Step 4b-8 (no reflux)
17.5	2.45	27	25	5.0	0.96	3.77	1.72	Step 4b-8 (no reflux)

4.5.1.3 MVRC Design

Starting from the CDiC in Step 2, the external heat integration is targeted in Step 3. The same procedure as for the HIDiC is followed, where A and CR now refer to external heat exchange area and compression ratio. The maximum heat exchange area is estimated using Eq. (4.2):

$$A_{max} = \frac{\min([3170, 3240])\text{kW}}{0.60\,\text{kW}\,\text{m}^{-2}\,\text{K}^{-1} \cdot 5\,\text{K}} = 1057\,\text{m}^2 \tag{4.10}$$

The development of the MVRC is illustrated in Table 4.6. Rather than using an increase in A of $0.3A_{max}$, a value of $0.5A_{max}$ is used for illustration as to reduce the number of rows in Table 4.6. Note that ΔT_{min} does not change with the heat exchange area, thereby simplifying the iteration steps.

In Step 5-6, a valve cooling for the MVRC of $Q_{vlv} = -450\,\text{kW}$ has been obtained. Without valve cooling, simulation shows that the vapour flow rate is raised from $102\,\text{mol}\,\text{s}^{-1}$ to $121\,\text{mol}\,\text{s}^{-1}$. Adiabatic throttling is assumed, which leads to a significant increase in the compressor duty without valve cooling, compared to the case with valve cooling (from 435 kW to 515 kW). This difference becomes zero using valve cooling with the provided duty.

Step 4b is investigated by adjusting the total number of trays but the optimal CDiC appears to result in the optimal MVRC.

The final MVRC design has a reboiler duty of $Q_{rbl} = 454\,\text{kW}$ and a condenser duty for condensing the vapour resulting from throttling of $Q_{vlv} = -450\,\text{kW}$. The TAC of the MVRC is lower than both that the CDiC and that of the HIDiC.

Table 4.6. Design Progress of the MVRC. Valve cooling is used in all cases with $Q_{vlv} = -450\,\text{kW}$.

A m^2	CR -	N_{rct} -	N_{str} -	ΔT_{min} K	OPEX $\text{M\$\,yr}^{-1}$	CAPEX M\$	TAC $\text{M\$\,yr}^{-1}$	Note
0	1.00	19	17	-38.3	1.35	0.87	1.52	Step 2-3
0	3.20	19	17	5.0	1.90	2.61	2.42	Step 4a-8
528.5	3.20	19	17	5.0	1.24	2.99	1.84	Step 4a-8
950.0	3.20	19	17	5.0	0.72	3.06	1.34	Step 4a-8
945.0	3.26	21	19	5.0	0.73	3.12	1.36	Step 4b-8

4.5.1.4 SRVC Design

Based on the nominal HIDiC with 19 trays in the rectifying section and 17 trays in the stripping section, the estimated required compression ratio for external heat integrations is based on Eq. (4.6):

$$CR_{ext} = \alpha / CR_{int} = 2.4/2.13 = 1.13$$

The progression of the SRVC design is illustrated in Table 4.7 in a similar representation of the previous design examples of HIDiC and MVRC. However, now the distinction between internal and external heat transfer becomes inevitable, and as a result the OPEX and CAPEX are omitted. It has been found that it is more economic to use the final HIDiC design for the starting point for the SRVC as the TAC is lower with 25 and 23 trays in the rectifying and stripping sections, respectively.

4.5.1.5 No Prior Configuration Specification

Using the general representation of a heat-integrated distillation column in Figure 4.1, it is possible to generate designs of any of the four configurations CDiC, HIDiC, MVRC, and SRVC. The generation of each configuration can be carried out by incrementally converting one configuration to another. This extends the search space for benchmarking studies and facilitates intermediate designs. An incremental design simulation study of the separation of benzene/toluene is illustrated in Figure 4.5. In this case, the TAC is depicted, but any specified function or constraint can be used as long as models are available. Starting from the one CDiC design, the remaining configurations are obtained by the following procedure: The MVRC (moving

Table 4.7. Design Progress of the SRVC.

A_{int} m^2	CR_{int} -	A_{ext} m^2	CR_{ext} -	N_{rct} -	N_{str} -	$\Delta T_{min,int}$ K	$\Delta T_{min,ext}$ K	TAC M\$ yr^{-1}	Note
30.1	2.49	0	1	19	17	5	-3.4	1.76	HIDiC design
30.1	2.49	0	1.13	19	17	5	3.8	1.80	CR_{ext} estimate
30.1	2.49	0	1.23	19	17	5	5	1.85	Step 5-8
30.1	2.49	356	1.23	19	17	5	5	1.45	4a-8 (no reboiler duty)
19.3	2.46	374	1.31	25	23	5	5	1.41	4b-8 (no reboiler duty)

left from the CDiC) is obtained by using the maximum possible external heat exchange area from Eq. (4.2) such that $T_{min} = T_{cnd} - T_{rbl} = 5\,\mathrm{K}$. When moving right from the CDiC in Figure 4.5, internal heat integration is considered and the internal heat exchange area is gradually increased until no reflux condition is achieved. In the transition from the HIDiC to the SRVC, external heat integration is considered, while maintaining A_{int} and CR_{int}. The external heat transfer area is gradually increased until its maximum. In the SRVC designs to the far right in Figure 4.5, the internal heat transfer areas are gradually decreased. Note that the conversion of the HIDiC into an SRVC could similarly be carried out using a smaller internal heat exchange area. In this example, the influence of changing the total number of trays has not been investigated.

4.5.2 Multicomponent Aromatic Separation

This example serves as a demonstration of the proposed algorithm on a multicomponent system. Provided the specifications in Table 4.8, the distillate and bottom product compositions can be estimated when assuming all toluene will leave the column in the distillate. The conventional distillation column design is provided by Wakabayashi and Hasebe [160], so the proposed design procedure can be applied directly. Atmospheric pressure is found to be suitable for the separation. The CDiC has 30 plates in the rectifying section and 25 plates in the stripping section. Hence, following the recommendations for pairing for internal heat integration in Table 4.2, 25 plates in each section should be paired. All the plates in the stripping

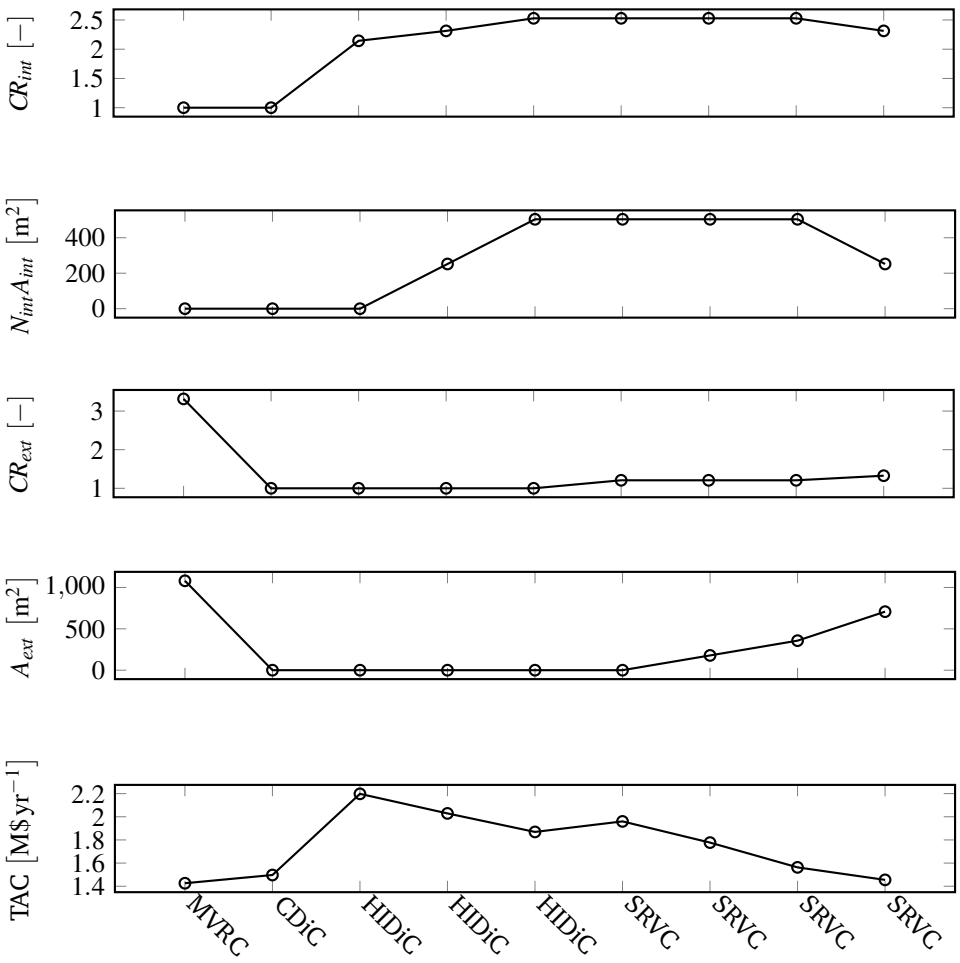

Figure 4.5. Continuous transition between configurations determined by compression ratios and heat exchange areas. *CR* denotes the compression ratio while $N_{int}A_{int}$ is the total area of heat exchangers for internal heat integration and A_{ext} is the external heat transfer area. The horisontal axes represent distillation column configurations.

section are paired with the first 25 plates of the rectifying section (counting from the top) such that they are in the same vertical height, resulting in the HIDiC.

The obtained configurations are summarised in Figure 4.6, in which the capital expenditures (CAPEX) is illustrated along with the operating expenditures (OPEX). The obtained results are compared to the novel HIDiC configuration called the 4-HIDiC, which is based on the Extended Ponchon-Savarit method [159] and has only four internally heat-integrated pairs. The 4-HIDiC outperforms the HIDiC as

Table 4.8. Feed specification of the separation of a multicomponent aromatic mixture.

Specification	Property	Unit	Value
Feed flow rate		kmol s^{-1}	55.6
Feed composition	Toluene (C7)	-	0.005
	Ethylbenzene (C8)	-	0.1
	p-Xylene (C8)	-	0.11
	m-Xylene (C8)	-	0.25
	o-Xylene (C8)	-	0.145
	Cumene (C9)	-	0.01
	n-Propylbenzene (C9)	-	0.022
	m-Ethyltoluene (C9)	-	0.158
	1,2,3-Trymethylbenzene (C9)	-	0.2
Liquid fraction		-	1
Feed pressure		kPa	101.3
Feed temperature		K	421.3
Stage pressure drop		kPa	0.70
Top purity specification	C9	-	0.007
Bottom purity specification	C8	-	0.015

a result of decreased CAPEX by using fewer, but larger, heat exchangers and lower duty of the compressor. At the same time the MVRC outperforms the HIDiC as well as the 4-HIDiC . The lowest OPEX but the highest CAPEX is obtained in the SRVC. Thus, in order to fully benefit from heat integration among stages one would prefer the SRVC, or alternatively stay with the MVRC. This suggests that tools for design decisions must be broadly applicable and be able to consider various alternatives in order to be versatile. It is not enough to merely compare HIDiC to CDIC. A framework, which is flexible and on a general form, is useful for such studies.

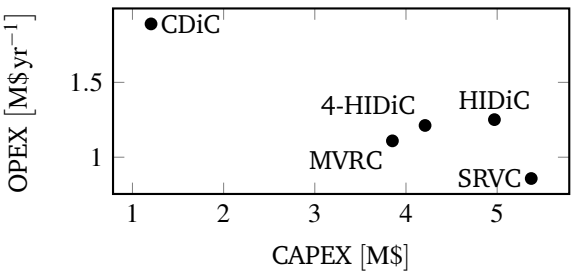

Figure 4.6. Illustration of the trade-off between OPEX and CAPEX for five configurations performing a separation of a multicomponent aromatic mixture.

4.6 Design Considerations and Discussion

A discussion of the design method is presented in this section. The discussion is based on qualitative considerations, simple models and the case study of benzene/-toluene, provided in section 4.5.1. The base case HIDiC design, resulting directly from the CDiC design, is employed.

4.6.1 Stripping Section Pressure

The selection of stripping section pressure, which is referred to as the feed stage pressure ($P_{\hat{N}_F}$), has been given little attention in the HIDiC design literature. The optimal design value of $P_{\hat{N}_F}$ is assumed to be a trade-off between operating and capital costs. The contributions to the operating costs are the addition of external utility (condenser and reboiler duties) and the cost of electricity for compression. A low pressure is favoured in terms of minimising the quality of the heat supplied as reboiler duty (e.g. reduced steam pressure). However, the compressor duty is a dominant factor in both OPEX and CAPEX in many cases. For example in the separation of benzene/toluene, the compressor accounts for 53% OPEX and 45% CAPEX. The compressor duty in Eq. (2.2) can be written for an as:

$$E = \frac{1}{\eta_{is}} V_{in} T_{in} C_P^V \left(CR^{R/C_P^V} - 1 \right) \tag{4.11}$$

where

$V_{in} =$ vapour flow through compressor [mole/s]
$T_{in} =$ temperature at compressor inlet [K]
$C_P^V =$ constant pressure heat capacity of vapour [$\mathrm{kJ\,mol^{-1}\,K^{-1}}$].

As it appears in Eq. (4.11), the compressor duty is proportional to the inlet temperature, which is determined by the operating pressure ($P_{\hat{N}_F}$). Furthermore, the compressor duty increases with the compression ratio to the power of R/C_P^V. This exponent is relatively small for larger molecules (e.g. monoatomic gas $R/C_P^V = 2/3$, diatomic $R/C_P^V = 2/5$ etc.). Hence, based on the inlet temperature, a low operating pressure is preferred in order to minimise the compressor duty. When the minimum temperature driving force (ΔT_{spec}) is infinitesimally small, the compression ratio can be approximated by the relative volatility for the MVRC (Eq. (4.5)). The temperature dependency of the relative volatility is typically small. Therefore, the influence of the operating pressure on the relative volatility, and hence the compression ratio in Eq. (4.11), can be neglected. It can be concluded, that the impact of the operating pressure on the inlet temperature (T_{in}) is more significant than the impact on the compression ratio.

It is found that indeed the compressor duty increases with the feed stage pressure, when investigating its impacts on the compressor duty, the CAPEX, and the OPEX by carrying out simulations for benzene/toluene (see Table 4.9). In addition, it is found in agreement with the analysis that the CAPEX increases with feed stage pressure as well. However, the opposite effect is observed for the OPEX. This is due to the fact that the required compression ratio increases as the fixed stage pressure drop becomes more significant when the operating pressure is lowered. As a result of this analysis, a low operating pressure in the low pressure section is desired. For this reason, it is proposed to reduce the pressure of the low pressure side of a compressor as first priority in step 6 (Figure 4.2). Furthermore, these results illustrate the importance of considering stage pressure drops when evaluating the economic performance of a heat-integrated configuration.

Table 4.9. Sensitivity on compressor duty, CAPEX and OPEX of column operating pressure when applying the design method on the separation of benzene/toluene.

$P_{\hat{N}_F}$	CR_{int}	T_{in}	E	CAPEX	OPEX
kPa	-	K	kW	M$	M$ yr^{-1}
75	2.59	357	388	3.87	1.03
101	2.45	367	394	3.92	1.02
125	2.37	374	401	4.00	1.02

4.6.2 Interplay Between Design Variables

When thermodynamic feasibility is realised (i.e. the minimum temperature driving force is positive), the expression for the internal heat transfer rate (Eq. (3.29)) states that an increase in ΔT by 1 unit corresponds to an increase in A by 1 unit. Increases in both OPEX and CAPEX result when ΔT is increased by compression. However, the increase in ΔT happens for all the pairs simultaneously. On the contrary, A must be increased for all pairings, which might result in a significant increase in CAPEX for a large number of heat-integrated stages. Thus, a trade-off between CAPEX and OPEX is not only reflected in choosing number of stages vs. reflux ratio as in CDiC but also generating a temperature driving force by increasing CR without increasing it excessively.

The relation between compression ratio and heat exchanger areas is investigated by carrying out HIDiC designs for obtaining reflux free operation of the separation of benzene/toluene. The result is illustrated in Figure 4.7. As expected, (Eq. (4.5)), compression ratios below the relative volatility have significant impact on the required total heat exchange area, since certain pairings have low heat transfer rates due to small temperature gradients. On the other hand, when the heat exchange

area is small, the compressor must compensate and provide large temperature gradients and thus a large compression ratio is required.

The optimal solution has both a low *CR* and a low *A* in figure 4.7. Hence, it is reasonable to base a the design on the minimum temperature driving force. If this is set reasonably low, the optimal trade-off of *CR* and *A* is expected to be achieved. Based on this analysis, it has been found useful to use the heat exchange area and the temperature driving force as design variables.

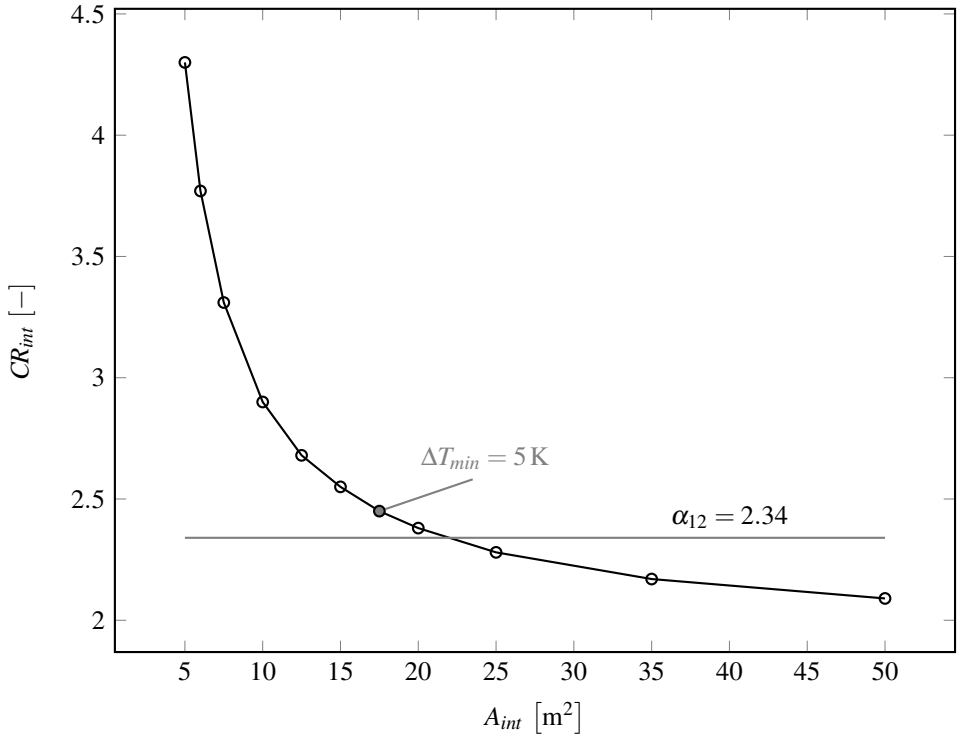

Figure 4.7. Relation between compression ratio and heat exchange area for the separation of benzene/toluene.

4.6.3 Constant Area Versus Constant Heat Duty

As indicated in Figure 4.1, the heat exchange area must be specified for each internal heat exchanger corresponding to every pair. Since the temperature driving forces vary along the column, constant heat transfer duties can lead to an uneven distribution of heat transfer area as illustrated in Figure 4.8. An alternative strategy is to design a constant heat transfer area for all stages. The total required heat

exchange areas are obtained is section 4.5.1 as $438\,m^2$ and $427\,m^2$ for respectively the constant heat transfer area ($A_{int,\hat{n}} = 30.1\,m^2,\ \hat{n} = 1,2,\ldots,N_{int}$) and for the constant internal heat transfer rates ($q_{\hat{n}} = 89.6\,kW,\ \hat{n} = 1,2,\ldots,N_{int}$ with $A_{int,\hat{n}}$ from Eq. (3.29)). The contribution of the internal heat exchangers for the constant heat exchange area approach on the CAPEX is 1.41 M$, while for the constant heat duty it is 1.35 M$. However, when considering the compressor duty, the constant heat duty design has a 7% higher compressor duty (from 394 to 421 kW) leading to a higher OPEX. The comparison between these strategies shows that (i) the total heat exchange area (3%) and the CAPEX (5%) is slightly larger for the constant heat exchange area approach, (ii) a strong coupling exists between the required heat exchange areas and the column temperature profile for the case of constant heat duties, (iii) from a practical view, however, it is simpler and most likely cheaper when only small variations in the heat exchange areas occur, and (iv) it appears more economically favoured to adopt a constant heat exchange area approach in terms of OPEX. It has been confirmed by others [154] that the constant heat exchange area approach for the separation of benzene/toluene results in the best economic performance.

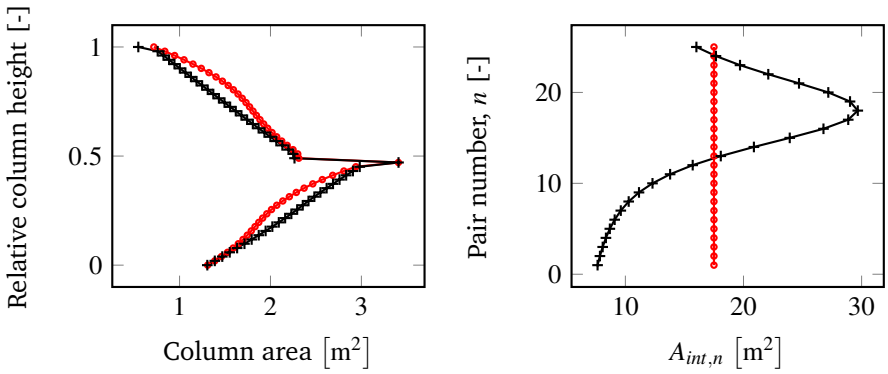

Figure 4.8. Estimated column area and the required heat exchange area for no reflux operation for two cases: Constant heat exchange area vs. constant heat duty for each pair. Legends: Constant A_{int} (—○—), Constant q_{int} (—+—).

4.6.4 Method Benchmarking

A summary of the resulting HIDiC designs, based on different methods for a separation of methanol/water into 90% top and 10% bottom purities, is given in Table 4.10. The methods have different purposes, which is reflected in the results. A remarkable difference among the illustrated design results are the obtained com-

pressor duties (E). The reason for this is that the considered methods do not adopt the minimum temperature approach. This approach can not be used in graphical methods due to the strong coupling with the mass and energy balances of the complete design. If the model framework developed in this work is available, it is claimed that proposed method can be conducted with less efforts than the considered graphical methods.

Table 4.10. Comparison of HIDiC designs using proposed method and literature methods.

Method	Design variables						
	N_{rct}	N_{str}	E	Q_{rbl}	$\sum q_n$	N_{ihx}	A_n
	-	-	kW	kW	kW	-	m^2
Proposed method	6	5	109.3	1428	662	4	26.7, 26.7, 26.7, 26.7
Ponchon-Savarit method [56]	5	4	261.2	1317	600	4	18.2, 10.8, 9.0, 8.4
Extended Ponchon-Savarit method [159]	3	6	250	1232	888	3	18.3, 19.5, 14.4

4.7 Conclusion

A design method that can cover the three heat-integrated distillation configurations is proposed; the mechanical-vapour recompression column (MVRC), the heat-integrated distillation column (HIDiC), and the secondary reflux and vaporisation column (SRVC). Following advantages of the design algorithm are claimed:

- It provides a systematic means of selecting the additional design variables of the MVRC, the HIDiC, and the SRVC
- It provides a systematic means of evaluating the most economically preferred configuration among the MVRC, the HIDiC, and the SRVC
- It is simple and intuitive
- It can explicitly cover multicomponent mixtures

However, on present form, an fully optimal design is not guaranteed.

In this chapter, the presented method has been successfully applied on the separation of two binary separations (benzene/toluene and methanol/water) and a multicomponent separation.

Chapter 5

Techno-Economic Feasibility Analysis

Techno-economic feasibility analyses are carried out for the heat-integrated distillation columns (HIDiC) separating benzene/toluene and propylene/propane. The techno-economic feasibility analysis address the physical realisation of heat transfer equipment, the possibility of entrainment flooding and weeping in different column arrangements, and benchmarking of alternative distillation configurations w.r.t. economy. A simple relation for evaluating the requirement for compressor vapour inlet super-heating is derived. Furthermore, an extensive economic feasibility analysis is presented covering ten industrial mixtures with different physical properties, to be separated in the conventional distillation column, the HIDiC, the mechanical vapour recompression column (MVRC), and the secondary reflux and vaporisation column (SRVC). It was found that the normal boiling point difference was correlated with the major design variables and performance indicators. In terms of the total annualised cost (TAC), the MVRC is the preferred configuration for the majority of the considered configurations. However, the HIDiC is the preferred configuration with respect to operating expenditures (OPEX) when the normal boiling point difference is below 10 K. The uncertainties in the OPEX for an MVRC and an HIDiC were quantified by the means of uncertainty analysis, and the most significant parameters on the OPEX uncertainty were identified for the two configurations.

The uncertainty and sensitivity analysis results were presented at the Distillation and Absorption conference [T. Bisgaard, J.K. Huusom, and J. Abildskov. Impact on model uncertainty of diabatization in distillation columns. *Proceedings of Distillation and Absorption*, pages 909–914, 2014].

5.1 Introduction

The conventional distillation column (CDiC), the mechanical vapour recompression column (MVRC), the heat-integrated distillation column (HIDiC), and the secondary reflux and vaporisation column (SRVC) are studied in this chapter. The economic feasibilities of the considered configurations are often linked to either the relative volatility [51, 48], the normal boiling point difference [86], or the resulting temperature profiles of the columns [142]. It is the aim of this chapter, to identify the links between the mixture properties, the design variables, and the economic feasibilities for the considered configurations. If such links exist, it is desired to use the physical properties of the mixtures to be separated as a means of determining the economically preferred distillation column configuration. Such an approach is similar to the framework proposed by Jaksland et al. [72] for conventional unit operations. The present analysis has been restricted to cover mainly binary mixtures; one multicomponent mixture is covered. However, the mixtures are carefully selected in order to cover a variety of the following physical properties:

- Difference in normal boiling points.
- Mean heat of vaporisation.
- Phase equilibrium behaviour (ideal, non-ideal, azeotropic etc.)

The phase equilibrium behaviour is used as a means to cover different resulting column temperature profiles rather than adjusting the product purities. Furthermore, the economic feasibility of a configuration is based on both the total annualised cost (TAC) and the operating expenditures (OPEX).

5.2 Methods and Tools

The considered case studies and the methods, used throughout this chapter, are briefly explained in this section. The terms technical feasibility and economic feasibility are defined.

5.2.1 Technical Feasibility

The following criteria must be satisfied in order to achieve technical feasibility of a given heat-integrated distillation configuration:

- Feasible solution: The first criteria for technical feasibility requires that a feasible solution to the distillation column model exists, given the feed and the product specifications.

- Realisation of internal heat transfer: The distillation column internals must have sufficient space for the installation of internal heat panels. The hydraulic feasibility indicator (HFI; Section 3.4) is suitable for this purpose. When HFI>1, the column can accommodate the specified heat exchange area by installing heat panels in the stripping section.
- Column capacity: Based on an estimated column cross sectional area, the possibility of using conventional sieve trays is investigated. Hence, no entrainment flooding or weeping must occur. In addition, the various column profiles of flows, heat transfer rates, temperatures and so on, provides valuable insights in the technical feasibility.
- Feasibility of compression: Condensation must not occur inside a compressor. Hence, the possibility of condensation of the compressed vapour must be investigated, and appropriate actions must be taken if it is the case. One action that can prevent condensation in the compressor is to superheat the compressor inlet vapour.

The above criteria are explained in detail in the following subsections.

5.2.1.1 Column Capacity

Based on conventional methods for investigating column tray capacities [57], the impact of introducing internal heat transfer is investigated w.r.t. entrainment flooding or weeping. Below the weeping point, at which the vapour flow rate is too low compared to the design flow rate, the required vapour dispersion can not be achieved. Furthermore, the vapour flow is not sufficient to prevent the liquid from passing through the perforations. The latter can be avoided by using bubble cap or valve trays. Entrainment flooding occurs when the vapour flow rate is too high. With increasing vapour flow rate, an increasing amount of liquid is entrained until a point where flooding occurs. As a result, the downcomers are filled and the column feed will be carried up through the column with the vapour. A large increase of pressure drop across the column is observed. Mathematically, flooding is avoided when $0 \leq u_{\text{crit},i} - u_i$, i.e. when the vapour velocity is below the flooding velocity (u_{crit}). Weeping is avoided when $0 \leq (H_\sigma + H_0) - (H_\sigma + H_0)_{crit}$, corresponding to the fact that the liquid head must not exceed the pressure drop from vapour passing through the perforations (H_0) and through the liquid due to surface tension (H_σ). The critical pressure drop $(H_\sigma + H_0)_{crit}$ depends on the liquid head, which is the sum of $h_{oW} + h_W$ [57].

The column sizing methods are usually based on the idea of avoiding flooding at nominal operation, but due to constructional implications of introducing inter-

nal heat transfer this might influence the tray capacities. One constructional implication is the gradually decreasing stripping section cross sectional area and the gradually increasing rectifying section cross sectional area from the column top to the bottom. As a result, the impacts of different design decisions (e.g. constant tray area vs. gradually changing tray area) on the technical feasibility are investigated. Three concentric arrangements are considered (Table 2.3):

- An arrangement, where the cross sectional area is constant throughout the column.
- A concentric arrangement with gradually changing cross sectional areas of the rectifying and stripping sections. The rectifying section constitutes the inner (tube) column and the stripping section constitutes the outer (shell) column.
- A 3-partition concentric arrangement, which is divided in three different partitions of equal height. The cross sectional areas of the inner rectifying section are different in each partition as a means to simplify the concentric arrangement. In this work, the cross sectional area of a partition is given by the mean value of the obtained cross sectional areas of the trays within the partition.

Table 5.1. Sieve tray dimensional parameters provided total cross sectional area.

Parameter	Unit	Value
Hole diameter	mm	6.35
Weir height	mm	50
Downcomer area per total area	-	0.1
Perforations area per active tray area	-	0.1
Tray thickness per hole diameter	-	0.72

5.2.1.2 Feasibility of Compression

The feasibility of compression (FOC) is defined by:

$$\mathrm{FOC} = \frac{\eta_{is}\bar{\lambda}}{\bar{C}_P^V \bar{T}_{nb}} - 1 \tag{5.1}$$

The FOB is derived by evaluating the change in the saturated temperature relative to the temperature change caused by isentropic compression. Condensation, due to compression, is undesired. Thus, the temperature increase, caused by compression, should be larger than the increase in the dew point temperature. This translates into a condition that states that FOC should be greater than zero. If the FOC is below zero, condensation might occur. This issue is not widely considered

in the HIDiC literature. However, Harwardt and Marquardt [51] address this issue by consistently preheating the compressor inlet by 5 K in all their case studies. The contribution of this preheater is considered as negligible compared to the total operating expenditures. However, it is essential for the realisation (technological feasibility) to investigate whether or not preheating is required.

5.2.2 Economic Feasibility

Economic feasibility is achieved if the total annualised cost (TAC) of a given configuration is equal to or lower than that of a CDiC. This is a simple definition as it is also important to analyse the capital and operating expenditures individually. Therefore, a different definition of the economic feasibility is also investigated, which requires that the operating expenditures (OPEX) of a given configuration are lower than that of a CDiC.

The payback period (PBP) is a complimentary indicator of the economic feasibility to the TAC. It is defined relative to the CDiC and thus represents the additional payback period of the additional investment:

$$\mathrm{PBP} = \frac{\mathrm{CAPEX}_{\mathrm{config}} - \mathrm{CAPEX}_{\mathrm{CDiC}}}{\mathrm{OPEX}_{\mathrm{CDiC}} - \mathrm{OPEX}_{\mathrm{config}}} \tag{5.2}$$

A simple equation for evaluating the economic feasibility of heat pump-assisted distillation columns was proposed by Pleşu et al. [130]. They used the analogy of a heat engine working between hot and cold reservoirs on a heat pump distillation column, in which separation was produced rather than work. In such a system, the efficiency of Carnot can be obtained based on the heat reservoir temperatures. They proposed a ratio of resulting work over the required energy investment is defined below [130]:

$$Q/W = \frac{T_{hk}\frac{D}{F}\bar{\lambda}}{T_{lk}^2\left[\Delta s_B + \frac{D}{F}(\Delta s_D - \Delta s_B) - \Delta s_F\right]} - \frac{T_{hk}^2}{T_{lk}(T_{hk} - T_{lk})} \tag{5.3}$$

where

$\Delta s_i =$ entropy of mixing of feed (F), distillate (D), or bottoms (B) [kJ mol^{-1} K^{-1}] (these are evaluated by using the relations in Table 3.1)

$T_{lk} =$ normal boiling point temperature of light key component [K]

$T_{hk} =$ normal boiling point temperature of heavy key component [K]

$\bar{\lambda} =$ geometric mean heat of vaporisation [kJ mol^{-1}]

The Q/W ratio represents the amount of energy units saved per energy unit provided for the heat pump. Hence, Q/W can take both negative and positive values. Pleşu et al. [130] propose a minimum value of 10 in order to obtain economic feasibility, which reflects a electricity cost to steam cost ratio of five and a Carnot

efficiency of two. Note that the geometric mean heat of vaporisation has been used rather than the distillate heat of vaporisation. It is assumed that this extension can describe the HIDiC as well as the heat pump-assisted distillation column, for which the expression was originally developed [130]. For a binary separation $D/F = (x_D - z)/(x_D - x_B)$.

5.2.3 Uncertainty and Sensitivity Analysis

An uncertainty analysis is carried out in order to quantify the uncertainty in the operating expenditures (OPEX) of a given configuration when the model parameters and the economic parameters are uncertain. Furthermore, a sensitivity analysis is employed in order to identify the parameters that cause the uncertainty in the OPEX. These are essential considerations when the economic feasibility of configurations is evaluated. The underlying theories for the uncertainty and sensitivity analysis are briefly stated in this section.

5.2.3.1 Monte Carlo Simulation

Any model can be represented in the general form:

$$\dot{\mathbf{x}} = \mathbf{f}(\mathbf{x}, \mathbf{u}, \boldsymbol{\theta}) \tag{5.4}$$

$$0 = \mathbf{h}(\mathbf{x}, \mathbf{u}, \boldsymbol{\theta}) \tag{5.5}$$

$$\mathbf{y} = \mathbf{g}(\mathbf{x}, \mathbf{u}, \boldsymbol{\theta}) \tag{5.6}$$

where

$\dot{\mathbf{x}} =$ the state derivative of length $N_{\mathbf{x}}$
$\mathbf{x} =$ the state variable vector of length $N_{\mathbf{x}}$
$\mathbf{u} =$ the input vector with length $N_{\mathbf{u}}$
$\boldsymbol{\theta} =$ the model parameter vector with length $N_{\boldsymbol{\theta}}$
$\mathbf{y} =$ output vector with length $N_{\mathbf{y}}$

The model parameter vector can be divided in two $\boldsymbol{\theta} = [\boldsymbol{\theta}^*, \boldsymbol{\theta}_*]^T$, where $\boldsymbol{\theta}_*$ represents the uncertain parameters of the parameter vector, while $\boldsymbol{\theta}^*$ represents the certain parameters.

Let $i = 1, 2, \ldots, N_{\mathbf{y}}$ denote the index of the model output, let $j = 1, 2, \ldots, N_{\boldsymbol{\theta}_*}$ denote the index of the uncertain parameter, and let $p = 1, 2, \ldots, N_p$ denote the Monte Carlo discretisation point. Hence, the model uncertainty can be evaluated by the Monte Carlo Method [102], in which the expectation and variance of the

model output are approximated by the following expressions:

$$\mu_i = \mathbf{E}(\mathbf{y}_i) \approx \frac{1}{N_p} \sum_{p=1}^{N_p} \mathbf{y}_i \tag{5.7}$$

$$\boldsymbol{\sigma}_i^2 = \mathbf{var}(\mathbf{y}_i) \approx \frac{1}{N_p - 1} \sum_{p=1}^{N_p} [\mathbf{y}_i - \mathbf{E}(\mathbf{y}_i)]^2 \tag{5.8}$$

If a sufficiently large sample size (N_p) is chosen, the sample space has been sufficiently covered, these estimates become good approximations to the real values. The sample space is discretised in points denoted by, p, and the Latin Hypercube Sampling technique [53] is used to effectively cover the uncertain parameter space.

5.2.3.2 Standardised Regression Coefficients

The propagation of the uncertainties associated with the individual uncertain parameters can be determined by the standardised regression coefficients (SRC). These are obtained by fitting a first order linear multivariate model of the uncertain parameters to the model output [145]:

$$y_{reg,i} = a_i + \sum_j b_{ij} \theta_{*,ij}$$

$$\beta_{ij} = \frac{\sigma_{\boldsymbol{\theta}_j}}{\sigma_{\mathbf{y}_i}} b_{ij}$$

The SRC (β_{ij}) can take values between [-1,1]. A value closer to 0 means least significance on the output. In addition, sum of the squared SRC must equal one for a successful linear model. Hence, the relative magnitude of β_{ji}^2 between the uncertain parameters $j = 1, 2, \ldots, N_{\boldsymbol{\theta}_*}$ can be interpreted as the relative significance on the output i.

5.2.3.3 Model Reduction

Due to the large number of required model evaluations (depending on N_p) when carrying out Monte Carlo simulations, a simplified model of the one presented in Chapter 3 is used. The simplified model is obtained by introducing additional assumptions:

- Constant molar overflow, meaning that changes in sensible heats have been neglected and mixtures have constant heats of vaporisation.
- Saturation pressures are described using the Clausius-Clapeyron equation instead of Eq. (3.8).

- Physical properties are no longer dependant on temperature, pressure and composition. This also implies a constant relative volatility.
- Ideal, binary mixtures.

The model variables are classified according to Eqs. (5.4)-(5.6):

$$\mathbf{x} = (x_1, ..., x_{N_S})^T \tag{5.9}$$

$$\mathbf{u} = (P_F, CR, L_{cnd}, V_{rbl}, F, z)^T \tag{5.10}$$

$$\boldsymbol{\theta} = (\lambda, T_{nb,1}, \Delta T_{nb}, \Delta P, U_{ihx}, A, C_P^V, S_{water}, S_{steam}, S_{electricity}, N_{rct}, N_{str})^T \tag{5.11}$$

$$\mathbf{y} = (\text{OPEX}) \tag{5.12}$$

where

$T_{nb,1} =$ normal boiling point temperature of light component [K]
$\Delta T_{nb} =$ normal boiling point temperature difference of components [K]
$\Delta P =$ Tray pressure drop [kPa]

The obtained model is similar to the one proposed by Huang et al. [60] if pressure drops were included, if the Antoine correlation was replaced by the Clausius-Clapeyron equation, and if column sections of different sizes were allowed.

5.3 Feasibility Indicators – Observations and Expectations

The selection of industrial binary separations are listed in Table 5.2. Both the Q/W ratio in Eq. (5.3) and the feasibility of compression in Eq. (5.1) are estimated and listed in the table. Some clear trends are observed: (i) The high Q/W ratios are observed for the mixtures with low relative volatilities meaning potential economic feasibilities, (ii) the FOC is negative for the mixtures comprised of large molecules as the heat capacities are high, which means that condensation due to compression might be a risk, and (iii) no significant relation between heats of vaporisation, Q/W and FOC are present. According to the Q/W estimates, mixtures with a relative volatility below 1.83 are expected to be economically feasible.

Table 5.2. Feasibility indicators of industrially relevant, binary mixtures. The list of mixtures and their relative volatilities are obtained from Seader et al. [137]. The mixtures are sorted according to increasing relative volatility. The physical properties are taken from NIST [120]. The estimation of Q/W is based on following separation: $x_D = 1 - x_B = 0.995$ and $z = 0.5$, while $\eta_{is} = 0.80$ in the FOC. The mean physical properties are represented by geometric mean values.

Mixture components Light/Heavy	α -	ΔT_{nb} K	$\bar{T}_{nb}$ K	$\bar{\lambda}$ kJ mol^{-1}	$\bar{C}_P^V$ kJ mol^{-1} K^{-1}	Q/W -	FOC -
1,3-Butadiene/vinylacetylene	1.16	7.5	272.3	23.6	0.00764	28	-0.1
Vinyl acetate/ethyl acetate	1.16	4.5	347.9	36.1	0.1061	66	-0.2
m-Xylene/o-xylene	1.17	4.7	414.6	41.5	0.1291	78	-0.4
Isopentane/n-pentane	1.30	8.1	305.1	25.6	0.1195	29	-0.4
Isobutane/n-butane	1.35	11.0	267.4	21.2	0.09757	16	-0.4
Ethylbenzene/styrene	1.38	9.7	414.1	42.4	0.1237	33	-0.3
Propylene/propane	1.40	5.5	228.3	16.1	0.06880	34	-0.2
Methanol/ethanol	1.44	13.7	344.6	40.2	0.05360	14	0.7
Water/acetic acid	1.83	18.0	382.1	45.4	0.04876	11	1.0
Ethylene/ethane	1.87	15.6	176.6	14.6	0.4745	4	0.4
Acetic acid/acetic anhydride	2.02	20.8	401.5	46.7	0.07945	7	0.2
Toluene/ethylbenzene	2.15	25.5	396.3	38.9	0.1149	6	-0.3
Propane/1,3-butadiene	2.18	37.5	249.1	18.7	0.07664	1	-0.2
Ethanol azeotrope/water	2.21	21.7	362.2	41.4	0.04943	5	0.9
Isopropanol/water	2.23	17.7	364.2	42.4	0.05785	9	0.6
Benzene/toluene	3.09	30.5	368.2	35.4	0.09246	3	-0.2
Methanol/water	3.27	35.4	355.0	38.8	0.04063	0	1.2
Cumene/phenol	3.76	30.0	439.7	50.9	0.1242	5	-0.3
Benzene/ethylbenzene	6.79	56.0	380.3	37.3	0.1025	-1	-0.2
Hydrogencyanide/water	11.2	74.2	334.0	31.8	0.05158	-2	0.5
Ethylene oxide/water	12.68	88.2	326.1	32.2	0.04197	-2	0.9
Formaldehyde/methanol	16.7	83.8	292.9	30.2	0.03949	-3	1.1
Water/ethylene glycol	81.2	97.3	419.0	51.0	0.05406	-3	0.8

5.4 Case Studies

Two case studies representing two classes of mixtures are presented: A wide-boiling mixture of benzene/toluene and a close-boiling mixture of propylene/propane.

5.4.1 Benzene/toluene

The separation of benzene/toluene is commonly considered a representative separation for illustrating the concepts of e.g. the HIDiC. The boiling point difference between the two components is 30.5 K as listed in Table 5.2. Therefore, the mixture is considered as a wide-boiling mixture. This mixture has a large difference in normal boiling points, which is reflected in the low $Q/W = 3$. According to the preliminary feasibility analysis, the separation of benzene/toluene is not expected to be economically feasible.

5.4.1.1 Conceptual Design

The designs of the four configurations (CDiC, MVRC, HIDiC, and SRVC) are already provided in Section 4.5.1. This section presents a detailed analysis of the technological and economic aspects of the internal heat integration. Therefore, this section mainly concerns the HIDiC, but a complete benchmark study is carried out for all the four configurations.

5.4.1.2 Technical Feasibility

The tray mole fractions, tray temperatures, and internal flow rates are shown in Figure 5.1 of an HIDiC along with the ones of a CDiC. As expected, the liquid and vapour flow rates are almost constant for the CDiC throughout the column, except at the feed location. In the HIDiC, the liquid and vapour flows gradually increases until a maximum is reached in the transition between the column sections. The mole fraction profile is significantly different in the HIDiC than in the CDiC. The shape of the CDiC mole fraction profile is caused by a pinch point as the operating point is close to the minimum reflux condition. The HIDiC has a more even composition profile due to internal heat integration [43]. The difference in the composition profiles are reflected in the temperature profiles. Furthermore, a temperature lift of 29 K, provided by the compressor, is illustrated in the temperature profile.

The estimated total tray cross sectional areas for each tray in a CDiC is approximately constant (Figure 5.2). In contrast, the variations of the internal flows in the HIDiC (Figure 5.1) causes significant variation in the total tray cross sectional area

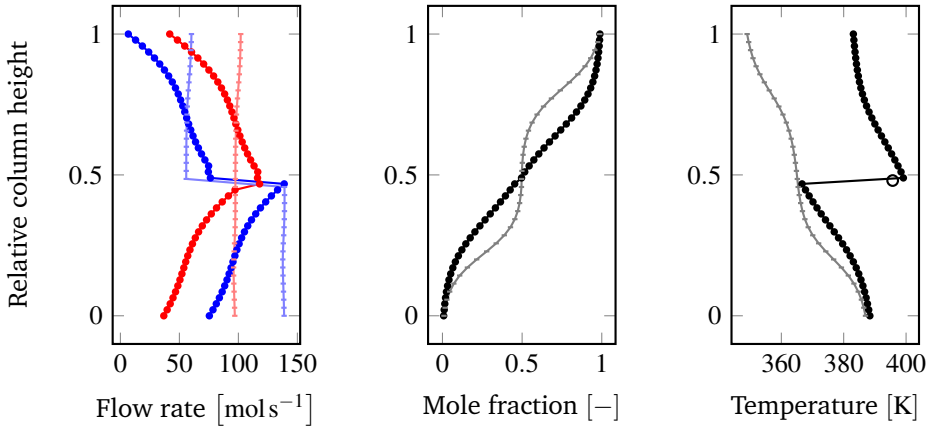

Figure 5.1. Tray internal flow rates, benzene mole fractions, and tempeartures of the HIDiC and the CDiC separating benzene/toluene. Legend: HIDiC: Mole fraction and temperature (—•—), liquid flow rate (—•—), vapour flow rate (—•—), temperature outlet of compressor (○). CDiC: Mole fraction and temperature (——), liquid flow rate (——), vapour flow rate (——).

profile in Figure 5.2. When combining the total tray cross sectional area of the trays that are heat-integrated, an approximately uniform combined total tray cross sectional area is achieved. This observation favours the concentric arrangement. The HFI is calculated and plotted in Figure 5.3. Based on the HFI profile, it can be concluded that the specified heat exchange areas (19.3 m^2 for each pair) can be realised as HFI>1 for almost every pair. In addition, the temperature driving forces seem reasonable compared to typical specifications in conventional heat exchangers.

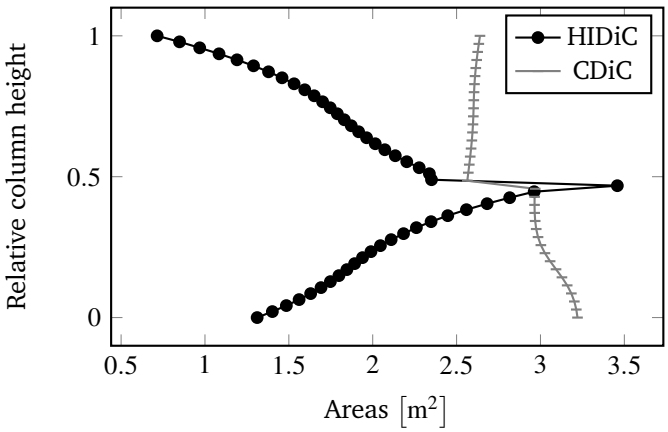

Figure 5.2. Required total tray areas for a HIDiC and a CDiC for the separation of benzene/toluene.

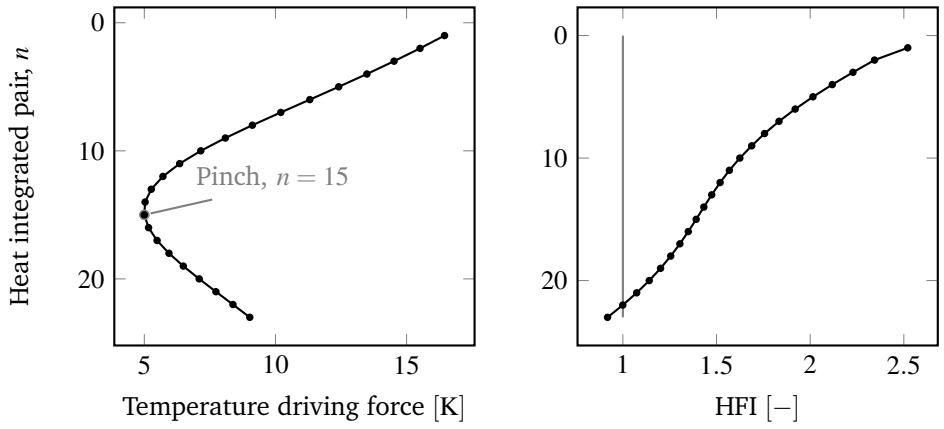

Figure 5.3. The temperature driving forces among heat-integrated pairs and the corresponding hydraulic feasibility indicator (HFI) for the separation of benzene/-toluene. Physical realisation of the specified heat exchange area ($A_{int} = 19.3\,\mathrm{m}^2$) is possible for HFI>1.

Ideally the column area profiles would follow that of Figure 5.2 for both the CDiC and the HIDiC. A column with a uniform cross sectional area is commonly used for the CDiC. An investigation of the possibility of simplifying the HIDiC structure is conducted. Figure 5.4 illustrates the implications of the three different arrangements (concentric, 3-partition concentric, uniform area) on the column capacity w.r.t. entrainment flooding and weeping. The results show that the concentric and the 3-partition concentric column arrangements are feasible. The uniform area column is not feasible because weeping is predicted in the top of the column. Weeping can be avoided by using other tray specifications or by using valve or bubble-cap trays. However, valve or bubble-cap trays take up more space inside a tray, and therefore reduce the available space for the required heat panels.

The feasibility of compression was reported for benzene/toluene in Table 5.2. Based on geometric mean pure component parameters the value is FOB=-0.2. By retrieving the properties of the inlet vapour stream from the simulation results and using these in Eq. (5.1), the FOB becomes:

$$\mathrm{FOB} = \frac{0.80 \cdot 29.62\,\mathrm{kJ\,mol^{-1}}}{0.1218\,\mathrm{kJ\,mol^{-1}\,K^{-1}} 366.7\,\mathrm{K}} - 1 = -0.4695$$

Hence, the same conclusion is resulted as the calculation based on the pure component properties. Because FOB is negative, it is expected that increasing the pressure of the saturated vapour, by means of isentropic compression, will result in a subcooled vapour. The obtained compressor outlet temperature from simulation agrees with the result; the temperature of the vapour outlet of the compressor is 396 K as

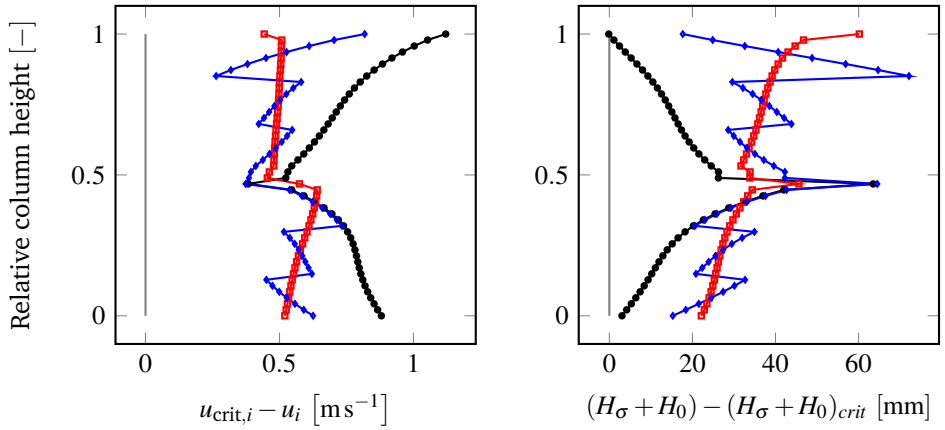

Figure 5.4. Column capacity investigation for flooding and weeping for three different column arrangements separating benzene/toluene. Legend: Constant column area (—•—), gradual changing area (—▫—), and 3-partitions arrangement (—⋄—). Problems with column capacity are predicted when values are below 0, which is illustrated with the vertical line (——).

indicated in Figure 5.1. Performing a *Py*-flash calculation of the compressor outlet vapour, a temperature of 400 K is obtained corresponding to the dew-point temperature. As the dew-point temperature is above the outlet temperature, the vapour is subcooled and condensation might occur. This observation is in accordance with the conclusion based on the FOC indicator. Even though the required duty to increase the compressor inlet temperature is low, this subject is rarely addressed in the HIDiC literature. The duties of raising the compressor inlet temperature by 5 K or 10 K are 67 kW and 135 kW, respectively. These values correspond to 6% and 12% of the reboiler duties in the HIDiC design, respectively. Because other minor costs are ignored in the economic model (e.g. electricity for pumping), the compressor preheating is not accounted for in evaluating the OPEX of the HIDiC separating benzene/toluene. As the compressor outlet temperature is among the highest temperatures in the column profile (Figure 5.1), the compressor preheating can not be realised by heat integration within the HIDiC.

5.4.1.3 Configuration Benchmarking

Key performance indicators of four distillation column configurations (CDiC, MVRC, HIDiC, and SRVC) are reported in Table 5.3. Even though the economics performance indicators are expected to be the most critical factor in deciding a preferred configuration, the increasing attention on environmental aspects, such as water and energy efficiency, make such factors increasingly important. This example clearly

illustrates the complexity and the necessity of proper benchmarking of the distillation configurations alternatives. For the separation of benzene/toluene, it is found that the MVRC is the preferred configurations w.r.t. TAC. However, a higher thermodynamic efficiency is obtained in the SRVC, while the water consumption is also the lowest. All the heat-integrated configurations suffer from a significant increase in CAPEX compared to the CDiC. An interesting observation is that the compressor duty is lowest for the HIDiC among the configurations employing compressors. The observation that the MVRC is the economically preferred configuration in terms of TAC is in agreement with the conclusions from similar studies [51]. However, not all literature agree on this fact (Table 2.6). Furthermore, this example illustrates the importance of considering multiple alternative configurations rather than only benchmarking e.g. the HIDiC against the CDiC.

Table 5.3. Performance indicators for the separation of benzene/toluene.

Performance indicator	Unit	Configuration			
		CDiC	MVRC	HIDiC	SRVC
Total trays	-	36	36	48	48
Second-law efficiency	-	0.153	0.356	0.296	0.416
CAPEX	M$	0.840	3.06	3.73	4.27
OPEX	M$ yr^{-1}	1.33	0.723	0.969	0.557
TAC	M$ yr^{-1}	1.50	1.34	1.72	1.41
PBP	yr	-	3.7	8.0	4.4
Water consumption	Mg yr^{-1}	4367	623	1668	74
HFI	-	-	0.92	0.92	
Hot utility	kW	3239	454	1124	0
Cold utility	kW	3172	-453	-1213	-54
Electricity	kW	0	435	402	447
Total integrated area	m^2	0	950	444	818

The equipment costing method provides additional information on the cost contribution of each of the equipment types for the distillation columns, i.e. columns, tray stacks, heat exchangers, and compressors. These contributions of the individual equipment are illustrated in Figure 5.5. It is clear that the dominating expense in the MVRC, the HIDiC, and the SRVC is the compressor, whereas the installation of 23 internal heat exchangers is of similar magnitude as the compressor cost in the HIDiC. In all the heat-integrated configurations, the gain from investing electrical energy is larger than the economic associated with the more expensive electricity. All heat-integrated distillation configurations reduce the energy consumption significantly.

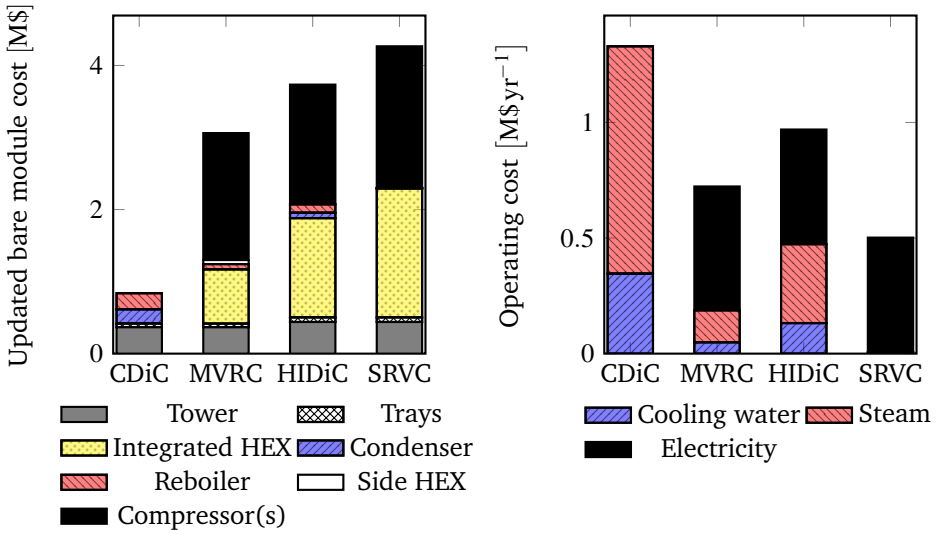

Figure 5.5. Breakdown of CAPEX and OPEX of different configurations separating benzene/toluene.

5.4.2 Propylene/propane

The temperature difference of the propylene/propane mixture is 5.5 K and the predicted $Q/W = 34$. This separation is considered relatively difficult due to its low relative volatility (approximately 1.40), but it is an important industrial separation.

5.4.2.1 Conceptual Design

The normal boiling points of propylene and propane are 225.46 K and 231.11 K, respectively, and hence the column operating pressure must be above atmospheric pressure. The bubble-point pressure of the distillate consisting of 99.5% propylene at 320 K is 2000 kPa. The temperature is selected such that cooling water can be used rather than a refrigerant. Therefore, it is assumed that the feed pressure is 200 kPa while the remaining feed specifications are the same as the ones reported in Table 5.7. Based on the Ponchon-Savarit method, a CDiC design was obtained with TAC=5.00 M\$ yr^{-1}, carried out in a distillation column with 94 trays in the rectifying and 96 trays in the stripping section. A column this large is not realistic to construct in one tower. Therefore, two separate columns must be constructed, i.e. a rectifying column and a stripping column, leading to a significant impact on the CAPEX. A reflux ratio of 18.4 is required and therefore the internal flow rates are large.

A remark on the simulation perspective is that due to the large number of stages,

and the fact that this system is modelled using an equation of state for both liquid and vapour phases (SRK), the convergence is time consuming. This application clearly illustrates the usefulness of using the BP Boiling method for generation of an initial guess (Step 6 in the model framework in Figure 3.4). In Matlab, 1541 equations are solved simultaneously in order to obtain a column simulation.

The design procedure described in Chapter 4 is followed and the designs of the CDiC, the MVRC, and the HIDiC are listed in Table 5.4. The number of trays was not altered as the CDiC design already contains an unreasonably large number of trays. Note that the feed stage pressure was reduced as a means to increase *CR* in the HIDiC, while the rectifying section pressure almost remained constant. Therefore, cooling water can still be used in the condenser. The SRVC is not included as a reboiler duty of zero was obtained in the HIDiC and hence no further heat integration is possible.

Table 5.4. Design specifications for the separation of propylene/propane.

Configuration	A_{int} m^2	CR_{int} -	A_{ext} m^2	CR_{ext} -	P_{N_F} kPa	N_{rct} -	N_{str} -	TAC $M\$\,yr^{-1}$
CDiC	0	1	0	1	2000	94	96	5.01
MVRC	0	1	2710	1.41	2000	94	96	3.87
HIDiC	40.1	1.37	0	1	1500	94	96	5.60

5.4.2.2 Technical Feasibility

The flow rate, mole fraction, and temperature profiles of the HIDiC separating propylene/propane are shown in Figure 5.6. The trends in the column profiles for the separation of propylene/propane are similar to those of the separation of benzene/toluene. As mentioned in the conceptual design of the CDiC, a large reflux ratio is required, hence the large molar flow rates, which exceed $1000\,mol\,s^{-1}$ (around $50\,kg\,s^{-1}$). The mole fraction profiles of the CDiC and HIDiC are similar as the ratio between liquid to vapour flow rates are similar in both configurations.

The temperature driving forces and the HFI are plotted for all the heat integrated pairs in Figure 5.7. The HFI becomes negative for the HIDiC because the assumptions behind the derivation of the HFI do not hold. The main assumption that causes the negative HFI relates to the downcomer. The required area of the stripping section is near zero due to the low required vapour flow. As the downcomer is assumed to take up 10% of the stripping section area, the estimation of its area can no longer be done using a rectangle, which is the underlying assumption. If the lower pairs are disregarded, placing heat fins inside the trays can provide sufficient heat change area. For the lower pairs, heat fins could be installed in

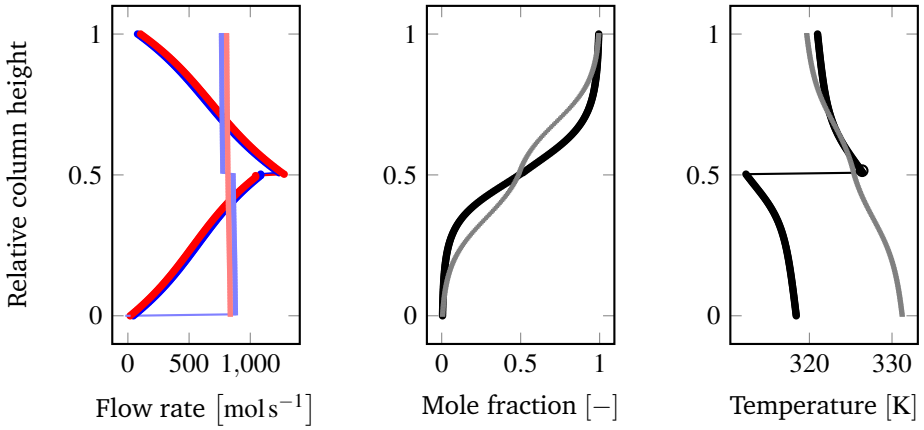

Figure 5.6. Tray internal flow rates, propylene mole fractions, and tempeartures of the HIDiC and the CDiC separating propylene/propane. Legend: HIDiC: Mole fraction and temperature (—•—), liquid flow rate (—•—), vapour flow rate (—•—), temperature outlet of compressor (○). CDiC: Mole fraction and temperature (——), liquid flow rate (——), vapour flow rate (——).

the rectifying section as this is not considered in the expression for HFI. But the overall conclusion from the HFI considerations is that the specified heat exchange area is not unreasonably large. Thus, realising the specified internal heat transfer is considered as being technically feasible.

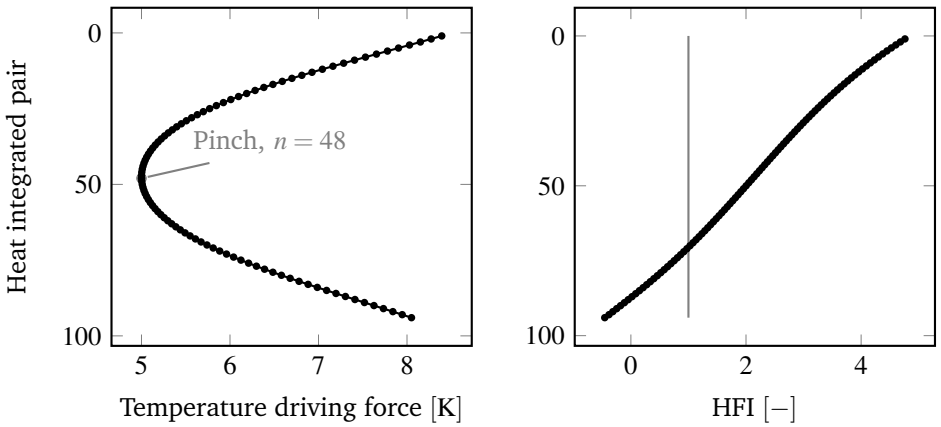

Figure 5.7. The temperature driving forces among heat integrated pairs and the corresponding hydraulic feasibility indicator (HFI) for the separation of propylene/propane. Physical realisation of the specified heat exchange area (A_{int} = 40.1 m^2) is possible for HFI>1.

The concentric arrangement is feasible, since neither entrainment flooding nor

weeping was predicted. The uniform area and the 3-partition concentric arrangements are infeasible (not illustrated). However, a concentric column with single-pass trays operates close to weeping condition. Olujic et al. [158] employed four-pass trays in a similar column, which might enhance the performance of the trays. The predicted compressor outlet temperature is 326.4 K and the predicted dew point temperature of the compressor outlet is 326.6 K. Therefore, compression is not feasible without preheating of the inlet vapour, which agrees with the observation using the FOB (FOB=-0.2). In this case, the required duty for increasing the compressor inlet temperature by 5 K is in the order of 500 kW. Again, the temperature of the distillate(321.9 K) and the bottoms (318.4 K) are below the compressor outlet temperature, and it not possible to obtain this duty by heat-integration.

5.4.2.3 Configuration Benchmarking

With respect to TAC (Table 5.5), the MVRC is the most favourable configuration, but when considering only the OPEX, a large potential exists for the HIDiC. The CAPEX is significantly larger in the HIDiC than those of the remaining configurations as a result of the 92 installed heat exchangers (see Figure 5.8). However, the OPEX is actually lower for the HIDiC as reboiler duty can be completely avoided. Yet, the compressor duty is higher in the HIDiC. This is caused by the higher vapour throughput in the compressor. The payback periods of both the MVRC and the HIDiC seem within reasonable limits. Furthermore, an additional configuration, the SIHIDiC, is introduced. The SIHIDiC is described below.

Table 5.5. Performance indicators for the separation of propylene/propane. The SIHIDiC is resulted by configuring pairing by using the approach of Chen et al. [23].

Performance indicator	Unit	Configuration			
		CDiC	MVRC	HIDiC	SIHIDiC
Second-law efficiency	-	0.0534	0.0876	0.0781	0.0730
CAPEX	M$	4.82	9.36	19.2	11.6
OPEX	M$ yr^{-1}	4.04	2.00	1.76	1.88
TAC	M$ yr^{-1}	5.01	3.87	5.60	4.20
PBP	yr	-	2.2	6.3	3.1
Water consumption	Mg yr^{-1}	13474	4260	1701	1852
HFI	-	-	-0.54	0.022	
Hot utility	kW	9793	1796	0	0
Cold utility	kW	-9787	-2584	-1247	-1357
Electricity	kW	0	952	1306	1392
Total integrated area	m^2	0	2515	3765	3450

It is clear that a distillation column performing the separation of propylene/propane

constitutes a significant investment. The estimated CAPEX of the column itself is almost five million US dollars due to the requirement of two tall and wide columns with a cross sectional area of around $10\,m^2$ and a high operating pressure. In the heat-integrated configurations, the large required internal flow rates lead to a large internal heat transfer area and therefore significant contributions to the CAPEX. The breakdown of the CAPEX and OPEX is presented in Figure 5.8, which reveals that over 50% of the CAPEX for the HIDiC is caused by the 94 installed internal heat exchangers. The OPEX of the MVRC and the HIDiC are significantly lower that that of the CDiC.

Figure 5.8 reveals that if improvements can be performed on the HIDiC design in order to reduce the CAPEX, the internal heat exchangers should be targeted for improvements. This is exactly the scope of the method proposed by Chen et al. [23]. This method can be incorporated in the proposed design method in Step 4c (Figure 4.2). The number of heat integrated pairs is, according to the method of Chen et al., reduced to three by choosing three trays in each section in the same vertical height. As a result, stages #2, #48, and #95 are paired with stages #99, #145, and #192. The resulting configuration is termed the Simplified Ideal HIDiC (SIHIDiC). The operating conditions of the SIHIDiC are similar to those of the HIDiC. The performance indicators and CAPEX and OPEX breakdown for the SIHIDiC are shown in Table 5.5 and Figure 5.8.

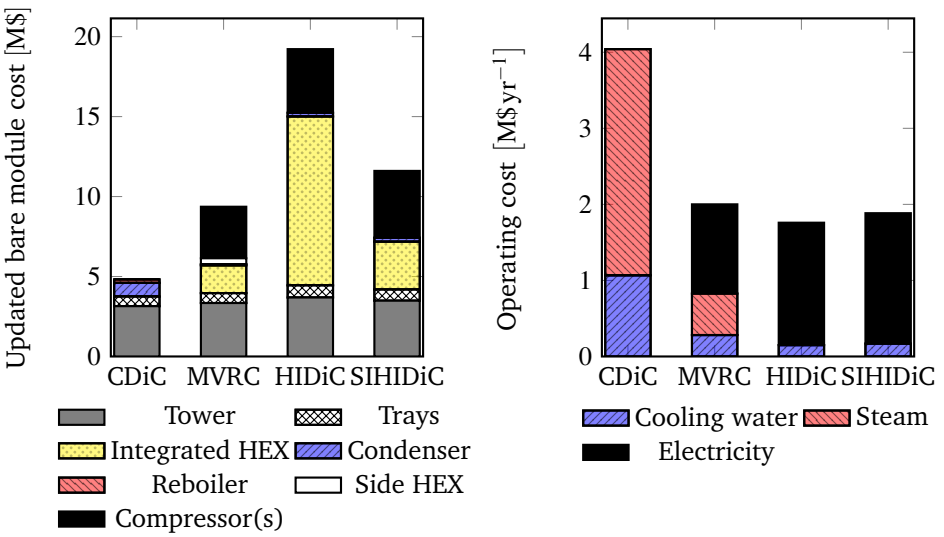

Figure 5.8. Breakdown of CAPEX and OPEX for the separation of propylene/propane.

5.4.3 Summary

It was shown that the concentric heat-integrated distillation column (HIDiC) containing sieve trays with conventional dimensions appears to be a technically feasible solution for the separation of both benzene/toluene and propylene/propane. Hence, the remaining considered separations in this chapter are assumed to be technically feasible. With respect to the economic feasibility, it has been shown that the mechanical vapour recompression column (MVRC) is a promising alternative to conventional distillation for both benzene/toluene and propylene/propane. The main advantage in the MVRC over the HIDiC and the SRVC is the lower CAPEX. In terms of OPEX, the application of the internal heat integrations seems very advantageous for both the separation of propylene/propane and benzene/toluene; the OPEX was lower for the SRVC in the case of benzene/toluene, while it was lower for the HIDiC in the case of propylene/propane. It was found that the MVRC still outperforms the HIDiC in terms of TAC after the number of heat-integrated stages was reduced from 94 to 3 for the separation of propylene/propane. Furthermore, it was illustrated that the FOB can be used for evaluating if super-heating is needed on the compressor inlet.

5.5 Feasibility Analysis

The aim of this section is to map the feasibility of the different configurations. This mapping is used to identify relations between the physical properties of the mixtures and the economic feasibility. Furthermore, the results are compared to the Q/W feasibility indicator.

5.5.1 Case Study Formulation

The following analysis are carried in a similar manner to the ones presented for benzene/toluene and propylene/propane. But only an overview of the results is reported and discussed. The developed design method (Chapter 4) was employed for all the reported mixtures (Table 5.6). In order to compare the results, all mixtures were separated under the same conditions, i.e. identical feed specifications, identical separation specifications, and identical economic parameters. The temperature difference and the heat of vaporisation are significant factors in the economic feasibility according to the Q/W (Eq. (5.3)). Hence, nine of the binary separations in Table 5.2 are selected and classified according to high or low normal boiling point difference, and high or low heat of vaporisation in Table 5.6. In addition, a multicomponent mixture was included; weighted averages based on the feed com-

position were used to estimate the physical properties of the mixture ($\alpha = 1.72$, $\bar{\lambda} = 44.43\,\mathrm{kJ\,mol^{-1}}$, and $\Delta T_{nb} = 22.75\,\mathrm{K}$, $C_P^V = 0.1402\,\mathrm{kJ\,mol^{-1}\,K^{-1}}$). This is a simple consideration, as the classification parameters are not dimensionless and because they are correlated. However, these parameters are still found useful as classification parameters since they are readily available. A common set of feed specifications, separation specifications and model parameters is summarised in Table 5.7. In the case of the azeotropic ethanol/water system, the feed composition and the product specifications were normalised by 0.87, which is the composition of the ethanol/water azeotrope. Furthermore, for the mixture of 9 aromatic components, the product purity specifications applied to the light C8 fraction and the heavy C9 fraction. The fact that all separations have common economic parameters enables fair comparative studies of the feasibilities among the configurations. In addition, by maintaining the feed and product specifications identical, the effect of the physical behaviours of the mixtures on the feasibility is isolated. All the configurations of Figure 3.1 are considered, namely the CDiC, the MVRC, the HIDiC, and SRVC.

Table 5.6. Considered mixtures for separation. Normal boiling point difference: High when $\Delta T_{nb} \geq 10\,\mathrm{K}$, otherwise low. Heat of vaporisation: High when $\bar{\lambda} \geq 33\,\mathrm{kJ\,mol^{-1}}$, otherwise low.

Mixture	VLE model		Classification	
	Liquid	Vapour	ΔT_{nb}	$\bar{\lambda}$
m-Xylene/o-xylene	Ideal	Ideal	Low	High
Isopentane/n-pentane	Ideal	Ideal	Low	Low
Propylene/propane	SRK	SRK	Low	Low
Methanol/ethanol	Ideal	Ideal	High	High
Acetic acid/acetic acid anhydride	UNIQUAC	Ideal	High	High
Ethanol azeotrope/water*	UNIFAC	Ideal	High	High
Benzene/toluene	Ideal	Ideal	High	High
Methanol/water	UNIFAC	Ideal	High	High
Benzene/ethylbenzene	Ideal	Ideal	High	High
9-Aromatics†	Ideal	Ideal	High	High

* mole fraction specifications were normalised by 0.87 (azeotropic point)
† 9-component mixture from Table 4.8, the feed composition was chosen as $z_1 = 0.005$, $z_i = 0.1244$ for $i = 2,3,\ldots,9$ with $i = 2,3,4,5$ representing the C8 fraction and $i = 6,7,8,9$ representing the heavy fraction.

5.5.2 Design Trends

All the obtained designs are presented in Table 5.8. In Figure 5.9, the correlations between the major design variables and the corresponding physical parameters of

the mixtures are presented, i.e. the relative volatility (α), the normal boiling point difference (ΔT_{nb}), and the mean heat of vaporisation ($\bar{\lambda}$).

It appears in Figure 5.9 that all the design variables except $CR_{ext,SRVC}$ are correlated with the normal boiling point difference. The propylene/propane separation is an outlier due to the non-ideal vapour phase. No significant correlations between the heat of vaporisation and any of the design variables is observed. The correlations between the relative volatilities and the design variables are not as significant as the normal boiling point differences.

A noticeable observation is the following. The azeotropic ethanol/water mixture HIDiC design was sensitive to the selection of the compression ratio in the sense that the minimum temperature driving force was sensitive to the compression ratio. This observation might indicate challenges w.r.t. operation of such HIDiC. The reason for this particular sensitivity is because the top product is an azeotrope. Thus, when the rectifying section pressure is increased by increasing the compression ratio, the azeotropic point is slightly affected. Hence, low-boiling azeotrope mixtures might be challenging to realise in an HIDiC.

Based on the observed correlations in Figure 5.9, simple expressions for the required total heat exchange areas and compression ratios for the HIDiC and the MVRC can be formulated as:

$$CR_{int} = 0.0381\Delta T_{nb} + 1.5936 \qquad (R^2 = 0.6768) \tag{5.13}$$

$$CR_{ext} = 0.0642\Delta T_{nb} + 1.7236 \qquad (R^2 = 0.7778) \tag{5.14}$$

$$\sum_n A_{int,n} = 128,043\Delta T_{nb}{}^{-1.75} \qquad (R^2 = 0.9455) \tag{5.15}$$

$$A_{ext} = 17,029\Delta T_{nb}{}^{-0.838} \qquad (R^2 = 0.9336) \tag{5.16}$$

The applications of these simple relations cover separations by an HIDiC or an MVRC of a pseudo-binary mixture into two pure components. These expressions can be useful in order to carry out preliminary evaluation of a given configuration. Furthermore, an important observation is that there is no significant relation between the shape of the temperature profiles and the design variables. Illustrations of all the temperature profiles are not provided. But for the separation of ethanol azeorope/water, a temperature pinch is observed for the lowest heat-integrated pair rather than in the middle of the heat-integrated part of the column, which is the case of benzene/toluene (Figure 5.3). A similar temperature pinch location is observed in the separation of methanol/water. Note in Table 5.8 that the presented case studies cover cases with equally large column sections (e.g. isopentane/n-pentane) and column sections of different sizes (e.g. ethanol azeotrope/water). Hence, it is assumed that this present analysis covers the cases of the analysis related to the

temperature profiles by Shenvi et al. [142].

Table 5.7. Feed specifications, purity specifications, and model parameters employed for the feasibility analysis (unless otherwise stated).

Class	Parameter	Unit	Value
Feed and separation specifications			
Feed	Flow rate	$\mathrm{mol\,s^{-1}}$	83.3
	Light component mole fraction	-	0.50
	Pressure	kPa	101.3
	Temperature	Saturated	
Distillate	Light component mole fraction	-	0.995
Bottoms	Heavy component mole fraction	-	0.995
Model parameters			
Internal heat exchanger	Heat transfer coefficient	$\mathrm{kW\,m^{-2}\,K^{-1}}$	0.60
General	Electricity price	$\mathrm{\$\,kWh^{-1}}$	0.14
	Steam ($P_{steam} > 200\,\mathrm{kPa}$)	$\mathrm{\$\,t^{-1}}$	$1.99 + 16.2(P_{steam} - 101.3\,\mathrm{kPa})^{0.05}$
	Cooling water (at 300 K)	$\mathrm{\$\,t^{-1}}$	0.080
	Year	-	2012
	Project life time	yr	5
	Service factor	-	0.904
	Materials	-	Carbon steel
Tray	Pressure drop	kPa	0.70
	Efficiency	-	0.80
	Flooding factor	-	0.80
	Void fraction	-	0.75
	Type	-	Sieve
	Spacing	mm	609.60 (24")
Condenser	Water temperature increase	K	5.0
	Heat transfer coefficient	$\mathrm{kW\,m^{-2}\,K^{-1}}$	0.60
	Type	-	Floating head
Reboiler	Heat transfer coefficient	$\mathrm{kW\,m^{-2}\,K^{-1}}$	1.420
	Difference between steam and reboiler temperature	K	10
	Type	-	Kettle reboiler
Compressor	Isentropic efficiency	-	0.80
	Motor efficiency	-	0.90
	Type	-	Centrifugal/motor

Table 5.8. Design specifications for the ten considered separations (Table 5.6).

Separation	Config.	A_{int}	CR_{int}	A_{ext}	CR_{ext}	N_{rct}	N_{str}
	m^2	-	m^2	-	-	-	
m-Xylene/o-xylene	CDiC	0	1	0	1	101	100
	MVRC	0	1	6325	3.01	100	101
	HIDiC	93.7	2.07	0	1	100	101
Isopentane/n-pentane	CDiC	0	1	0	1	59	59
	MVRC	0	1	2441	2.01	59	59
	HIDiC	50.75	1.78	0	1	59	59
	MVRC	45.5	1.80	53.5	1.25	63	63
Propylene/propane	See Table 5.4						
Methanol/ethanol	CDiC	0	1	0	1	32	32
	MVRC	0	1	1953	2.773	32	32
	HIDiC	37.1	2.23	0	1	38	38
	SRVC	37.1	2.23	326	1.25	38	38
Acetic acid/acetic acid anhydride	CDiC	0	1	0	1	23	30
	MVRC	0	1	1389	2.81	23	30
	HIDiC	30.6	2.36	0	1	29	36
	SRVC	30.6	2.36	216	1.20	29	36
Ethanol azeotrope/water	CDiC	0	1	0	1	47	8
	MVRC	0	1	1771	3.42	47	8
	HIDiC	88.2	2.48	0	1	47	8
	SRVC	88.2	2.48	353.5	1.24	47	8
Benzene/toluene	CDiC	0	1	0	1	19	17
	MVRC	945	3.26	0	1	19	17
	HIDiC	19.3	2.46	0	1	25	23
	SRVC	19.3	2.46	374	1.31	25	23
Methanol/water	CDiC	0	1	0	1	30	6
	MVRC	0	1	902	4.78	30	6
	HIDiC	24.8	3.90	0	1	30	6
	SRVC	24.8	3.90	397.5	1.11	30	6
Benzene/ethylbenzene	CDiC	0	1	0	1	10	10
	MRVC	0	1	553	5.21	10	10
	HIDiC	8.02	3.32	0	1	12	12
	SRVC	8.02	3.32	365	1.55	12	12
Aromatics	CDiC	0	1	0	1	38	38
	MRVC	0	1	2424	2.897	38	38
	HIDiC	47.2	2.20	0	1	50	50
	SRVC	47.2	2.202	208	1.40	50	50

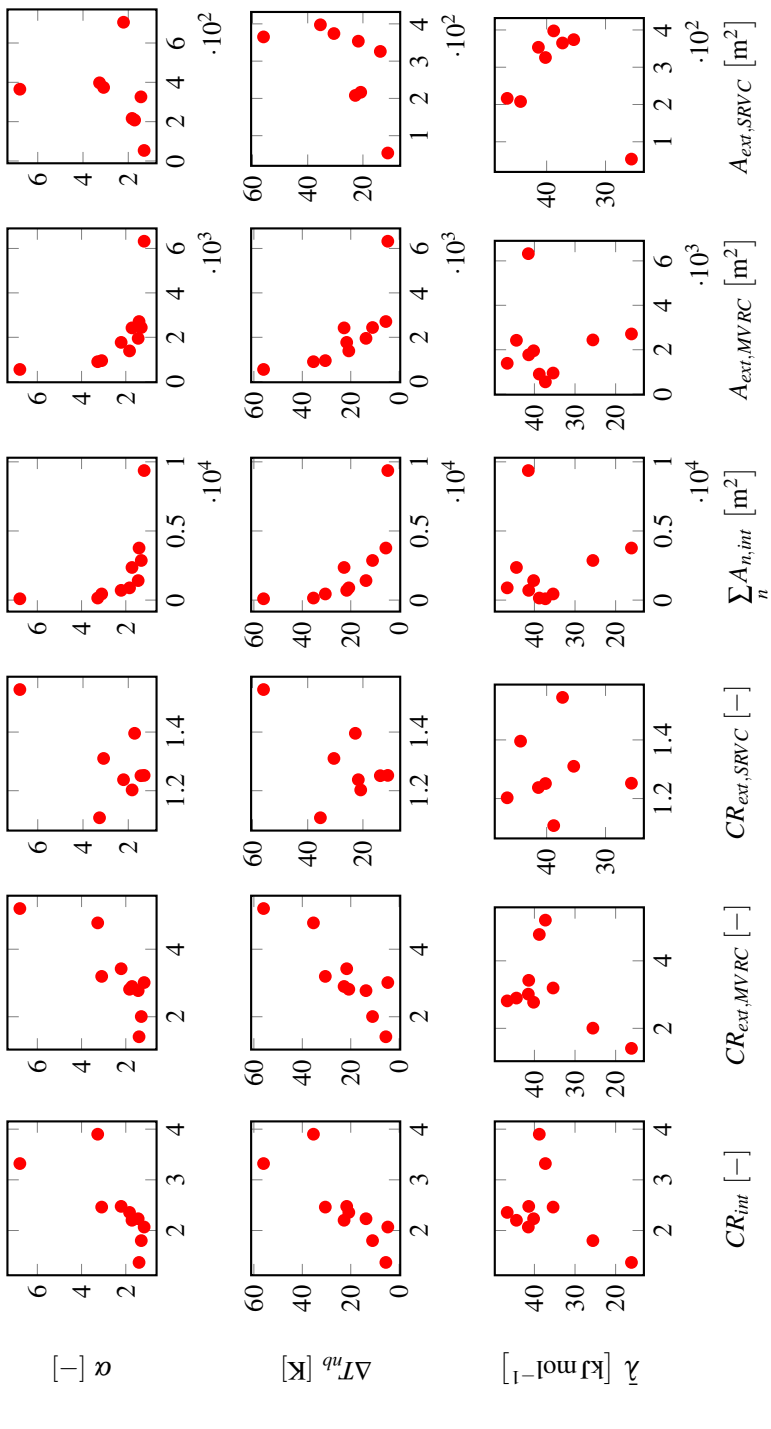

Figure 5.9. Correlation between design parameters and mixture properties. CR_{int}=internal compression ratio for HIDiC and SRVC, $CR_{ext,config}$=external compression ratio for a given configuration (MVRC or SRVC), $\sum_n A_{int,n}$=sum of internal heat transfer area for HIDiC and SRVC, $A_{ext,config}$=external heat transfer area for a given configuration (MVRC or SRVC).

Table 5.9. Estimated specific heat transfer area for internal heat integration (Φ) and total concentric cross sectional area (A_{CT}; see Section 3.4.3).

Mixture -	Φ $m^2\,m^{-3}$	A_{CT}
m-Xylene/o-xylene	4.2	93.7
Isopentane/n-pentane	5.1	50.8
Propylene/propane	4.5	40.1
Methanol/ethanol	16.3	37.1
Acetic acid/acetic acid anhydride	11.3	30.6
Ethanol azeotrope/water	41.6	88.2
Benzene/toluene	7.6	19.3
Methanol/water	31.4	24.8
Benzene/ethylbenzene	4.6	8.0
9-Aromatics	5.1	47.2

Based on the design specifications and column simulations, the specific heat transfer areas (Φ, Eq. (2.4)) are estimated for internal heat transfer for the ten considered mixtures. The resulting specific heat transfer areas are given in Table 5.9. When comparing these required specific heat transfer areas to the values, obtained in experiments (Table 2.3), the reported shell-and-tube arrangements ($1.9\,m^2\,m^{-3}$ [58]) do not meet the required specific heat transfer areas. However, both the structured plate arrangement ($52.7\,m^2\,m^{-3}$ [19]) and the concentric lift tray arrangement ($19.9\,m^2\,m^{-3}$ [122]) can achieve the required specific heat transfer areas. Furthermore, it is expected that heat panels installed inside conventional trays can accommodate the required heat transfer area.

5.5.3 Quantification of OPEX Uncertainty

Due to of a lack of experience related to the design of e.g. the HIDiC, it is important to investigate the impact of uncertain design parameters on the economic evaluation. Both the OPEX and the CAPEX appears in the TAC. The uncertainty of the CAPEX is reported as 20% by Biegler et al. [9]. The uncertainty of the OPEX is therefore needed, in order to benchmark the configurations under uncertainty. Consider a scenario where a design of either the CDiC, the MVRC, or the HIDiC has been constructed, based on a nominal parameter set. Considering that some of the parameters are uncertain, the following questions are answered by this analysis:

- How are uncertainties in the parameters reflected in the OPEX if the operational variables of the CDiC, the MVRC, or the HIDiC must compensate for these?

- What is the variance of the estimated OPEX for each configuration?
- Which uncertain parameters have the most significant contribution to the variance?

The uncertain parameters are assumed to be uniformly distributed. The uncertain parameters and their bounds are listed below:

- Heat of vaporisation, $0.90\ \lambda_0 \leq \lambda \leq 1.10\ \lambda_0$
- Tray pressure drop, $0.80\ \Delta P_0 \leq \Delta P \leq 1.20\ \Delta P_0$
- Overall heat transfer coefficient, $0.80\ U_{ihx,0} \leq U_{ihx} \leq 1.20\ U_{ihx,0}$
- Constant pressure heat capacity of the vapour, $0.90\ C^V_{P,0} \leq C^V_P \leq 1.10\ C^V_{P,0}$
- Ratio of steam price to electricity price, $0.80(S_{electricity}/S_{steam})_0 \leq (S_{electricity}/S_{steam}) \leq 1.20(S_{electricity}/S_{steam})_0$.

The nominal uncertain parameters (given by the subscript "0"), the remaining parameters, and the common design variables are listed in Table 5.10.

Table 5.10. Nominal input and parameters for the two classes of mixtures.

Parameter	Unit	Value
P_{str}	kPa	101.3
λ	$\mathrm{kJ\,mol^{-1}}$	33
$T_{nb,1}$	K	350
S_{steam}	$\mathrm{\$\,kJ^{-1}}$	$10.4 \cdot 10^{-6}$
ΔP_0	kPa	0.70
$U_{ihx,0}$	$\mathrm{kW\,m^{-2}\,K^{-1}}$	0.60
$C^V_{P,0}$	$\mathrm{kJ\,mol^{-1}\,K^{-1}}$	0.070
$(S_{electricity}/S_{steam})_0$	-	3.8

Two mixtures with different normal boiling point differences were considered as this parameter was identified as the must important physical parameter (Section 5.5.2): A mixture with a large normal boiling point difference ($\Delta T_{nb} = 30$) and a mixture with a low normal boiling point difference ($\Delta T_{nb} = 5.0$). The number of stages were calculated using the Fenske-Underwood-Gilliland procedure based on the nominal values listed in Table 5.11. The reflux-to-minimum-reflux ratio was chosen as 1.05. The designs were carried out such that the compression ratios (CR) were adjusted to satisfy the minimum temperature driving force condition in Eq. (4.4), and such that heat transfer areas (A) were adjusted to minimise conventional utilities. The conventional utilities are minimised by imposing the constraint

$\min([L_{cnd}, V_{rbl}]) = 0$ for the HIDiC and $\min([Q_{cnd}, Q_{rbl}]) = 0$ for the MVRC. For all configurations, the remaining degrees of freedom (L_{cnd} and V_{rbl}) were chosen such that the purity constraints were fulfilled. The feed specifications and economic parameters are identical of those in Table 5.7. A Monte Carlo sample size of $N_p = 1000$

Table 5.11. Nominal design for the two classes of mixtures.

ΔT	Configuration	N_{rct}	N_{str}	L_{cnd}/F	V_{rbl}/F	CR	A
K	-	-	-	-	-	-	m^2
30	CDiC	19	18	0.696	1.20	1	0
30	MVRC	19	18	0.696	1.20	3.44	1096
30	HIDiC	19	18	0	0.50	2.53	24.9
5.0	CDiC	90	89	5.92	6.42	1	0
5.0	MVRC	90	89	5.92	6.42	2.98	5885
5.0	HIDiC	90	89	0	0.50	2.07	75.3

was used for each design (rows in Table 5.11) leading to 6000 column simulations. For every sample, a new set of input variables (L_{cnd}, V_{rbl}, CR) were obtained in order to satisfy the purity constraints and minimum utility constraints. Based on the new set of input variables, the OPEX was calculated. The resulting OPEX estimates are illustrated in Figure 5.10. The OPEX of CDiC is relatively unaffected by the uncertain parameters and therefore the variance is low. It can be concluded with 95% confidence that the OPEX is lower of the MVRC than the HIDiC for the wide-boiling mixture. However, for the close-boiling mixture, the confidence intervals overlap. The obtained standard deviations for the 30 K mixture are 6.3% for the MVRC and 4.2% for the HIDiC. The obtained standard deviations for the 5 K mixture are 12.5% for the MVRC and 10.7% for the HIDiC.

The uncertain parameters, which are responsible for the variances, are identified by the global sensitivity analysis (Section 5.2.3). The obtained SRC values are plotted in Figure 5.11. As the sums of the SRC's do not add up to one for the CDiC, no linear correlation between the uncertain parameters and the OPEX estimates could be obtained. This is believed to be due to the fact that only the latent heat of vaporisation affects the OPEX of the CDiC. The relative significance of the uncertain parameters are represented by the magnitude of the SRC values. Thus, the ratio between the electricity and the steam prices is the dominating parameter. In the MVRC, the tray pressure drop is also a significant uncertain parameter, while the overall heat transfer coefficient is significant for the HIDiC. The heat of vaporisation does not have a significant impact on the uncertainties.

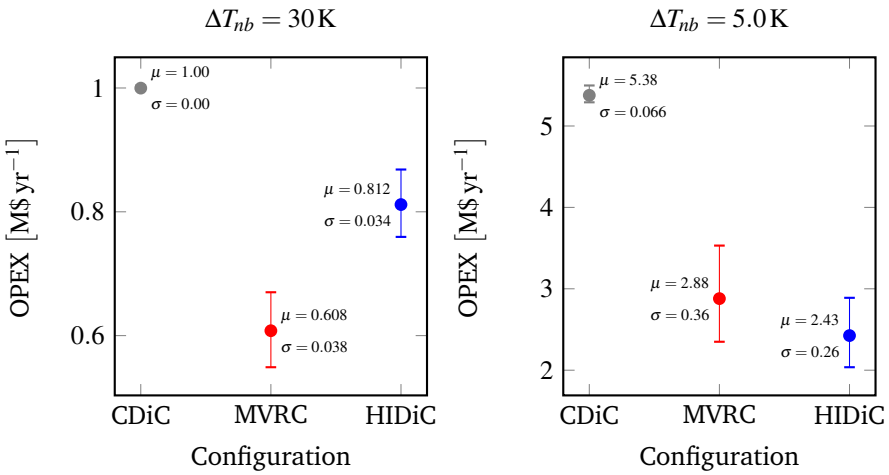

Figure 5.10. OPEX estimate for the CDiC, the MVRC and the HIDiC performing separations of two different mixtures under uncertain design parameters. The error bars represent 5% and 95% confidence intervals. Expectation (μ) and standard deviation σ are given in [M\$ yr^{-1}].

5.5.4 Benchmarking

The remaining task is to relate the economic feasibility of the considered configurations for the ten case studies to the physical parameters. Based on the conclusion from the previous section, the major design variables are correlated with the normal boiling point differences (Eqs. (5.13)-(5.16)). Hence, such correlation is also expected for the economic feasibility.

An uncertainty in the CAPEX of 20% is assumed [9]. The relative standard deviations in the OPEX for two separations of varying ΔT_{nb} were obtained in Section 5.5.3. For each configurations, a linear correlation between the relative standard deviation and ΔT_{nb} was used to estimate the uncertainty of the OPEX. As the SRVC was not considered in the uncertainty analysis, the uncertainty of its OPEX is assumed to be identical to that of the HIDiC. When standard deviations below zero were obtained by the linear correlation, these were fixed at zero. The uncertainty of the TAC is thus obtained by combining the contributions from the CAPEX and OPEX. The resulting uncertain TAC's for different mixtures and configurations are illustrated in Figure 5.12. It can be concluded that the MVRC outperforms the considered configurations in most of the cases. A similar conclusion was reported by Harwardt and Marquardt [51].

When plotting the TAC of the resulting configurations for the normal boiling point differences, trends amond the binary separations are obtained for the dif-

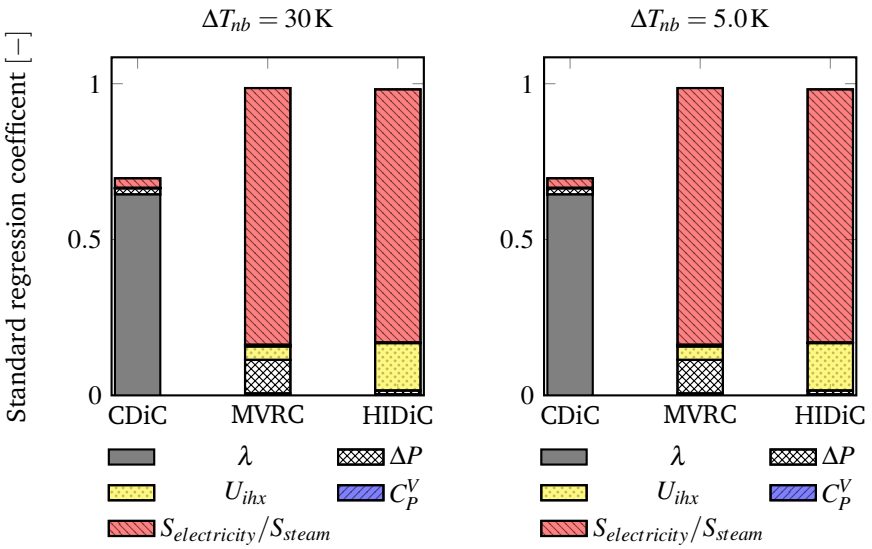

Figure 5.11. Standard regression coefficient (SRC) values of the OPEX for the CDiC, the MVRC and the HIDiC performing separations of two different mixtures under uncertain design parameters. The relative significance of a parameter on the OPEX estimate of a configuration is proportional to the size of the area occupied by the parameter.

ferent distillation column configurations (see Figure 5.13). The multicomponent mixture of the aromatics do not follow the trend of the TAC of the binary mixtures. However, as will be shown below, the trends of the binary mixtures are followed surprisingly well when considering relative performance indicators (relative to the CDiC design).

The obtained relative performance indicators for the considered case studies are illustrated in Figure 5.14. The performance indicators of the CDiC were used as the scaling factor, except for the compressor duties. The compressor duties of the CDiC are zero and thus the reboiler duty of the CDiC was used instead. It appears that also for the performance indicators, the normal boiling point difference shows a reasonable correlation. One significant observation of the relative OPEX is that the HIDiC is the favoured configuration for $\Delta T_{nb} < 10\,\mathrm{K}$. The MVRC and the SRVC have similar relative OPEX in the interval $10\,\mathrm{K} \leq \Delta T_{nb} < 25\,\mathrm{K}$ and hence the simpler should be considered. For higher normal point temperature differences ($\Delta T_{nb} \geq 25\,\mathrm{K}$), the SRVC is an attractive configuration.

The link between the Q/W ratio and the economic feasibility is investigated. It was claimed that a value of $Q/W \geq 10$ is a reasonable estimate for economic feasibility (i.e. $\mathrm{TAC} < \mathrm{TAC}_{\mathrm{CDiC}}$) of a heat pump-assisted distillation column configuration

[130]. Based on the result in Figure 5.15, this simple consideration holds well for the HIDiC, since the relative TAC, according to the trend, is below 1 after around $Q/W = 10$. For the MVRC and the SRVC, the plot indicates that these configurations are preferred in terms of TAC for all mixtures with $Q/W \geq 0$.

5.6 Conclusion

A techno-economic analysis of heat-integrated distillation columns has been presented in this chapter. Four configurations were considered, namely the conventional distillation column (CDiC), the mechanical vapour recompression column (MVRC), the heat-integrated distillation column (HIDiC), and the secondary reflux and vaporisation column (SRVC). It has been illustrated by simulation of the separation of benzene/toluene that it is possible, by using heat panels, to realise a HIDiC. Detailed economic analysis of the separations of benzene/toluene and propylene/propane showed that the capital expenditure of configurations with internal heat integration comprises a significant drawback to such configurations. Hence, the reductions in the operating expenses are difficult to justify when considering the significant capital investment. Significant reductions in the operating expenses were, however, achieved by the HIDiC for the separation of propylene/propane.

A comprehensive study of nine binary mixtures and one multicomponent mixture being separated in the four different distillation configurations was conducted and analysed w.r.t. economic feasibility. The presented design method was successfully applied to the ten separations. The difference in normal boiling points was found to be the determining parameter for the feasibility. A measure for the heat required for distillation per work required (Q/W) was evaluated. It was found that economic feasibility for any of the three heat-integrated distillation configurations (MVRC, HIDiC, SRVC) was achieved for $Q/W \geq 0$.

The completely heat-integrated SRVC performs the best in terms of OPEX, second-law efficiency, and water consumption with only a slightly increased CAPEX compared to the HIDiC. Interestingly, the following intervals of the normal boiling differences are identified for choosing the preferred configuration among the HIDiC or MVRC in terms of OPEX:

- $\Delta T_{nb} < 10\,\mathrm{K}$: The HIDiC
- $10\,\mathrm{K} \leq \Delta T_{nb}$: The MVRC

These relations are simplified but they provide actual quantifications of the limits, which divide the optimal solutions of the heat-integrated distillation configurations.

Considering the large expected uncertainties in the CAPEX estimates, the favourable OPEX in the HIDiC for $\Delta T_{nb} < 10\,\mathrm{K}$ justifies the need for dynamic analyses in the subsequent chapters.

All performance indicators, as well as the design variables, correlate surprisingly well with the normal boiling point differences. Therefore, correlations for estimating the total required heat exchanger area and compression ratio for the MVRC and the HIDiC were proposed. These are not only useful as preliminary estimates of the operating and capital expenses, but also for good estimates for the conceptual design of such configurations. In addition, it was found that the compressor duty of a heat pump-assisted distillation column configuration usually lies within 10-15% of the reboiler duty of a corresponding conventional distillation column.

Finally, uncertainty and sensitivity analysis showed that, when building an MVRC or an HIDiC, the operating expenses are subject to a large uncertainty for close-boiling separations with a relative standard deviation above 10%. The most significant uncertain parameter is the ratio between the cost of energy supplied by steam over the cost of energy supplied as electricity. The second-most significant parameters are the tray pressure drop for the MVRC and the overall heat transfer coefficient for the HIDiC.

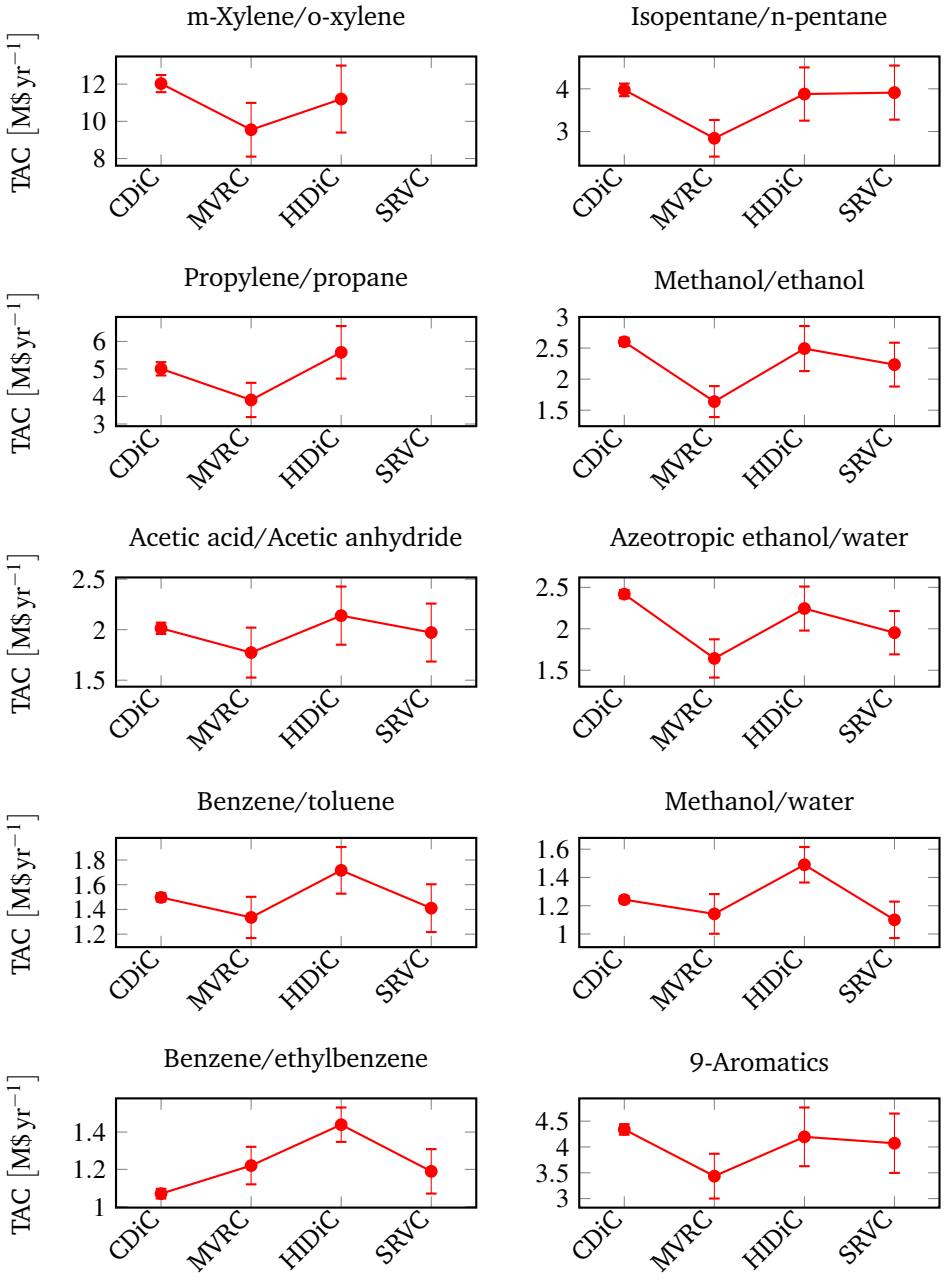

Figure 5.12. Benchmarking of the four distillation column configurations (CDiC, MVRC, HIDiC, and SRVC) w.r.t. TAC. The TAC=CAPEX/5+OPEX (annual basis), which accounts for uncertainty in OPEX and CAPEX.

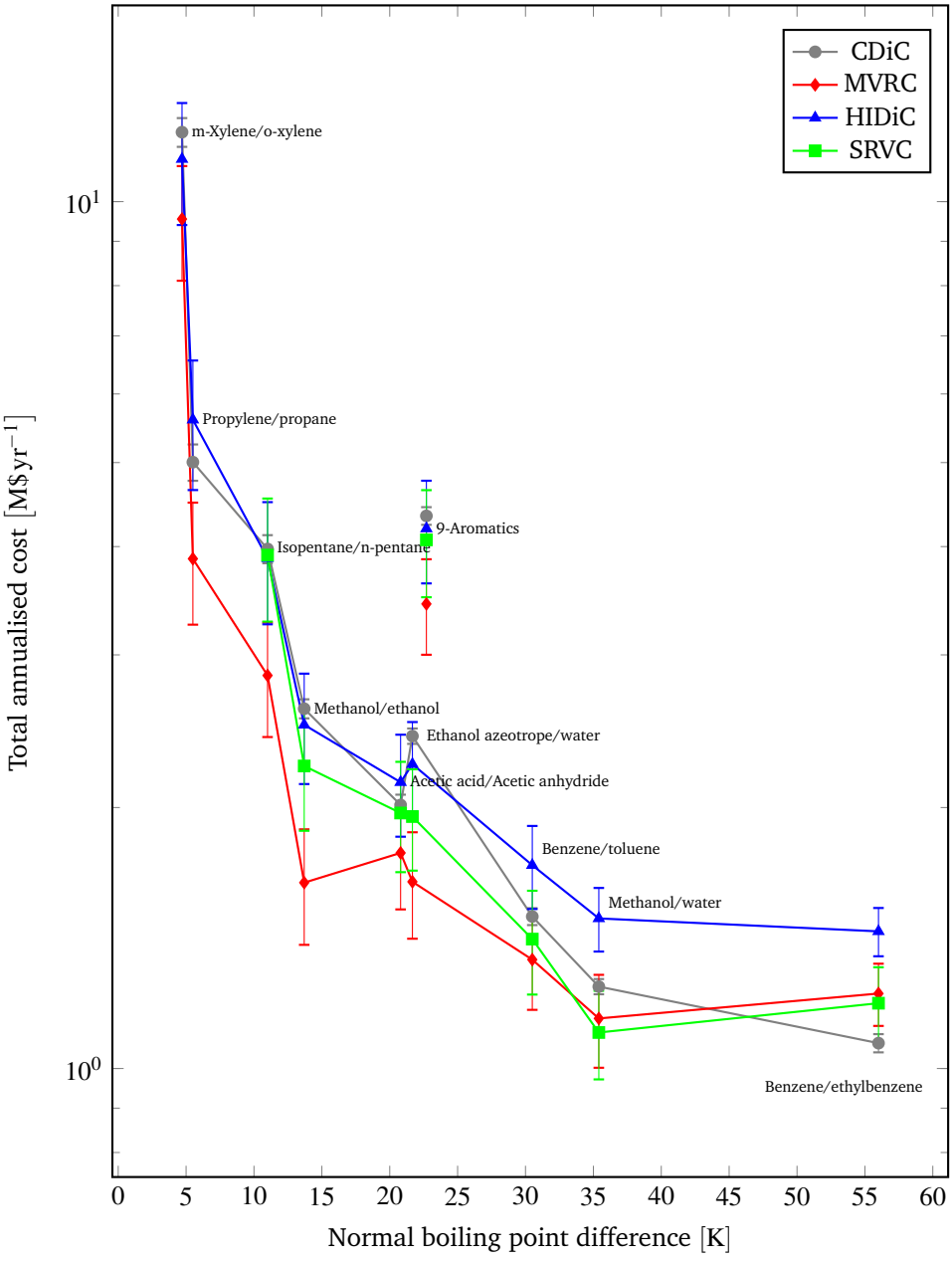

Figure 5.13. Correlation between normal boiling point difference and total annualised cost (TAC) illustrated using logaritmic axes. The TAC=CAPEX/5+OPEX (annual basis), which accounts for uncertainty in OPEX and CAPEX.

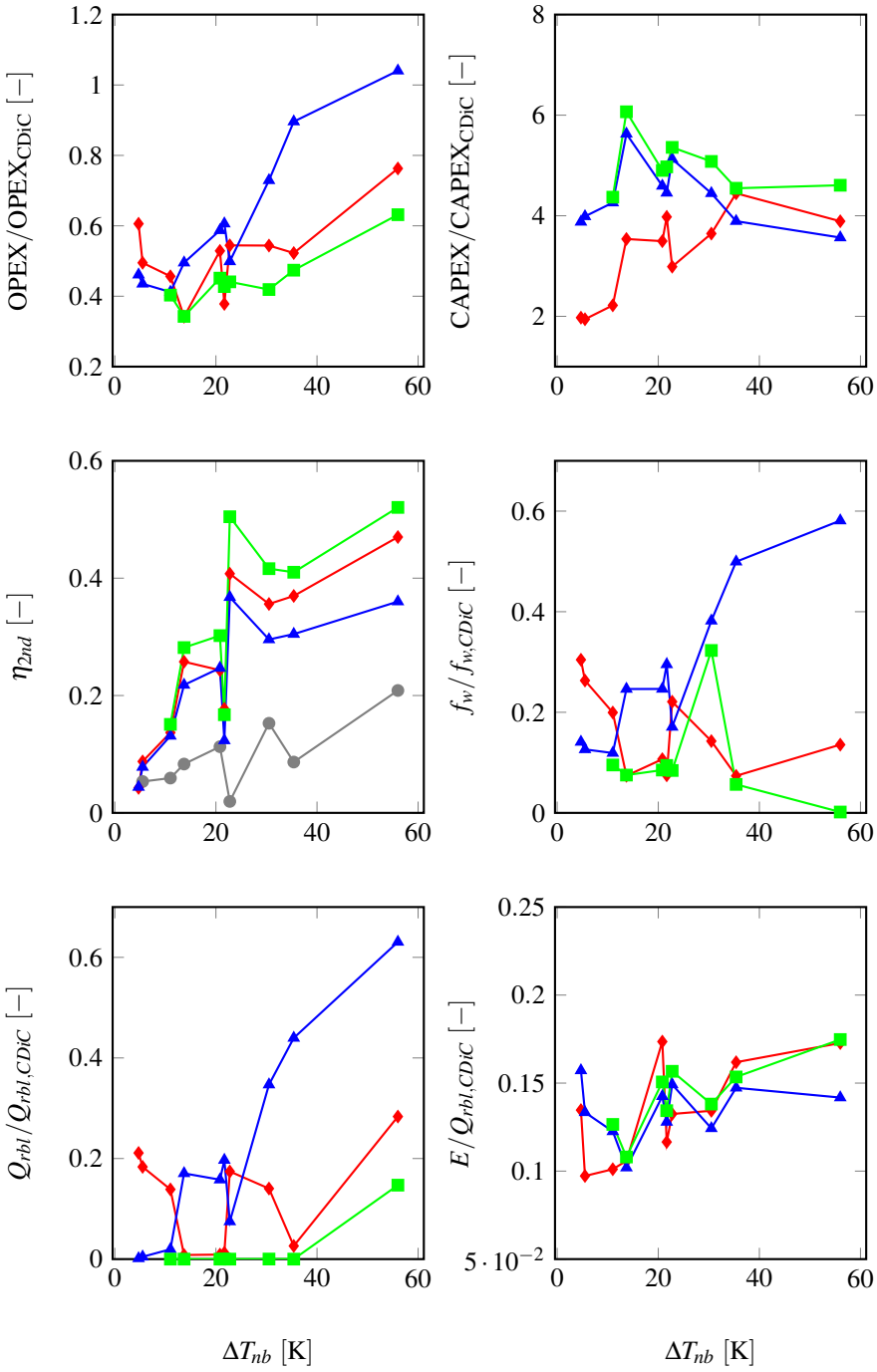

Figure 5.14. Relative performance indicators. f_w is the water consumption, η_{2nd} is the second-law efficiency. Legend: CDiC (—●—), MVRC (—◆—), HIDiC (—▲—), and SRVC (—■—).

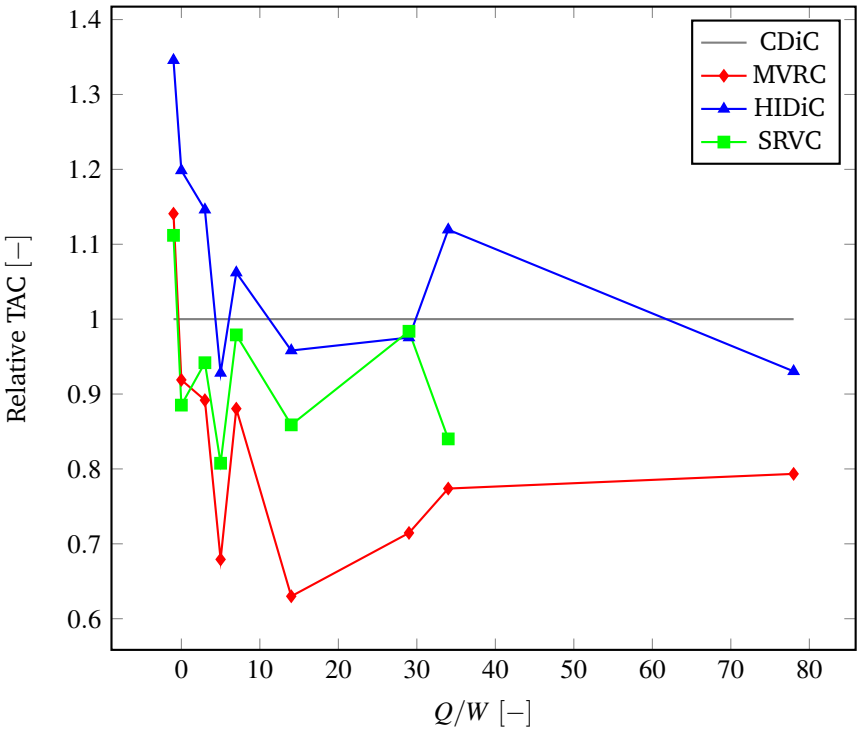

Figure 5.15. Heat required for distillation per work required (Q/W) and relative total annualised cost for the nine binary mixtures. The relative TAC $=$ TAC/TAC$_{\text{CDiC}}$.

Chapter 6

Stabilising Control

The fundamental problem of obtaining a stabilising control structure of the concentric heat-integrated distillation column (HIDiC) is addressed in this chapter. The economic plantwide control method by Larsson and Skogested was adopted for solving the problem in a systematic manner [T. Larsson and S. Skogestad. Plantwide control–a review and a new design procedure. *Model Ident Control*, 21(4):209–240, 2000]. A control structure of the regulatory control layer is devised, based on generic considerations and numerical studies. These numerical studies are based on open-loop considerations and various tools for controllability analysis. The proposed regulatory control layer is evaluated by dynamic simulations. The performance, in terms of setpoint tracking of the controlled variables and the possibility of entrainment flooding and weeping, was investigated in dynamic simulations. It was concluded that stable operation in both aspects could be achieved for the proposed control structure. The significance of including pressure dynamics and accounting for the stabilising control layer is illustrated by dynamic open-loop simulations, where the obtained responses are compared to the responses of a simplified model, available in literature.

This chapter is based on work conducted in collaboration with Professor Sigurd Skogestad during an exchange period at the Norwegian University of Science and Technology, Trondheim,

Norway.

The results of this chapter were used in an accepted conference contribution for DYCOPS 2016 [T. Bisgaard, S. Skogestad, J.K. Huusom, and J. Abildskov. Optimal operation and stabilising control of the concentric heat-integrated distillation column. *11th IFAC International Symposium on Dynamics and Control of Process Systems – Trondheim, Norway*, 2016]. Early progress on this problem was presented during the Nordic Process Control Workshop 2015 (NPCW19) in Norway.

6.1 Introduction

Internal heat transfer takes place in both the heat-integrated distillation column (HIDiC) and the secondary reflux and vaporisation column (SRVC). These configurations show potential favourable economic performances compared to the mechanical vapour recompression column (MVRC) and the conventional distillation column (CDiC). As a result, the dynamic behaviour of the HIDiC is studied in this chapter, as it is used to represent the behaviour of similar configuration with internal heat transfer (including the SRVC).

Simple control theory is briefly explained in this section; starting from a presentation of a common control hierarchy in a chemical plant, a systematic economic plantwide control design procedure, and the purpose of stabilising control.

6.1.1 Control Hierarchy

The control system of a chemical plant can be divided into levels that are performing actions at different time scales and different partitions of the chemical plant. This division is called a control hierarchy and is illustrated in Figure 6.1.

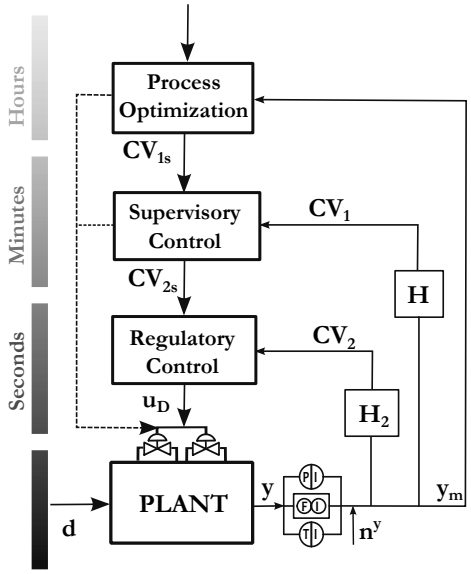

Figure 6.1. Control hierachy [104].

Starting from the top of the control hierarchy, the purpose of the different layers are as follows [149]:

- **Process optimisation**: The purpose of this layer is to ensure plantwide opti-

mal performance. For example, the objectives of this layer can be achieved by carrying out plantwide steady state optimisation. The optimal solution from the plantwide optimisation routine is distributed locally to unit operations or groups of unit operations and provides the setpoint(s) of the supervisory control layer.

- **Supervisory control layer**: This layer provides local, optimising control by keeping the controlled variables at the setpoint provided from the layer above. The controlled variables in this layer must be carefully selected in order to ensure near-optimal operation when kept at the given setpoint. Hereby, the optimisation load is distributed locally in order to reduce the time delay between the optimisation layer and the process itself. Hence, the control objectives of this layer are economic rather than stabilisation. The output from this layer is the setpoints to the lower regulatory layer.

- **Regulatory control layer**: The role of the regulatory control layer is to provide fast stabilisation of the process. The setpoints from the supervisory layer are directly translated into actuator actions in the regulatory layer.

- **Plant:** The dynamic behaviour of the plant is dictated by the dynamic control degrees of freedom, which are specified in the above layer. Measurements are taken on the plant in order to describe the current state of the process. These measurements are inputs for the above layers.

The scopes of this chapter are related to the investigation of the distillation column dynamics and the design of the regulatory layer. Stabilisation of a plant or a process is an essential task and it has not been addressed systematically for a HIDiC. This work considers control degrees of freedom, which are very similar to the corresponding actuators in a real HIDiC.

6.1.2 Economic Plantwide Control (Part 1)

A sequential, systematic method for designing the entire control system illustrated in Figure 6.1 is proposed by Larsson and Skogestad [89, 149]. This method can be summarised as shown in Figure 6.2. The method is divided into a top-down analysis, which relates to the top layers of the hierarchy in Figure 6.1, and a bottom-up analysis (Steps 5-7), which relates to the integration of the top-down analysis in relation to the bottom layers in the hierarchy. Hence, the top-down analysis (Steps 1-3) mainly involves steady state simulation, and the bottom-up part mainly involves dynamic simulation with Step 4 working as the link between the two. An overview of the method combined with a collection of practical rules are collected

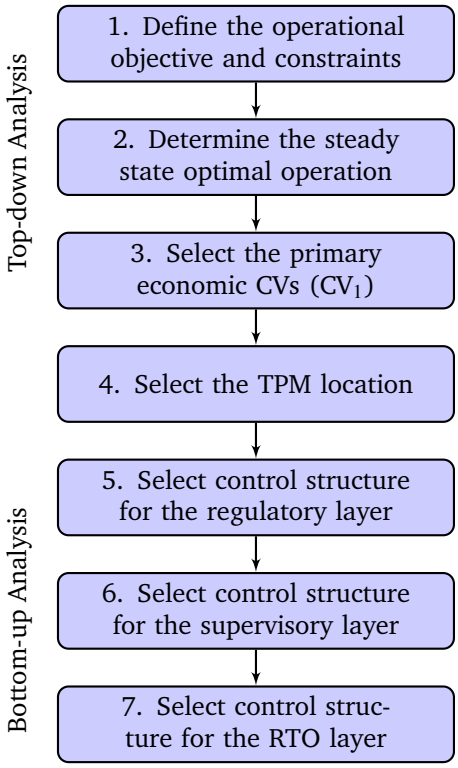

Figure 6.2. Economic plantwide control method [89, 149]. CV: Controlled variable; TPM: Throughput manipulator; RTO: Realtime optimisation. Step 4 serves as a transition between the top-down and the bottom-up analyses.

by Minasidis et al. [104]. The work by Minasidis et al. is the basis of the following introduction of the method. In Step 1, the overall operation objective is formulated, which often is economic. An objective function is formulated reflecting the operation objective and the associated degrees of freedom are identified. Expected economic disturbances are also identified in this step. The operation conditions for every economic disturbance scenario of optimal operation is identified in Step 2 by solving the optimisation problem, which arises from the formulated objective function. The knowledge gained from the identification of optimal operation is in Step 3 applied to select the primary controlled variables ($\mathbf{CV}_1$). The primary controlled variables are typically controlled in the supervisory layer (see Figure 6.1). In Step 4, the throughput manipulator (TPM) is selected, which has a significant impact on the decisions related to the following steps. When the TPM is selected, the bottom-up part starts in Step 5, where the control structure in the regulatory layer is selected. This selection covers the pairing of the secondary controlled variables

($\mathbf{CV}_1$) with the process actuators ($\mathbf{u_D}$ in Figure 6.1). Following the selection of regulatory layer in Step 5, a similar selection of the supervisory layer is performed in Step 7. Thus, the $\mathbf{CV}_1$'s are paired with the $\mathbf{CV}_2$. The final step is Step 7, in which the process optimiser is located. This typically consists of a real-optimisation layer (RTO) that provides the optimal setpoints. In some cases, a well-designed supervisory layer can make the RTO layer redundant.

6.1.3 Stabilising Control

The concept of stabilising control covers the actions of the regulatory layer, i.e. the adjustments in process actuators in order to maintain stable operation. Stable operation means that drifts in operation are avoided. This generally corresponds to controlling liquid holdups and pressures. Furthermore, the temperature profile of a distillation column behaves like a drifting variable, as it can be illustrated as a level between the light components in the top and the heavy components in the bottom [150]. Thus, abnormal operation caused by composition changes is avoided by controlling the temperature.

The main objective of the regulatory layer is to provide stabilisation of the plant in both a mathematical sense (eliminate integrating processes) and a practical sense (avoid drift in operation). This is realised by stable and robust control, which should work under all the conditions imposed by the economic supervisory layer. The regulatory layer is an indispensable part of a plant or unit operation, as stability is closely related to safety. Another objective of the regulatory layer is to provide fast control as illustrated in Figure 6.1, which is reflected in the selection of the controlled variables ($\mathbf{CV}_2$) and their pairing with the actuators. A rule of thumb is formulated by Minasidis et al. [104], which suggests that the pairing of a controlled and a manipulated variable should be carried out in such a way that the physical distance between the corresponding measurement and actuator is minimised. This rule is adopted throughout this chapter and is referred to as the "pair close" rule.

As a single unit operation is the focus rather than that of an entire plant, the TPM position has no significant importance. As a result, the design of the regulatory layer can be performed without considering Steps 1-4, based on dynamic analysis and general guidelines [104]. This approach is applied in this chapter.

6.1.4 Proportional-Integral Control

Proportional-integral-derivative controllers are most often referred to as PID controllers. PID controllers are feedback controllers, which act on a deviation from a specified setpoint of a controlled variable. In this work, PI controllers have been

found sufficient, thereby ignoring the derivative (D) action. The deviation between the desired setpoint and the measured output is termed the error. The error is defined as:

$$e(t) = y_{set}(t) - y_m(t) \tag{6.1}$$

where

$e(t) =$ error of controlled variable k at time t
$y_{set}(t) =$ setpoint of the controlled variable k
$y_m(t) =$ measured value of the controlled variable k

The control action, u, can be written in terms of the error:

$$u(t) = u(t=0) + K_c \left(e(t) + \frac{1}{\tau_I} \int_0^t e(\tau) d\tau \right) \tag{6.2}$$

$u(t) =$ controller action
K_c proportional gain (controller tuning parameter)
τ_I integral gain (controller tuning parameter) [s]

The values of K_c and τ_I can be obtained by using tuning rules. The Skogestad Internal-mode control method (SIMC) [148] has been adopted in this work. This method requires only one tuning parameter, the desired closed-loop time constant (τ_c), along with a transfer function describing the relation between the manipulated and the controlled variable. The notation $u \rightarrow y$ is used to represent a control loop, in which u is manipulated to control y.

6.1.5 Case Study

A concentric HIDiC separating benzene/toluene is considered in this chapter. The considered concentric HIDiC design is summarised in Table 6.1 and the model parameters are given in Table 5.7. Conventional column sizing has been employed using the tray dimensional parameters listed in Table 5.1. This design leads to a gradually increasing rectifying section diameter when moving from the top to the bottom, while the stripping section diameter is gradually decreasing. The trend in the column diameter and the column design is illustrated in Figure 6.3. As a result, the nominal tray liquid holdups vary along the column. Based on the considerations of Section 5.4, it is assumed that a uniform heat transfer area, among the heat-integrated stages, can be achieved by installing heat panels within the column structure.

6.2 Operation Analysis

Generic considerations of a general HIDiC are presented, relating to the identification of the manipulated and the controlled variables.

Table 6.1. Design and nominal operation point if the concentric HIDiC.

Class	Specification	Unit	Value
Feed	Flow rate	$\mathrm{mol\,s^{-1}}$	83.3
	Benzene mole fraction	-	0.50
	Pressure	kPa	101.3
	Temperature	K	365.3
Distillate	Benzene mole fraction	-	0.99
Bottoms	Benzene mole fraction	-	0.01
Design	Trays in the rectifying section	-	25
	Trays in the stripping section	-	23
	Heat exchange area per tray	$\mathrm{m^2}$	19.3
	Column cross sectional area	$\mathrm{m^2}$	See Figure 5.2
	Condenser holdup	mol	12,550
	Reboiler holdup	mol	22,626
	Tray holdups (min/max)	mol	355 / 1610
Operation	Compression ratio	-	2.306
	Feed location pressure	kPa	101.3
	Reflux flow rate	$\mathrm{mol\,s^{-1}}$	0.8333
	Reboiler duty	kW	1175

6.2.1 Operational Degrees of Freedom

A general representation of a HIDiC with actuators and indicators is given in Figure 6.4. The indicators are also shown in the figure. The indicators and their selection will be discussed in more detail below. The number of actuators corresponds to the number of operational degrees of freedom. These are listed in Table 6.2. Because the HIDiC is considered an isolated process as part of a plant, the feed flow rate is not considered as an operation degree of freedom and is hence considered as the TPM.

The HIDiC considered (Figure 6.4) has seven operational degrees of freedom reflected in six valves and one compressor setting. Four of the valves are manipulating flow rates directly (V-1, V-2, V-4, and V-6). In a real set-up, the valves V-3 and V-5 are manipulating the flow rates of cooling water and steam. However, in simulation it is assumed that these valves can directly manipulate the corresponding duties of the condenser (Q_{cnd}) and the reboiler (Q_{rbl}), respectively. The operational degrees of freedom, represented by valves V-1, V-2, V-3, V-4, and V-5, are identical to those of the conventional distillation column (CDiC). When converting the CDiC into the HIDiC, three additional operational degrees of freedom arise. First of all, the introduction of the compressor adds an additional operational degree of freedom, the compressor setting (C-1). The compressor setting of a real process could be its rotational speed, but in this work it is represented by the compressor duty.

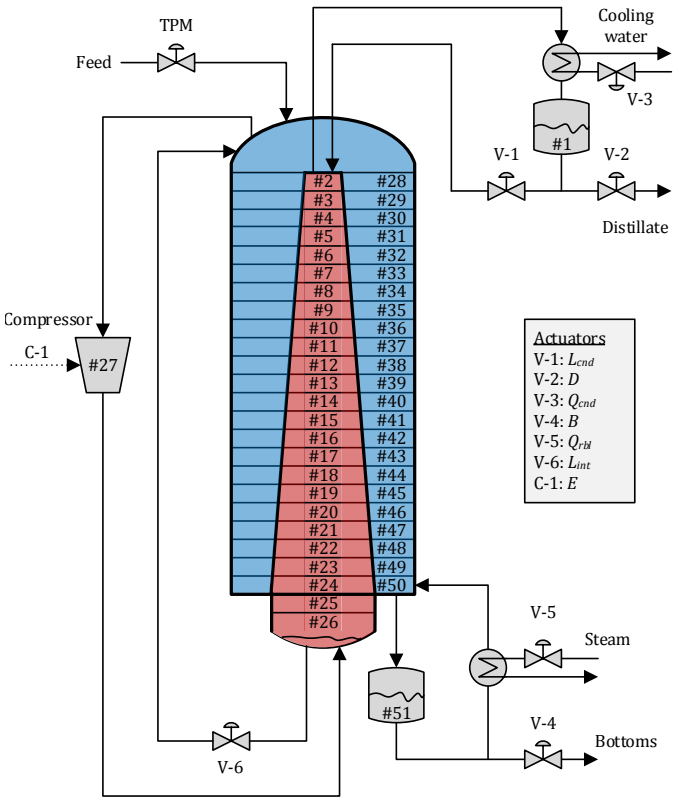

Figure 6.3. A concentric HIDiC with actuators separating benzene/toluene.

Ho et al. [55] argue that a pressure regulator valve should be used for controlling the rectifying section outlet liquid pressure in order to avoid liquid maldistribution in its entry point in top of the stripping section. However, it is presumed that this pressure is self-regulating and that a reasonable liquid pressure can be achieved if the level controller valve and/or the outlet nozzle (entry) are dimensioned appropriately. As a result of physically separating the two column sections, the flow rate of the liquid between the two sections must be regulated, which can be done by valve V-6. A similar degree of freedom analysis is provided by Ho et al. [55] for several simpler HIDiC configurations. The difference between the actuators by Ho et al. and the actuators in Table 6.2, is that Ho et al. used the compressor rotation speed rather than the duty.

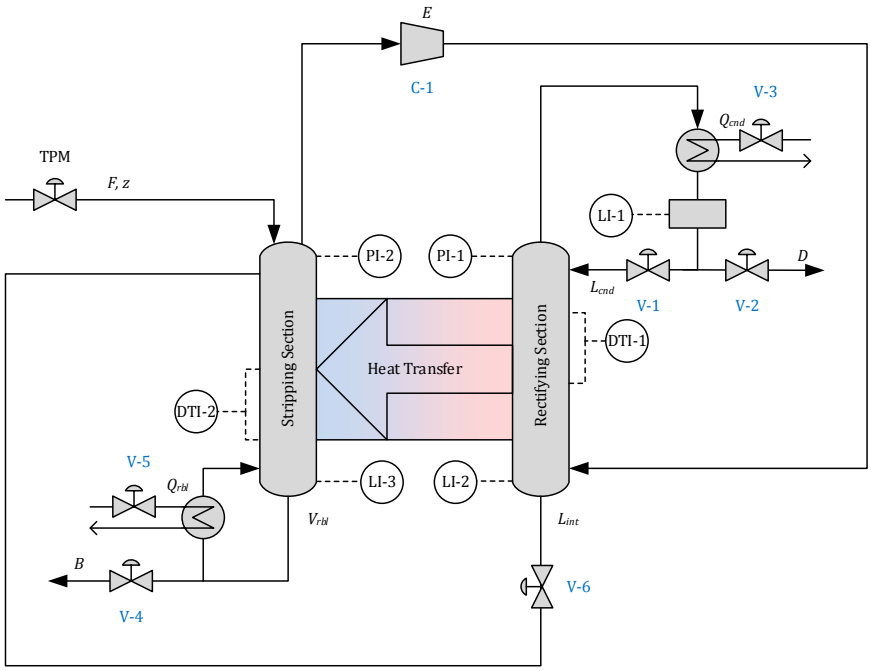

Figure 6.4. Conceptual representation of the HIDiC with actuators and measurement indicators.

6.2.2 Identification of Secondary Controlled Variables ($\mathbf{CV}_2$)

The secondary controlled variables are identified by analysis of the HIDiC illustrated in Figure 6.4. Potential drifting variables are identified in a systematic manner using the guidelines by Minasidis et al. [104]. All selected secondary controlled variables constitutes $\mathbf{CV}_2$. These are listed below:

- **Temperature profile:** The temperature profile must be controlled, which is equivalent to controlling one composition in the column. In this work, the possibility of composition control is left for the economic objectives presented in Chapter 7. This approach enables the supervisory layer to manipulate the setpoint of the temperature profile controller. Due to this possible coupling to the supervisory layer, the temperature control is suggested to be carried out in the column section containing the more valuable component. Therefore, the design of the temperature controller is case specific and the following scenarios must be considered: The top product is more valuable and the bottom

Table 6.2. Identification and classification of degrees of freedom assuming given feed flow rate.

Label	Operation degrees of freedom	Steady state degrees of freedom
V-1	Reflux flow, L_{cnd}	Reflux flow rate, L_{cnd}
V-2	Distillate flow, D	Condenser holdup*, M_{cnd}
V-3	Condenser duty, Q_{cnd}	Stripping section pressure, P_{str}
V-4	Bottoms flow, B	Reboiler holdup*, M_{rbl}
V-5	Reboiler duty, Q_{rbl}	Boilup flow rate, V_{rbl}
V-6	Intermediate flow, L_{int}	Intermediate holdup*, M_{int}
C-1	Compressor duty	Rectifying section pressure, P_{rct}

* No steady state effect

product is more valuabe. In addition to stabilisation, temperature control provides several benefits as e.g. indirect level control, indirect composition control, and reduces the interactions in any composition control loops. Since pressure dynamics are expected to play a significant role in the stabilisation of a HIDiC, it is proposed to control a temperature difference across a column section. This provides a simple built-in pressure compensation at an increased complexity of controller design as two sensors must be located rather than one. The criteria for selecting the column temperature measurement(s) are given by Skogestad [150]:

- The location should be within the column rather than at the column ends,
- control temperature in the column end where composition control is most important (usually the case for the more valuable product),
- locate the temperature where the steady state sensitivity is large ("maximum gain rule"),
- for dynamic reasons, one should avoid locating a temperature sensor in a region with a small temperature change from one stage to the next (avoid "flat" temperature profile),
- use an input in the same end as the temperature sensor since the temperature loop must be fast, and
- avoid using an input that may saturate.

The sensor for measuring the difference in temperatures is referred to as a differential temperature indicator (DTI) in Figure 6.4.

- **Section Pressures:** A pressure is a measure of a vapour holdup and therefore closely resembles an integrating process. It is expected that the pressures of

both column sections, i.e. that of the rectifying section (P_{rct}) and that of the stripping section (P_{str}), must be controlled for stabilisation. A similar, explicit treatment of the control of the pressures in both column sections has not been encountered in literature. This might be due to the fact that the pressures do have some degree of self-regulation. For example, an increase in the rectifying section pressure leads to an increase in the tray temperatures and therefore the amount of internal heat integration increases. As heat is removed in the rectifying section due to heat integration, the pressure decreases as vapour is condensed. However, as the change in internal heat transfer affects the separation, the above control layers might prevent it. The pressure stabilisation gives rise to some valuable analysis of this particular behaviour. Pressure sensors can in principle be placed in any tray of each section. Hence, the preferred position is investigated from a stabilisation point of view. The location of pressure sensors can also have economic implications [90, 101]. The pressure sensors are called pressure indicators (PI) in Figure 6.4.

- **Liquid holdups:** Dynamic holdups act as pure integrators and are therefore unstable. In most cases, in particular for non-reactive systems, the holdups do not have impact on the steady state and are therefore not considered. However, holdups act as buffer tanks in a dynamic system and influence the time constants of e.g. the composition responses. As a result, these effects are included in these studies. Similar to conventional distillation, the condenser holdup (M_{cnd}) and the reboiler holdup (M_{rbl}) must be controlled. Due to the physical separation of the rectifying section and the stripping section, it is not certain that gravity is used to transport the liquid from the rectifying section to the stripping section, nor it is certain that the pressure difference between the sections can stabilise the liquid holdup. Therefore, it is expected that the bottom holdup of the rectifying section (M_{int}) must be controlled. The subscript "int" is used for intermediate as referring to in-between the column sections. Liquid holdups can be measured directly in the corresponding tanks. The sensors for measuring the liquid holdups are called level sensors and are displayed in Figure 6.4 using the abbreviation "LI" for level indicator.

- **Liquid pressure:** The pressure of the liquid entering the low-pressure stripping section from the high-pressure rectifying section must be controlled such that the entrance of the liquid in the stripping section does not cause disruption in entrance location. The pressure of the entering liquid should be adjusted to approximately that of the pressure of the entrance location.

- **Internal hydraulics:** In this work, simulations indicated that most HIDiC

designs have no external reflux. A small, but consistent, liquid reflux might be needed to keep the separation efficiency above a certain limit in the upper trays. In some cases, this might lead to an economic loss and therefore the minimum liquid reflux flow rate is a fixed back-off value.

6.3 Design of Regulatory Layer

The design of the regulatory layer denotes the pairing of the manipulated variables $\mathbf{u_D}$ with the measurements $\mathbf{y}$ of the secondary controlled variables $\mathbf{CV}_2$:

$$\mathbf{u_D} = [L_{cnd}, D, Q_{cnd}, B, Q_{rbl}, L_{int}, E]^T \tag{6.3}$$

$$\mathbf{y} = [M_{cnd}, M_{rbl}, M_{int}, P_{rct}, P_{str}, \Delta T, L_{cnd}]^T \tag{6.4}$$

Note that the liquid reflux flow rate L_{cnd} is listed as a measurement in order to reflect that it is considered as a secondary control variable.

Generally, simple PI controllers (or PID) are desired in the regulatory control layer. The pairing is done sequentially in the order of the following subsections. The simple Skogestad IMC (SIMC) rules [148] are employed for tuning of the PI controllers. Therefore, model identification is carried out on rigorous dynamic responses in order to obtain low-order transfer functions. The considered transfer functions are an integrating process, a first-order transfer function, a second-order transfer function, and a second-order transfer function with numerator dynamic transfer function. Time delays are included for all the considered transfer functions. The only decision variable related to the tuning is the desired closed-loop time constant (τ_c) when a transfer function has been obtained.

6.3.1 Liquid Holdup Control

Based on the "pair-close" rule, the only options for the control of the condenser holdup is the distillate flow rate ($D \rightarrow M_{cnd}$) and the liquid intermediate flow rate to control the intermediate holdup ($L_{int} \rightarrow M_{int}$). The most obvious way of controlling the reboiler holdup is by the bottoms flow rate ($B \rightarrow M_{rbl}$) rather than by the boil-up rate, which is dictated by the reboiler duty. Note that the distillate flow rate is the only option for controlling the condenser holdup. Note that contrary to a conventional distillation column, the reflux flow rate is close to saturation for the HIDiC ($L_{cnd} = 0.8333\,\mathrm{mol\,s^{-1}}$). Therefore, the liquid reflux flow rate is an infeasible candidate as the manipulated variable. In this work, it is assumed that the dynamics of the intermediate holdup is identical to that of the remaining trays. As a result, the intermediate flow rate is described by the Francis weir formula in Eq. (3.35). This has a similar response to that of a simple P controller.

Actuator dynamics are neglected in this work, so the simple integrating processes are obtained:

$$\frac{\Delta M_{cnd}(s)}{\Delta D(s)} = -\frac{1}{s} \tag{6.5}$$

$$\frac{\Delta M_{rbl}(s)}{\Delta B(s)} = -\frac{1}{s} \tag{6.6}$$

where

$s =$ the independent variable in the Laplace domain

$\Delta =$ deviation from steady state

These transfer functions can be derived mathematically as shown in Illustration 6.1. A value of $\tau_c = 120\,\mathrm{s}$ was considered as a reasonable value, since it is not critical to keep the holdups tightly controlled.

Illustration 6.1. Derivation of transfer functions for liquid holdup.
Take the example of the condenser. Its total mass balance is

$$\frac{M_{cnd}}{dt} = V_2 - L_{cnd} - D.$$

Taking the Laplace transform on both sides and introducing deviation variables yields:

$$s\Delta M_{cnd}(s) = \Delta V_2(s) - \Delta L_{cnd}(s) - \Delta D(s),$$

which leads to:

$$\frac{\Delta M_{cnd}(s)}{\Delta V_2(s)} = \frac{1}{s}, \quad \frac{\Delta M_{cnd}(s)}{\Delta L_{cnd}(s)} = -\frac{1}{s}, \quad \frac{\Delta M_{cnd}(s)}{\Delta D(s)} = -\frac{1}{s}$$

A similar approach applies to the intermediate holdup and the reboiler holdup.

6.3.2 Pressure and Temperature Control

As the nominal reflux flow rate is expected to be low, the remaining actuators are Q_{cnd}, Q_{rbl}, and E, which can be used to control P_{rct}, P_{str}, and ΔT. Usually, from a stabilisation point of view, the selection of the location of the pressure sensor is not important. As a result, the column section pressures are measured in the top of the column sections. According to the guidelines listed in Section 6.2.2, the controlled temperature should be sensitive to the inputs in steady state and must not be located at a flat region in the temperature profile. As it was argued to control a temperature difference in the HIDiC, it is proposed to locate a tray i, whose temperature must be subtracted from the temperature in the top of the rectifying section (T_2) if ΔT is located in the rectifying section, or from the temperature in the bottom of the

stripping section (T_{N_S-1}) if ΔT is located in the stripping section. These column end temperature measurements represent the stable part of ΔT, which provides pressure compensation. By considering the steady state gains of step changes in the potential manipulated variables (Q_{cnd}, Q_{rbl}, and E) in all possible combinations of $\Delta T = T_2 - T_k,\ k = 3,4,\ldots,N_F - 1$, it was found that the combination $\Delta T = T_2 - T_{17}$ had the largest gain. Interestingly, the temperature at stage #17 corresponds to the pinched pair, i.e. the location where the temperature gradient responsible for internal heat transfer is the smallest (see Figure 5.3). This result appears reasonable, as simulations have shown that changes in operation can move the pinch location thereby indicating sensitivity to operational changes. Based on this reflection, the pinch location is a suitable starting point for defining ΔT for any separation.

A similar analysis was carried out for the case, where the temperature profile must be controlled in the stripping section. Again, it was found by simulation that the more sensitive controlled variable is $\Delta T = T_{43} - T_{50}$, which corresponds to the temperature difference between the heat transfer pinch location (stage #43) and the bottom of the stripping section (stage #50). When ΔT is evaluated for both column sections, the rectifying section temperature difference will be denoted $(\Delta T)_{rct}$ and the stripping section temperature difference will be denoted $(\Delta T)_{str}$.

Typically, in conventional columns, the pressure of the entire column is controlled by the condenser duty. The reason why this is not the case for the HIDiC is the significant amount of heat integration. The nominal condenser duty is $-1240\,\mathrm{kW}$, while the total nominal amount of heat, exchanged in the rectifying section, is $-2181\,\mathrm{kW}$. Hence, the total amount of internal heat transfer is twice the amount of the condenser duty. Therefore, significant dynamic interactions are expected. The individual initial responses of the three controlled variable candidates (P_{rct}, P_{str}, and ΔT) subject to $\pm 1\%$ step changes in the manipulated variable candidates (Q_{cnd}, Q_{rbl}, and E) are illustrated in Figure 6.5. Order transfer functions of as low order as possible have been fitted to the dynamic responses of the full model. These responses are illustrated in Figure 6.5. A visual representation of the match between the fitted responses and the actual reposes is provided in the figure as well. In general, the fitted transfer functions were able to describe both the actual dynamics in the initial responses and to predict the resulting steady states.

When considering both options for controlling the temperature profile ($\Delta(\Delta T)_{rct}$ and $\Delta(\Delta T)_{str}$), the system matrix $\mathbf{G}(s)$ can be represented in the following way:

$$\begin{bmatrix} \Delta P_{rct} \\ \Delta P_{str} \\ \Delta(\Delta T)_{rct} \\ \Delta(\Delta T)_{str} \end{bmatrix} = \mathbf{G}(s) \begin{bmatrix} \Delta Q_{cnd} \\ \Delta Q_{rbl} \\ \Delta E \end{bmatrix} \tag{6.7}$$

The obtained transfer functions based on the best match can be represented by the system matrix:

$$\mathbf{G}(s) = \begin{bmatrix} \frac{4.444\cdot10^{-3}(24.87s+1)}{(937.2s+1)(7.351s+1)} & \frac{3.807\cdot10^{-3}e^{-3.422s}}{(935.9s+1)(18.19s+1)} & \frac{5.218\cdot10^{-3}(93.56s+1)e^{-1.806s}}{(809.3s+1)(17.25s+1)} \\ \frac{2.220\cdot10^{-3}e^{-2.742s}}{895.1s+1} & \frac{1.915\cdot10^{-3}e^{-5.185s}}{915.2s+1} & \frac{0.8678\cdot10^{-3}(-657.9s+1)}{(1026s+1)(4.066s+1)} \\ \frac{-58.40\cdot10^{-3}(26.77s+1)}{(1920s+1)(2.265s+1)} & \frac{6.921\cdot10^{-3}(1285s+1)}{(2503s+1)(2499s+1)} & \frac{0.2707\cdot10^{-3}(-17465s+1)e^{-108.5s}}{(2819s+1)(356.0s+1)} \\ \frac{-46.77\cdot10^{-3}(-42.74s+1)e^{-5.075s}}{(2364s+1)(21.04s+1)} & \frac{-16.26\cdot10^{-3}(-140.3s+1)}{(1944s+1)(11.06s+1)} & \frac{-54.54\cdot10^{-3}(953.5s+1)e^{-18.18s}}{(1932s+1)(250.4s+1)} \end{bmatrix} \tag{6.8}$$

In all transfer function representations, the pressures are given in bar. Both the initial responses in Figure 6.5 and the obtained transfer functions in Eq. (6.8) witness the rather complex dynamics of the HIDiC. For example, an inverse response is observed in the responses for P_{str} when E is changed. Furthermore, the response of ΔT to changes in E has a small steady state gain but a complicated dynamic response, which the low-order transfer functions are not able to capture. The obtained transfer function is a second-order transfer function with numerator dynamics with inverse response. However, it does not capture the initial response, which is in the same direction of the final response.

The steady state relative gain array (RGA) [17] can be used to assist in the decision on the pairing of the manipulated and controlled variables for decentralised control. RGA elements close to unity are preferred and must not be negative. If temperature control must be carried out in the rectifying section, $\Delta(\Delta T)_{str}$ is omitted in Eq. (6.8) and a 3×3 system matrix ($\mathbf{G}_{rct}(s)$) is obtained. The following RGA is obtained:

$$\mathbf{G}_{rct}(s=0) = 10^{-3}\begin{bmatrix} 4.4440 & 3.8070 & 5.2180 \\ 2.2200 & 1.9150 & 0.8678 \\ -58.4000 & 6.9210 & 0.2707 \end{bmatrix} \Rightarrow$$

$$\mathbf{\Gamma} = \mathbf{G}_{rct} \otimes \left(\mathbf{G}_{rct}^{-1}\right)^T = \begin{bmatrix} -0.0549 & -0.4396 & \mathbf{1.4945} \\ 0.1754 & \mathbf{1.3192} & -0.4945 \\ \mathbf{0.8795} & 0.1204 & 0.0000 \end{bmatrix}$$

The structure of the RGA is identical to Eq. (6.8) with controlled variables in rows and manipulated variables in columns. The final suggestion for pairing is highlighted in the RGA as boldface numbers, which leads to $Q_{cnd} \rightarrow \Delta T$, $Q_{rbl} \rightarrow P_{str}$ and $E \rightarrow P_{rct}$. The two latter pairings are intuitive, but the former pairing is not. However, it was found that it should be possible to use the condenser duty for controlling the temperature profile. These three resulting control loops appear to be feasible by considering both the steady state RGA and the initial responses (Figure 6.5). Furthermore, the obtained pairings are in accordance with the "pair close" rule.

A similar analysis of the RGA is carried out for the temperature difference located in the stripping section. In this case, the RGA becomes:

$$\mathbf{G}(s=0) = 10^{-3}\begin{bmatrix} 4.4440 & 3.8070 & 5.2180 \\ 2.2200 & 1.9150 & 0.8678 \\ 46.7700 & -16.2600 & -54.5400 \end{bmatrix} \Rightarrow$$

$$\mathbf{\Gamma} = \mathbf{G} \otimes \left(\mathbf{G}^{-1}\right)^T = \begin{bmatrix} 0.9089 & -1.3934 & \mathbf{1.4846} \\ -0.6172 & \mathbf{2.1090} & -0.4918 \\ \mathbf{0.7083} & 0.2845 & 0.0073 \end{bmatrix}$$

A similar pairing is obtained when choosing the pairing resulting in RGA elements close to unity (indicated in RGA as boldface numbers). It might seem undesirable to control the stripping section temperature profile with the condenser duty when having the "pair close" rule in mind. But as illustrated previously, the sum of the internal heat integration is larger than the condenser duty itself. In fact, the effect on the opposite section might be at least as significant due the self-regulating behaviour as discussed in Section 6.2.2. For both locations of ΔT, the dominant factor for the resulting pairing is the direct coupling between the compressor duty and the rectifying section pressure. This is illustrated by the significant gain for the rectifying section pressure compared to the remaining controlled variables, which is clear in the last column in the steady state gain matrix $\mathbf{G}(s=0)$.

A remark on the illustrated dynamic responses for a CDiC in Figure 6.5 is that these responses have both larger time constants and smaller gains than those of the HIDiC. For example, the steady state gain matrix is:

$$\mathbf{G}^{\mathbf{CDiC}}(s) = \begin{bmatrix} \frac{\Delta P_{rct}}{\Delta Q_{cnd}} & \frac{\Delta P_{rct}}{\Delta Q_{rbl}} \\ \frac{\Delta P_{str}}{\Delta Q_{cnd}} & \frac{\Delta P_{str}}{\Delta Q_{rbl}} \end{bmatrix} = 10^{-3}\begin{bmatrix} 2.474 & 2.515 \\ 2.072 & 2.245 \end{bmatrix}$$

6.3.3 Liquid Pressure and Internals Hydraulics Control

These two control loops will not be considered in this work, as they are not modelled. The liquid preessure of the intermediate liquid flow has no impact on the model solution as the enthalpy is independent of pressure (see Eq. (3.17)). It was discussed previously that the liquid reflux should be kept low, but at the same time it should be kept at a non-zero value in order to keep the top trays wetted. A flow controller is needed to satisfy this requirement. As the liquid reflux is a model input, no controller is required in this work.

6.3.4 Recommendations and Discussion

A list of the fundamental controllers of a HIDiC constituting the stabilising control structure in the regulatory layer can be summarised:

- V-6(L_{int}) $\rightarrow M_{int}$: Level control (LC). The dynamics are not considered in this work.
- V-1 $\rightarrow L_{cnd}$: Flow control (FC).
- V-2(D) $\rightarrow M_{cnd}$: Level control (LC).
- V-4(B) $\rightarrow M_{rbl}$: Level control (LC).
- V-5(Q_{rbl}) $\rightarrow P_{str}$: Pressure control (PC).
- V-3(Q_{cnd}) $\rightarrow \Delta T$: Differential temperature control (DTC). Note that this structure is independent on the location of the measurement of the column temperature profile.
- C-1(E) $\rightarrow P_{rct}$: Pressure control (PC).

The items in the above list are presented in the order of the proposed sequential tuning procedure. Level controllers have no significant interactions with the remaining loops and should therefore be tuned and implemented first. The latter three loops are sorted according to an increasing desired closed-loop time constant (τ_c). Furthermore, the resulting control structures for stabilising a HIDiC for the two considered cases (distillate or bottoms valuable product) are illustrated in Figure 6.6. Based on the results, it should be able to design the regulatory control structure for any HIDiC as most considerations are generic. The control of the temperature profile based on the temperature measurements of the pinch locations requires evaluation of several different mixtures. As seen in Chapter 5, it appears that common separations have a heat transfer pinch location near the middle of the column sections. According to the previous analysis, the heat-integrated tray, involved in a heat transfer pinch location in the considered column section, appears to be a suitable candidate for temperature profile control. This statement is explored by simulation in the following section.

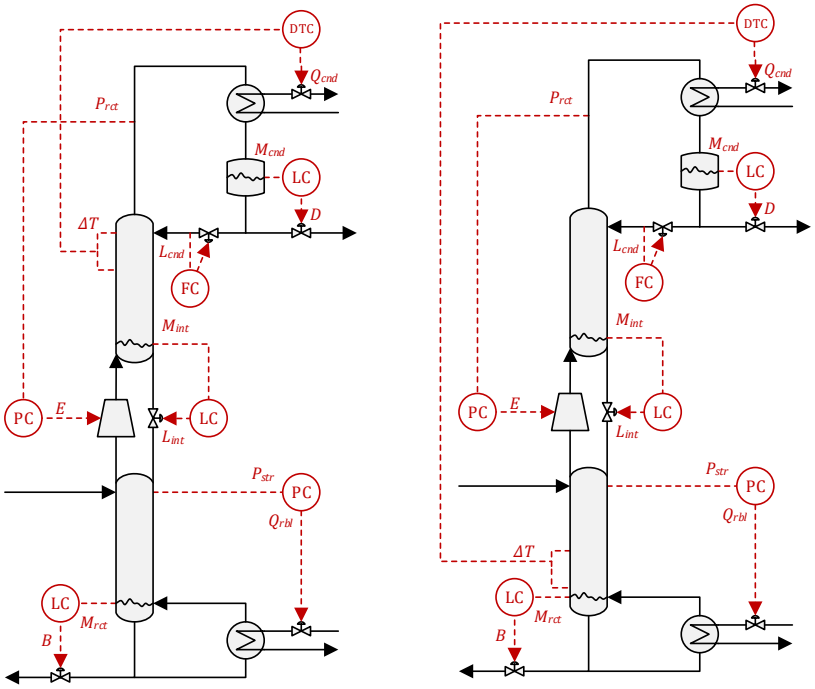

(a) Distillate more valuable product, which requires control of the rectifying section temperature profile.

(b) Bottoms more valuable product, which requires control of the stripping section temperature profile.

Figure 6.6. Regulatory layer control structures depending on product values. LC: Level controller, PC: Pressure controller, DTC: Differential temperature controller, FC: Flow controller.

6.4 Dynamic Evaluations

In this section, the developed regulatory control layer structure is evaluated by simulation. Benzene/toluene is used as the model feed mixture, while it is assumed that the distillate is the more valuable product. Hence, the evaluation concerns the control structure shown in Figure 6.6(a).

6.4.1 Tuning

Sequential tuning was carried out in the order, displayed in Table 6.3 (starting from the top). The table provides the identified first-order models, the desired closed-loop time constant, and the resulting controller parameters. Desired closed-

loop time constants were chosen in the order of minutes because large actions are undesired in the pressure control loops. In addition, numerical convergence issues in the differential equation solver were encountered for more tightly controlled pressure loops.

The manipulation of the steam supply, and hence the reboiler duty, is reasonably fast. Therefore, the desired closed-loop time constant of this loop is chosen as $\tau_{c,Q_{rbl}\rightarrow P_{str}} = 90\,\text{s}$. The rectifying section pressure control loop were chosen to be the slowest as it is desirable to run the compressor with as few operational changes as possible ($\tau_{c,E\rightarrow P_{rct}} = 180\,\text{s}$). Finally, the desired closed-loop time constant of the loop involving the condenser duty is chosen as $\tau_{c,Q_{cnd}\rightarrow \Delta T} = 120\,\text{s}$ since Skogestad [150] recommends to have a rather fast temperature controller. A benefit of choosing the largest desired closed-loop time constant for the control loop involving the compressor is that this loop has smaller interactions on the remaining loops. As a result, this loop requires less controller action, as it acts upon disturbances after the faster and more interactive loops have acted.

6.4.2 Regulatory Layer Performance

The following scenario is used for testing the control structure:

- $t \geq 0\,\text{h}$: +20% step response in feed flow rate (F)
- $t \geq 2.5\,\text{h}$: +5% step response in benzene mole fraction (z_1)
- $t \geq 5\,\text{h}$: +100% in reflux ratio (L_{cnd}) such that $L_{cnd}^{set} = 1.668\,\text{mol}\,\text{s}^{-1}$
- $t \geq 7.5\,\text{h}$: +5% step change in stripping section pressure (P_{str}^{set})

The former two changes correspond to disturbance changes and the latter two correspond to setpoint changes. The setpoint changes simulate the action of the above supervisory control layer (Figure 6.1), which will be developed in Chapter 7. The dynamic responses subject to the formulated test scenario are illustrated in Figure 6.7. The composition responses are not shown in the figure as they will be the focus in the following subsection. Satisfactory setpoint tracking was obtained with acceptable smoothness of the manipulated variables. Furthermore, stability w.r.t. entrainment flooding and weeping was checked using the method of Section 5.2.1. Neither entrainment flooding nor weeping were encountered in the dynamic simulation. It can thus be concluded that stabilisation of the HIDiC has successfully been obtained.

An additional scenario was tested, corresponding to a case, where the temperature control loop is not active (Figure 6.7). Reasonably stable operation was

Table 6.3. Sequential tuning (ordered) of the concentric HIDiC with dynamic responses. In each row, the above control loops are closed. The unit of the pressures is bar. Legend: Dynamic responses (——), fitted transfer functions, $\mathbf{G}(s)$ (- - -).

Loop	Response		Controller parameters		
	Δy vs. t/τ_c	$\mathbf{G}(s)$	τ_c s	K_c	τ_I s
$D \rightarrow M_{cnd}$	Not shown	$\frac{-1}{s}$	120	$-8.333 \cdot 10^{-3}$	480.0
$B \rightarrow M_{rbl}$	Not shown	$\frac{-1}{s}$	120	$-8.333 \cdot 10^{-3}$	480.0
$Q_{rbl} \rightarrow P_{str}$	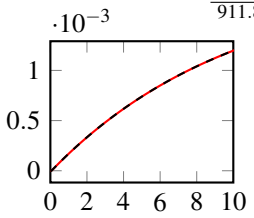	$\frac{1.915 \cdot 10^{-3}}{911.8s+1} e^{-5.436s}$	90	$4.989 \cdot 10^{3}$	381.7
$Q_{cnd} \rightarrow \Delta T$	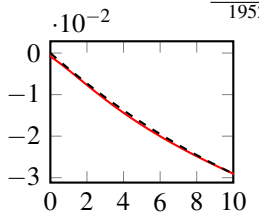	$\frac{-63.22 \cdot 10^{-3}}{1952s+1}$	120	-257.3	480.0
$E \rightarrow P_{rct}$	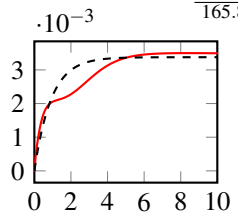	$\frac{3.377 \cdot 10^{-3}}{165.8s+1}$	180	272.7	165.8

achieved but ΔT deviates significantly from its nominal value. The scenario with the temperature controller inactive is relevant in the situation of HIDiC startup as mentioned in Table 2.8. Furthermore, the temperature loop is not always included in simulations as will be discussed in the following subsection. However, the simulation shows that the temperature control loop plays a significant role.

6.4.3 Open-loop Responses

Simple distillation column models are available for the HIDiC, which for example assume constant molar overflow, including the simpler model of Huang et al. [60]. Extra efforts are required using the proposed model in Chapter 3 for composition open-loop responses, compared to the simpler model of Huang et al. In order to investigate the impact of the model choice, the parameters are translated into the required parameters in the simple model using mean values of the relative volatility and the heat of vaporisation, while the remaining design variables were kept identical (compression ratio, separation specifications, molar holdups etc.). As the tray pressure drop is not considered in the simple model, the resulting temperature driving forces for internal heat transfer were larger for the Huang model. Therefore, an internal heat transfer area of $A = 11.2\,\mathrm{m}^2$ for every stage was used in order to obtain a similar value of the reflux flow rate. This is reasonable because the simple model does not account for the pressure dependency of the relative volatility. Since the two section pressures are fixed in the Huang model, they should be stabilised in the proposed model as well for comparison. Pressure stabilisation can not be achieved in the HIDiC without affecting the energy balance, and thus it is assumed that a fair comparison between the models can be obtained when the proposed pressure stabilisation loops are active.

Dynamic simulation is carried out and significant dissimilarities are obtained in the two models (Figure 6.8). Similar trends of dynamic responses in the top and bottom compositions are observed for feed flow rate and feed composition step responses. Furthermore, the gains associated with these responses are of similar magnitude, except the bottom composition response caused by a feed flow rate step change. One explanation of this could be due to the fact that the effect of the sensible heat of the throttled liquid is accounted for in the presented model. In particular, the compression ratio step responses are very different, which is due to the way that the pressure dynamics are accounted for in the presented model. In addition, the composition open-loop responses are shown for the fully implemented regulatory control layer, i.e. with the temperature control loop closed. As expected, the temperature control loop provides indirect composition control, which leads to a significant reduction in the required control efforts by eventual composition

control loops.

6.5 Conclusions

A decentralised control structure of the regulatory layer was derived based on a systematic analysis of the concentric heat-integrated distillation column (HIDiC). The HIDiC has seven variables that must be controlled in order to stabilise the column operation. Five of the seven variables were considered in simulation. Suggestions for the locating of the temperature measurements are provided. A case study of the separation of benzene/toluene was presented, and satisfactory stabilisation was achieved. Following characteristics were observed of the developed regulatory layer:

- Good feed disturbance rejection
- Good setpoint tracking when subject to setpoint changes
- No entrainment flooding or weeping subject to both feed disturbances and regulatory control loop setpoint changes

Based on the achieved results, it must be stressed that the pressure dynamics are important to consider, when performing dynamic simulations. This is due to the strong coupling between pressure, temperature and compositions, which are not normally present in a conventional distillation column. In order to emphasise this claim, the model was benchmarked against a simpler model with the constant molar overflow-assumption. In particular, a significant mismatch was observed in dynamic composition responses subject to step changes in the compression ratio. This observation illustrates the need for including pressure dynamics, when conducting dynamic simulations of the heat-integrated distillation column.

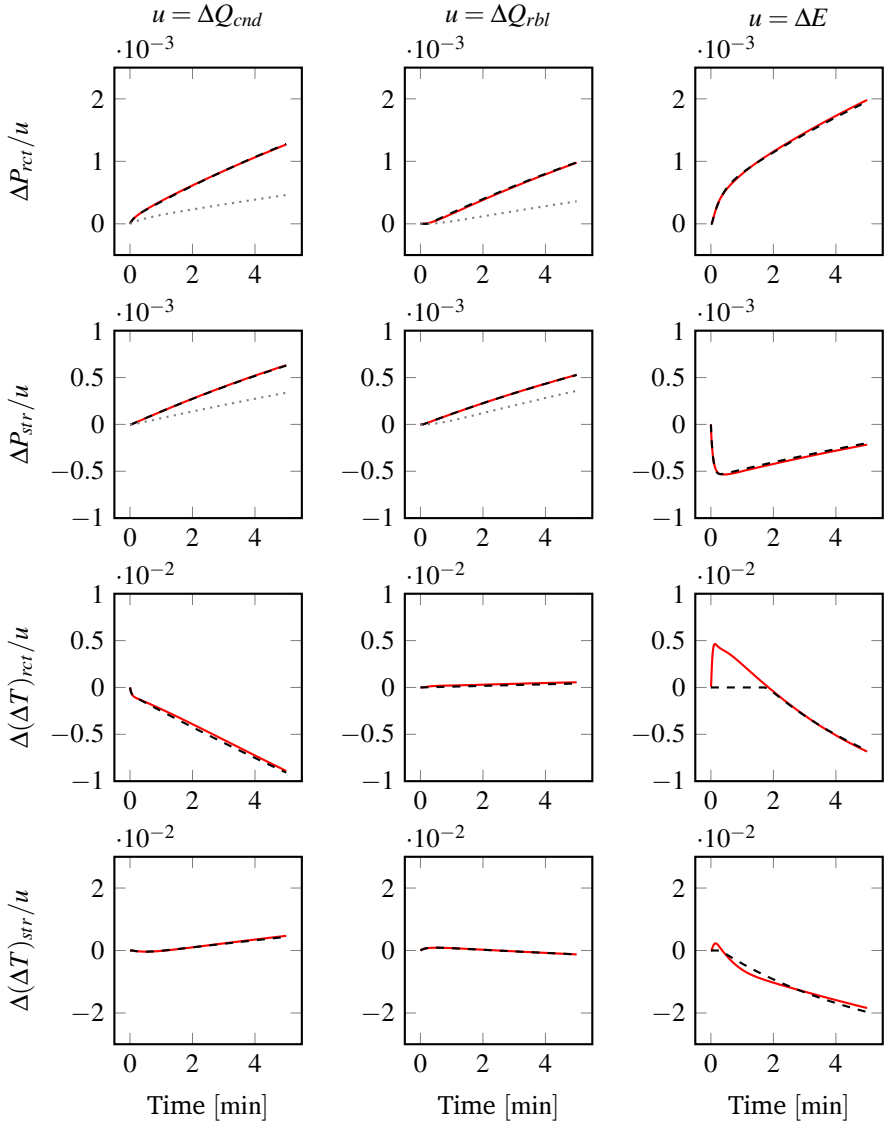

Figure 6.5. Initial responses of the HIDiC separating benzene/toluene. Dynamic responses are illustrated for a CDiC with similar specifications carrying out the same separation for comparison. Legend: Full order model response (——); Identified low-order model (- - -); CDiC response (·····).

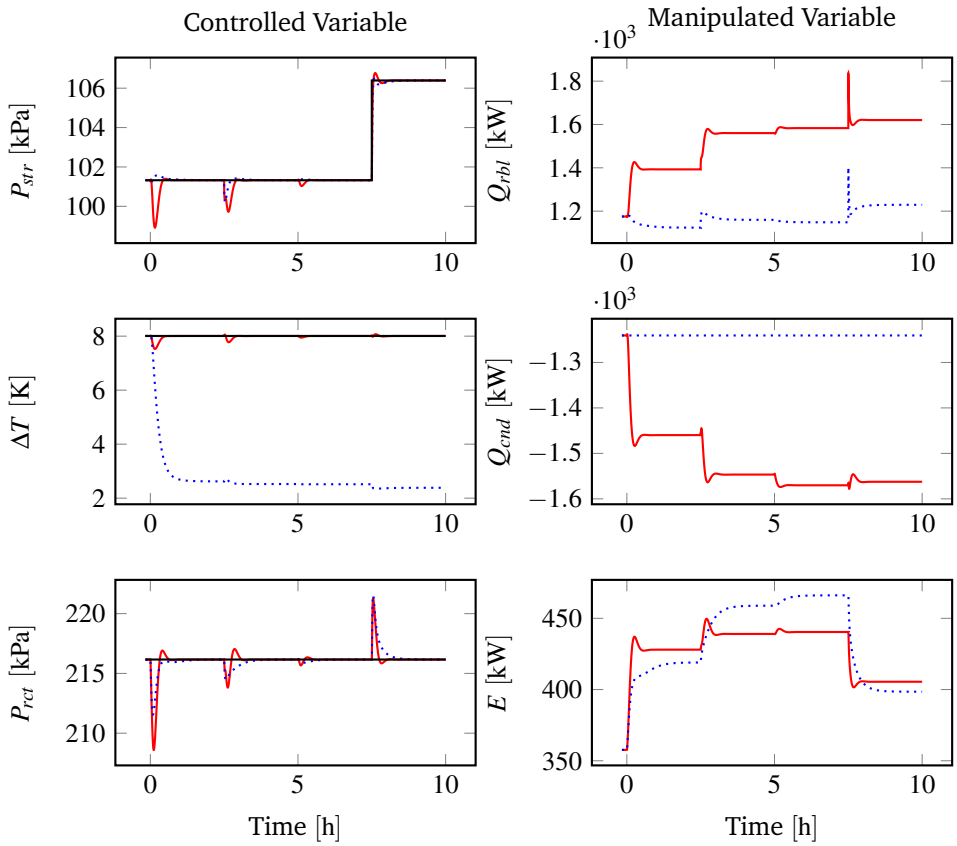

Figure 6.7. Dynamic responses in controlled and manipulated variables of the considered pressure and temperature control loops. Legend: All loops closed (——), only pressure loops closed (·····), setpoint (——).

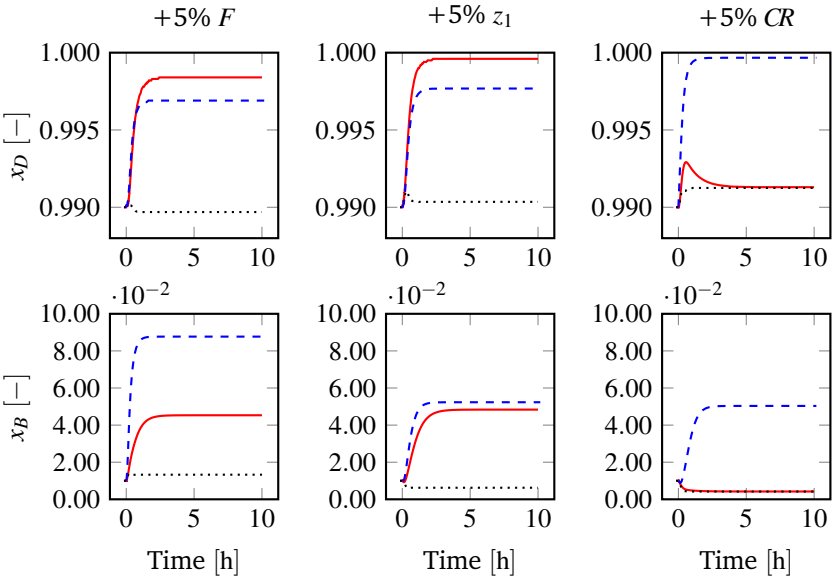

Figure 6.8. Dynamic responses in top and bottom compositions to step responses in the feed flow rate (F), benzene feed mole fraction (z_1), and compression ratio (CR). Legend: Model including holdup and pressure stabilisation (——), model including holdup, pressure and temperature stabilisation (·····), and the simpler model by Huang et al. [60] (- - -).

Chapter 7

Optimising Control

Optimal operation of a heat-integrated distillation column with compressor(s) is formulated. The optimal operation is identified for a concentric heat-integrated distillation column separating benzene/toluene. A control structure of the supervisory control layer is devised and evaluated by simulation. The findings of the case study are generalised and a control structure of the concentric HIDiC is formulated and presented. The economic plant-wide control method by Larsson and Skogested was adopted for devising the control structure in a systematic manner [T. Larsson and S. Skogestad. Plantwide control–a review and a new design procedure. *Model Ident Control*, 21(4):209–240, 2000]. The previously developed regulatory control layer was combined with the supervisory control layer, and simulations were carried out for evaluating the performance w.r.t. tracking of the optimal operation.

This chapter is based on work conducted in collaboration with Professor Sigurd Skogestad during an exchange period at the Norwegian University of Science and Technology, Trondheim, Norway.

A part of this chapter was is presented in the conference proceedings of DYCOPS 2016 [T. Bisgaard, S. Skogestad, J.K. Huusom, and J. Abildskov. Optimal operation and stabilising control of the concentric heat-integrated distillation column. *11th IFAC International Symposium on Dynamics and Control of Pro-*

cess Systems – Trondheim, Norway, 2016]. Early progress on this problem was presented during the Nordic Process Control Workshop 2015 (NPCW19) in Norway.

7.1 Introduction

One important goal of control, after stabilisation of a plant, is ensuring optimal operation. As will be described in the following subsection, these two tasks are linked in the sense that the stabilising control structure must act upon the changes performed by the optimising control structure.

7.1.1 Economic Plant-wide Control (Part 2)

In Section 6.1.2, a method for designing an economic plant-wide control structure was described. According to the method (Figure 6.2), it is recommended to start with the top-down design followed by the bottom-up design. However, it was found more suitable to present the design of the control structure of the regulatory layer (Step 5) from the bottom-up analysis (Chapter 6) prior to the top-down analysis provided in this chapter. The top-down analysis covers Step 1-4 of the economic plant-wide control design procedure. The argument for this is that only one unit operation is considered, and therefore Step 5 can be performed for a given operating point. Hence, this chapter presents the application of the top-down analysis of the economic plant-wide control method on a heat-integrated distillation column configuration.

7.1.2 Optimising Control

The supervisory control layer is located on top of the regulatory control layer in the control hierarchy (illustrated in Figure 6.1). The main objective of this layer is to ensure near-optimal operation by controlling carefully selected variables, called the primary controlled variables ($\mathbf{CV}_2$). The criteria for selecting the primary controlled variables is that the economic loss must be low during disturbances, while the primary controlled variables are kept constant. The economic loss is defined as the deviation of the actual value of the operating objective function from the optimal value. In many cases, this implies that active constraints should be selected as primary controlled variables [104], while the remaining primary controlled variables are selected based on the concept of self-optimising variables [149].

It was concluded, in relation to the development of the regulatory control layer, that stabilisation of the pressure is important, and that adding a temperature controller in the stabilisation layer could significantly enhance the overall stabilisation performance. Since the pressure difference of the two column sections is essential for the separation capability of an HIDiC, the study of the optimal operation is important. The procedure of devising the supervisory control layer and its evaluation are presented in the following sections.

7.1.3 Case Study

The feed specifications, separation specifications, and parameter specifications of the separation of benzene/toluene are provided in Section 6.1.5. Based on the provided design, it is desired to identify the optimal operating point. The procedure for obtaining the optimal operating point is illustrated in Figure 7.1. In Step 1, the conceptual design is developed of a HIDiC, which separates a given mixture of benzene/toluene into 99.5% pure benzene in the distillate and 99.5% toluene in the bottoms products. The design, satisfying these specifications, was presented previously (Section 4.5.1). In Step 2, the column internals are designed. The concentric HIDiC is considered. The tray geometrical parameters are taken from Table 5.1 and the total cross sectional areas of each tray were estimated as described in Section 3.4. Using this approach, the design summarised in Table 6.1 was obtained. Note, that this approach accounts for e.g. tray pressure drop increases with increasing vapour loading, and therefore represents a realistic HIDiC column. Based on this column design, the identification of the optimal operating point is carried out in Step 3. The identification of the optimal operating point is carried out as a part of the top-down design procedure, which is described in the following sections.

Figure 7.1. Case study design procedure.

7.2 Top-down Design

This analysis considers the operation aspect only. It is the purpose of this section to define the optimal operating point based on a given column design. Hence, an optimisation degrees of freedom analysis and the identification of the optimal operating point will be described in this section.

7.2.1 Definition of Optimal Operation

The economic objective of operation is to maintain optimum trade-off between separation quality and operating costs associated with the compressor and reboiler. The product prices are $1.04\,\$\,kg^{-1}$ for benzene (distillate), $0.853\,\$\,kg^{-1}$ for toluene (bottoms) [64] and the feed price is assumed to be $0.50\,\$\,kg^{-1}$. The objective func-

tion (J [=] $\$\,\mathrm{kg}^{-1}$) becomes:

$$\begin{aligned}
\min J = \frac{1}{MW_F F}\,[&0.50 - 1.04 MW_D D - 0.853 MW_B B \\
&+ \left(1.99 + 16.2(P_{steam} - 101.3)^{0.05}\right) f_{steam} \\
&+ 0.080 \cdot 10^{-3} f_{cw} + 3.89 \cdot 10^{-5} E\Big] \qquad (7.1)\\
s.t. \; & 0.99 \leq x_D \\
& 0.99 \leq 1 - x_B \\
& E \leq 550\,\mathrm{kW} \\
& 101.3\,\mathrm{kPa} \leq P_i \leq 600\,\mathrm{kPa}, \quad i = 1,2,\ldots,N_S \\
& 0.01 F_0 \leq L_i \leq 200\,\mathrm{mol\,s}^{-1}, \quad i = 1,2,\ldots,N_S - 1 \\
& 0.01 F_0 \leq V_i \leq 150\,\mathrm{mol\,s}^{-1}, \quad i = 2,3,\ldots,N_S
\end{aligned}$$

where

$f_{cw} =$ mass flow rate of cooling water [$\mathrm{kg\,s}^{-1}$]
$f_{steam} =$ mass flow rate of steam at pressure P_{steam} [$\mathrm{kg\,s}^{-1}$]
$F_0 =$ nominal feed flow rate [$\mathrm{mol\,s}^{-1}$]

Note that the specified product requirements in Eq. (7.1) are less strict than the product requirements, which form the basis of the conceptual design. This reflects a typical practice of conceptual design, where a given distillation column design is oversized in order to improve the operation flexibility. This ensures that the required purities can be satisfied when subject to disturbances and thus increases the flexibility of operation. Additional constraints are imposed reflecting the limitations of the capacity of the equipment. These bounds are fixed by the mechanical strength of the equipment. The upper limits of the internal flow rates were assumed to be +50% of the nominal design values. The lower limits were assumed to be 1% of the feed flow rate in order to avoid the possibility of certain trays drying out. A maximum compressor duty was also assumed as +50% of the design value. The design value refers to the values, forming the basis of the conceptual design.

The number of operational degrees of freedom was provided in Table 6.2 in Section 6.2.1. In this context, it was argued that the considered HIDiC has eight operational degrees of freedom, of which four have no steady state effect, and thus no impact on the cost function in Eq. (7.1). The remaining four variables with steady state effects are thus:

$$\mathbf{u}_1 = [L_{cnd}, Q_{rbl}, P_{str}, CR]^T \qquad (7.2)$$

Note that the compression ratio (CR) is used to represent the rectifying section pressure P_{rct}.

Table 7.1. Nominal, optimal operation of HIDiC for the separation of benzene/-toluene. The optimum for a CDiC with same specifications is shown for comparison.

	Variable	Unit	Configuration	
			CDiC	HIDiC
Design degrees of freedom	P_{str}	kPa	101.3	101.3
	CR	-	-	2.306
	L_{cnd}	$\mathrm{mol\,s^{-1}}$	60.15	0.8333
	Q_{rbl}	kW	3304	1175
Cost function	J	$\$\,\mathrm{mol^{-1}}$	-0.4323	-0.4342
Constraints (bold: active)	x_D	-	**0.9900**	**0.9900**
	$1-x_B$	-	0.9987	**0.9900**
	$\min L_i$	$\mathrm{mol\,s^{-1}}$	55.66	**0.8333**
	$\max L_i$	$\mathrm{mol\,s^{-1}}$	141.8	136.9
	$\min V_i$	$\mathrm{mol\,s^{-1}}$	97.69	35.3
	$\max V_i$	$\mathrm{mol\,s^{-1}}$	102.2	113.1
	$\min P_i$	kPa	**101.3**	**101.3**
	$\max P_i$	kPa	135.8	234.0
	E	kW	-	357.6
	$T_{cnd}-T_{cw,out}$	K	48.48	75.20

7.2.2 Optimal Operation Point

The solver "fmincon" in Matlab is used to solve the non-linear programming problem in Eq. (7.1) using the sequential quadratic programming algorithm. The solution is listed in Table 7.1. For comparison, the optimal operating point of a corresponding conventional distillation column (CDiC) carrying out the same separation is presented. This approach is applied for a CDiC by Jacobsen and Skogestad [70], who report a negative objective function and other similar trends in the optimal solution of the CDiC. A negative sign of the objective function indicates that a profit is obtained. The cost function is lower for the HIDiC than the CDiC, which illustrates the capability of reducing the operating expenditures (OPEX) in a HIDiC compared to a CDiC. In the CDiC, the bottom composition constraint is not active (Table 7.1). This reflects the fact that benzene is the more valuable component and therefore the loss of benzene content in the bottoms product is low. In the HIDiC, both composition constraints are active, which reflects the strong coupling between the distillate and bottom compositions because the internal heat integration affects both compositions simultaneously.

The result of the optimisation has four active constraints for the HIDiC, which are x_D, x_B, P_{str}, and L_{cnd} as indicated in boldface numbers in Table 7.1. The num-

ber of optimisation degrees of freedom corresponds to the number of required primary controlled variables. It is generally suggested to control the active constraints [104], and thus the active constraint variables are selected as candidates as the primary controlled variables.

The sensitivities of the four identified primary controlled variables on the objective function are illustrated in Figure 7.2. If a nominal value of a primary controlled variable represent a flat optimum, limited economic benefit of control is obtained and other variables should be investigated. No flat optimum regions are observed and therefore the considered variables (x_D, x_B, P_{str}, and L_{cnd}) are suitable as primary controlled variables. Before the final decision of which variables are selected as primary controlled variables, the active constraint regions must be mapped. This is done in the following subsection.

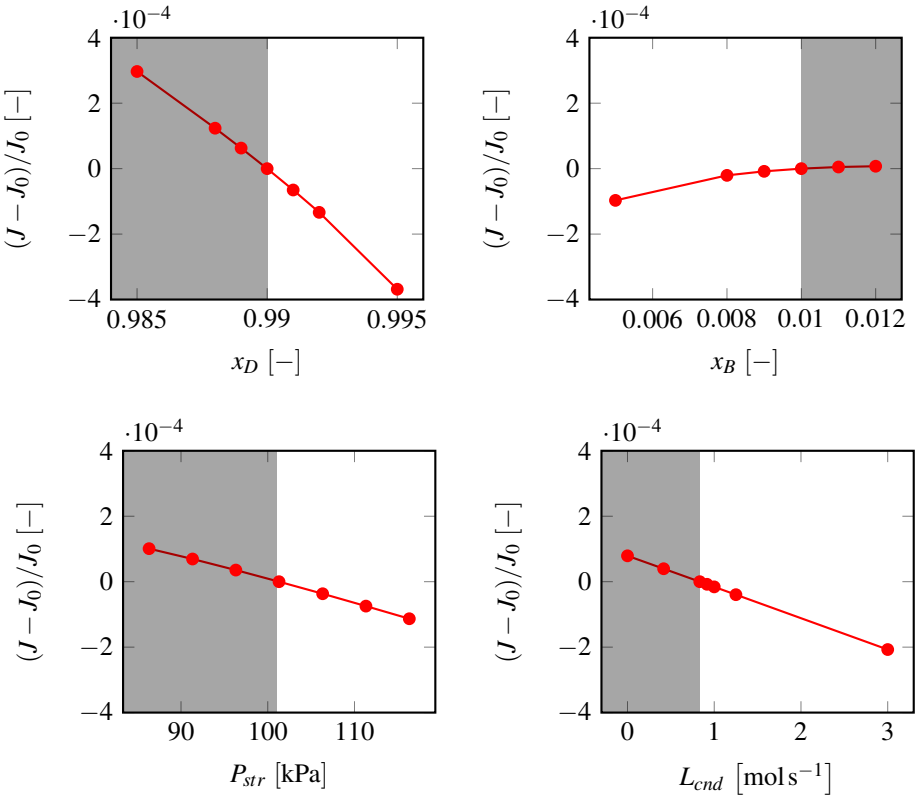

Figure 7.2. Relative sensitivity in the objective function of perturbations in the candidate primary controlled variables. The shaded areas represent infeasible regions. J_0 is the nominal objective function.

7.2.3 Active Constraint Regions

The expected economic disturbances are the feed flow rate and the feed composition. The expected disturbance ranges are between -20% and +20% for the feed composition (10% increment) and -20% and +40% for the feed flow rate (10% increment). Table 7.1 only reflects the optimal operation conditions for the nominal disturbance values. It is desired to identify the active constraints and the objective function values for every possible disturbance scenario. This identification was carried out by the "brute force" method, which requires a discretisation of the two-dimensional disturbance space. For this purpose, a 5×7 grid was adopted, leading to 35 nodes. In each of the 25 nodes, the optimal solution was manually obtained by solving Eq. (7.1) and the active constraints were recorded. When the complete disturbance space was covered, the different active constraint regions were identified based on the obtained active constraints for the individual nodes. The resulting map of active constraint regions is illustrated in Figure 7.3.

The active constraint Region I clearly dominates in Figure 7.3. Different constraints become active at relatively high feed flow rates (above +30%). At these high feed flow rates, the maximum vapour flow rate constraint (Region II) or maximum compressor duty (Region III) constraint become active. The following identified active constraint regions are:

I: $\mathbf{AC} = \{x_D, x_B, P_{min}, L_{min}\}$

II: $\mathbf{AC} = \{x_D, x_B, P_{min}, V_{max}\}$

III: $\mathbf{AC} = \{x_D, x_B, P_{min}, E_{max}\}$

The variables refer to the bounds defined in Eq. (7.1). It is observed, that the objective function becomes more sensitive to the feed flow rate as the feed flow rate increases. This is because the internal heat transfer rates do not scale with feed flow rate, as the heat exchange area is fixed. To compensate for the increased feed flow rate, either the compressor duty must increase in order to increase the temperature driving force (and thus the internal heat transfer rate), or the reboiler duty must increase. However, the tray pressure drops increases with increasing reboiler duty.

In principle, a control structure of the supervisory layer should be defined for each active region. But for the considered concentric HIDiC, the active constraint Region I dominates most of the disturbances encountered. As a result, only the following primary controlled variables are considered:

$$\mathbf{CV}_2 = [x_D, x_B, P_{str}, L_{cnd}]^T \tag{7.3}$$

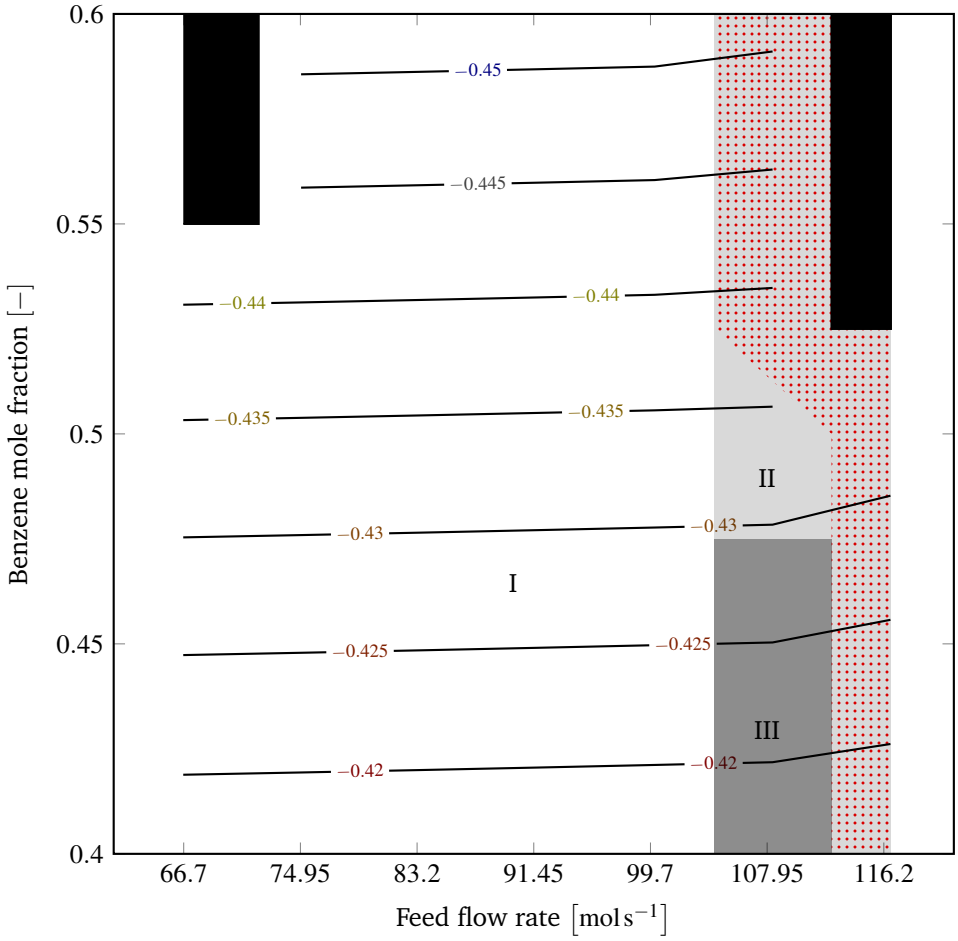

Figure 7.3. Active constraint regions with objective function contours [\$kg^{-1}]. The active constraint regions are represented by roman numbers and they are: I: $x_D, x_B, P_{min}, L_{min}$; II: $x_D, x_B, P_{min}, V_{max}$; III: $x_D, x_B, P_{min}, L_{min}, E_{max}$; The black region represents infeasibility. The subscripts "min" and "max" refers to the limits in Eq. 7.1 of the corresponding varibles. Flooding is predicted in the dotted region.

In the following section, the control structure based on these primary controlled variables will be devised.

7.3 Supervisory Control Layer Design

The design of the supervisory control layer involves several decisions, including the pairing, the controller type, and eventual coordination between the control loops.

The simplest structure of the supervisory control layer is a decentralised scheme, but in some cases the interactions between the loops are large, resulting in poor dynamic performance. In such cases, the supervisory controller, or part of it, may be multi-variable. For example, it could be a 3×3-pairing for a model predictive controller (MPC), which changes the setpoints of ΔT, P_{rct} and P_{str}. However, one disadvantage of multi-variable control is the increased required computational effort.

In this work, a supervisory control layer consisting of PI controllers was selected for the concentric HIDiC, which leads to a control structure of cascade controllers (regulatory and supervisory control layers). In the previous analysis, it was shown that all active constraint variables should be controlled, i.e. the top composition (x_D), the bottom composition (x_B), the stripping section pressure (P_{str}) and the liquid reflux rate (L_{cnd}). These variables are primary controlled variables as they ensure near optimal economic performance when kept constant during disturbances. Previously, a stabilising control structure was devised for both the case, where the distillate product is more valuable, and the case, where the bottom product is more valuable. Hence, the design of the supervisory control layer follows the same approach.

7.3.1 More Valuable Top Product

Generally, it is suggested to manipulate the setpoint of the temperature profile controller (ΔT^{set}) for controlling the composition of the more valuable component. Hence, the cascade loop employing a composition controller (CC) is used ($\Delta T^{set} \rightarrow x_D$). Using the "pair close" rule (Section 6.1.3), it is decided to control the bottom composition (x_B) by the stripping section pressure ($P_{str}^{set} \rightarrow x_B$). However, as the stripping section pressure is also a primary controlled variable, the output from the bottom composition controller (the stripping section pressure setpoint (P_{str}^{set})) must be controlled by an additional controller. This additional controller manipulates the setpoint of the rectifying section in order to control the stripping section setpoint ($P_{rct}^{set} \rightarrow P_{str}^{set}$). The final control structure, consisting of both the regulatory control and supervisory control layer, is illustrated in Figure 7.4(a).

7.3.2 More Valuable Bottom Product

The case where the bottom product is more valuable, the control of the temperature profile in the stripping section is carried out by manipulating the condenser duty. This leads to the situation where the setpoint of the temperature profile controller (ΔT^{set}) must be manipulated by a bottom composition controller ($\Delta T^{set} \rightarrow x_B$). This

might appear counter-intuitive as the physical distance between the bottom product and the condenser duty is large, which opposes the "pair close" rule. However, it is argued that this is reasonable due to the two following reasons. The first reason is the fact that the RGA analysis strongly favoured the pairing between the condenser duty and the temperature profile controller in Chapter 6. The second reason is that the actual "distance" between the bottoms product and the condenser duty is close due to internal heat integration, i.e. the time delay is smaller than in a conventional distillation column. Finally, it is proposed to control the top composition by manipulating the rectifying section pressure setpoint ($P_{rct}^{set} \rightarrow x_D$), while the optimal value of the stripping section is passed directly through the supervisory layer to the stripping section. The resulting control structure with both the regulatory control and supervisory control layer for this case is illustrated in Figure 7.4(b).

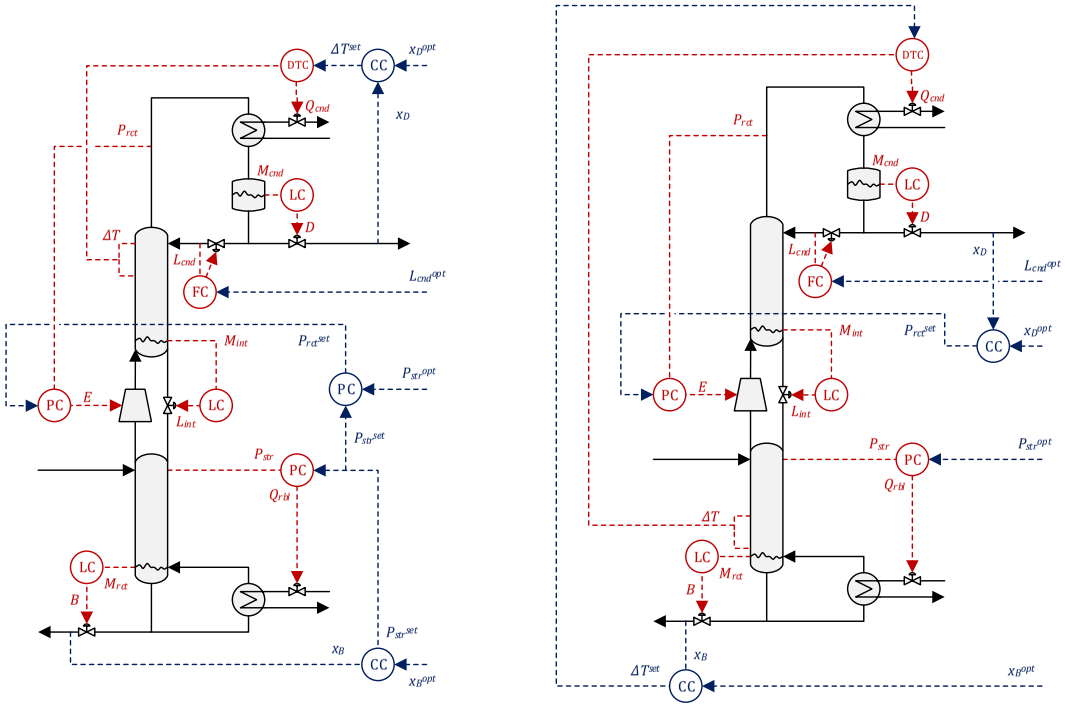

(a) Distillate more valuable product.

(b) Bottoms more valuable product.

Figure 7.4. Control structures for a HIDiC. Red lines represent the regulatory control loops and blue lines represent supervisory control loops (cascade). LC: Level controller, PC: Pressure controller, DTC: Difference temperature controller, FC: Flow controller, CC: composition controller.

7.4 Dynamic Evaluation

In this section, the developed supervisory layer control structure, combined with the regulatory layer, is evaluated by dynamic simulation. The distillate is the more valuable product for the separation of benzene/toluene and thus the final control structure of Figure 7.4(a) is employed.

7.4.1 Tuning

A sequential tuning was carried out in the order displayed in Table 7.2. The table includes the identified first-order models, the desired closed-loop time constants, and the resulting controller parameters. Since the controllers of the supervisory layer act as cascade controllers, desired closed-loop time constants ten times larger than those of the slave loops from the regulatory control layer were used.

7.4.2 Evaluation

The developed control structure consisting of a regulatory and a supervisory layer is evaluated for the different disturbance scenarios, given below.

7.4.2.1 Single Disturbance Scenarios

The following disturbance scenarios are used to investigate the performance of the control layers. The dynamic responses for feed flow rate step changes are illustrated in Figure 7.5, given the scenario:

- $0 < t \leq 15\,\text{h}$: +10% feed flow rate
- $15\,\text{h} < t$: Feed flow rate reset ($F = F_0$)

The dynamic responses for feed composition step changes are illustrated in Figure 7.6, given the scenario:

- $0 < t \leq 15\,\text{h}$: +10% feed composition
- $15\,\text{h} < t$: Feed composition reset ($z = z_0$)

Both the disturbance scenarios lead to a new steady state after approximately 15 h. The primary controlled variables ($\mathbf{CV}_1$) are shown in the left columns of Figure 7.5 and Figure 7.6. These ($\mathbf{CV}_1$) are controlled by the supervisory control layer by adjusting the setpoints of $\mathbf{CV}_2$, which are illustrated in the middle columns. The $\mathbf{CV}_2$ are controlled by the regulatory control layer by adjusting the actuators $\mathbf{u}_D$ in the columns to the right. Both disturbance scenarios are controlled reasonably

Table 7.2. Sequential tuning (ordered) of the concentric HIDiC with dynamic responses. In each row, the above control loops are closed. The unit of the pressures is bar. Legend: Dynamic responses (——), fitted transfer functions, $\mathbf{G}(s)$ (- - -).

Loop	Response		Controller parameters		
	Δy vs. t/τ_c	$\mathbf{G}(s)$	τ_c s	K_c	τ_I s
$\Delta T^{set} \rightarrow x_D$	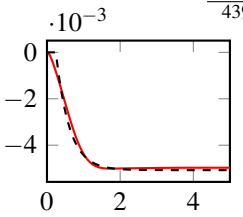	$\frac{-5.074 \cdot 10^{-3}}{439.4s+1} e^{-293.8s}$	1200	-57.97	439.4
$P^{set}_{str} \rightarrow x_B$	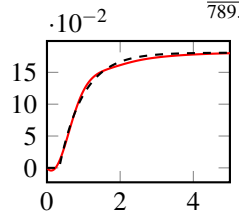	$\frac{0.1809}{789.4s+1} e^{-401.3s}$	1200	2.726	789.4
$P^{set}_{rct} \rightarrow P^{set}_{str}$	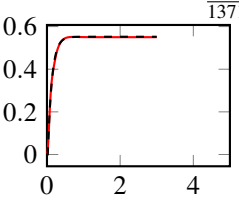	$\frac{0.5523}{1371s+1} e^{-267.8s}$	12,000	0.2023	1.371

well. As expected, the distillate compositions are more tightly controlled than the bottoms compositions because the temperature controller is located in the rectifying section.

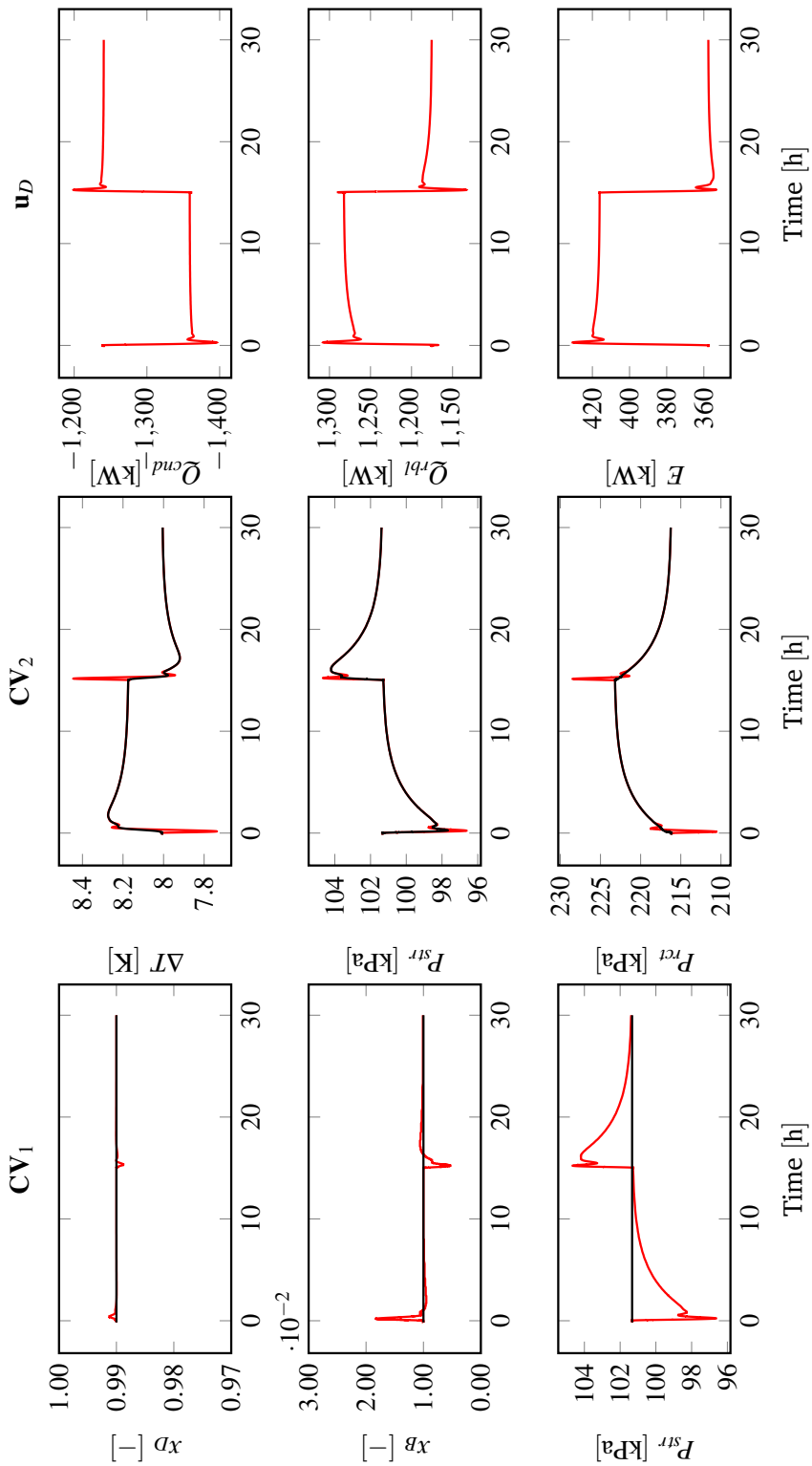

Figure 7.5. Dynamic responses in controlled and manipulated variables to step changes in the feed flow rate. Legend: All loops closed (——), setpoint (——).

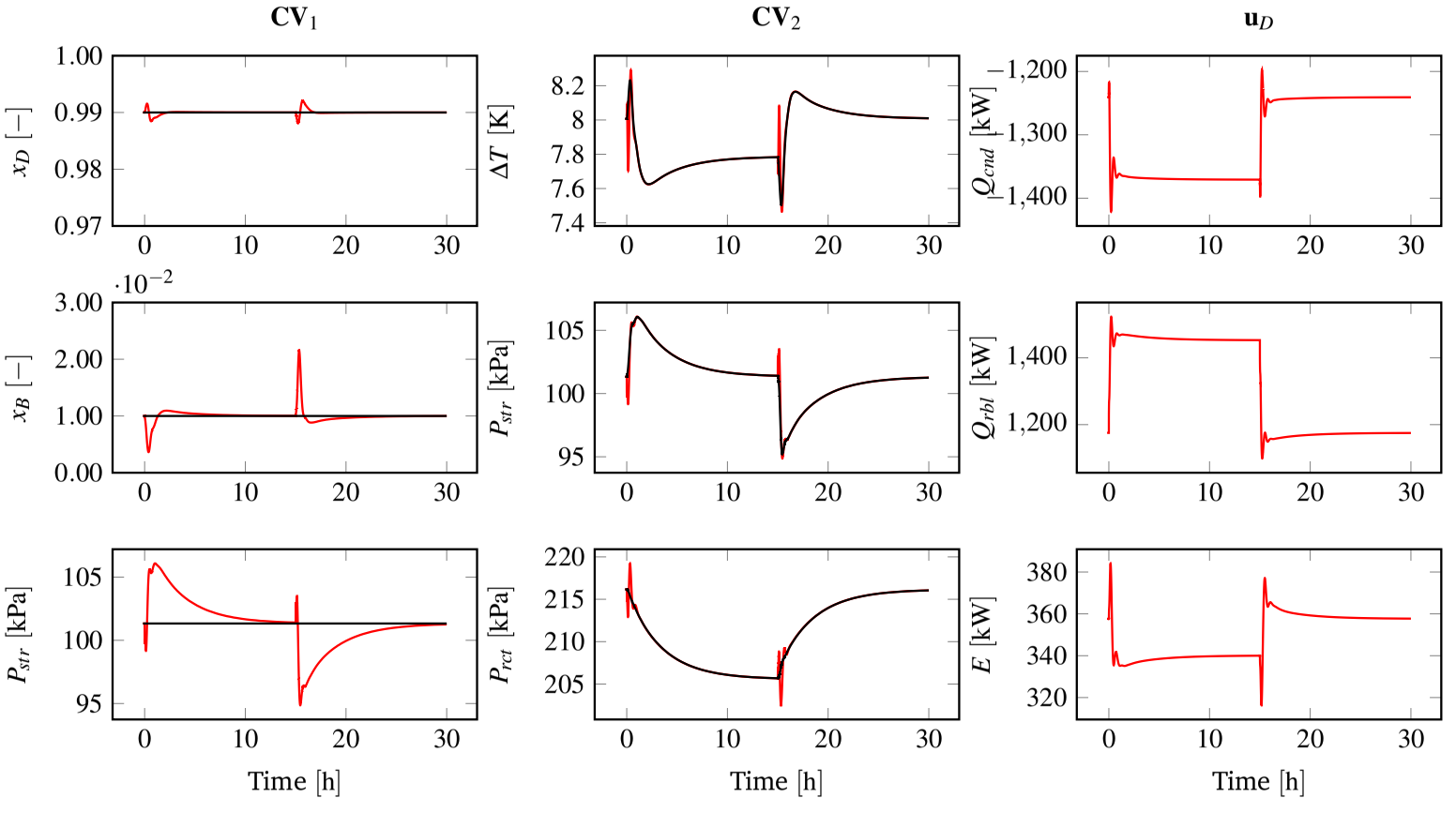

Figure 7.6. Dynamic responses in controlled and manipulated variables to step changes in the feed composition. Legend: All loops closed (——), setpoint (——).

7.4.2.2 Mixed Disturbance Scenario

As the objective of the supervisory control layer is to improve the economic performance of the HIDiC, only the economic disturbance variables are considered for evaluation. The following disturbance scenario is formulated:

- $t \geq 0\,\text{h}$: +10% feed flow rate ($F = 1.10F_0$)
- $t \geq 2.5\,\text{h}$: +10% feed composition ($z = 1.10z_0$)
- $t \geq 5.0\,\text{h}$: -10% feed flow rate from nominal value ($F = 0.90F_0$)
- $t \geq 7.5\,\text{h}$: Feed composition reset ($z = z_0$)

The resulting dynamic responses are illustrated in Figure 7.7. All controlled variables are kept reasonably close to their setpoints in the simulations. Neither entrainment flooding nor weeping were predicted. The capability of the supervisory control layer of ensuring optimal operation is investigated in Figure 7.8. The figure depicts the achieved instantaneous objective function in terms of $\$\,\text{s}^{-1}$ along with the optimal objective function.

7.5 Conclusion

A control structure of a supervisory control layer was systematically developed for a concentric HIDiC based on the separation of benzene/toluene. The optimal operating point was identified for the expected disturbances (feed flow rate and feed composition). Furthermore, the active constraint regions were identified. The purities of the distillate and the bottom product, the stripping section pressure, and the liquid reflux ratio were identified as the primary controlled variables. Designs of the supervisory control layer for the following two cases were proposed: A case, where the distillate is the more valuable product stream and a case, where the bottom product is the more valuable product stream. Dynamic simulations were performed for the separation of benzene/toluene, for which the distillate product is the more valuable stream. Acceptable performance of the developed control structure (combined regulatory and supervisory control layers) was obtained.

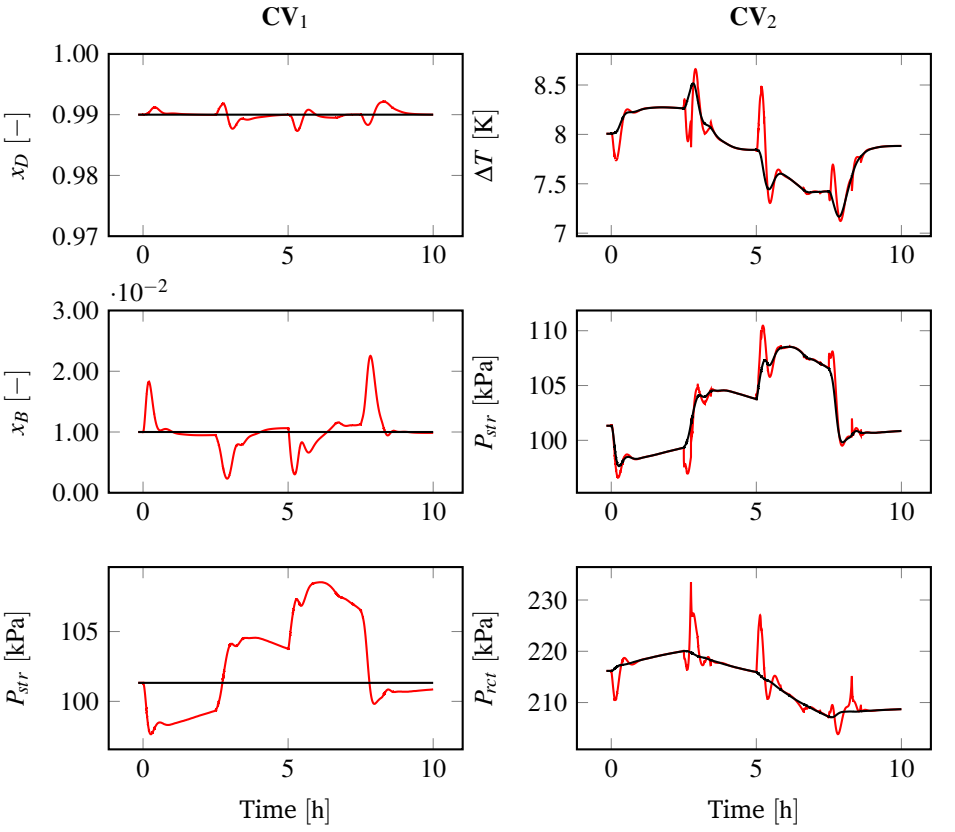

Figure 7.7. Dynamic responses in controlled and manipulated variables (regulatory layer setpoints) of the supervisory layer. Legend: All loops closed (——), setpoint (——).

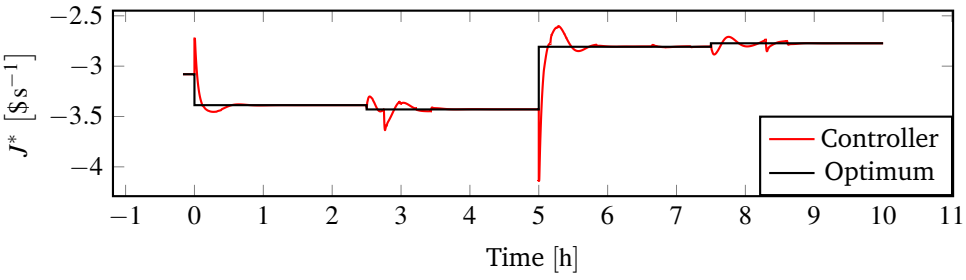

Figure 7.8. Evaluation of the tracking of the optimal operating point given by the solution to Eq. (7.1).

Chapter 8

Thesis Conclusions

Introducing heat-integration in distillation by the means of compression results in a trade-off between operating expenditures (OPEX) and capital expenditures (CAPEX). The heat-integrated distillation column (HIDiC) offers a low OPEX but a high CAPEX, relative to conventional distillation. The high CAPEX relates to the investment costs of the compressor and the internal heat exchangers. The mechanical vapour recompression column also offers lower OPEX and higher CAPEX than conventional distillation. It was found that the HIDiC offers the lowest OPEX among the considered distillation column configurations for binary separations with a normal boiling point difference below 10 K. For binary separations with a normal boiling point difference above 10 K, the secondary reflux and vaporisation column (SRVC) has the lowest OPEX. It is expected that these findings will facilitate a focused development of cheap and simple heat panels in order to reduce the CAPEX of internal heat exchangers.

A systematic modelling and conceptual design framework was developed, which is tailor-made for the four considered configurations: The MVRC, the HIDiC, the SRVC, and the conventional distillation column. The framework allows static and dynamic benchmarking of all configurations. The model accounts for vital phenomena such as pressure dynamics, liquid tray hydraulics, and sensible heat effects. Due to the general structure of the model, a possibility exists for incorporating additional heat-integrated distillation column configurations with one or more compressors. Another benefit of the general model formulation is that it allows a fair basis for comparison when conducting configuration benchmark studies. All model equations for the individual configurations are solved within the same framework, and therefore the same economic model, the same model parameters, etc.

In order to study a realistic operation of a concentric HIDiC, a regulatory control layer and a supervisory control layer were devised and evaluated by simulation. The

control structure designs were based on general consideration and a numerical case study of the separation of benzene/toluene. Hence, recommendations are given on the control structures of both control layers.

This work has addressed two main areas in the development and understanding of using compressors in heat-integrated distillation. The first area is the economic feasibility, which was described above. The second area is the technical feasibility. The study of the separation of benzene/toluene has been adopted to show that:

- The specified uniform heat integration area by design can be realised within the HIDiC.
- Additional utility should be considered; the vapour inlet to the compressor must be superheated in order to avoid condensation within the compressor.
- Neither entrainment flooding nor weeping were encountered in three column arrangements: A HIDiC with uniform column area, a concentric HIDiC with gradually changing rectifying section area, and a simplified concentric HIDiC, in which the rectifying section area is gradually decreased over three partitions.
- The HIDiC can be operated steadily using a proposed, decentralised regulatory control layer. Steady operation means in this context that the drifting variables were maintained at their setpoints and that no entrainment flooding or weeping were observed during dynamic simulations. This conclusion is based on the concentric HIDiC.
- The HIDiC can be operated steadily and with good tracking of an economic objective function using a decentralised, supervisory control layer on top of the regulatory control layer. This conclusion is based on the concentric HIDiC.

Chapter 9

Future Directions

The main concern of the development of the heat-integrated distillation column (HIDiC) is the understanding of the realisation of internal heat-integration on an industrial scale. Among the proposed column arrangements for addressing this, are the shell-and-tube arrangement, the concentric arrangement, and the structured plate arrangement. Based on the findings in this work and in literature, some drawbacks of the mentioned arrangements are:

- The shell-and-tube arrangement has negative effects on the separation.
- The concentric arrangement can only accommodate the required heat exchange area by installing heat panels within the structure.
- The shell-and-tube arrangement and the structured plate arrangement only exist as packed columns.
- The realisation of internal heat integration is constrained by the construction cost.

It has been found that the construction cost of internal heat exchangers is the main economic bottleneck. One option is to reduce the number of internal heat exchangers, while another option is to improve the design of the internal heat exchangers. Computational fluid dynamics (CFD) is a powerful simulation tool, which can be employed to develop, innovate, and optimise the column arrangement for realising internal heat transfer. Using CFD, the implications w.r.t. heat transfer and mass transfer of realising internal heat integration in distillation can be quantified. Based on these quantifications, the heat and mass transfer phenomenons can be fully understood and appropriate measures can be taken in order to improve designs. In addition, economic construction constraints can be investigated by simulation, thereby reducing possible costs associated with experimental testing. In

relation to the experimental observation, the concentric arrangement with trays and heat panels, and the structured plate arrangements, appear to be good candidates for industrial-scale HIDiC applications. Furthermore, determinations of the overall heat transfer coefficients inside various internal heat-integrated distillation column arrangements are well documented in literature.

The developed model is only designed for performing dynamic simulations of ideal vapour systems. The propylene/propane distillation column was found to be a feasible economic alternative to the mechanical vapour recompression column (MVRC). Furthermore, it was found that pressure dynamics were essential in the study of the operation of the HIDiC. Because the propylene/propane distillation column has almost two hundreds trays, pressure propagations within the column are significant for the operation. Thus, it is essential to study the operation of a HIDiC carrying out such a separation. The developed model must be extended to cover such separations, i.e. a differential-algebraic equation (DAE) system must be formulated and solved.

Automatising the proposed design method has not been completed in this study. If such automation is successful, a possibility for conducting extensive combinatorial studies arises, in order to arrive at a true optimal structure. This approach will then be an alternative to the super structure-based approach of Harward and Marquardt [51].

Bibliography

[1] Economic indicators. Technical report, Chemical Engineering, 2012.

[2] Danske nøgletal. http://www.ens.dk/info/tal-kort/statistik-nogletal/nogletal/danske-nogletal, 2015. December, 2015.

[3] U.S. Energy Information Adminstration. Petroleum and other liquids. www.eia.gov, 2015. January, 2016.

[4] William H. Aitken. Apparatus for combined heat and mass transfer, 1998. US Patent 5,722,258.

[5] J.R. Alcántara-Avila and H.-Y. Lee. *Process Intensification in Chemical Engineering. Design Optimization and Control*, chapter 5 Heat-Integrated Intensified Distillation Processes. J.G. Segovia-Hernández, A. Bonilla-Petriciolet, 1st edition. edition, 2016.

[6] T.R. Andersen. *Optimal Design and Operation of Process Integrated Distillation*. PhD thesis, Technical University of Denmark, 2002.

[7] K. Aso, H. Matsuo, H. Noda, T. Takada, and N. Kobayashi. Heat integrated distillation operation, 1998. US Patent 5,783,047.

[8] F.E. Becker and A.I. Zakak. Heat recovery in distillation by mechanical vapor recompression. *Proceedings from the Eighth Annual Industrial Energy Technology Conference*, pages 705–709, 1986.

[9] L.T. Biegler, I.E. Grossmann, and A.W. Westerberg. *Systematic Methods of Chemical Process Design*. Prentice-Hall Inc., New Jersey. USA, 1st edition. edition, 1997.

[10] T. Bisgaard, J.K. Huusom, and J. Abildskov. Dynamic effects of diabatization in distillation columns. *Proceedings of the 10th European Workshop on*

Advanced Control and Diagnostics (ACD 2012), 2012.

[11] T. Bisgaard, J.K. Huusom, and J. Abildskov. Dynamic effects of diabatization in distillation columns. *Computer-aided Chemical Engineering*, 32:1015–1020, 2013.

[12] T. Bisgaard, J.K. Huusom, and J. Abildskov. A modeling framework for conventional and heat integrated distillation columns. *10th IFAC International Symposium on Dynamics and Control of Process Systems – Mumbai, India*, pages 373–378, 2013.

[13] T. Bisgaard, J.K. Huusom, and J. Abildskov. Impact on model uncertainty of diabatization in distillation columns. *Proceedings of Distillation and Absorption*, pages 909–914, 2014.

[14] T. Bisgaard, J.K. Huusom, and J. Abildskov. Modeling and analysis of conventional and heat-integrated distillation columns. *AIChE Journal*, 61(12):4251–4263, 2015.

[15] T. Bisgaard, J.K. Huusom, and J. Abildskov. Conceptual design of heat-integrated distillation columns with compressors. 2016.

[16] T. Bisgaard, S. Skogestad, J.K. Huusom, and J. Abildskov. Optimal operation and stabilising control of the concentric heat-integrated distillation column. *11th IFAC International Symposium on Dynamics and Control of Process Systems – Trondheim, Norway*, 2016.

[17] E.H. Bristol. On a new measure of interaction for multivariable process control. *IEEE Transactions on Automatic Control*, 11(1):133–134, 1966.

[18] A.J. Brugma. Fractional distillation of liquid mixtures, especially petroleum, 1937. US Patent 2,471,134.

[19] O.S.L. Bruinsma, T. Krikken, J. Cot, M. Saric, S.A. Tromp, Ž. Olujic, and A.I. Stankiewicz. The structured heat integrated distillation column. *Chem Eng Res Des*, 90(4):458–470, 2012.

[20] J. Cabrera-Ruiz, A. Jiménez-Gutiérrez, and J.G. Segovia-Hernández. Assessment of the implementation of heat-integrated distillation columns for the separation of ternary mixtures. *Ind Eng Chem Res*, 50(4):2176–2181, 2011.

[21] I.T. Cameron, C.A. Ruiz, and R. Gani. A generalized model for distillation columns–ii: Numerical and computational aspects. *Comput Chem Eng*, 10(3):199–211, 1986.

[22] J.C. Campbell, K.R. Wigal, V. Van Brunt, and R.S. Kline. Comparison of energy usage for the vacuum separation of acetic acid/acetic anhydride using

an internally heat integrated distillation column (hidic). *Separ Sci Technol*, 43(9–10):2269–2297, 2008.

[23] H. Chen, K. Huang, and S. Wang. A novel simplified configuration for an ideal heat-integrated distillation column (ideal hidic). *Sep Purif Technol*, 73(2):230–242, 2010.

[24] J. de Graauw, M.J. Steenbakker, A. de Rijke, Z. Olujic, and P.J. Jansens. Heat integrated distillation column, 2010. US Patent 7,678,237.

[25] G. de Koeijer and R. Rivero. Entropy production and exergy loss in experimental distillation columns. *Chem Eng Sci*, 58(8):1587–1597, 2003.

[26] G.M. de Koeijer and S. Kjelstrup. Minimizing entropy production rate in binary tray distillation. *Int J Thermodyn*, 3(3):105–110, 2000.

[27] A. de Rijke. *Development of a Concentric Internally Heat Integrated Distillation Column (HIDiC)*. PhD thesis, Technische Universiteit Delft, 2007.

[28] A. de Rijke, W. Tesselaar, M.A. Gadalla, Z. Olujic, and P.J. Jansens. Heat and mass transfer characteristics of an annular sieve tray. *IChemE Symposium Series No. 152*, pages 181–189, 2006.

[29] M.F. Doherty and J.D. Perkins. On the dynamics of distillation processes–iv uniqueness and stability of the steady state in homogeneous continuous distillations. *Chem Eng Sci*, 37(3):381–392, 1982.

[30] J.A. Ferré, F. Castells, and J. Flores. Optimization of a distillation column with a direct vapor recompression heat pump. *Industrial and Engineering Chemistry Process Design and Development*, 24(1):128–132, 1985.

[31] R.E. Fitzmorris and R.S.H. Mah. Improving distillation column design using thermodynamic availability analysis. *AIChE J*, 26(2):265–273, 1980.

[32] Z. Fonyo and P. Mizsey. Economic applications of heat pumps in integrated distillation systems. *Heat Recovery Syst CHP*, 14(3):249–263, 1994.

[33] Aa. Fredenslund, J. Gmehling, and P. Rasmussen. *Vapor-liquid Equilibrium Using UNIFAC. A Contribution Method.* Elsevier, USA, 1st edition. edition, 1977.

[34] D.C. Freshwater. Thermal economy in distillation. *Institution of Chemical Engineers – Transactions*, 29(1):149–160, 1951.

[35] C. Fuentes and W.L. Luyben. Control of high-purity distillation columns. *Industrial and Engineering Chemistry Process Design and Development*, 22(3):361–366, 1983.

[36] T. Fukushima, M. Kano, O. Tonomura, and S. Hasebe. Dynamics and control of heat integrated distillation column (hidic). *International Symposium on Advanced Control of Chemical Processes*, pages 629–634, 2006.

[37] M. Gadalla, L. Jiménez, Z. Olujic, and P.J. Jansens. A thermo-hydraulic approach to conceptual design of an internally heat-integrated distillation column (i-hidic). *Comput Chem Eng*, 31(10):1346–1354, 2007.

[38] M. Gadalla, Z. Olujic, A. de Rijke, and P.J. Jansens. A thermo-hydraulic approach to conceptual design of an internally heat-integrated distillation column (i-hidic). *European Symposium on Computer-Aided Process Engineering*, 18:181–186, 2004.

[39] M. Gadalla, Z. Olujic, A. de Rijke, and P.J. Jansens. A new approach to the design of internally heat-integrated tray distillation columns. *European Symposium on Computer-Aided Process Engineering*, 20:805–810, 2005.

[40] M. Gadalla, Z. Olujic, L. Sun, A. de Rijke, and P.J. Jansens. Pinch analysis-based approach to conceptual design of internally heat-integrated distillation columns. *Chem Eng Res Des*, 83(8):987–993, 2005.

[41] M.A. Gadalla. Internal heat integrated distillation columns (ihidics)-new systematic design methodology. *Chem Eng Res Des*, 87(12A):1658–1666, 2009.

[42] R. Gani, C.A. Ruiz, and I.T. Cameron. A generalized model for distillation columns–i: Model description and applications. *Comput Chem Eng*, 10(3):181–198, 1986.

[43] P. Le Goff, T. Cachot, and R. Rivero. Exergy analysis of distillation processes. *Chem Eng Technol*, 19(6):478–485, 1996.

[44] S. Gopichand, T.O. Omideyi, J. Kasprzycki, and S. Devotta. The economics of heat pump assisted distillation systems–ii. analysis of ethanol-water mixtures. *J Heat Recov Syst*, 4(4):271–280, 1984.

[45] R. Govind. Dual distillation column, 1987. US Patent 4,681,661.

[46] F. Gross, E. Baumann, A. Geser, D.W.T. Rippin, and L. Lang. Modelling, simulation and controllability analysis of an industrial heat-integrated distillation process. *Comput Chem Eng*, 22(1–2):223–237, 1998.

[47] R. Gutiérrez-Guerra, J. Cortez-González, R. Murrieta-Dueñas, J.G. Segovia-Hernández, S. Hernández, and A. Hernández-Aguirre. Design and optimization of heat-integrated distillation column schemes through a new robust methodology coupled with a boltzmann-based estimation of distribution al-

gorithm. *Ind Eng Chem Res*, 53(27):11061–11073, 2014.

[48] R. Gutiérrez-Guerra, R. Murrieta-Dueñas, J. Cortez-González, J.G. Segovia-Hernández, S. Hernández, and A. Hernández-Aguirre. Design and optimization of hidic distillation columns using a boltzmann-based estimation of distribution algorithm: Influence of volatility. *Proceedings of Distillation and Absorption*, pages 655–660, 2014.

[49] D. Hänggi and I. Meszaros. Vapor recompression: Distillation without steam. *Sulzer Technical Review 1/99*, pages 32–34, 1999.

[50] A. Harwardt, K. Kraemer, and W. Marquardt. Identifying optimal mixture properties for hidic application. *Proceedings of Distillation and Absorption*, pages 55–60, 2010.

[51] A. Harwardt and W. Marquardt. Heat-integrated distillation columns: Vapor recompression or internal heat integration? *AIChE J*, 58(12):3740–3750, 2012.

[52] G.G. Haselden. Distillation process and apparatus, 1977. US Patent 4,025,398.

[53] J.C. Helton and F.J. Davis. Latin hypercube sampling and the propagation of uncertainty in analyses of complex systems. *Reliab Eng Syst Safe*, 81(1):23–69, 2003.

[54] E.J. Henley and J.D. Seader. *Equilibrium-Stage Separation Operations in Chemical Engineering*. John Wiley & Sons, Inc, USA, 1st edition. edition, 1981.

[55] T. Ho, C. Huang, J. Lin, and L. Lee. Dynamic simulation for internally heat-integrated distillation columns (hidic) for propylene-propane system. *Comput Chem Eng*, 33(6):1187–1201, 2009.

[56] T.-J. Ho, C.T. Huang, L.-S. Lee, and C.-T. Chen. Extended ponchon-savarit method for graphically analyzing and designing internally heat-integrated distillation columns. *Ind Eng Chem Res*, 49(1):305–358, 2010.

[57] C.D. Holland. *Fundamentals of Multicomponent Distillation*. McGraw-Hill Book, Inc., USA, 1st edition. edition, 1981.

[58] K. Horiuchi, K. Yanagimoto, K. Kataoka, and M. Nakaiwa. Energy-saving characteristics of heat integrated distillation column technology applied to multi-component petroleum distillation. *IChemE Symposium Series No. 152*, pages 172–180, 2006.

[59] K. Huang, W. Liu, J. Ma, and S. Wang. Externally heat-integrated double

distillation column (ehiddic): Basic concept and general characteristics. *Ind Eng Chem Res*, 49(3):1333–1350, 2010.

[60] K. Huang, M. Nakaiwa, T. Akiya, K. Aso, and T. Takamatsu. A numerical consideration on dynamic modeling and control of ideal heat integrated distillation columns. *J Chem Eng Jpn*, 29(2):344–351, 1996.

[61] K. Huang, L. Shan, Q. Zhu, and J. Qian. Design and control of an ideal heat-integrated distillation column (ideal hidic) system separating a close-boiling ternary mixture. *Energy*, 32(11):2148–2156, 2007.

[62] K. Huang, L. Shan, Q. Zhu, and J. Qian. Adding rectifying/stripping section type heat integration to a pressure-swing distillation (psd) process. *Appl Therm Eng*, 28(8–9):923–932, 2008.

[63] K. Huang, S. Wang, K. Iwakabe, L. Shan, and Q. Zhu. Temperature control of an ideal heat-integrated distillation column (hidic). *Chem Eng Sci*, 62(22):6486–6491, 2007.

[64] ICIS. `www.icis.com`, 2015. August, 2015.

[65] International Energy Agency. Energy technology perspectives 2012. Technical report, International Energy Agency, 2012.

[66] K. Iwakabe, M. Nakaiwa, K. Huang, K. Matsuda, T. Nakanishi, T. Ohmori, A. Endo, and T. Yamamoto. An internally heat-integrated distillation column (hidic) in japan. *IChemE Symposium Series No. 152*, pages 900–911, 2006.

[67] K. Iwakabe, M. Nakaiwa, K. Huang, T. Nakanishi, A. Røsjorde, T. Ohmori, A. Endo, and T. Yamamoto. Energy saving in multicomponent separation using an internally heat-integrated distillation column (hidic). *Appl Therm Eng*, 26(13):1362–1368, 2006.

[68] K. Iwakabe, M. Nakaiwa, K. Huang, T. Nakanishi, A. Røsjorde, T. Ohmori, A. Endo, and T. Yamamoto. Performance of an internally heat-integrated distillation column (hidic) in separation of ternary mixtures. *J Chem Eng Jpn*, 39(4):417–425, 2006.

[69] E.W. Jacobsen and S. Skogestad. Multiple steady states in ideal two-product distillation. *AIChE J*, 37(4):499–511, 1991.

[70] M.G. Jacobsen and S. Skogestad. Active constraint regions for optimal operation of distillation columns. *Ind Eng Chem Res*, 51(7):2963–2973, 2012.

[71] F. Jaing, J. Quan, T. Hamaguchi, Y. Ota, and Y. Hashimoto. Design and control of hidic. *SICE-ICASE International Joint Conference, Bexco, Busan, Korea*, pages 5727–5730, 2006.

[72] C.A. Jaksland, R. Gani, and K.M. Lien. Separation process design and synthesis based on thermodynamic insights. *Chem Eng Sci*, 50(3):511–530, 1995.

[73] A.K. Jana. Heat integrated distillation operation. *Appl Energ*, 87(5):1477–1494, 2010.

[74] A.K. Jana. Advances in heat pump assisted distillation column: A review. *Energy Convers Manage*, 77:287–297, 2014.

[75] E. Jensen. Rectification apparatus using a heat pump, 2011. US Patent 7,972,423.

[76] W. Jiang, J. Khan, and R.A. Dougal. Dynamic centrifugal compressor model for system simulation. *J Power Sources*, 158(2):1333–1343, 2006.

[77] E.S. Jimenez, P. Salamon, R. Rivero, C. Rendon, K.H. Hoffmann, M. Schaller, and B. Andersen. Optimization of a diabatic distillation column with sequential heat exchangers. *Ind Eng Chem Res*, 43(23):7566–7571, 2004.

[78] S.S. Jogwar and P. Daoutidis. Dynamics and control of vapor recompression distillation. *J of Process Contr*, 19(10):1737–1750, 2009.

[79] M. Kano, T. Fukushima, H. Makita, and S. Hasebe. Multiple steady-states in a heat integrated distillation column (hidic). *J Chem Eng Jpn*, 40(10):824–831, 2007.

[80] M. Kano, H. Makita, and S. Hasebe. Prediction of multiple steady states in distillation through simple mass and heat balance analysis. *Ind Eng Chem Res*, 50(3):1346–1351, 2011.

[81] K. Kataoka, H. Noda, T. Mukaida, G. Nishimura, and H. Yamaji. Boost to bioethanol distillation by internal heat-integrated distillation column (hidic). *Advanced Chemical Engineering Reasearch*, 3, 2014.

[82] Y.H. Kim. Internally and partially heat-integrated distillation system for ternary separation. *Ind Eng Chem Res*, 50(9):5733–5738, 2011.

[83] B. Kiran and A.K. Jana. Introducing vapor recompression mechanism in heat-integrated distillation column: Impact of internal energy driven intermediate and bottom reboiler. *AIChE J*, 61(1):118–131, 2015.

[84] B. Kiran, A.K. Jana, and A.N. Samanta. A novel intensified heat integration in multicomponent distillation. *Energy*, 41(1):443–453, 2012.

[85] A.A. Kiss. Distillation technology-still young and full of breakthrough opportunities. *J Chem Technol Biotechnol*, 89(4):479–498, 2013.

[86] A.A. Kiss, S.J. Flores Landaeta, and C.A. Infante Ferreira. Towards energy ef-

ficient distillation technologies - making the right choice. *Energy*, 47(1):531–542, 2012.

[87] A.A. Kiss and Ž. Olujic. A review on process intensification in internally heat-integrated distillation columns. *Chem Eng and Process: Process Intensification*, 86:125–144, 2014.

[88] Jr.P.A. Kolodzie and M. van Winkle. Discharge coefficienfts through perforated plates. *AIChE J*, 3(3):305–312, 1957.

[89] T. Larsson and S. Skogestad. Plantwide control–a review and a new design procedure. *Model Ident Control*, 21(4):209–240, 2000.

[90] H. Li. *Modelling for Predictive Control*. PhD thesis, Technical University of Denmark, 2007.

[91] X. Liu, M.A. Longhua, and Q. Jixin. Thermodynamic analysis and optimization on energy savings of ideal internal thermally coupled distillation column. *Chinese J Chem Eng*, 8(1):57–63, 2000.

[92] X. Liu and J. Qian. Modeling, control, and optimization of ideal internal thermally coupled distillation columns. *Chem Eng Technol*, 23(3):235–241, 2000.

[93] X. Liu, Y. Zhou, L. Cong, and F. Ding. High-purity control of internal thermally coupled distillation columns based on nonlinear wave model. *J of Process Contr*, 21(6):920–926, 2011.

[94] R.S.H. Mah, Jr.J.J. Nicholas, and R.B. Wodnik. Distillation with secondary reflux and vaporization: A comparative evaluation. *AIChE J*, 23(5):651–658, 1977.

[95] D. Maiti, A.K. Jana, and A.N. Samanta. A novel heat integrated batch distillation scheme. *Appl Energ*, 88(12):5221–5225, 2011.

[96] H. Makita, T. Fukushima, M. Kano, and S. Hasebw. Analysis of multiple steady-states in a heat integrated distillation column (hidic). *PSE ASIA*, 2007.

[97] S.V. Mali and A.K. Jana. A partially heat integrated reactive distillation: Feasibility and analysis. *Sep Purif Technol*, 70(1):136–139, 2009.

[98] A. Mane. A new intensified heat integration in distillation column. *Ind Eng Chem Res*, 49(19):9534–9541, 2010.

[99] K. Matsuda, K. Iwakabe, K. Kubo, A. Horiguchi, Y. Weifang, H. Kosuge, S. Kataoka, T. Yamamoto, T. Ohmori, and M. Nakaiwa. Rate-based modeling for internally heat-integrated distillation column (hidic) in binary system. *J Jpn Pet Inst*, 50(3):162–168, 2007.

[100] K. Matsuda, K. Iwakabe, and M. Nakaiwa. Recent advances in internally heat-integrated distillation columns (hidic) for sustainable development. *J Chem Eng Jpn*, 45(6):363–372, 2012.

[101] M. Mauricio-Iglesias, T. Bisgaard, H. Kristensen, K.V. Gernaey, J. Abildskov, and J.K. Huusom. Pressure control in distillation columns: A model-based analysis. *Ind Eng Chem Res*, 53(38):14776–14787, 2014.

[102] N. Metropolis and S. Ulam. The monte carlo method. *J Am Stat Assoc*, 44(247):335–341, 1949.

[103] K. Meyer, L. Ianniciello, J.E. Nielsen, T. Bisgaard, J.K. Huusom, and J. Abildskov. Hidic – design, sensitivity and graphical representation. *Proceedings of Distillation and Absorption*, pages 727–732, 2014.

[104] V. Minasidis, S. Skogestad, and N. Kaistha. Simple rules for economic plantwide control. *Computer-aided Chemical Engineering*, 37:101–108, 2015.

[105] T.J. Mix, J.S. Dweck, M. Weinberg, and R.C. Armstrong. Energy-conservation in distillation. *Chem Eng Prog*, 74(4):49–55, 1978.

[106] A. Miyzaki, J.R. Alcántara-Avila, K.-I. Sotowa, and T. Horikawa. Trade-off assessment between controllability and energy savings in internally and externally heat integrated distillation structures. *ADCONP2014*, pages 426–431, 2014.

[107] C.A. Muhrer, M.A. Collura, and W.L. Luyben. Control of vapor recompression distillation columns. *Ind Eng Chem Res*, 29(1):59–71, 1990.

[108] J.F. Mulia-Soto and A. Flores-Tlacuahuac. Modeling, simulation and control of an internally heat integrated pressure-swing distillation process for bioethanol separation. *Comput Chem Eng*, 35(8):1532–1546, 2011.

[109] K. Naito, M. Nakaiwa, K. Huang, A. Endo, K. Aso, T. Nakanishi, T. Nakamura, H. Noda, and T. Takamatsu. Operation of a bench-scale ideal heat integrated distillation column (hidic): an experimental study. *Comput Chem Eng*, 24(2–7):495–499, 2000.

[110] M. Nakaiwa, K. Huang, A. Endo, K. Naito, M. Owa, T. Akiya, T. Nakane, and T. Takamatsu. Evaluating control structures for a general heat integrated distillation column (general hidic). *Comput Chem Eng*, 23(1):851–854, 1999.

[111] M. Nakaiwa, K. Huang, A. Endo, T. Ohmori, T. Akiya, and T. Takamatsu. Internally heat-integrated distillation columns: A review. *Chem Eng Res Des*, 81(1):162–177, 2003.

[112] M. Nakaiwa, K. Huang, K. Naito, A. Endo, T. Akiya, T. Nakane, and T. Taka-

matsu. Parameter analysis and optimization of ideal heat integrated distillation columns. *Comput Chem Eng*, 25(4–6):737–744, 2001.

[113] M. Nakaiwa, K. Huang, K. Naito, A. Endo, M. Owa, T. Akiya, T. Nakane, and T. Takamatsu. A new configuration of ideal heat integrated distillation columns (hidic). *Comput Chem Eng*, 24(2–7):239–245, 2000.

[114] M. Nakaiwa, K. Huang, M. Owa, T. Akiya, T. Nakane, M. Sato, and T. Takamatsu. Characteristics of energy savings in an ideal heat-integrated distillation column (hidic). *Energy Conversion Engineering Conference*, 3:1587–1591, 1997.

[115] M. Nakaiwa, K. Huang, M. Owa, T. Akiya, T. Nakane, M. Sato, T. Takamatsu, and H. Yoshitome. Potential energy savings in ideal heat-integrated distillation column. *Appl Therm Eng*, 18(11):1077–1087, 1998.

[116] M. Nakaiwa, K. Huang, M. Owa, T. Akiya, T. Nakane, and T. Takamatsu. Operating an ideal heat integrated distillation column with different control algorithms. *Comput Chem Eng*, 22(1):389–393, 1998.

[117] M. Nakaiwa, T. Wakabayashi, and A. Tamakoshi. Heat integrated distillation apparatus, 2013. US Patent 8,440,056 B2.

[118] T. Nakanishi, T. Takamatsu, M. Nakaiwa, K. Aso, H. Noda, and N. Kuratani. A case study of hidic design and energy saving. *Comput Chem Eng*, 23(1):855–858, 1999.

[119] N.M. Nikačevic, A.E.M. Huesman, P.M.J. Van den Hof, and A.I. Stankiewicz. Opportunities and challenges for process control in process intensification. *Chem Eng and Process: Process Intensification*, 52(1):1–15, 2012.

[120] NIST. Nist chemistry webbook. `http://webbook.nist.gov/chemistry/`, 2016. Juni, 2014.

[121] H. Noda, N. Kuratani, T. Mukaida, M. Kaneda, K. Kataoka, H. Yamaji, and M. Nakaiwa. Plate efficiency and heat transfer characteristics in heat-integrated distillation. *Asian Pacific Confederation of Chemical Engineers congress*, 2005.

[122] H. Noda, T. Mukaida, M. Kaneda, K. Kataoka, and M. Nakaiwa. Internal column-to-column heat transfer characteristics for energy-saving distillation system. *IChemE Symposium Series No. 152*, pages 737–744, 2006.

[123] H. Noda, T. Takamatsu, K. Aso, T. Nakanishi, K. Yoshida, M. Nakaiwa, T. Mukaida, and N. Kuratani. Development on a coaxial heat integrated distillation column (hidic). *Korean J Chem Eng*, 17(5):593–596, 2000.

[124] H. Noda, H. Yamaji, N. Kurantani, and K. Kataoka. Multi-structure internal heat exchange type distillation tower, 2010. US Patent 7,846,303.

[125] Z. Olujic, F. Fakhri, A. de Rijke, J. de Graauw, and P.J. Jansens. Internal heat integration – the key to an energy-conserving distillation column. *J Chem Technol Biotechnol*, 78(2–3):241–248, 2003.

[126] Z. Olujic, M. Jödecke, A. Shilkin, G. Schuch, and B. Kaibel. Equipment improvement trends in distillation. *Chem Eng and Process: Process Intensification*, 48(6):1089–1104, 2009.

[127] T.O. Omideyi, J. Kasprzycki, and F.A. Watson. The economics of heat pump assisted distillation systems–i. a design and economic model. *J Heat Recov Syst*, 4(3):187–200, 1984.

[128] T.O. Omideyi, M.G. Parande, J. Kasprzycki, and S. Devotta. The economics of heat pump assisted distillation systems iii–a comparative analysis on three alcohol mixtures. *J Heat Recov Syst*, 4(4):281–286, 1984.

[129] F.B. Petlyuk, V.M. Platonov, and D.M. Slavinskii. Thermodynamically optimal method for separating multicomponent mixtures. *International Chemical Engineering*, 5:555, 1965.

[130] V. Pleşu, A.E.B. Ruiz, J. Bonet, and J. Llorens. Simple equation for sustainbility of heat pump use in distillation. *Computer-aided Chemical Engineering*, 33:1327–1332, 2012.

[131] G.H.S.F. Ponce, M. Alves, J.C.C. Miranda, R.M. Filho, and M.R.W. Maciel. Using an internally heat-integrated distillation column for ethanol-water separation for fuel applications. *Chem Eng Res Des*, 95:55–65, 2015.

[132] J.L. Pulido, E.L. Martinez, A.R.R. Bineli, M.R. Wolf, and R.M. Filho. Heat transfer study in a concentric stage of an internally heat-integrated distillation column (hidic) using cfd simulation. *Proceedings of the World Congress on Engineering and Computer Science*, 2, 2010.

[133] C.A. Ruiz, I.T. Cameron, and R. Gani. A generalized dynamic model for distillation columns–iii. study of startup operations. *Comput Chem Eng*, 12(1):1–14, 1988.

[134] M.A. Salim, M. Sadasivam, and A.R. Balakrishnan. Transient analysis of heat pump assisted distillation systems. 1 the heat pump. *Int J Energy Res*, 15(2):123–135, 1991.

[135] M.A. Salim, M. Sadasivam, and A.R. Balakrishnan. Transient analysis of heat pump assisted distillation systems. 2 column and system dynamics. *Int*

J Energy Res, 15(2):137–148, 1991.

[136] J.P. Schmal, H.J. Van Der Kooi, A. De Rijke, Ž. Olujic, and P.J. Jansens. Internal versus external heat integration: Operational and economic analysis. *Chem Eng Res Des*, 84(5):374–380, 2006.

[137] J.D. Seader, E.J. Henley, and D.K. Roper. *Separation Process Principles. Chemical and Biochemical Operations*. John Wiley & Sons, Inc, USA, 3rd edition. edition, 2003.

[138] Jr.D. Seader. Continuous distillation apparatus and method, 1980. US Patent 4,234,391.

[139] H. Shahandeh, J. Ivakpour, and N. Kasiri. Feasibility study of heat-integrated distillation columns using rigorous optimization. *Energy*, 74:662–674, 2014.

[140] H. Shahandeh, J. Ivakpour, and N. Kasiri. Internal and external hidics (heat-integrated distillation columns) optimization by genetic algorithm. *Energy*, 64:875–886, 2014.

[141] H. Shahandeh, M. Jafari, N. Kasiri, and J. Ivakpour. Economic optimization of heat pump-assisted distillation columns in methanol-water separation. *Energy*, 80:496–508, 2015.

[142] A.A. Shenvi, D.M. Herron, and R. Agrawal. Energy efficiency limitations of the conventional heat integrated distillation column (hidic) configuration for binary distillation. *Ind Eng Chem Res*, 50(1):119–130, 2011.

[143] S.P. Shirsat. Letter to the editor - modeling, simulation and control of an internally heat integrated pressure-swing distillation process for bioethanol separation. *Comput Chem Eng*, 53:201–202, 2013.

[144] L. Shu, L. Chen, and H. Sun. Performance optimization of a diabatic distillation-column by allocating a sequential heat-exchanger inventory. *Appl Energ*, 84(9):893–903, 2007.

[145] G. Sin, K. Gernaey, M.B. Neumann, M.C.M. van Loosdrecht, and W. Gujer. Global sensitivity analysis in wastewater treatment plant model applications: Prioritizing sources of uncertainty. *Water Res*, 45(2):639–651, 2011.

[146] S. Skogestad. Dynamics and control of distillation columns - a critical survey. *Model Ident Control*, 18(3):177–217, 1997.

[147] S. Skogestad. Dynamics and control of distillation columns: A tutorial introduction. *Chem Eng Res Des*, 75(6):539–562, 1997.

[148] S. Skogestad. Simple analytic rules for model reduction and pid controller tuning. *J of Process Contr*, 13(4):291–309, 2003.

[149] S. Skogestad. Control structure design for complete chemical plants. *Comput Chem Eng*, 28(1–2):217–234, 2004.

[150] S. Skogestad. The dos and don'ts of distillation column control. *Chem Eng Res Des*, 85(A1):13–23, 2007.

[151] S. Skogestad and M. Morari. Understanding the dynamic behavior of distillation columns. *Ind Eng Chem Res*, 27(10):1848–1862, 1988.

[152] J.M. Smith and H.C. Van Ness. *Introduction to Chemical Engineering Thermodynamics*. McGraw-Hill Book, Inc., Singapore, 4th edition. edition, 1986.

[153] D.R. Summers, M.W. Pilling, and D.C. Wiesman. Mega tower design considerations. *Proceedings of Distillation and Absorption*, pages 230–235, 2014.

[154] B. Suphanit. Design of internally heat-integrated distillation column (hidic): Uniform heat transfer area versus uniform heat distribution. *Energy*, 35(3):1505–1514, 2010.

[155] B. Suphanit. Optimal heat distribution in the internally heat-integrated distillation column (hidic). *Energy*, 36(7):4171–4181, 2011.

[156] T. Takamatsu, M. Nakaiwa, K. Huang, T. Akiya, H. Noda, T. Nakanishi, and K. Aso. Simulation oriented development of a new heat integrated distillation column and its characteristics for energy saving. *Comput Chem Eng*, 21(Suppl.):243–247, 1997.

[157] G.D. Ulrich and P.T. Vasudevan. How to estimate utility costs. Technical report, Chemical Engineering, 2006.

[158] Ž. Olujic, L. Sun, A. de Rijke, and P.J. Jansens. Conceptual design of an internally heat integrated propylene-propane splitter. *Energy*, 31(15):3083–3096, 2006.

[159] T. Wakabayashi and S. Hasebe. Design of heat integrated distillation column by using h-xy and t-xy diagrams. *Comput Chem Eng*, 56(13):174–183, 2013.

[160] T. Wakabayashi and S. Hasebe. Higher energy saving with new heat integration arrangement in heat integrated distillation column (hidic). *Proceedings of Distillation and Absorption*, pages 57–63, 2014.

[161] T. Wakabayashi and T. Nakao. Stripper for separating process in aromatic component processing apparatus and method for operating the same, 2014. US Patent 0083839 A1.

[162] S.M. Walas. *Chemical Process Equipment. Selection and Design*. Butterworth-Heinemann, USA, 1st edition. edition, 1990.

[163] J.C. Wang and G.E. Henke. Tridiagonal matrix for distillation. *Hydrocarbon Processing*, 45(8):155–163, 1966.

[164] L. Wang, M. Kano, and S. Hasebe. Effect of multiple steady-states on operation strategy and control structure for a heat integrated distillation column (hidic). *19th European Symposium on Computer Aided Process Engineering*, 26:447–451, 2009.

[165] L. Wang, M. Kano, and S. Hasebe. Effect of operation strategy and control structure on multiple steady-states of heat integrated distillation column (hidic). *J Chem Eng Jpn*, 43(10):857–864, 2010.

[166] L. Wang, H. Makita, M. Kano, and S. Hasebe. Dynamic start-up model of heat integrated distillation column. *PSE ASIA*, 2007.

[167] Y. Wang, K. Huang, and S. Wang. A simplified scheme of externally heat-integrated double distillation columns (ehiddic) with three external heat exchangers. *Ind Eng Chem Res*, 49(7):3349–3364, 2010.

[168] B. Wittgens and S. Skogestad. Evaluation of dynamic models of distillation columns with emphasis on the initial response. *Model Ident Control*, 21(2):83–103, 2000.

[169] R.O. Wright. Fractionation apparatus, 1949. US Patent 2,471,134.

[170] L. Xu, D. Chen, B. Yan, and X. Yuan. Experimental investigation on heat exchange and separation performance of an annular structured internal heat-integrated distillation column. *Chinese J Chem Eng*, 22(10):1087–1091, 2014.

[171] X. Yuan, L. Xu, D. Chen, Y. Luo, and K. Yu. Reversibility analysis for design optimization of an internally heat-integrated distillation column. *Chem Eng Technol*, 36(7):1147–1156, 2013.

[172] X. Zhang, K. Huang, H. Chen, and S. Wang. Comparing three configurations of the externally heat-integrated double distillation columns (ehiddics). *Comput Chem Eng*, 35(10):2017–2033, 2011.

[173] Y. Zhu and X. Liu. Dynamics and control of high purity heat integrated distillation columns. *Ind Eng Chem Res*, 44(23):8806–8814, 2005.

[174] Y. Zhu and X. Liu. Investigating control schemes for an ideal thermally coupled distillation column (itcdic). *Chem Eng Technol*, 28(9):1048–1055, 2005.

Appendix A

Model Impelementation Documentation

A.1 Model Hierarchy

An overview of the model implementation hierarchy is provided in Figure A.1.

A.2 Database

A database of chemical species with physical data was generated. This database contains 45 compounds. Furthermore, a corresponding database of UNIFAC parameters is established, which can describe the 45 compounds by including 17 different groups. The databases are established as Microsoft Excel files.

A.3 Implementation

The implementation is illustrated through a description of the developed Matlab functions. A list of these is given in Table A.1.

Table A.1. Matlab functions descriptions. The Matlab functions are sorted alpabetically.

Function	Short description
`f_activity_coefficient`	Calculate activity coefficient; the options for calculating the activity coefficients are Wilson, UNIQUAC and UNIFAC.

Continued on next page

Table A.1 – continued from previous page

Function	Short description
f_column	The main function, which evaluates all model equations in order to obtain the state derivatives
f_column_definitions	Based on the user input, the data is organised in one variable of the structure data type
f_comp2idx	Obtains an index corresponding to a string of a component name.
f_density	The density of the liquid is calculated based on the DIPPR 105 correlation
f_design_column	Solves all algebraic equations consisting of conservative, constitutive and constraint equations, in order to obtain a accurate steady state.
f_design_internals	Determines valve constants for valve equations based on steady state data. The valve constants are only significant in dynamic simulations.
f_equilibrium_constant	Calculates the equilibrium constant based on specified thermodynamic methods
f_fenske_underwood_gililand	Provides a column design by the Fenske-Underwood-Gililand method for conventional distillation columns.
f_fit_binary	Fits the binary interaction parameters of a thermodynamic model to provided experimental data.
f_flash	For a mixture with zero degrees of freedom (Gibb's phase rule), this function provides remaining mixture properties based on user input. E.g. if liquid mole fraction and temperature are known, pressure and vapour mole fractions can be calculated. This method is given explicitly, but the function also contains iterative methods as e.g. boiling point method for finding temperature and vapour phase composition given liquid phase composition and pressure.
f_flow	Determines the internal flows based on empirical formulas. Liquid flow given by the Francis weir formula and vapour flow through perforations equation.
f_fugacity_coefficient	Calculate fugacity coefficient; the option for calculating the fugacity coefficient is the Soave-Redlich-Kwong equation of state.

Continued on next page

Table A.1 – continued from previous page

Function	Short description
`f_heat_transfer`	Calculates internal heat transfer; only internal heat transfer between stages is implemented.
`f_initialize_database`	Extracts required pure component data and binary interaction parameter data from the databases. The extracted data depends on the user input of required thermodynamic models. The data is stored in a variable of the structure data type.
`f_optimize_operation`	Attempts to optimise the operating point for a given column design.
`f_performance_indicators`	Calculates all performance indicators described in Section 3.4 based on a steady state solution.
`f_ponchon_savarit`	Provides a column design by the Ponchon-Savarit method for conventional distillation columns.
`f_phase_diagram`	Calculates *xy*, *Txy*, *hxy*, or driving force phase diagram.
`f_state_function`	The reference state has been chosen as pure components in ideal gas state at 298.15 K. The constant pressure heat capacity from DIPPR 107 correlation.
`f_surface_tension`	The surface tension is calculated by the Full DIPPR 106 correlation.
`f_vapor_pressure`	Vapour pressure based on DIPPR 101 correlation.
`f_visualize_column`	Provides a graphical representation of a specified distillation column.
`f_Wang_Henke`	Provides a steady state solution based on the extended version of the Wang-Henke bubble-point method. This method is described in Appendix D.

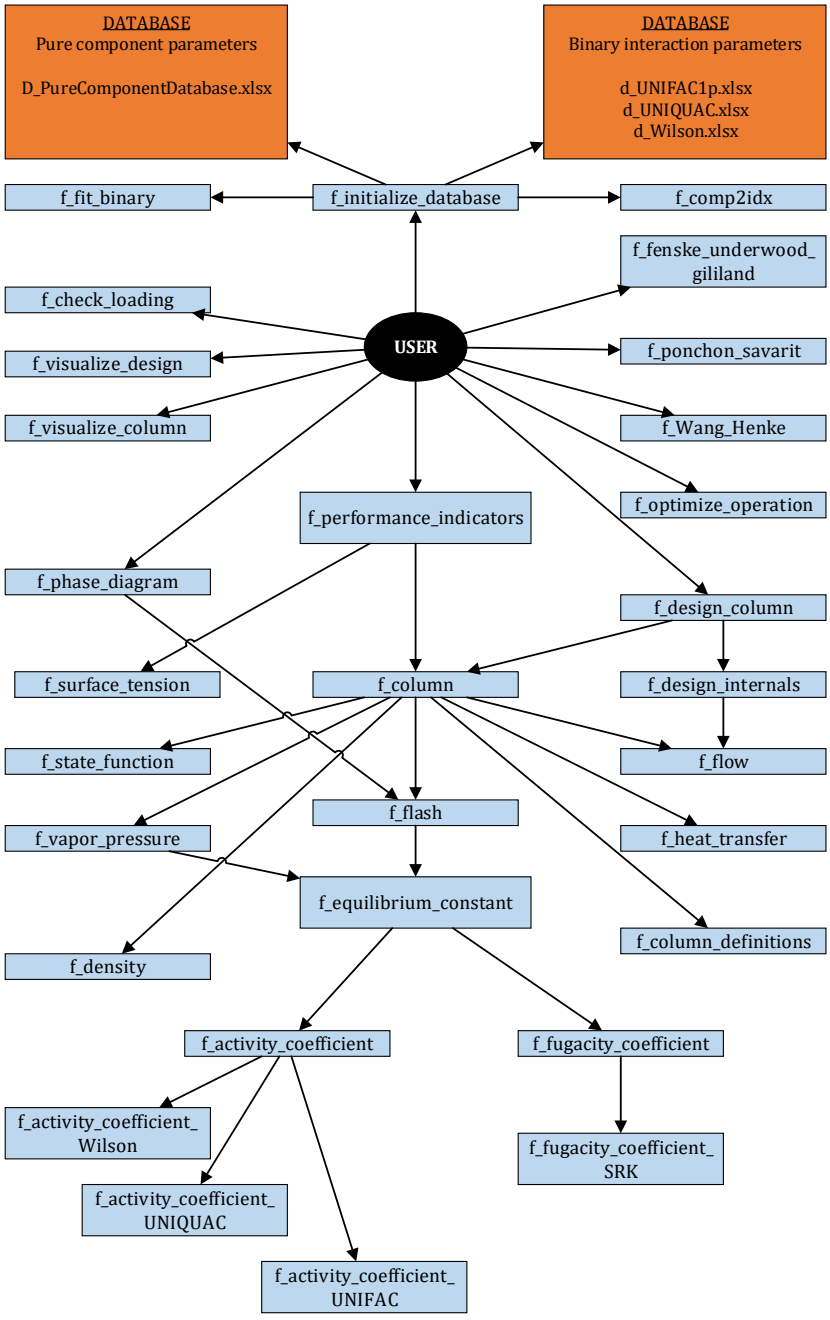

Figure A.1. Model implementation hierarchy illustrating the links between the Matlab functions listed in Table A.1.

Appendix B

Mathematical Derivations

The mathematical derivations applied throughout the thesis are collected in this appendix.

B.1 State Functions

The ideal vapour enthalpy of a pure component at temperature T is obtained by mathematical integration of the constant pressure heat capacity ($c^V_{P,i,j}$):

$$\begin{aligned} h^V_{i,j} &= \int_{T=T_{ref}}^{T_i} c^V_{P,i,j} dT \\ &= \left[A_j T + \frac{B_j C_j \cosh\left(C_j/T\right)}{\sinh\left(C_j/T\right)} - \frac{D_j E_j \sinh\left(E_j/T\right)}{\cosh\left(E_j/T\right)} \right]_{T=T_{ref}}^{T_i} \end{aligned}$$

Similarly, the vapour entropy of a pure component at temperature T is obtained by mathematical integration:

$$\begin{aligned} s^V_{i,j} &= \int_{T=T_{ref}}^{T_i} \frac{c^V_{P,i,j}}{T} dT \\ &= \Bigg[A \ln T + D_j \ln\left(e^{2E_j/T} + 1\right) - B_j \ln\left(e^{2C_j/T} - 1\right) \\ &\quad + \frac{2C_j B_j}{T}\left(\frac{1}{e^{2C_j/T} - 1} + 1\right) \\ &\quad + \frac{2E_j D_j}{T}\left(\frac{1}{e^{2E_j/T} + 1} - 1\right) \Bigg]_{T=T_{ref}}^{T_i} \end{aligned}$$

The ideal liquid constant pressure heat capacity can be obtained through differentiation:

$$\begin{aligned} c_{P,i,j}^{L} =& \frac{\partial}{\partial T}\Delta_{vap}h_{i,j} \\ =& -\frac{2B_jC_j^2}{T_i^3\sinh\left(C_j/T_i\right)^2} + \frac{2B_jC_j^3\cosh\left(C_j/T_i\right)}{T_i^4\sinh\left(C_j/T_i\right)^3} \\ & -\frac{2D_jE_j^2}{T_i^3\cosh\left(E_j/T_i\right)^2} + \frac{2D_jE_j^3\sinh\left(E_j/T_i\right)}{T_i^4\cosh\left(E_j/T_i\right)^3} \end{aligned}$$

B.2 Derivatives Chain Rule Algebra

Following approach is employed for converting liquid energy holdup derivatives into temperature derivatives. The liquid is assumed to be incompressible, which implies $u_j^L = h_j^L$. Hence:

$$\begin{aligned} \frac{d}{dt}(u^L M_T^L) =& \frac{d}{dt}(h^L M_T^L) \\ =& M_T^L\frac{dh^L}{dt} + h^L\frac{dM_T^L}{dt} \end{aligned}$$

The time derivative of the enthalpy is:

$$\begin{aligned} \frac{dh^L}{dt} =& \frac{d}{dt}\sum_{j=1}^{N_C} x_j h_j^L \\ =& \sum_{j=1}^{N_C}\left(h_j^L\frac{dx_j}{dt} + x_j\frac{dh_j^L}{dt}\right) \\ =& \sum_{j=1}^{N_C}\left(h_j^L\frac{dx_j}{dt} + x_j c_{P,j}^L\frac{dT}{dt}\right) \end{aligned}$$

Here the chain rule was used:

$$\frac{dh_j^L}{dt} = \frac{\partial h_j^L}{\partial T}\frac{dT}{dt} = c_{P,j}^L\frac{dT}{dt} \tag{B.1}$$

was substituted. The energy holdup derivatives can thus be expressed in temperature derivatives:

$$\frac{dT}{dt} = \frac{1}{C_P^L}\left(\frac{d}{dt}(h^L M_T^L) - M_T^L\sum_{j=1}^{N_C} h_j^L\frac{dx_j}{dt} + h^L\frac{d}{dT}M_T^L\right) \tag{B.2}$$

When the vapour phase energy holdup derivatives must be expressed in terms of temperature derivatives, one has to account for the relation between enthalpy and internal energy $u = h - PV$. Thus, the internal energy derivative of a vapour

phase when assuming constant total vapour holdup:

$$\begin{aligned}
\frac{d}{dt}(u^V M_T) &= M_T \frac{du^V}{dt} \\
&= M_T \frac{d}{dt}(h^V - RT) \\
&= M_T \left(\frac{dh^V}{dt} - R\frac{dT}{dt} \right) \\
&= M_T \left(\frac{d}{dt} \sum_{j=1}^{N_S} h_j^V y_j - R\frac{dT}{dt} \right) \\
&= M_T \left(\sum_{j=1}^{N_S} \frac{d}{dt}(h_j^V y_j) - R\frac{dT}{dt} \right) \\
&= M_T \left(\sum_{j=1}^{N_S} h_j^V \frac{dy_j}{dt} + \sum_{j=1}^{N_S} y_j \frac{dh_j^V}{dt} \right) - M_T R\frac{dT}{dt}
\end{aligned}$$

Using chain rule $dh_j^V/dt = (\partial h_j^V/\partial T)(dT/dt)$ (similar to Eq. B.1) with the definition $\partial h_j^V/\partial T = C_{P,j}^V$:

$$\begin{aligned}
\frac{d}{dt}(u^V M_T) M_T \left(\sum_{j=1}^{N_S} h_j^V \frac{dy_j}{dt} + \sum_{j=1}^{N_S} y_j \frac{\partial h_j^V}{\partial T}\frac{dT}{dt} \right) - M_T R\frac{dT}{dt} \\
M_T \left(\sum_{j=1}^{N_S} h_j^V \frac{dy_j}{dt} + \frac{dT}{dt} \sum_{j=1}^{N_S} y_j C_{P,j}^V \right) - M_T R\frac{dT}{dt} \\
M_T \sum_{j=1}^{N_S} h_j^V \frac{dy_j}{dt} + M_T \frac{dT}{dt} C_P^V - M_T R\frac{dT}{dt}
\end{aligned}$$

Implying:

$$\frac{dT}{dt} = \frac{\frac{d}{dt}(u^V M_T) - M_T \sum_{j=1}^{N_S} h_j^V \frac{dy_j}{dt}}{M_T C_P^V - M_T R} \tag{B.3}$$

B.3 Compressor Feasibility

Compression is feasible if the compression is dry, i.e. condensation does not occur when a saturated vapour is compressed. Given an initial saturated condition (T_{in}, P_{in}). If the pressure is increased from the initial condition by compression, the increase in the saturation temperature must not exceed the temperature resulting from isentropic compression in the new state. If the temperature drops below the saturation temperature (below dew-point), condensation occurs. It is assumed that this formulated condition can be simplified in terms of derivatives. The condition is assumed to correspond to the condition, where the increase in the actual tempera-

ture, due to compression, must larger than the increase in saturation temperature:

$$\frac{dT}{dP} \leq \frac{dT^{sat}}{dP} \Rightarrow \frac{\partial P}{\partial T^{sat}} \leq \frac{\partial P}{\partial T} \tag{B.4}$$

The pressure is the only thermodynamic degree of freedom as only one phase and constant composition is considered. The saturated condition obeys the Clausius-Clapeyron equation:

$$\frac{dP}{dT^{sat}} = \frac{P\lambda}{T^2 R} \tag{B.5}$$

The derivative associated with the actual state is derived form Eq. (3.33):

$$\frac{dP}{dT} = \frac{P_{in} C_P^V \left[\eta_{is}\left(\frac{T}{T_{in}} - 1\right) + 1\right]^{C_P^V}}{R\eta_{is} T_{in}\left[\eta_{is}\left(\frac{T}{T_{in}} - 1\right) + 1\right]} \tag{B.6}$$

Inserting Eq. (B.5) and (B.6) into Eq. (B.4) and evaluating the expression for $T = T_{in} \approx \bar{T}_{nb}$:

$$\bar{T}_{nb} \leq \frac{\eta_{is}\lambda}{C_P^V} \approx \frac{\eta_{is}\bar{\lambda}}{\bar{C}_P^V} \Rightarrow \frac{\eta_{is}\bar{\lambda}}{\bar{C}_P^V \bar{T}_{nb}} - 1 \geq 0 \tag{B.7}$$

It is assumed that the inlet vapour to the compressor is the geometric mean normal boiling point temperature $\bar{T}_{nb}$ of the components. This is reasonable because the compressor in a HIDiC is placed above the feed stage and the stripping section is usually operated at atmospheric pressure.

B.4 Compression Ratio

The purpose of this section is to show the derivation of an approximate expression for the compression ratio, which is valid for the heat-integrated distillation column (HIDiC) and the mechanical vapour recompression column (MVRC). Consider a conventional distillation column (CDiC) with a uniform pressure on each tray (P), i.e. ignoring pressure drops. The lowest temperature is in the condenser and the highest temperature is in the reboiler. This temperature difference will thus be the largest among the possible arrangements of heat integration. If the temperature of the condenser is raised to or above that of the reboiler temperature by means of compression, the column is divided in a high pressure section (HP) and a low pressure section (LP). The location of the sections depends on the location of the compressor; for example, for the HIDIC, the HP section is the rectifying section and the LP section is the stripping section. The pressures are termed $P_{HP} = CR\ P_{LP}$ for the HP section and $P_{LP} = P$ for the LP section, with CR being the compression ratio. The condition for the temperature driving force becomes

$$T_{cnd} = T_{rbl} + \Delta T \Rightarrow T_{bp,1}|_{P_{HP}} = T_{bp,2}|_{P_{LP}} + \Delta T \tag{B.8}$$

where ΔT is additional increase in temperature above the reboiler temperature. In Eq. (B.8), the condenser is assumed to consist of pure component 1 such that the temperature is the boiling point of component 1 at pressure P_{HP} ($T_{bp,1}|_{P_{HP}}$), and the reboiler is assumed to consist of pure component 2 at pressure P_{LP} ($T_{bp,2}|_{P_{LP}}$). Using the normal condition as reference ($P_{atm} = 101.32\,\text{kPa}$), the Clausius-Clapeyron equation states:

$$\left(\frac{1}{T_{bp,1}|_{P_{atm}}} - \frac{R}{\lambda}\ln\frac{CRP_{LP}}{P_{atm}}\right)^{-1} = \left(\frac{1}{T_{bp,2}|_{P_{atm}}} - \frac{R}{\lambda}\ln\frac{P_{LP}}{P_{atm}}\right)^{-1} + \Delta T \Leftrightarrow \tag{B.9}$$

$$CR = \exp\left[\frac{\lambda}{RT_{bp,1}} - \ln\frac{P_{LP}}{P_{atm}} - \frac{\frac{\lambda}{RT_{bp,2}} - \ln\frac{P_{LP}}{P_{atm}}}{1 + \frac{\Delta T}{T_{bp,2}} - \frac{R\Delta T}{\lambda}\ln\frac{P_{LP}}{P_{atm}}}\right] \tag{B.10}$$

where R is the universal gas constant and λ is the heat of vaporisation assumed constant and identical for both components.

In the special case for $\Delta T = 0$ K, Eq. (B.10) reduces to

$$CR = \exp\left[\frac{\lambda}{R}\left(\frac{1}{T_{bp,1}} - \frac{1}{T_{bp,2}}\right)\right] = \alpha_{12} \tag{B.11}$$

where α_{12} is the relative volatility. Hence, a simple estimate of the required compression ratio can be calculated by Eq. (B.11).

Appendix C

Supplementary Material for Economic Model

The values of the Souder-Brown factor, presented in the book of Biegler et al. [9], has been read off and implemented as a look-up table in the Matlab implementation. An illustration generated by the look-up table is shown in Figure C.1.

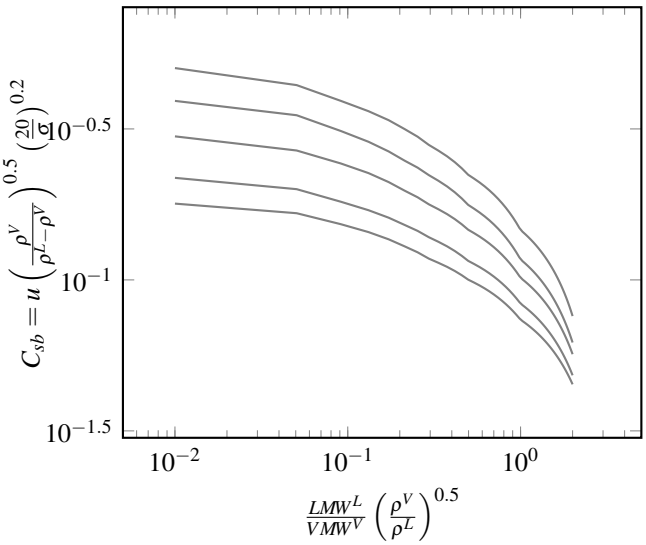

Figure C.1. Souder-Brown factor for column internals [9].

Appendix D

Extended BP Method

The BP Method [163] provides a readily programmed, rapid solution procedure for a certain set of input specifications. By using temperatures and vapour flow rates as tear variables, all mass-energy-sum-enthalpy balances (MESH) can be solved sequentially. In particular, the mass balances w.r.t. the liquid mole fractions become linear and thus a tridiagonal matrix is obtained. This tridiagonal matrix is then solved by a modified Gaussian-elimination algorithm referred to as the Thomas Algorithm. The BP Method has been extended by including an extra step that handles internal heat integration. However, as temperatures are tear variables this step becomes straight forward. The Extended BP Method is illustrated in Figure D.1.

Step 1: Specify degrees of freedom

The specifications are:

- Feed temperature (T_F), pressure (P_F), composition (z_F), and enthalpy (h_F) and stage locations (N_F)
- Stage pressures (P_i) for $i = 1,2,\ldots,N_S$. Specifying the stage pressures also dictates the positions of the comperssor/throttling valves.
- Flow rate of liquid sidestreams (U_i) and vapour sidestreams (W_i) for $i = 1,2,\ldots,N_S$. Note that the distillate flow rate is designed as U_1.
- External heat transfer rates (Q_i) at all stages but the first (condenser) and the last (reboiler), i.e. for $i = 2,3,\ldots,N_S-1$
- Total number of stages (N_S)
- Reflux ratio ($RR = L_1/U_1$)

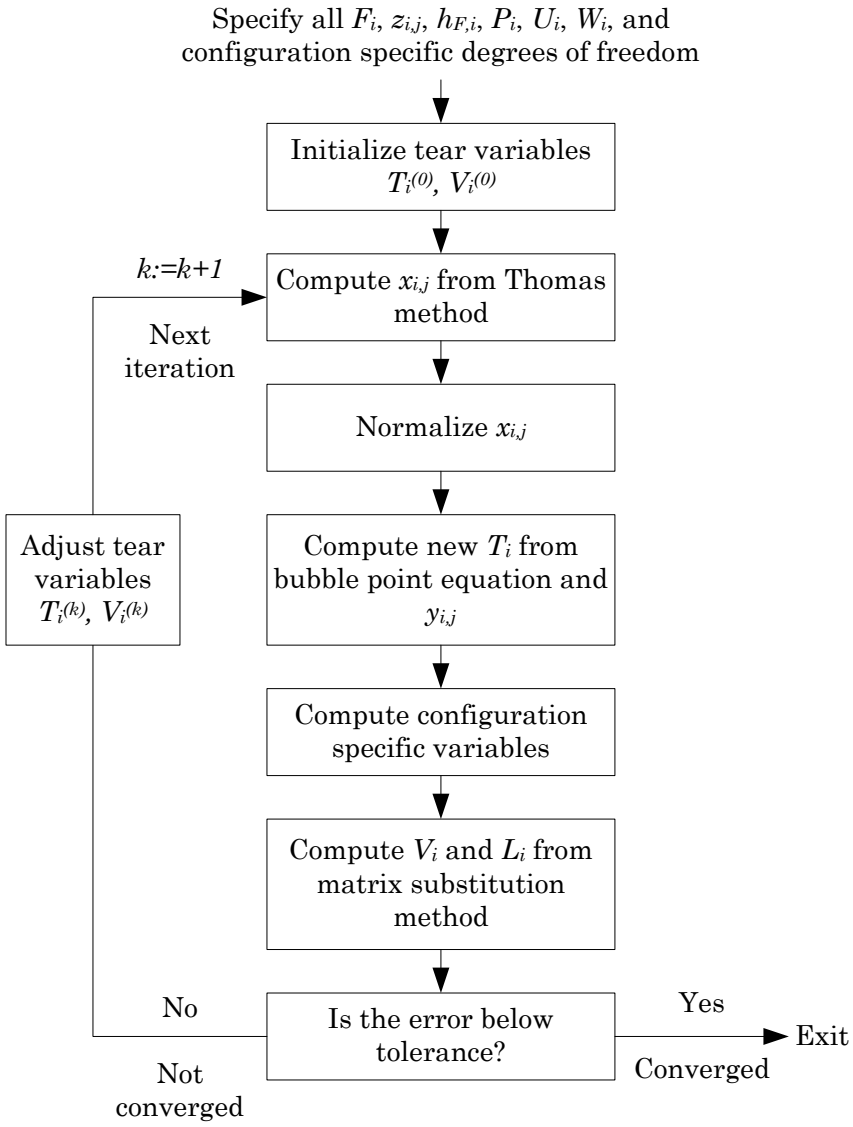

Figure D.1. Extended BP Algorithm.

- Top vapour flow rate (V_1)

- The pairing of heat-integrated stages (see Section 3.3.4)

Step 2: Initialise tear variables

The tear variables are V_i and T_i for all N_S stages. For conventional distillation columns, it is sufficient to initialise the tear variables using linear interpolation of top and bottom bubble-point temperatures based on the specified product compositions, and by assuming constant-molar interstage flows for the vapour flow rates. In this work, the initialisation is carried out as described below.

A uniform temperature initialisation has been employed based on averaged feed conditions:

$$T_i = T_{bp}|_{P_i,\bar{z}}, \quad i = 1,2,\ldots,N_S \tag{D.1}$$

where

$T_{bp} =$ bubble point [K]

$P_i =$ specified stage pressure [kPa]

$\bar{z} =$ averaged feed composition [-]

Using the temperature initialisation in Eq. (D.1), internal heat integration can be included in the initialisation of the vapour flow, as a higher temperature is obtained through the pressure variations. The vapour flow rate profile can thus be initialised using:

$$V_i = (U_1 - L_1) + \sum_{k=i}^{N_S} \left(F_k(1-q_k) + \frac{q_k}{\Delta h_{vap,k}} \right), \quad i = 2,3,\ldots,N_S \tag{D.2}$$

where

$\Delta h_{vap,k} =$ heat of vaporisation at the specified conditions and temperature from eq. (D.1).

Step 3: Compute x from tridiagonal matrix algorithm

Due to the tridiagonal matrix structure, the mass balances can be solved successively starting from the top stage ($i = 1$):

$$B_{i,j} = -(V_{i+1} + \sum_{k=1} i\,(-V_1 + F_k - W_k - U_k) + (V_i + W_i)\,K_{i,j} \tag{D.3}$$

$$C_{i,j} = V_{i+1} K_{i+1,j} \tag{D.4}$$

$$D_{i,j} = -F_i z_{i,j} \tag{D.5}$$

$$p_{i,j} = \frac{C_j}{B_j} \tag{D.6}$$

$$q_{i,j} = \frac{D_j}{B_j} \tag{D.7}$$

From stage $i = 2, 3, \ldots, N_S - 1$:

$$A_i = V_i + \sum_{k=1}^{i-1} (F_k - W_k - U_k) \tag{D.8}$$

$$B_{i,j} = -\left[V_{i+1} + \sum_{k=1}^{i} (F_i - W_i - U_i) + U_i + (V_i + W_i) K_{i,j} \right] \tag{D.9}$$

$$C_{i,j} = V_{i+1} K_{i+1,j} \tag{D.10}$$

$$D_{i,j} = -F_i z_{i,j} \tag{D.11}$$

$$p_{i,j} = \frac{C_{i,j}}{B_{i,j} - A_i p_{i-1,j}} \tag{D.12}$$

$$q_{i,j} = \frac{D_{i,j} - A_i q_{i-1,j}}{B_{i,j} - A_i p_{i-1,j}} \tag{D.13}$$

And the last stage $i = N_S$:

$$A_i == V_i + \sum_{k=1}^{i-1} (F_k - W_k - U_k) \tag{D.14}$$

$$B_{i,j} = -\left[\sum_{k=1}^{i} (F_k - W_k - U_k) + U(i) + (V_i + W_i) K_{i,j} \right] \tag{D.15}$$

$$D_{i,j} = -F_i * z_{i,j} \tag{D.16}$$

$$q_{i,j} = \frac{D_{i,j} - A_i q_{i-1,j}}{B_{i,j} - A_i p_{i-1,j}} \tag{D.17}$$

The liquid mole fraction can be obtained successively starting running in reverse order from $i = N_S, N_S - 1, \ldots, 1$:

$$x_{N_S,j} = q_{N_S,j} \tag{D.18}$$

$$x_{i,j} = q_{i,j} - p_{i,j} x_{i+1,j}, \quad i = N_S - 1, N_S - 2, \ldots, 1 \tag{D.19}$$

Note that the equilibrium factors of each component at stage i is obtained using the state of the previous iteration $K^{(k)} = f(T^{(k-1)}, P^{(k-1)}, x^{(k-1)}, y^{(k-1)})$.

Step 4: Normalise x

The liquid mole fractions are normalised according to the formula:

$$x_{i,j} := \frac{x_{i,j}}{\sum_{k=1}^{N_C} x_{i,k}} \tag{D.20}$$

The normalisation requires the mole fractions to be updated, and therefore the operator ":=" meaning "replaced by".

Step 5: Compute new T and y from bubble-point equation

Two phases are considered with N_C components. This gives N_C thermodynamic degrees of freedom according to Gibb's phase rule. Since all x and P are known, the temperature and vapour mole fractions at equilibrium can be obtained by a bubble-point calculation. This calculation depends on the types of models used, but a general form is:

$$0 = f(T^{(k)}, P^{(k)}, x^{(k)}, y^{(k)}) \tag{D.21}$$

Which can be solved to obtain $T^{(k)}$ and $y^{(k)}$.

In this work, the compressor/valve stage is included as stages in the BP Method, and therefore the temperature of these stages must be calculated according to the equation:

$$T_i = T_{i+1}\left(1 + \frac{1}{\eta}\left[\left(\frac{P_i}{P_{i+1}}\right)^{(\kappa_i - 1)/\kappa_i} - 1\right]\right) \tag{D.22}$$

Step 6: Compute configuration specific variables

In this step, all liquid and vapour enthalpies are calculated (see Section 3.3.2):

$$h^L = f(T, P, x) \tag{D.23}$$

$$h^V = f(T, P, y) \tag{D.24}$$

In addition, the internal heat transfer rates are calculated (see Section 3.3.4):

$$q = f(T) \tag{D.25}$$

Finally, the external duties compressor duty (E), condenser duty (Q_1), and the reboiler duty (Q_{N_S}) are calculated using:

$$E_i = V_{i+1}(h_i^V - h_{i+1}^V) \tag{D.26}$$

$$Q_1 = (L_1 + U_1)h_1^L + (V_1 + W_1)h_1^V - V_2 h_2^V - F_1 h_{F,1} - E_1 - q_1 \tag{D.27}$$

$$Q_{N_S} = V_1 h_1^V + L_{N_S} h_{N_S}^L - \sum_{k=1}^{N_S}\left(F_k h_{F,k} - U_k h_k^L - W_k h_k^V\right) - \sum_{k=1}^{N_S - 1}(Q_k) - \sum_{k=1}^{N_S} E - \sum_{k=1}^{N_S} q \tag{D.28}$$

Note that the above equations are extended from the original method as presented by Seader et al. [137].

Step 7: Compute V and L from matrix substitution method

The liquid and vapour flow rates are updated using energy balances:

$$\alpha_i = h_{i-1}^L - h_i^V \tag{D.29}$$

$$\beta_i = h_{i+1}^V - h_i^L \tag{D.30}$$

$$\gamma_i = \sum_{k=1}^{i-1} (-V_1 + F_k - W_k - U_k)\left(h_i^L - h_{i-1}^L\right) + F_i(h_i^L - h_{F,i}) + W_i(h_i^V - h_i^L) - Q_i - q_i - E_i - U_i h_i^L \tag{D.31}$$

$$V_{i+1} = \frac{\gamma_i - \alpha_i * V_i}{\beta_i} \tag{D.32}$$

$$L_i = V_{i+1} + \sum_{k=1}^{i} (-V_1 + F_k - W_k - U_k) \tag{D.33}$$

Step 8: Evaluate tolerance

The iteration stop criterion:

$$\frac{1}{N_S}\left(\sum_{i=1}^{N_S}\left[\frac{T_i^{(k)} - T_i^{(k-1)}}{T_i^{(k)}}\right] + \sum_{i=1}^{N_S}\left[\frac{V_i^{(k)} - V_i^{(k-1)}}{V_i^{(k)}}\right]\right) \leq \varepsilon \tag{D.34}$$

In this work, the tolerance $\varepsilon = 10^{-8}$. If the criteria in Eq. (D.34) is not satisfied, the iteration number (k) is increased by one and the algorithm is repeated from Step 2.

Appendix E

Design Method Comparison

This appendix serves as a comparison of the presented design method in Chapter 4 to existing design methods. The employed existing methods are the Ponchon-Savarit method [56] and the Extended Ponchon-Savarit method [159].

Detailed descriptions of the individual, reviewed design methods are not provided in this section, but their steps are systematically described in relation to the considered separation. For derivation and further information on the design methods see the provided references along with the reviews. For a basis of comparison, the separation of methanol/water with the specifications listed in Table E.1. This binary mixture has a non-ideal behaviour as a result of hydrophilic interactions, which is expected to result in column design with column sections of different sizes. As the heat-integrated pairs of the column stages is an essential element in a design method of a HIDiC, the design outcomes from the two considered methods should be compared. In addition, the separation is sufficiently easy such that it can be carried out in a reasonably low amount of stages. Therefore graphical methods can be easily represented with sufficient readability.

Table E.1. Separation for testing the design methods.

Variable	Unit	Value
Components	-	Methanol/water
VLE Model	-	UNIFAC 1p VLE
Feed flow rate	$\mathrm{mol\,s^{-1}}$	69.4
Composition	-	0.58
Feed pressure	kPa	101.3
Feed temperature	K	344.85
Distillate composition	-	0.9
Bottoms composition	-	0.1

E.1 Nominal Design

The nominal design is obtained using the proposed design algorithm outlines in Chapter 4. The optimal CDiC design based on TAC has 6 trays in the rectifying section and 5 trays in the stripping section. The TAC for the CDiC is $0.90\,\mathrm{M\$\,yr^{-1}}$. It turns out that the optimal HIDiC design has the same number of stages with five heat-integrated pairs. The TAC for the HIDiC is $0.98\,\mathrm{M\$\,yr^{-1}}$. Thus the TAC is higher for the HIDiC than the CDiC. The reboiler duty is $Q_{rbl} = 1428\,\mathrm{kW}$ and the compressor duty is $E = 109.3\,\mathrm{kW}$. This is obtained with 5 heat-integrated pairs with areas of $26.7\,\mathrm{m^2}$ and a compression ratio of 1.685.

E.2 Ponchon-Savarit

Method Summary

This design method closely resembles a direct application of the original Ponchon-Savarit method for adiabatic distillation columns [54]. A systematic application of the Ponchon-Savarit to a diabatic distillation column was published by Ho et al. [56], and it is summarised in Figure E.1. Following separation formulation in step 1, the mass balances are solved in step 2 based on the provided specifications. In step 3, the pressures for the stripping and the rectifying sections are specified. The *hxy*-diagram is constructed in step 4 comprised of bubble-point and dew-point lines for both the two section pressures. In step 5 a constant, stage-wise, internal heat transfer rate is specified, enabling stepping by drawing of top-down and bottom-up lines in step 6 as in the conventional Ponchon-Savarit Method. When the stepping is finished or can not converge, the design is evaluated for feasibility in step 7 (temperature driving forces etc.). Finally, the compressor is characterised by its vapour throughput in step 8, and all duties are calculated in step 9. The heat exchange areas are estimated in step 9.

Design

Given the feed specifications listed in Table E.1, a component balance and a total mass balance can be solved simultaneously:

$$Fz = Dx_D + Bx_B$$
$$F = D + B$$

With $z = 0.58$, $x_D = 0.9$, $x_B = 0.1$, and $F = 69.4\,\mathrm{mol\,s^{-1}}$, the solution is $D = 41.7\,\mathrm{mol\,s^{-1}}$ and $B = 27.8\,\mathrm{mol\,s^{-1}}$. In step 3, the stripping section pressure is set identical to

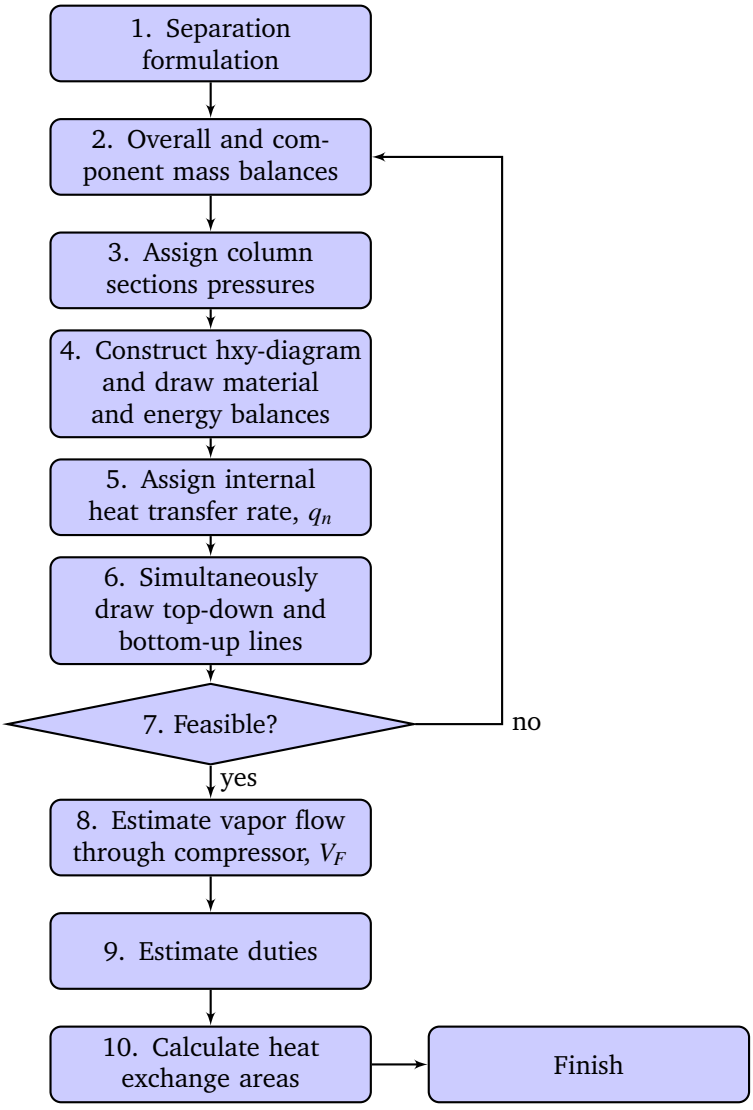

Figure E.1. Ponchon-Savarit Method for HIDiC design by Ho et al. [56].

the feed pressure $P_{str} = 101.3\,\text{kPa}$. It is recommended that the rectifying section pressure is selected such that the temperature difference between the dew point temperature of the top product and the bubble-point temperature of the bottoms product should be significant. A minimum temperature difference of 10 K is suggested by the authors. The bubble-point temperature of the bottoms product is 360.8 K. For the same separation, Ho et al. [56] propose a rectifying section pressure of 202.6 kPa. However, at this pressure the dew-point temperature of the top product is only 360.1 K and does not fulfil the suggested minimum temperature difference. By manual iterations, a rectifying section pressure of 350 kPa was found to be satisfactory giving a minimum temperature difference of 15.6 K. The equilibrium data are represented in an *hxy*-diagram in step 4 along with lines representing the overall mass and energy balances. Using this line, the sum of the compressor and the reboiler duties divided by the bottoms flow rate can be estimated, obtaining $(E + Q_{rbl})/B = 56.8\,\text{kJ mol}^{-1}$. As a result $E + Q_{rbl} = 1578\,\text{kW}$. The minimum overall heat transfer rate ($q_{HT}^{min} = 504.3\,\text{kW}$) is estimated graphically in order to provide insights in selecting the internal heat transfer rate later in the following step. Based on the minimum overall heat transfer rate, a value of internal heat transfer $q_n = 150\,\text{kW}$ is chosen. No direct guidelines for selecting q_n is provided and iterations of this variable might be necessary for obtaining a feasible design. A design pinch is reached if work and equilibrium lines become parallel, which leads to an infeasible design and adjustments in design are required. In step 6, the simultaneously top-down and bottom up lines drawing is performed. The construction of the lines is carried out by alternating between equilibrium and work lines, which are straight lines. The work lines are shifted by a vertical distance proportional to the internal heat transfer $q/B = 5.4\,\text{kJ mol}^{-1}$. The resulting design has four heat-integrated pairs with five trays in the rectifying section and four trays in the stripping section. The temperature driving forces of the four pairs are estimated as 13.8 K, 23.2 K, 27.8 K, and 30.0 K from top to bottom, leading to heat exchange areas of $18.2\,\text{m}^2$, $10.8\,\text{m}^2$, $9.0\,\text{m}^2$, and $8.4\,\text{m}^2$ using $U = 0.60\,\text{kW m}^{-2}\,\text{K}^{-1}$. The vapour flow through the compressor is estimated in step 8 using the component and overall mass balances of the rectifying section:

$$0 = V_F - L_{R1} - D$$
$$0 = V_F y_F - L_{R1} x_{R1} - D y_T$$

Using $D = 41.7\,\text{mol s}^{-1}$, $y_T = 0.9$ and by reading $x_R = 0.64$ and $y_F = 0.81$ from the *hxy*-diagram, $L_{R1} = 23.6\,\text{mol s}^{-1}$ and $V_F = 65.3\,\text{mol s}^{-1}$ result. The latter, $V_F = 65.3\,\text{mol s}^{-1}$, is the vapour flow through the compressor.

The compressor duty (E) is calculated using eq. (2.2). Inserting the values

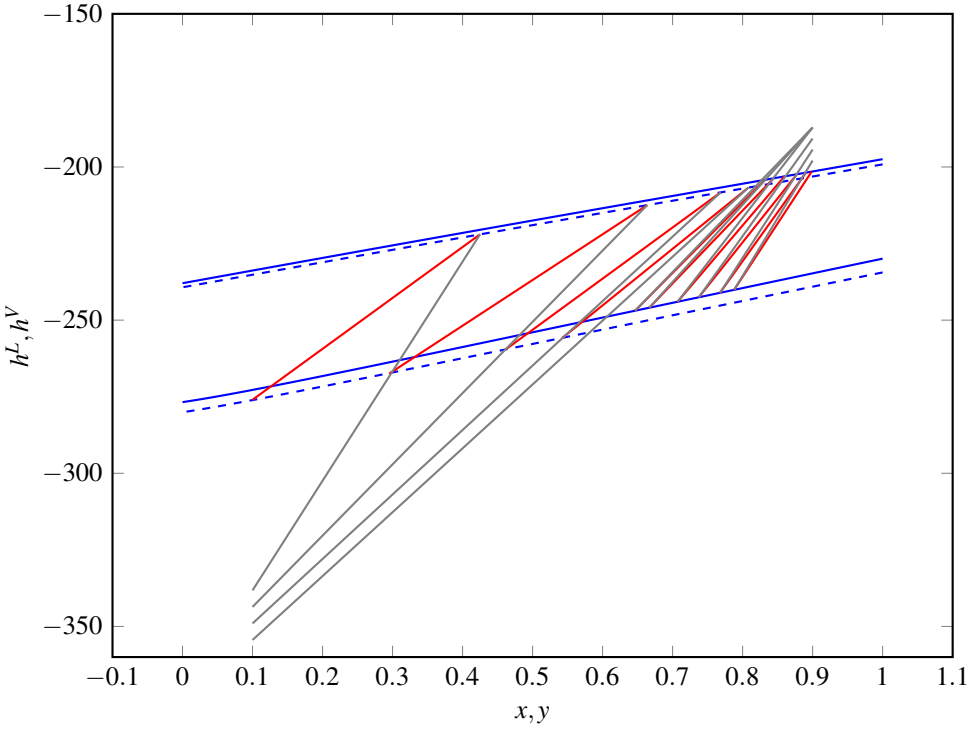

Figure E.2. HIDiC design obtained by the Ponchon-Svararit method.

$\kappa = 1.23$, $R = 0.008\,314\,\mathrm{kJ\,mol^{-1}\,K^{-1}}$, $P_{out} = 350.0\,\mathrm{kPa}$, $P_{in} = 101.3\,\mathrm{kPa}$, $T_{N_F} = 345\,\mathrm{K}$, and the vapour flow through the compressor from step 8, a duty of $E = 261.2\,\mathrm{kW}$ is obtained. The reboiler duty is hence obtained by subtracting compressor duty from the overall heat duty obtained in step 4, giving $Q_{rbl} = 1317\,\mathrm{kW}$.

Results and Discussion

With the *hxy*-diagram and the corresponding final column design in Figure E.2, the Ponchon-Savarit Method has provided a feasible HIDiC design. The Ponchon-Savarit method provides a relatively simple, graphical approach for HIDiC design. However, the method only serves as a means to give a rapid feasible solution (estimating duties) and is therefore not suited for fine-tuning the design as the stepping in the *hxy*-diagram is time consuming. This is also a impractical if iterations are required. The major limitations of the design method is that it does not supply any generic guidelines for selecting the compression ratio, the pairing of the stages, and at which stages internal heat integration should take place.

E.3 Extended Ponchon-Savarit

Method Summary

Wakabayashi and Hasebe [159] claimed to address the weaknesses of the method by Ho et al. [56] in a method referred to as the Extended Ponchon-Savarit Method. The method starts with separation formulation in step 1 and the full procedure is summarised in Figure E.3. The HIDiC design takes its starting point (step 2) in a conventional distillation column design. In step 3, the number of stages in the two column sections will provide insights for specifying bounds of these values, whereas the reboiler duty of the conventional distillation provides a reasonable estimate of the required hot utilities. For example a specification of a HIDiC reboiler duty could be half that of a CDiC. The specification of the compressor duty depends on experience. In addition, the number of pairings must be specified. The ideal conditions for heat exchange in the stripping section (reversible distillation curves, RDC) are calculated in step 4, followed by a specification of internal heat integration duties and drawing of bottom-up lines in step 5. Step 6 ensures that the stripping section design is in accordance to the desired design as specified in step 3. The rectifying section is designed using top-down lines in steps 7-9 as in steps 4-6 resulting in design of the rectifying section. Finally, in step 10, the required heat exchange areas are calculated.

Design

A column pressure of 101.3 kPa is selected based on the feed pressure. Ponchon-Savarit stepping for a CDiC is carried out using a reflux ratio to minimum reflux ratio of 1.2 resulting in 4 stages in both column sections and a reboiler duty of $Q_{rbl}^{CDiC} = 2054\,\text{kW}$. In step 3, based on the CDiC design, the range of number of stages in the stripping and rectifying sections are specified as $2 \leq N_{str} \leq 6$ and $2 \leq N_{rct} \leq 6$. In addition, a compressor duty of $E = 250\,\text{kW}$ and an energy saving of 40% corresponding to $822\,\text{kW}$ is assumed. Hence, the reboiler duty of the HIDiC is $Q_{rbl} = 1232\,\text{kW}$. These numbers are in the same order of the obtained design using the Ponchon-Savarit Method as described previously. The ideal ideal conditions for heat exchange in the stripping section are calculated in step 4. The reversible distillation curves (RDC) are plotted along with the *hxy* data and are used as a tool for selecting the ideal heat-integrated stages in both sections. Since a distillation column has a finite number of stages, the RDC is approximated by the "operating locus". The drawing of the operating locus is a part of the HIDiC design procedure, and it is drawn such that the vertical distance between itself and the RDC

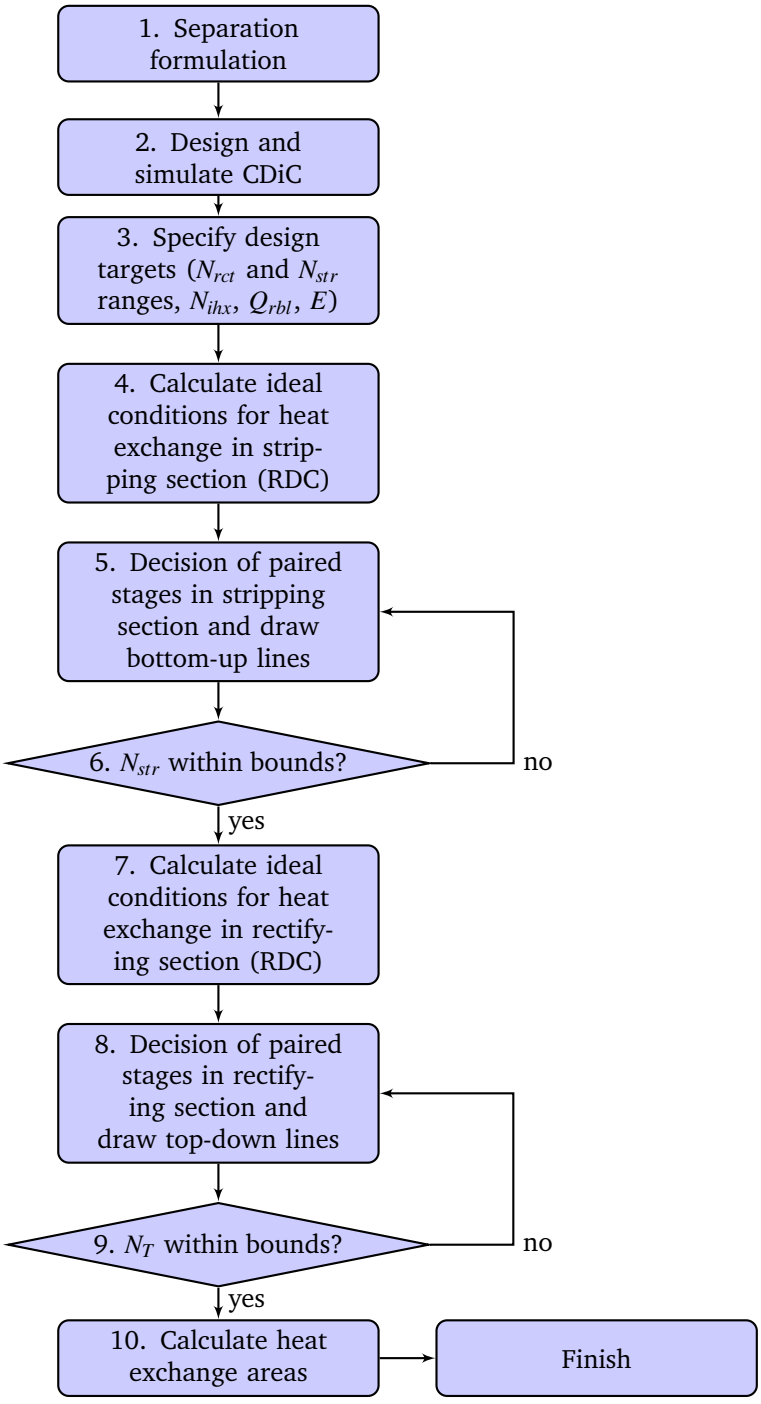

Figure E.3. Extended Ponchon-Savarit Method for HIDiC design by Wakabayashi and Hasebe [159].

must be approximately the same at any composition. The rectifying section RDC is shifted by an additional heat input to the stripping section, $\Delta h = 20\,\mathrm{kJ\,mol^{-1}}$ to obtain a shifted RDC (S-RDC). In the composition ranges where the operating locus is horizontal, the corresponding stages are adiabatic, whereas a vertical displacement corresponds to a diabatic stages. The operating locus for the stripping section is obtained by following the rules provided, which results in 3 heat-integrated stages in the stripping section. The resulting duties are $q_3 = 222\,\mathrm{kW}$, $q_2 = 333\,\mathrm{kW}$, and $q_3 = 333\,\mathrm{kW}$. The construction of the bottom-up lines are carried out by letting the operating locus determine the position of the heat-integrated stages. A total of 6 stages in the stripping section are resulted with the 3 stages below the feed stage being heat-integrated. The obtained $N_{str} = 6$ is within the bounds specified in step 3. Based on the defined compressor duty, the rectifying section pressure must be established for step 7. The vapour flow through the compressor consists of several contributions [159]: The top vapour leaving the stripping section, the vapour fraction caused by flashing the feed at the stripping section pressure, and the vapour fraction cased by flashing the bottoms liquid from the rectifying section at the stripping section pressure. The following balances are solved for the stripping section:

$$
\begin{aligned}
0 &= L_{str,in} - V_{str,out} - B \\
0 &= L_{str,in} x_{str,in} - V_{str,out} y_{str,out} - B x_B \\
0 &= L_{str,in} h^L_{str,in} - V_{str,out} h^V_{str,out} - B h^L_B + \sum_{i=1}^{N_{ihx}} q_i + Q_{rbl}
\end{aligned}
$$

By using $x_{str,in} = 0.58$ and $h^L_{str,in} = -254\,\mathrm{kJ\,mol^{-1}}$ assumed from feed, with $h^L_B = -276\,\mathrm{kJ\,mol^{-1}}$, $h^V_{str,out} = -207\,\mathrm{kJ\,mol^{-1}}$, and $\sum_{i=1}^{N_{ihx}} q_i = 888\,\mathrm{kW}$, one obtain $L = 85.2\,\mathrm{mol\,s^{-1}}$, $V = 57.4\,\mathrm{mol\,s^{-1}}$, and $y = 0.81$. $h^V_{str,out}$ is the vapour enthalpy at the same condition of the liquid stream entering the stripping section ($x_{str,in}$, $h^L_{str,in}$). Assuming a rectifying section pressure of $P_{rct} = 350.0\,\mathrm{kPa}$, the distribution of the two phases of the throttled liquid is estimated, as the enthalpy is the intersection of the feed equilibrium line and the bubble-point line at 350.0 kPa. The overall composition is 0.616 with the enthalpy of $-248.4\,\mathrm{kJ\,mol^{-1}}$. Carrying out a flash calculation a vapour fraction of 0.108 is obtained and thus the vapour contribution from the throttled liquid is $0.108/(1-0.108)\cdot 85.2\,\mathrm{mol\,s^{-1}} = 10.3\,\mathrm{mol\,s^{-1}}$. The contribution from flashing the feed stream is zero since it is a saturated liquid. The vapour flow through the compressor is thus $\hat{V}_{S1} = 67.7\,\mathrm{mol\,s^{-1}}$. Using equation (2.2) with the estimated compressor throughput and the values from step 8-9 in the Ponchon-Savarit method by Ho et al. [56], a pressure, $P_{out} = 320.2\,\mathrm{kPa}$ is obtained. In step 7, The RDC of the rectifying section is constructed. The S-RDC for the rectifying section is uniquely

determined by passing through the point, obtained by extrapolating the total mass balance to the distillate composition. The operating locus for the rectifying section is also constructed based on provided guidelines. The top-down lines are drawn and 3 stages are resulted excluding the condenser. It is found that the condenser must be paired with two stages in the rectifying section whereas the 2$^{\text{nd}}$ stage must also be heat-integrated. The obtained $N_{rct} = 3$ is within the bounds specified in step 3. In step 10, the heat exchange areas are calculated resulting in $18.3\,\text{m}^2$, $19.5\,\text{m}^2$, and $14.4\,\text{m}^2$.

Results and Discussion

The graphical solution is presented in figure E.4. The resulting design is more complicated in the sense that heat integration does not take place in the same vertical height. In fact, the user must specify how many heat-integrated pairs the solution must contain. This can be both a strength and a weakness. This is because novel configurations can be obtained, but the arrangement of the heat integration is restricted to stabbed-in type heat exchangers. This has proven useful in an industrial set-up [161]. A useful aspect of the method is that the impact of different design decisions can be investigated, while maintaining the energy savings constant as these are specified in Step 3. However, when specifying the energy savings, feasibility can not always be ensured.

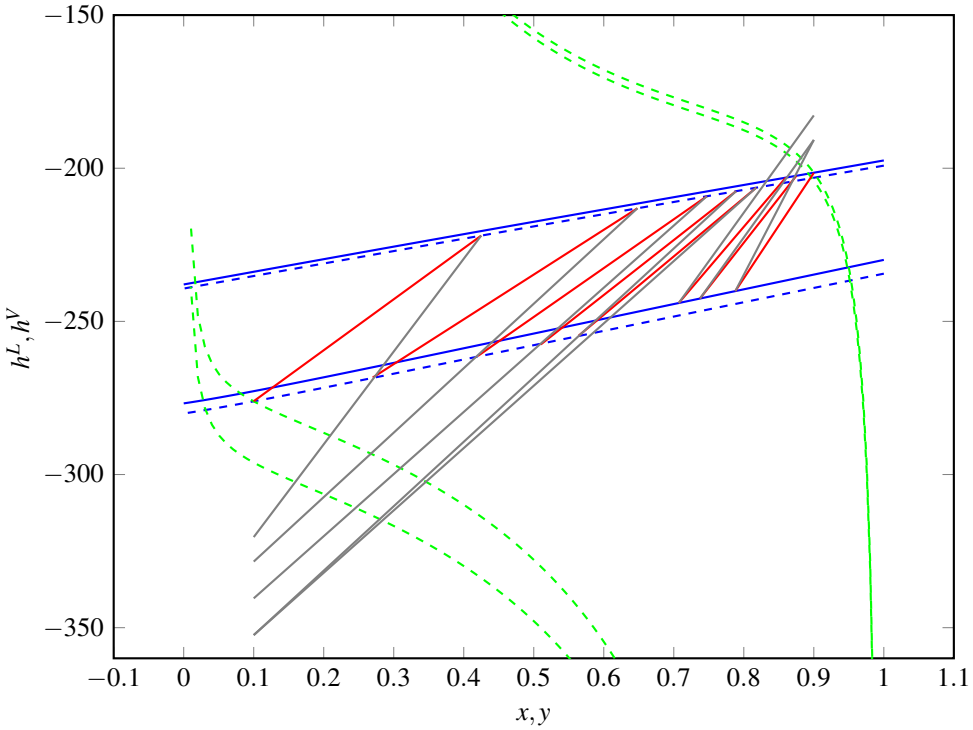

Figure E.4. HIDiC design obtained by the extended Ponchon-Svararit method.

Appendix F

Notation

Symbol	Definition	Unit
Roman symbols		
A_{ihx}	Internal heat exchange area	m^2
A_a	Active tray area	m^2
A_{CT}	Concentric total cross sectional area	m^2
A_d	Downcomer area	m^2
A_p	Perforations area	m^2
A_t	Tray area	m^2
A_T	Total cross sectional area	m^2
b	Availability function	$\mathrm{kJ\,mol^{-1}}$
c_P^L	Constant pressure heat capacity of liquid	$\mathrm{kJ\,mol^{-1}\,K^{-1}}$
c_P^V	Constant pressure heat capacity of vapour	$\mathrm{kJ\,mol^{-1}\,K^{-1}}$
CR	Compression ratio	-
d	Column diameter	m
e	Controller error	Varies
E	Electrical energy flow rate	kW
f	Mass flow rate	$\mathrm{kg\,s^{-1}}$
f_F	Feed thermal condition	-
F	Feed flow rate	$\mathrm{mol\,s^{-1}}$
FF	Flooding factor	-
g	Gravitation constant	$\mathrm{m\,s^{-2}}$
h^L	Enthalpy of liquid	$\mathrm{kJ\,mol^{-1}}$
h^V	Enthalpy of vapour	$\mathrm{kJ\,mol^{-1}}$

Continued on next page

Continued from previous page

Symbol	Definition	Unit
H_{cl}	Clear liquid height	m
H_{oW}	Liquid height over weir	m
H_S	Tray spacing	m
H_t	Tray thickness	m
H_W	Weir height	m
K_c	Controller gain	Varies
l	Column length	m
L	Liquid flow rate	$\mathrm{mol\,s^{-1}}$
M	Molar holdup	mole
M_T	Total molar holdup	mole
MW	Molecular weight	$\mathrm{kg\,mol^{-1}}$
N_{cnd}	Number of condensers (0 or 1)	-
N_{cpr}	Number of compressors	-
N_{ihx}	Number of heat-integrated stages	-
N_{rbl}	Number of reboilers (0 or 1)	-
N_{rct}	Number of trays in rectifying section	-
N_S	Number of stages	-
N_{str}	Number of trays in the stripping section	
N_T	Number of trays	-
N_F	Feed stage	-
P	Pressure	kPa
P^{sat}	Saturated pressure	kPa
Q	External heat transfer rate	kW
q	Internal heat transfer rate	kW
R	Universal gas constant	$\mathrm{kJ\,mol^{-1}\,K^{-1}}$
RR	Reflux ratio	-
s	Laplace domain independent variable	
s^L	Entropy of liquid	$\mathrm{kJ\,mol^{-1}\,K^{-1}}$
s^V	Entropy of vapour	$\mathrm{kJ\,mol^{-1}\,K^{-1}}$
S	Price	$\mathrm{\$\,kg^{-1}}$
t	Time	s
T	Temperature	K
T_s	Temperature of sink/source	K
T_σ	Temperature of surroundings	K
u	Internal energy	$\mathrm{kJ\,mol^{-1}}$

Continued on next page

Continued from previous page

Symbol	Definition	Unit
U	Liquid side stream flow rate	$\mathrm{mol\,s^{-1}}$
U_{hex}	Overall heat transfer coefficient of a conventional heat exchanger	
U_{ihx}	Overall heat transfer coefficient for heat integration	$\mathrm{kg\,m^{-2}\,K^{-1}}$
v	Molar volume	$\mathrm{m^3\,mol^{-1}}$
V	Vapour flow rate	$\mathrm{mol\,s^{-1}}$
V_{rbl}	Reboiler vapour flow rate	$\mathrm{mol\,s^{-1}}$
W	Vapour side stream flow rate	$\mathrm{mol\,s^{-1}}$
W_{lost}	Lost work	kW
W_{min}	Minimum work	kW
x	Liquid mole fraction	-
y	Vapour mole fraction	-
y_m	Measured variable	Varies
y_{set}	Setpoint	Varies
z	Feed mole fraction	-
Boldface symbols		
$\mathbf{CV}_1$	Primary controlled variables	-
$\mathbf{CV}_2$	Secondary controlled variables	-
$\mathbf{u}_D$	Actuators	-
$\mathbf{x}$	State variables	-
$\mathbf{y}$	Output vector	-
$\boldsymbol{\beta}$	Standard regression coefficient vector	-
$\boldsymbol{\theta}$	Parameter vector	-
$\boldsymbol{\theta}^*$	Certain parameters	-
$\boldsymbol{\theta}_*$	Uncertain parameters	-
Greek symbols		
Δh_{vap}	Heat of vaporisation	$\mathrm{kJ\,mol^{-1}}$
ΔP	Pressure drop	kPa
γ	Activity coefficient	-
η	Efficiency	-
θ_{dT}	Downcomer area per total cross sectional area	-
θ_{pa}	Area of perforations per active tray area	-
κ	Isentropic expansion factor	-

Continued on next page

Continued from previous page

Symbol	Definition	Unit
λ	Constant heat of vaporisation	$\mathrm{kJ\,mol^{-1}}$
$\hat{\lambda}$	Geometric mean constant heat of vaporisation	$\mathrm{kJ\,mol^{-1}}$
ρ	Density	$\mathrm{kg\,m^{-3}}$
τ_c	Desired closed-loop time constant	s
τ_I	Controller integral time	s
Φ	Specific heat transfer area	$\mathrm{m^2\,m^{-3}}$
Abbreviations		
BC	Bare module cost	
CAPEX	Capital expenditures	
CDiC	Conventional distillation column	
CE PCI	Chemical Engineering Plant Cost Index	
cnd	Condenser	
cpr	Compressor	
CV	Controlled variable	
DTI	Differential temperature indicator	
FOC	Feasibility of compression	
HIDiC	Heat-integrated distillation column	
HFI	Hydraulic feasibility indicator	
ihx	Internal heat exchange	
LI	Level indicator	
MF	Module factor	
MPF	Material and pressure correction factor	
MV	Manipulated variable	
MVRC	Mechanical vapour recompression column	
OC	Operating cost	
OPEX	Operating expenditures	
PI	Pressure indicator	
PID control	Proportional-integral-derivative control	
rbl	Reboiler	
rct	Rectifying section	
RTO	Real-time optimisation	
SRC	Standardised regression coefficients	
SRVC	Secondary reflux and vaporisation column	

Continued on next page

Continued from previous page

Symbol	Definition	Unit
TAC	Total annualised cost	
TPM	Throughput manipulator	
UBMC	Updated bare module cost	
VLE	Vapour-liquid equilibrium	
vlv	Throttling valve	